

NPS ARCHIVE
1969
CROMER, C.

AN INVESTIGATION OF THE NONLINEAR
DYNAMIC RESPONSE OF CYLINDRICAL
SHELLS UNDER TRANSIENT PRESSURE

by

Charles Clinton Cromer

UNITED STATES NAVAL POSTGRADUATE SCHOOL



THESIS

AN INVESTIGATION OF THE NONLINEAR
DYNAMIC RESPONSE OF CYLINDRICAL
SHELLS UNDER TRANSIENT PRESSURE

by

Charles Clinton Cromer

April 1969

*This document has been approved for public re-
lease and sale; its distribution is unlimited.*

T135361

AN INVESTIGATION OF THE NONLINEAR DYNAMIC RESPONSE
OF CYLINDRICAL SHELLS UNDER TRANSIENT PRESSURE

by

Charles Clinton Cromer
Lieutenant Commander, United States Navy
B.S., Illinois Institute of Technology, 1957

Submitted in partial fulfillment of the
requirements for the degree of

DOCTOR OF PHILOSOPHY

from the

NAVAL POSTGRADUATE SCHOOL
April 1969

NPS ARCHIVE
1969
CROMER, C.

~~CONFIDENTIAL~~
~~C.I.~~

ABSTRACT

A numerical algorithm was developed for computing the nonlinear dynamic response of a ring-stiffened, nearly circular cylindrical shell of finite length under transient, axisymmetric radial loads of arbitrary axial distribution. Nonlinear Donnell-type equations were solved using Fourier series expansions of the dependent variables in the circumferential coordinate, modified finite difference approximations of the axial derivatives, and Newmark's beta-method, combined with Gauss elimination, for the time integration.

The response of a simply supported shell under an exponentially decaying, uniform pressure was computed for peak pressures and total impulses between the static buckling limit and the dynamic buckling limit. Near the dynamic buckling limit, the exponential growth of the static buckling modes dominated; but as the peak pressure was reduced, the parametrically excited Mathieu modes became increasingly important. The significance of damping, the initial imperfections, and nonlinear coupling was also investigated.

TABLE OF CONTENTS

	PAGE
LIST OF TABLES	9
LIST OF FIGURES	11
TABLE OF SYMBOLS AND ABBREVIATIONS	15
ACKNOWLEDGEMENTS	21
CHAPTER	
I. INTRODUCTION	23
Scope of the Investigation	23
Historical Review	25
Rings and Unstiffened Cylinders	25
Dynamic Stability of Ring-stiffened Shells	33
New Features of the Investigation	35
Organization and Preview	37
II. FORMULATION OF THE PROBLEM	39
Introduction	39
Coordinate System	39
Strain-displacement Relations	40
Shell	40
Rings	43
Constitutive Relations.	45
Equations of Motion	47
Boundary Conditions	51
Nondimensional Equations	52
Nondimensional Variables	52
Nondimensional Equations of Motion	53

Nondimensional Boundary Conditions	55
Simply Supported	55
Clamped	56
Response Symmetric to Midspan	56
III. DEVELOPMENT OF THE NUMERICAL MODEL	57
Introduction	57
Fourier Series Expansions	57
Form of the Series Expansions	59
Reduction to Two Independent Variables . .	62
Equations of Motion	62
Boundary Conditions	64
Simply Supported	65
Clamped	65
Response Symmetric to the Midspan . .	66
Modified Finite Differences	66
Superiority of Modified Differences	
over Conventional Differences	70
Adaptation to the Nonlinear Problem . . .	71
Finite Difference Grid and Notation . .	71
Difference Expressions for Derivatives .	73
Evaluation of Nonlinear Terms	74
Location of Rings	75
Difference-differential Equations	76
Equations of Motion	76
Boundary Conditions	79
Simply Supported	79

Clamped	80
Response Symmetric to Midspan	81
IV. SOLUTION OF THE NUMERICAL MODEL	82
Solution Procedure	82
Solution of the Axial and Circumferential	
Equations	83
Applicable Methods	83
Gauss Elimination	84
Recursion Relations	85
Computation of P_K^n Matrices	87
Computation of x_K^n Matrices	88
Back Substitution	89
Time Integration	90
Integration Procedure	92
The Beta Parameter	93
Convergence Rate and Computational Errors .	97
Computer Program	99
Calculation of the Circumferential Stress	
at a Typical Location	100
Verification of Computer Program	103
Linear Test Cases	104
Moving Step Load	104
Uniform Harmonic Load	105
V. NUMERICAL RESULTS	110
Introduction	110
Statement of the Problem	110
Shell Properties	110

Initial Imperfection	111
Load	112
Previous Investigations of the Problem . . .	112
Anderson and Lindberg's Investigation . .	113
Hyperbolic Response	115
Mathieu Instability	118
McIvor and Lovell's Contribution	121
Investigation of the Problem by the Methods	
Developed in this Study	122
Preliminaries	122
Minimum Number of Axial Grid Points . .	122
Selection of the Participating Modes . .	124
Results	130
Case A	130
Case B	137
Comparison with Anderson and Lindberg's	
Findings	142
Comparison with McIvor and Lovell's	
Findings	145
Maximum Stresses	146
Case C	147
Case D	153
Critical Loading Based Upon Maximum	
Stress	156
Axial Wave Form of Responding Modes . .	158
Random Imperfections	161

Significance of Intermodal Coupling of the Flexural Modes	162
Significance of Coupling Terms in Mode Zero Equations	166
VI. SUMMARY, FINDINGS, AND RECOMMENDATIONS FOR FUTURE WORK	169
Summary	169
Findings	172
Recommendations for Future Work	177
LIST OF REFERENCES	179
APPENDIX A. INCONSISTENCY OF THE CONVENTIONAL DIFFERENCES	184
APPENDIX B. ADAPTATION OF MODIFIED DIFFERENCES TO NONLINEAR EQUATIONS	199
Evaluation of Nonlinear Terms	199
In-plane Forces, λ_1 , and λ_2	199
Nonlinear Terms η_ξ , $\eta_{\xi\theta}$, and η_θ	204
Boundary Conditions on Displacements	206
APPENDIX C. DEFINITIONS OF CONSTANTS AND MATRICES	208
APPENDIX D. COMPUTER PROGRAM	212
Fortran Variables	212
Description of the Program	212
Input Requirements	229
User Alterations to Obtain Uncoupled Solutions	239

Storage Requirements and Execution

Time	241
Program Listing	242

LIST OF TABLES

TABLE	PAGE
I. Stability and Convergence Limits	95
II. Natural Frequencies, Natural Periods, and Buckling Pressures Predicted by Equations of Anderson and Lindberg [19]	116
III. Response of Individual Modes Without Extraction of Energy from Axisymmetric Mode, $p_o = 6.37 \times 10^{-4}$, $\tau_o = 208$	126
IV. Case A, Amplifications and Stresses, $t_o = 3.0$ msec ($\tau_o = 208$), Zero Damping	131
V. Case B, Amplifications and Stresses, $t_o = 1.0$ msec ($\tau_o = 69.3$), Zero Damping	140
VI. Case C, Amplifications and Stresses, $t_o = 3.0$ msec ($\tau_o = 208$), Damping Included	151
VII. Case D, Amplifications and Stresses, $t_o = 1.0$ msec ($\tau_o = 69.3$), Damping Included	155
VIII. Effect of Magnitude of Initial Imperfection, $P_o = 70$ psi, $t_o = 3.0$ msec, Zero Damping	163
IX. Amplifications with Total and Limited Intermodal Coupling, $P_o = 70$ psi, $t_o = 3.0$ msec, $w_1^n = 1.0 \times 10^{-5}$, Zero Damping	165
X. Response of Individual Modes without Energy Extraction from the Axisymmetric Mode, $P_o = 70$ psi ($p_o = 6.37 \times 10^{-4}$), $t_o = 3.0$ msec ($\tau_o = 208$)	167

XI. Description of Fortran Variables	213
--	-----

LIST OF FIGURES

FIGURE		PAGE
2.1	Geometry and Coordinates of Shell	40
2.2	Displacements and Rotation of a Typical Ring .	42
2.3	Positive Directions of Forces and Moments . . .	46
3.1	Staggered Finite Difference Mesh	68
3.2	Spatial Discretization using Modified Differences	72
4.1	Relationship Between Mesh Nodes and Index K of Equation (4.2)	86
4.2	Acceleration vs. Time for $\beta = 1/4, 1/6,$ and $1/8$	94
4.3	Dependency of Convergence Rate and Computational Errors on Length of Time Increment $\beta = 1/6$ (Ref. [42])	98
4.4	Quarter-span Response to a Moving Step Load . .	106
4.5	Response of Mid-span to a Uniform Harmonic Pressure	108
5.1	Mathieu Stability Chart for Harmonic Uniform Pressure	120
5.2	Mathieu Stability Chart for Exponentially Decaying Uniform Pressure, $P_O = 70$ psi ($p_O = 6.37 \times 10^{-4}$), $t_O = 3.0$ msec ($\tau_O = 208$)	128
5.3	Case A, Response of Modes 5, 6, 7, and 14, $P_O = 60$ psi ($p_O = 5.46 \times 10^{-4}$), $t_O = 3.0$ msec ($\tau_O = 208$), Zero Damping	133

5.4	Case A, Response of Modes 5, 6, 7, 8, and 14 $P_O = 70 \text{ psi}$ ($p_O = 6.37 \times 10^{-4}$), $t_O = 3.0$ msec ($\tau_O = 208$), Zero Damping	134
5.5	Case A, Response of Modes 5, 6, 7, 8, and 14 $P_O = 77 \text{ psi}$ ($p_O = 7.01 \times 10^{-4}$), $t_O = 3.0$ msec ($\tau_O = 208$), Zero Damping	135
5.6	Case A, Maximum Amplification of Hyperbolic Modes	138
5.7	Case B, Maximum Amplification of Hyperbolic Modes	143
5.8	Critical Loading for Amplification of 1000 . .	144
5.9	Case C, Response of Modes 5, 6, 7, and 14, $P_O = 60 \text{ psi}$ ($p_O = 5.46 \times 10^{-4}$), $t_O = 3.0$ msec ($\tau_O = 208$), Damping Included	148
5.10	Case C, Response of Modes 5, 6, 7, 8, and 14 $P_O = 70 \text{ psi}$ ($p_O = 6.37 \times 10^{-4}$), $t_O = 3.0$ msec ($\tau_O = 208$), Damping Included	149
5.11	Case C, Response of Modes 5, 7, and 14 $P_O = 77 \text{ psi}$ ($p_O = 7.01 \times 10^{-4}$), $t_O = 3.0$ msec ($\tau_O = 208$), Damping Included	150
5.12	Case C, Maximum Circumferential Stress vs. Peak Pressure, $t_O = 3.0 \text{ msec}$ ($\tau_O = 208$), Damping Included	154
5.13	Case D, Maximum Circumferential Stress vs. Peak Pressure, $t_O = 1.0 \text{ msec}$ ($\tau_O = 69.3$), Damping Included	157

5.14	Critical Loading Based on Stress,	
	$\sigma_{yp} = 42$ ksi, Damping Included	159
5.15	Axial Variation of (a) Hyperbolic Modes,	
	(b) Mathieu Modes, $p_o = 6.37 \times 10^{-4}$,	
	$\tau_o = 208$	160
A.1a	"Whole" Station Mesh - Modified Differences. . .	196
A.1b	"Half" Station Mesh - Modified Differences . . .	196
B.1	Finite Difference Stations	202
B.2	Finite Difference Stations at the End $\xi = 0$. . .	207
D.1	Input Format	230
D.2	Execution Time, $\tau = 0$ to 200	243

TABLE OF SYMBOLS AND ABBREVIATIONS

a	radius of a perfect circular cylindrical shell
a^r	radius of centroidal circle of a ring
A_r	cross sectional area of the rings
A^n	2x2 matrix, (4.2) ¹
B	extensional rigidity of the shell
B_K^n	2x2 matrix, (4.2)
c	nondimensional damping coefficient
C	damping coefficient
C^n	2x2 matrix, (4.2)
C_1, \dots, C_5	ring coefficients
C_{ITT}^n	Fourier coefficient of the product $\bar{w}_\theta w_\theta$
C_{ITX}^n	Fourier coefficient of the product $\bar{w}_\theta w_\xi$
C_{IXT}^n	Fourier coefficient of the product $\bar{w}_\xi w_\theta$
C_{IXX}^n	Fourier coefficient of the product $\bar{w}_\xi w_\xi$
C_{TT}^n	Fourier coefficient of the nonlinear term $\frac{1}{2}w_\theta^2$
C_{XT}^n	Fourier coefficient of the nonlinear term $w_\xi w_\theta$
C_{XX}^n	Fourier coefficient of the nonlinear term $\frac{1}{2}w_\xi^2$
C_T	St. Venant's torsion constant of the rings
d	nondimensional spacing of finite difference mesh

¹Numbers in parenthesis indicate the equation in which the matrix is first defined or used.

d_1, \dots, d_9	constants
D	bending rigidity of the shell
\bar{e}	eccentricity of the rings
e	\bar{e}/a
E, E_r	Young's modulus of the shell, ring material
f^n	2x1 matrix, (4.11)
g_K^n	2x1 matrix, (4.4)
G_r	shear modulus of ring material
h	thickness of the shell
H	the set of whole stations in the finite difference mesh at which the rings are located
H_j	the member of the set H corresponding to the j^{th} ring
H^n	2x2 matrix, (4.11)
I	impulse per unit area
I_x, I_z	centroidal moments of inertia of a ring cross section
k	half stations of the finite difference mesh
K	whole stations of the finite difference mesh
l	L/a
L	length of the cylindrical shell
m	number of half stations in the finite difference mesh
M	number of whole stations in the finite difference mesh
M_x, M_y	bending moments
M_{xy}, M_{yx}	twisting moments
n	Fourier index
\bar{n}_θ	nondimensional magnitude of the circumferential stress at the surface of the shell

n_θ, n_ξ	nondimensional in-plane forces
$n_{\xi\theta}$	nondimensional in-plane shear force
N_r	number of rings
N_x, N_y	in-plane normal forces
N_{xy}, N_{yx}	in-plane shear forces
$n_\theta^n, n_\xi^n, n_{\xi\theta}^n$	Fourier coefficients of $n_\theta, n_\xi, n_{\xi\theta}$
O^n	2x2 matrix, (4.11)
p	nondimensional pressure
P	pressure
p_{cr}^n	nondimensional static buckling pressure of the n^{th} mode
P_K^n	2x2 matrix, (4.5a)
R^n	2x2 matrix, (4.12)
R_j^n	the contribution of the ring at station H to the radial equilibrium equation of Fourier index n
s^n	2x1 matrix, (4.12)
t	time
T	shortest nondimensional period of the modes of oscillation of the finite difference model
T_n	nondimensional period of the n^{th} flexural mode
\mathcal{T}	kinetic energy
$\mathcal{T}_s, \mathcal{T}_r$	kinetic energy of the shell, ring
u	U/a
U	axial displacement of the shell midsurface
u^n	Fourier coefficient of u
U^r	axial displacement of the centroid of a ring
v	V/a
V	circumferential displacement of the shell mid-surface

v^n	Fourier coefficient of v
v^r	circumferential displacement of the centroid of a ring cross section
\bar{w}	\bar{W}/a
$\bar{\bar{w}}$	unstrained displacement of shell midsurface from midsurface of the perfect circular cylindrical shell
\bar{w}^n	Fourier coefficient of \bar{w}
w^*	$\bar{w} + w$
\dot{w}^n	nondimensional radial velocity of the n^{th} mode
\ddot{w}^n	nondimensional radial acceleration of n^{th} mode
\ddot{w}_1^n	nondimensional radial acceleration, used in iterative procedure
w	W/a
w^n	Fourier coefficient of w
W	radial displacement of the shell midsurface from the unstrained midsurface of the nearly circular cylindrical shell
w_i^n	amplitude of the imperfection mode of the form $w_i^n \sin \frac{\pi \xi}{l} \cos n\theta$
w^r	radial displacement of the centroid of a ring
\mathcal{W}	work function
\mathcal{W}_L^o	work done by applied forces on the shell in a virtual displacement
\mathcal{W}_s^o	negative of the strain energy of the shell, work function of the shell
\mathcal{W}_r^o	negative of the strain energy of the rings, work function of the rings
x	axial coordinate
x_K^n	$2 \times l$ matrix, (4.5a)
\bar{y}	defined by $d\bar{y} = a^r dy/a$

z	radial coordinate
z_K^n	2x1 matrix, (4.3)
α	h/a
β	Chapter II: angle of twist of ring cross section Chapter IV: parameter of Newmark beta-method
γ_{xy}	shear strain
δ	operator for a variation in the calculus of variations sense
$\delta()$	Dirac delta function
δ_{ij}	Kronecker delta
$\Delta\tau$	increment in τ
ϵ	convergence parameter
ϵ_x, ϵ_y	strains of the shell midsurface
ϵ_θ^r	circumferential strain of ring
η_θ^n	Fourier coefficient of the nonlinear product $n_\theta (w,_{\theta\theta} + \bar{w},_{\theta\theta})$
η_ξ^n	Fourier coefficient of the nonlinear product $n_\xi (w,_{\xi\xi} + \bar{w},_{\xi\xi})$
$\eta_{\xi\theta}^n$	Fourier coefficient of the nonlinear product $2n_{\xi\theta} (w,_{\xi\theta} + \bar{w},_{\xi\theta})$
θ	y/a
$\lambda 1^n, \lambda 2^n$	functions of the displacement w^n in the axial and circumferential equations
$\Lambda 1^n, \Lambda 2^n$	functions of the displacement w^n
μ	characteristic length corresponding to the width of a ring
ν	Poisson's ratio
ξ	x/a
Π	potential energy

Π^n	potential energy of the n^{th} mode
$\bar{\Pi}^n$	$2\Pi^n/\pi a B$
ρ, ρ_r	mass density of the shell, ring material
σ_{yp}	yield point stress of shell material
σ_θ	circumferential stress at midsurface of the shell
$\sigma_{\theta B}$	circumferential stress at the surface of the shell due to bending
$\sigma_{\theta s}$	circumferential stress at the surface of the shell
τ	nondimensional time
τ_0	nondimensional time constant
ϕ	angle of twist of ring per unit circumferential length
χ_x, χ_y	changes of curvature of the midsurface of the shell
χ_{xy}	twist of the midsurface of the shell
χ_1^r, χ_2^r	changes of curvature of the rings
Ω	frequency
Ω_n	natural frequency of the n^{th} flexural mode

ABBREVIATIONS

in	inches
ksi	thousands of pounds per square inch
msec	milliseconds
psi	pounds per square inch
$()', \xi$	$\partial()/\partial\xi$, where ξ is a spatial coordinate
(\cdot)	$\partial()/\partial\tau$

ACKNOWLEDGEMENTS

I first wish to express my profound gratitude to Professor R. E. Ball, my advisor, for suggesting this topic, for his advice and assistance, and for his continuous encouragement.

I also wish to thank Professor J. E. Brock, Professor T. H. Gawain, Professor G. H. Lindsey, and Professor E. J. Stewart, the other members of my Doctoral Committee, for their helpful counselling.

The staff of the Computer Facility of the Naval Post-graduate School was cooperative in providing assistance and computing time.

Special thanks is also due to the Naval Weapons Laboratory, Dahlgren, Virginia, for their financial support of the research.

Finally, but by no means least, I wish to express appreciation to Mary Louise and to young Laura and David for their patience and encouragement.

CHAPTER I

INTRODUCTION

I. SCOPE OF THE INVESTIGATION

This dissertation considers the general nonlinear dynamic response of a nearly circular, nearly cylindrical, ring-stiffened shell of finite length subjected to a transient, axisymmetric radial load.

The research was part of a project for the Naval Weapons Laboratory, Dahlgren, Virginia, to analytically predict the dynamic response of the large NWL shock tube [1]¹ under operational loading conditions. The various sections of the shock tube can be idealized as thin, ring-stiffened, circular cylindrical shells having either clamped or simply supported ends. The operating loads can be described as internal, propagating, axisymmetric pulses having pressures both higher and lower than ambient atmospheric pressure. In the unloaded condition, the midsurface of the shell deviates from a perfect circular cylinder, but the unloaded shell was assumed to be stress free. Due to this initial imperfection of the shell, the dynamic response will not be axisymmetric even though the loading may be axisymmetric.

¹Numbers within brackets refer to items in the List of References, page 179.

Although there has been a great deal of recent interest in problems of this nature,² there are, in fact, no previous analyses that are fully capable of solving the problem.

Consequently, an algorithm was developed for the numerical solution to the Donnell-type, nonlinear differential equations that describe the general dynamic response of the idealized shock tube sections to a transient, axisymmetric, radial load of arbitrary time history and axial distribution. Some of the features of the method were demonstrated by computing the dynamic response of a simply supported shell under an exponentially decaying, uniform pressure. The peak pressures and the total impulses of the loads considered fall between the static buckling limit and the dynamic buckling limit. In addition, the significance of viscous damping, of the initial imperfections, and of the nonlinear coupling was investigated.

²The analysis is applicable to structures other than the NWL shock tube. For instance, a missile or submarine engulfed by a blast front presents a similar structural dynamics problem.

II. HISTORICAL REVIEW

Rings and Unstiffened Cylinders

The nonlinear dynamic response of circular cylindrical shells has received considerable attention over the past twenty years, with the Russians doing much of the early work in the field. For example, the 1956 book by the Russian V. V. Bolotin [2] is a classic in the field of dynamic instability. In it the works of most of the early Russian investigators are described in some detail.

One of the earliest articles to appear in the American literature was a 1961 translation from the Russian of a 1958 paper by V. L. Agamirov and A. S. Vol'mir [3]. In this paper the Bubnov-Galerkin method was used to obtain an approximate solution for the response of a closed cylindrical shell subjected to a hydrostatic loading that increased linearly with time. They assumed a function for the spatial variation of both the initial imperfection and the total deflection, allowing for variation in the axial and circumferential directions. Thus, the problem was reduced to the numerical solution of a single nonlinear ordinary differential equation in the time dependent amplitude of the displacement function.

In 1961, J. C. Yao [4] published one of the first American papers to appear in the field. He investigated the stability of an infinite cylinder under a uniform radial pressure applied as a rectangular shaped function of time.

The motion was assumed to consist of a uniform radial displacement plus one flexural mode having two waves around the circumference. The only coupling retained was the influence of the axisymmetric mode on the flexural mode. The flexural mode was shown to respond in an oscillatory or exponential manner depending on the magnitude of the pressure.

The Agamirov and Vol'mir paper [3] was followed in 1962 by another translation from the Russian of a 1960 paper by Y. I. Kadashevich and A. K. Pertsev [5]. They investigated the response of a finite cylindrical shell loaded by uniform radial pressure applied as a step function in time. They used combinations of two axisymmetric modes and one nonaxisymmetric mode to represent the initial imperfection and the radial displacement. However, these modes did not satisfy the boundary conditions. Using Lagrange's equations, ordinary, coupled, nonlinear differential equations were obtained which accounted for the radial inertia of all three oscillatory modes. These equations were integrated numerically to obtain the time histories of the modes. The critical load was defined as the load which caused stresses in excess of the ultimate strength of the shell material. This paper is considered most significant because it retained all the nonlinear coupling between the three modes. Most later works do not retain all of the coupling terms.

Another very significant paper was published by Yao [6] in 1963. He investigated the dynamic stability of closed cylindrical shells under several combinations of harmonic and static loads. He assumed the radial motion to consist of a uniform quasi-static displacement plus a small, nonaxisymmetric, flexural perturbation that satisfied the boundary conditions.³ As in his earlier work [4], Yao retained only the influence of the axisymmetric mode on the flexural mode. The governing equation for the motion of the perturbation was an ordinary differential equation with a harmonically varying coefficient, namely, the classical Mathieu equation.⁴ When a flexural mode corresponded to a point in an unstable region of the Mathieu stability chart, the response of the shell was assumed to be unstable. Yao concluded that a shell not only can withstand static loads up to the classical buckling load, but also can endure an additional harmonic load so long as the harmonic component does not render any of the flexural modes unstable.

³The radial inertia of the axisymmetric mode was neglected.

⁴The solution to the Mathieu equation is either oscillatory and bounded, or oscillatory and unbounded, depending on the parameters [7]. The unbounded condition is known as parametric resonance or dynamic instability. The distinction between a bounded response and one that is unbounded is determined from the Mathieu stability chart.

In late 1963, J. D. Wood and L. R. Koval [8] presented the results of their investigation of the stability of an axially loaded shell subjected to a time dependent uniform radial pressure. Their assumptions and method of solution were essentially the same as those employed by Yao [4, 6]. However, they did not neglect the radial inertia of the axisymmetric mode as Yao had done.

In 1964, J. N. Goodier and I. K. McIvor [9] published a paper which considered the response of an infinitely long shell subjected to nearly axisymmetric, radial impulse of low intensity. Mathieu's equation governed the early growth of the flexural modes. Since the impulse was of low intensity, a single dominant flexural mode could be identified from the Mathieu stability chart. They assumed the radial displacement to consist of a uniform radial mode plus the single dominant flexural mode. The fully coupled motion of these two modes was computed numerically. During the motion, the axisymmetric mode and the flexural mode exchanged energy in a cyclic manner because of the total coupling between the two modes. Although the flexural mode corresponded to an unstable point on the stability chart, its motion remained bounded since only a finite amount of energy was imparted to the shell by the load. This paper demonstrated that the motion of a flexural mode is not necessarily unbounded even though its early growth is associated with a point in an unstable region of the Mathieu stability chart.

H. E. Lindberg [10], in a companion to the above paper, investigated the dynamic buckling of thin shells under very intensive impulsive loads. He found that many short wavelength flexural modes were excited to large amplitudes, and that buckling occurred as the result of hyperbolic growth, rather than any oscillatory growth.

In 1964, R. S. Roth and J. M. Klosner [11] investigated the dynamic response of a cylindrical shell subjected to an axisymmetric, axial step load. They used a Donnell-type shell theory and assumed that the radial displacements and the initial imperfection were comprised of a linear combination of four discrete modes, all of which did not satisfy the boundary conditions. Radial inertial forces in all modes were considered. The Galerkin-Ritz method was used to obtain the coupled, ordinary, nonlinear differential equations in the time dependent coefficients. The resulting equations were then integrated numerically. Prior to this work, the Russians Kadashevich and Pertsev [5] were apparently the only ones who had accounted for the simultaneous, coupled motion of more than one flexural mode.

In 1965, a survey article by R. M. Evan-Iwanowski [12] reviewed the state of the art on the parametric resonance of structures. The bibliography is very comprehensive with numerous references to the early Russian work. In this article Evan-Iwanowski suggested that future work should be devoted to study of the interaction between the dynamic and parametric responses.

M. P. Bienick, T. C. Fan, and L. M. Lackman's 1966 paper [13] investigated the dynamic stability of a cylindrical shell under a uniform radial pressure, applied harmonically or as a ramp function of time. The axisymmetric deflection state varied as a half sine wave along the axis, thus satisfying the simply supported boundary conditions. One flexural mode of arbitrarily small magnitude was assumed to comprise the perturbed state. It also satisfied the boundary conditions. The effects of the radial inertia in both modes were included. The stability problem was reduced to Mathieu's equation for both types of loads. Under the ramp loading, they found that not one, but several flexural modes were unstable if the shell was short.

The first works devoted to the dynamic stability of a cylindrical shell loaded by a moving axisymmetric load were by G. A. Hegemeir [14, 15] in 1966 and 1967. The shell was infinite in length, and the load moved at constant velocity, leading to a steady state condition. Hegemeir, like Yao [6] and Bienick, Fan, and Lackman [13], investigated the stability of the nonaxisymmetric response with respect to arbitrarily small perturbations. However, the governing equation was not the Mathieu equation.

In 1966, T. C. Fan [16] retained the axial and circumferential inertia in an investigation of the dynamic stability of a simply supported cylinder loaded by uniform radial pressure applied as a ramp function of time. His

results showed that neglecting the axial and circumferential inertial forces has little effect on the stability of small flexural perturbations. This seems to be the only study of the significance of the axial and circumferential inertial forces.

In 1966, M. H. Lock [17], like Goodier and McIvor [9], studied the response of a ring, or an infinitely long cylinder, but under step loads instead of impulsive loads. Using finite deflection theory, he computed the coupled motion of the axisymmetric mode and one nonaxisymmetric mode. The conditions for instability to small perturbations were shown to be necessary for the existence of large displacements, but not sufficient. Significant to the present investigation, he showed that a flexural mode could be excited to large amplitude in either of two ways: (1) When the magnitude of the load exceeded the static buckling load of a mode, that mode grew in essentially an exponential manner with time until limited by nonlinear effects. (2) A flexural mode could also be excited to large amplitudes by the oscillation of the axisymmetric mode, and the growth was an oscillation of increasing amplitude, as in parametric resonance.

A 1965 report by H. E. Lindberg, et al. [18] and the subsequent 1968 article by D. L. Anderson and H. E. Lindberg [19] are of considerable interest to this dissertation. They presented two theoretical models, a tangent modulus model for plastic behavior and an elastic model,

for predicting the dynamic loads required to buckle a cylindrical shell. Only the elastic model is of interest here. This model made use of a Donnell-type shell theory which accounted for initial imperfections. The radial motion was assumed to consist of a uniform radial displacement plus nonaxisymmetric flexural modes that satisfied the simply supported boundary conditions. The spatial distribution of the initial imperfection was taken to be the same as that assumed for the flexural mode shapes. Following Yao [4, 6], Wood and Koval [8], and Bienick, Fan, and Lackman [13], the influence of the axisymmetric mode on the flexural modes was the only coupling retained. No coupling was retained which might extract energy from the uniform radial mode, nor was any coupling between flexural modes retained. An exponentially decaying uniform load and a linearly decaying uniform load were considered. The maximum displacement of several flexural modes was found by numerical integration, and buckling was assumed to have occurred whenever the maximum displacement of any mode exceeded one thousand times the initial imperfection in that mode. Only the lower frequency, exponentially growing buckling modes were considered. The parametrically excited modes were not treated. The authors reasoned that these modes would dissipate energy locally by plastic flow and, hence, would eventually dampen out before causing deflections large enough to buckle the shell.

The most recent work is the paper by I. K. McIvor and E. G. Lovell [20] which appeared in late 1968. They studied the dynamic response of finite length cylindrical shells subjected to a uniform radial impulse. They assumed a set of modal displacement functions that simplified some of the algebra, but did not satisfy end conditions of usual interest. By first using a small nonaxisymmetric perturbation approach that retained only the influence of the axisymmetric mode on the flexural mode, Mathieu's equation was obtained. They then determined from the Mathieu stability diagram the four or five flexural modes having the highest initial growth rate. Using these modes and the axisymmetric mode, and retaining all coupling between modes, they employed the Runge-Kutta integration method to compute the response of each mode to the uniform radial impulse. A slight irregularity in the impulse was used to initiate the response of each nonaxisymmetric mode. They found that the modes underwent beat-like oscillations accompanied by a continual exchange of energy between modes. The stress levels attained during the nonsymmetric motion were much higher than those developed in an axisymmetric dynamic response to the same load.

Dynamic Stability of Ring-stiffened Shells

The treatment of discrete ring stiffeners in a nonlinear dynamic analysis would provide a suitable topic for

a dissertation in itself. In the course of this research, a brief study of the problem was conducted, and a seemingly suitable method of analysis was selected. It is not the only method, and perhaps not even the best method. A complete review of the related literature is deemed to be beyond the scope of this study. Only a few references are mentioned to provide a starting point for an interested reader.

In a 1967 dissertation, W. K. Dietz [21] investigated the dynamic response of eccentrically reinforced, circular cylindrical shells subjected to dynamic axial loads. He considered only shells with closely spaced stiffeners and treated the structure as an equivalent orthotropic shell. The Galerkin method was used to obtain a set of ordinary, nonlinear differential equations in time which were integrated by employing a predictor-corrector method.

J. M. Klosner and H. N. Franklin [22] presented a report in 1968 which dealt briefly with the dynamic instability of long reinforced cylindrical shells under axial loads. They, like Dietz, treated an equivalent orthotropic shell and used the Galerkin method to obtain the governing differential equations of motion. The equations were integrated by the Runge-Kutta method.

The analysis of the rings contained in this dissertation is essentially an adaptation of a method used by D. L. Block [23] in a 1968 report dealing with the influence

of discrete ring stiffeners and prebuckling deformations on the static buckling of axially loaded shells.

III. NEW FEATURES OF THE INVESTIGATION

The studies which have been reviewed in the proceeding section appear inadequate for one or more of the following reasons:

1. The motion can not be predicted after onset of nonaxisymmetric motion.
2. The boundary conditions are not satisfied by the assumed displacement functions.
3. Coupling due to nonlinear effects is only partially retained.
4. The assumed displacements are not general enough; or an insufficient number of modes have been included to encompass both the higher frequency, parametrically excited modes and the exponentially growing, lower frequency, buckling modes.
5. The analyses do not handle loads which depend on the axial coordinate.

The algorithm developed in this dissertation is more general than any of the earlier analyses and does not contain any of the above shortcomings. This is accomplished by the use of the following new features:

1. The displacements are expanded in Fourier series in the circumferential coordinate. The series are then truncated, and only the significant modes are retained. Those modes which do not respond can be discarded. As many as fifteen modes are included, and this number can be increased at the expense of increased computing time. In this study all of the nonlinear coupling between the modes is retained, and enough modes are included to simultaneously encompass the parametrically excited modes and the exponentially growing buckling modes.
2. A set of modified finite differences is employed for the derivatives with respect to the axial coordinate for the first time in a nonlinear shell problem. These modified differences are shown to be superior to the conventional difference approximations to derivatives.
3. The iterative Newmark beta-method is employed for the time integration of the radial equations of motion. The axial and circumferential displacements are obtained by Gauss elimination during each iteration.

4. The boundary conditions are consistently observed.
5. Axisymmetric radial loads of arbitrary time variation and axial form can be readily handled.
6. Initial imperfections symmetric about a plane through the axis and of arbitrary axial distribution are accounted for.
7. Viscous damping forces are included in the equations of motion.
8. The effects of discrete, eccentrically located ring stiffeners have been included in the analysis.

IV. ORGANIZATION AND PREVIEW

The main body of the dissertation is divided into six chapters. The present introductory chapter is followed by the development of the equations of motion in Chapter II. In Chapter III, a numerical model is developed that replaces the partial differential equations of Chapter II with difference-differential equations in the time variable. In Chapter IV, methods for generating a solution to the difference-differential equations are considered, the computer program is briefly described, and the tests which were conducted to verify the computer program are discussed. Numerical results for a problem, a problem similar to one considered earlier by Anderson and Lindberg [19] and McIvor

and Lovell [20], are presented in Chapter V along with studies of the significance of damping, of the initial imperfection, and of nonlinear coupling. Chapter VI contains a summary of the work, the new findings, and recommendations for future work in the field.

Four appendices contain some of the minor details of the development of the algorithm and a complete documentation of the computer program, including instructions for preparation of input data cards and other information necessary for the operation of the program.

CHAPTER II

FORMULATION OF THE PROBLEM

I. INTRODUCTION

In this chapter the governing nonlinear differential equations for the dynamic response of a ring-stiffened, nearly circular cylindrical shell of finite length are derived. A Donnell-type nonlinear theory [24, 25] that accounts for initial imperfections in the shape of the shell is used to describe the shell response; the discrete circular rings are treated by linear beam and elementary torsion theories. The shell and ring materials are assumed to be homogeneous, isotropic, and elastic; and the rings may be fabricated from a different material than the shell. The centroids of the ring cross sections are eccentrically located with respect to the midsurface of the shell. Radial inertial forces of the shell and the rings have been included; but their axial, circumferential, and rotatory inertial forces have been neglected. Viscous type damping has been included to account for dissipative effects.

II. COORDINATE SYSTEM

The motions of the shell of length L will be referred to the fixed coordinate system shown in Figure 2.1. The positive direction of the axial coordinate x , the

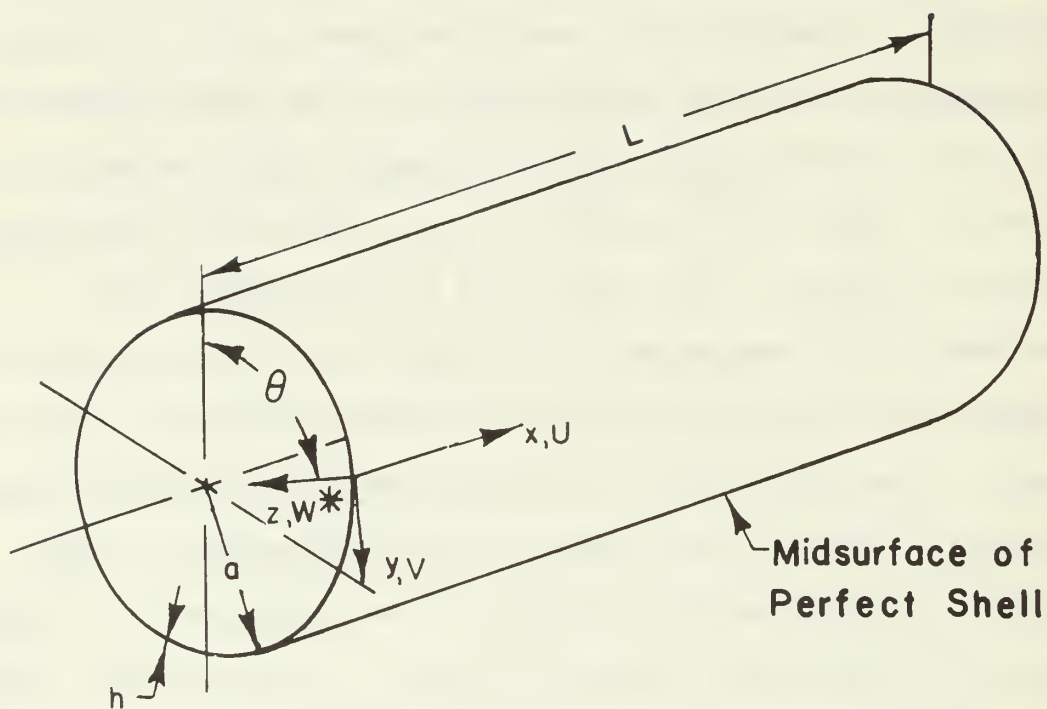


FIGURE 2.1

GEOMETRY AND COORDINATES
OF SHELL

circumferential coordinates y and θ , the radial coordinate z , the axial displacement U , the circumferential displacement V , and the radial displacement W^* are as indicated in Figure 2.1. The origin of the coordinate system is located at the midsurface of a perfectly circular cylinder of radius a . The ends of the shell are located at $x = 0$ and $x = L$. The shell thickness is denoted by h .

The motion of a ring will be described by the displacements of the centroid of the ring cross section U^r , V^r , and W^r , and the rotation about a normal to the cross section β , with positive directions as indicated in Figure 2.2. The distance \bar{e} between the centroid of a ring cross section and the midsurface of the shell is positive when the rings are on the outside of the shell.

III. STRAIN-DISPLACEMENT RELATIONS

Shell

In the Donnell-type nonlinear theory, the relations between the midsurface strains and displacements are given by [25]

$$\epsilon_x = U_{,x} + \frac{1}{2} (W_{,x})^2 + W_{,x} \bar{W}_{,x} \quad (2.1a)$$

$$\epsilon_y = V_{,y} - \frac{W}{a} + \frac{1}{2} (W_{,y})^2 + W_{,y} \bar{W}_{,y} \quad (2.1b)$$

$$\gamma_{xy} = U_{,y} + V_{,x} + W_{,x} W_{,y} + \bar{W}_{,x} \bar{W}_{,y} + W_{,x} \bar{W}_{,y} \quad (2.1c)$$

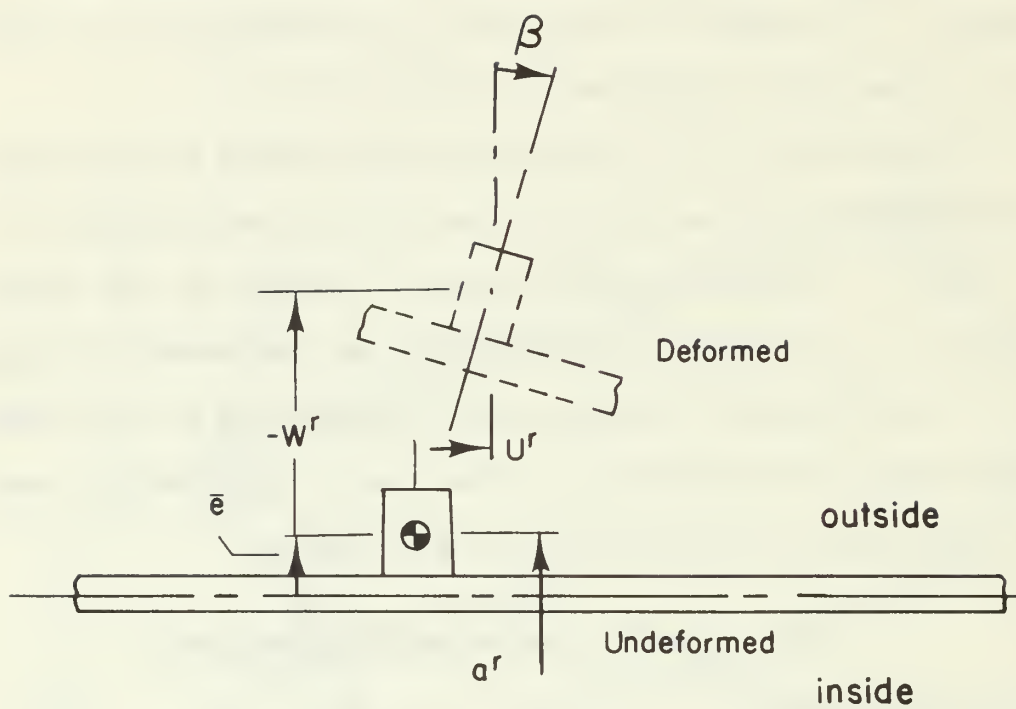


FIGURE 2.2
DISPLACEMENTS AND ROTATION
OF A TYPICAL RING

$$\chi_x = W,_{xx} \quad (2.1d)$$

$$\chi_y = W,_{yy} \quad (2.1e)$$

$$\chi_{xy} = W,_{xy} \quad (2.1f)$$

where ϵ_x and ϵ_y are the extensional strains, γ_{xy} is the shear strain, χ_x and χ_y are the curvature changes, χ_{xy} is the twist, W is the radial displacement of the midsurface of the nearly circular cylinder, and \bar{W} is the radial deviation of the unstrained midsurface from the midsurface of a perfectly circular cylindrical shell. Hence

$$W^* = W + \bar{W}$$

Here, and in the sequel

$$(\quad),_x = \frac{\partial(\quad)}{\partial x}$$

$$(\quad),_{yy} = \frac{\partial^2(\quad)}{\partial y^2}$$

Rings

The rings are assumed to be circular in shape and radially thin compared to their radius a^r . The strain-displacement relations taken for the rings are the ones used by G. D. Galletly [26] in his investigation of the free linear vibration of ring-stiffened shells. The strains of the centroid of the ring are given by

$$\left. \begin{aligned}
 \chi_1^r &= -\frac{1}{a^r} \left(\beta + \frac{U^r_{,\theta\theta}}{a^r} \right) \\
 \chi_2^r &= \frac{1}{(a^r)^2} (W^r + W^r_{,\theta\theta}) \\
 \phi &= \frac{1}{a^r} \left(-\beta_{,\theta} + \frac{U^r_{,\theta}}{a^r} \right) \\
 \epsilon_\theta^r &= \frac{1}{a^r} (V^r_{,\theta} - W^r)
 \end{aligned} \right\} (2.2)$$

where χ_1^r is the curvature change in the plane normal to the ring, χ_2^r is the curvature change in the plane of the ring, ϕ is the angle of twist per unit circumferential length, and ϵ_θ^r is the circumferential strain.

Assuming β to be small, $\bar{e} \ll a$, and that \bar{W} and $\bar{W}_{,x}$ are zero at the point of attachment, the displacements and rotation of the ring can be geometrically related to the shell displacements [26]. This leads to

$$\left. \begin{aligned}
 W^r &= W \\
 \beta &= W_{,x} \\
 U^r &= U + \bar{e} \beta \\
 V^r &= V + \bar{e} W_{,y}
 \end{aligned} \right\} (2.3)$$

and the radius of the ring is given by

$$a^r = a + \bar{e}$$

Thus, the ring strains can be expressed in terms of the shell displacements. Substituting (2.3) into (2.2) and noting that $(\)_{,\theta} = a(\)_{,y}$ gives

$$\left. \begin{aligned}
 \chi_1^r &= -\frac{1}{a^r} [W,_{x} + \frac{a^2}{a^r} (U,_{yy} + \bar{e} W,_{xyy})] \\
 \chi_2^r &= \frac{1}{(a^r)^2} (W + a^2 W,_{yy}) \\
 \phi &= \frac{a}{a^r} (-W,_{xy} + \frac{U,_{y} + \bar{e} W,_{xy}}{a^r}) \\
 \epsilon_{\theta}^r &= \frac{a}{a^r} (V,_{y} + \bar{e} W,_{yy} - \frac{W}{a})
 \end{aligned} \right\} (2.4)$$

Note that (2.4) does not contain \bar{W} , the initial imperfection of the shell. This is due to the fact that the initial imperfection \bar{W} and its slope $\bar{W},_x$ have been taken equal to zero where the rings are attached.

IV. CONSTITUTIVE RELATIONS

The resultant forces and moments per unit length of shell midsurface are obtained by integrating the stresses over the thickness. The normal forces are N_x and N_y , the shear forces are N_{xy} and N_{yx} , the bending moments are M_x and M_y , and the twisting moments are M_{xy} and M_{yx} . The positive directions of these forces and moments and the applied pressure P are as shown in Figure 2.3.

The stress resultants are related to the strains by the relationships

$$N_x = B(\epsilon_x + \nu \epsilon_y) \quad (2.5a)$$

$$N_y = B(\epsilon_y + \nu \epsilon_x) \quad (2.5b)$$

$$N_{xy} = N_{yx} = \frac{1-\nu}{2} B \gamma_{xy} \quad (2.5c)$$

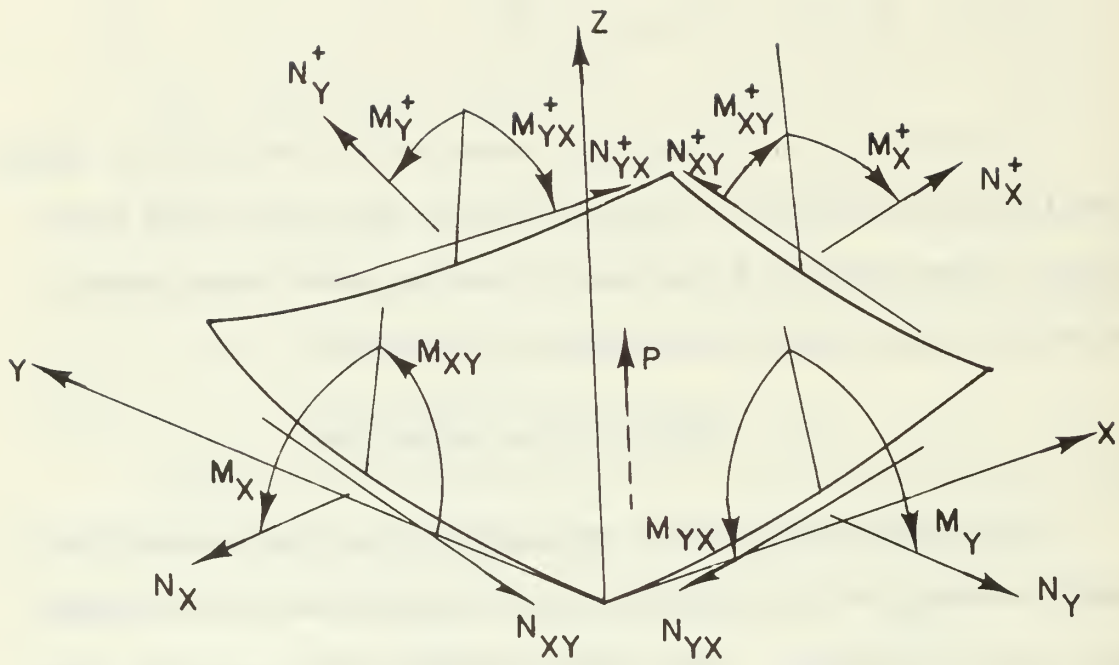


FIGURE 2.3

POSITIVE DIRECTIONS OF FORCES AND MOMENTS

$$M_x = -D(\chi_x + \nu\chi_y) \quad (2.5d)$$

$$M_y = -D(\chi_y + \nu\chi_x) \quad (2.5e)$$

$$M_{xy} = -M_{yx} = (1 - \nu) D\chi_{xy} \quad (2.5f)$$

where ν is Poisson's ratio, and B and D are the extensional and flexural rigidities, respectively, defined by

$$\left. \begin{aligned} B &= \frac{Eh}{1-\nu^2} \\ D &= \frac{Eh^3}{12(1-\nu^2)} \end{aligned} \right\} (2.6)$$

Young's modulus is denoted by E .

V. EQUATIONS OF MOTION

The governing equations of motion are derived in this section by means of Hamilton's Principle. For the case where nonconservative forces are present, Hamilton's principle states that [27]

$$\delta \int_{t_1}^{t_2} (\mathcal{W} + \mathcal{T})_{dt} = 0 \quad (2.7)$$

where \mathcal{W} is the total work function, \mathcal{T} is the total kinetic energy, and t is the time coordinate, t_1 and t_2 being arbitrary times.

The total work function is the sum of the work function of the external pressure and damping force \mathcal{W}_L , the work function of the shell \mathcal{W}_S , and the work function of the rings \mathcal{W}_R .

Thus

$$\mathcal{W} = \mathcal{W}_L + \mathcal{W}_S + \mathcal{W}_r \quad (2.8)$$

The variation of \mathcal{W}_L is given by

$$\delta \mathcal{W}_L = - \int_0^L \int_0^{2\pi a} (C W_{,t} - P) \delta W \, dy \, dx \quad (2.9)$$

where C is the viscous damping coefficient. The terms $CW_{,t}$ and P are held constant during the variation.

The variation of \mathcal{W}_S is given by

$$\begin{aligned} \delta \mathcal{W}_S = - \int_0^L \int_0^{2\pi a} [N_x \delta \epsilon_x + N_{xy} \delta \gamma_{xy} + N_y \delta \epsilon_y \\ - M_x \delta \chi_x + 2M_{xy} \delta \chi_{xy} - M_y \delta \chi_y] \, dy \, dx \end{aligned} \quad (2.10)$$

The in-plane forces and moments are also held constant during the variation.

The contribution \mathcal{W}_r of the ring forces to the total work function is taken as the negative of the strain energy in the rings. Hence, $\delta \mathcal{W}_r$ is given by [26]

$$\begin{aligned} \delta \mathcal{W}_r = - \frac{1}{2\mu} \sum_{j=1}^{N_r} \delta \int_0^{2\pi a^r} [E_r I_z (\chi_1^r)^2 + E_r I_x (\chi_2^r)^2 \\ + G_r C_T (\phi)^2 + E_r A_r (\epsilon_\theta^r)^2] \, d\bar{y} \, \delta(x-x_j) \, dx \end{aligned} \quad (2.11)$$

where

μ	characteristic length
I_x, I_z	moments of inertia of the ring cross section with respect to axes passing through the centroid of the ring
A_r	cross sectional area of the ring
C_T	St. Venant's torsion constant for the ring [28]
$\delta(\)$	Dirac delta function, not to be confused with the symbol used to denote a variation
N_r	number of rings
E_r	Young's modulus of the ring material
G_r	shear modulus of the ring material
ρ_r	mass density of the ring material
j	subscript which associates a variable with the j^{th} ring; for example, x_j is the x-coordinate of the j^{th} ring
$d\bar{y} = \frac{a^r}{a} dy$	

The Dirac delta function has been introduced here to allow the integration of $\delta \mathcal{W}_r$ to be carried out over the length of the shell. This technique has been used by Block [23] and is necessary in order to combine \mathcal{W}_L , \mathcal{W}_S , and \mathcal{W}_r in a double integration form. It requires the introduction of a characteristic length μ that corresponds to the width of a ring.

The total kinetic energy of the structure is given by

$$\mathcal{T} = \mathcal{T}_s + \mathcal{T}_r \quad (2.12)$$

where \mathcal{T}_s is the kinetic energy of the shell and \mathcal{T}_r is the kinetic energy of the ring. Only the radial velocities will be included in the kinetic energy of the shell and of the ring; the axial, circumferential, and rotatory inertia of both the rings and the shell are assumed to be negligible. Thus, the kinetic energy of the shell is given by

$$\mathcal{T}_s = \frac{\rho h}{2} \int_0^L \int_0^{2\pi a} (w, t)^2 dy dx \quad (2.13)$$

where ρ is the mass density of the shell material. The kinetic energy of the rings is given by

$$\mathcal{T}_r = \frac{\rho_r A_r}{2\mu} \sum_{j=1}^{N_r} \int_0^L \int_0^{2\pi a^r} (w, t)^2 d\bar{y} \delta(x-x_j) dx \quad (2.14)$$

Substituting (2.8) and (2.12) into (2.7) yields

$$\delta \int_{t_1}^{t_2} (\mathcal{W}_L + \mathcal{W}_s + \mathcal{W}_r + \mathcal{T}_s + \mathcal{T}_r) dt = 0 \quad (2.15)$$

Substituting (2.1) into (2.10); (2.4) into (2.11); and (2.9), (2.10), (2.11), (2.13), and (2.14) into (2.15) and performing the variation yield the following equations of dynamic equilibrium

$$\begin{aligned} N_{x,x} + N_{xy,y} + \sum_{j=1}^{N_r} \left[\frac{E_r I_z}{a\mu} (w,_{xyy} + a u,_{yyy}) \right. \\ \left. + \bar{e} a w,_{xyyy} \right]_j - \frac{G_r C_t}{a\mu} \left(\frac{1}{a} u,_{yy} - w,_{xyy} \right)_j \delta(x-x_j) = 0 \end{aligned} \quad (2.16)$$

$$\begin{aligned}
N_{Y,Y} + N_{XY,X} - \sum_{j=1}^{N_r} \frac{E_r A_r}{\mu} (V_{,YY} - \bar{e} W_{,YYY} \\
- \frac{1}{a} W_{,Y})_j \delta(x-x_j) = 0
\end{aligned} \tag{2.17}$$

$$\begin{aligned}
D\nabla^4 W = N_X (W_{,XX} + \bar{W}_{,XX}) + 2N_{XY} (W_{,XY} + \bar{W}_{,XY}) \\
+ N_Y (W_{,YY} + \bar{W}_{,YY}) + \frac{1}{a} N_Y + P - CW_{,t} - \rho h W_{,tt} - \sum_{j=1}^{N_r} \frac{\rho_r A_r}{\mu} (W_{,tt})_j \\
+ \sum_{j=1}^{N_r} \left[\frac{E_r I_z}{\mu a^2} (W_{,XX} + a U_{,xyY} + 2\bar{e} a W_{,xxyY} - \bar{e} a^2 U_{,xyyyy} \right. \\
+ \bar{e}^2 a^2 W_{,xxyyyy})_j - \frac{E_r I_x}{\mu a^4} (W + 2a^2 W_{,YY} + a^4 W_{,YYYY})_j \\
+ \frac{E_r A_r}{\mu a^2} (\bar{e} a^2 V_{,yyy} + a V_{,yy} - \bar{e} a^2 W_{,yyyy} - 2\bar{e} a W_{,yy} - W)_j \\
\left. + \frac{G_r C_T}{\mu a} (U_{,xyY} - a W_{,xxyY})_j \right] \delta(x - x_j)
\end{aligned} \tag{2.18}$$

VI. BOUNDARY CONDITIONS

The variational procedure also yields the admissible boundary conditions [29].

Simply Supported

The boundary conditions that correspond to simply supported ends are

$$\begin{aligned}
 V &= 0 \\
 W &= 0 \\
 M_x &= 0 \\
 N_x &= 0
 \end{aligned}
 \qquad \text{at } x = 0, L
 \tag{2.19}$$

Clamped

The boundary conditions that correspond to clamped ends are

$$\begin{aligned}
 U &= 0 \\
 V &= 0 \\
 W &= 0 \\
 W_{,x} &= 0
 \end{aligned}
 \qquad \text{at } x = 0, L
 \tag{2.20}$$

VII. NONDIMENSIONAL EQUATIONS

Nondimensional Variables

The nondimensional variables and parameters that will be used in the analysis are defined by

$$\left.
 \begin{aligned}
 \xi &= \frac{x}{a} & \eta &= \frac{L}{a} & \theta &= \frac{y}{a} \\
 \tau &= \frac{t}{a} \left(\frac{E}{\rho(1-\nu^2)} \right)^{\frac{1}{2}} \\
 u &= \frac{U}{a} & v &= \frac{V}{a} & w &= \frac{W}{a} & \bar{w} &= \frac{\bar{W}}{a} \\
 p &= P \frac{a(1-\nu^2)}{Eh} \\
 c &= C \left(\frac{1-\nu^2}{E\rho} \right)^{\frac{1}{2}}
 \end{aligned}
 \right\}
 \tag{2.21a}$$

$$\begin{aligned}
n_{\xi} &= N_x \frac{1-v^2}{Eh} & n_{\theta} &= N_y \frac{1-v^2}{Eh} & n_{\xi\theta} &= N_{xy} \frac{1-v^2}{Eh} \\
\alpha &= \frac{h}{a} & e &= \frac{\bar{e}}{a} \\
C_1 &= \frac{E_r}{E} \frac{I_x (1-v^2)}{a^2 h \mu} \\
C_2 &= \frac{\rho_r}{\rho} \frac{A_r}{h \mu} \\
C_3 &= \frac{E_r}{E} \frac{A_r (1-v^2)}{h \mu} \\
C_4 &= \frac{E_r}{E} \frac{I_z (1-v^2)}{a^2 h \mu} \\
C_5 &= \frac{E_r}{E} \frac{C_T (1-v^2)}{2a^2 h \mu}
\end{aligned} \tag{2.21b}$$

Nondimensional Equations of Motion

Expressing the equations of motion (2.16), (2.17), and (2.18) in terms of the above non-dimensional quantities leads to the three equations

$$\begin{aligned}
n_{\xi,\xi} + n_{\xi\theta,\theta} + \sum_{j=1}^{N_r} [C_4 (w_{,\xi\theta\theta} + u_{,\theta\theta\theta\theta} + ew_{,\xi\theta\theta\theta})_j \\
+ C_5 (w_{,\xi\theta\theta} - u_{,\theta\theta})_j] \delta(\xi - \xi_j) = 0
\end{aligned} \tag{2.22a}$$

$$n_{\theta,\theta} + n_{\xi\theta,\xi} + \sum_{j=1}^{N_r} C_3 (w_{,\theta} + ew_{,\theta\theta\theta} - v_{,\theta\theta})_j \delta(\xi - \xi_j) = 0 \tag{2.22b}$$

$$\begin{aligned}
\frac{1}{12} \alpha^2 \nabla^4 w &= n_{\xi} (w,_{\xi\xi} + \bar{w},_{\xi\xi}) + 2n_{\xi\theta} (w,_{\xi\theta} + \bar{w},_{\xi\theta}) \\
&+ n_{\theta} (w,_{\theta\theta} + \bar{w},_{\theta\theta}) + n_{\theta} + p - \frac{c}{\alpha} \dot{w} - [\ddot{w} + \sum_{j=1}^{N_r} C_2 \ddot{w}_j \delta(\xi - \xi_j)] \\
&+ \sum_{j=1}^{N_r} [C_4 (w,_{\theta\theta} + u,_{\xi\theta\theta} + 2ew,_{\xi\xi\theta\theta} + eu,_{\xi\theta\theta\theta\theta} \quad (2.22c) \\
&+ e^2 w,_{\xi\xi\theta\theta\theta\theta})_j - C_1 (w + 2 w,_{\theta\theta} + w,_{\theta\theta\theta\theta})_j \\
&+ C_3 (ev,_{\theta\theta\theta} + v,_{\theta} - e^2 w,_{\theta\theta\theta\theta} - 2e w,_{\theta\theta} - w)_j \\
&+ C_5 (u,_{\xi\theta\theta} - w,_{\xi\xi\theta\theta})_j] \delta(\xi - \xi_j)
\end{aligned}$$

Here $(\dot{}) = \partial()/\partial\tau$.

The in-plane forces N_x , N_y , and N_{xy} can be expressed as functions of the displacements U , V , and W by combining the constitutive relations, (2.5a)-(2.5c), and the strain-displacement relations (2.1a)-(2.1c). In nondimensional form

$$n_{\xi} = u,_{\xi} + \frac{1}{2}(w,_{\xi})^2 + \bar{w},_{\xi} w,_{\xi} + v[v,_{\theta} - w + \frac{1}{2}(w,_{\theta})^2 + \bar{w},_{\theta} w,_{\theta}] \quad (2.23a)$$

$$n_{\theta} = v,_{\theta} - w + \frac{1}{2}(w,_{\theta})^2 + \bar{w},_{\theta} w,_{\theta} + v[u,_{\xi} + \frac{1}{2}(w,_{\xi})^2 + \bar{w},_{\xi} w,_{\xi}] \quad (2.23b)$$

$$n_{\xi\theta} = \frac{1-v}{2} (v,_{\xi} + u,_{\theta} + w,_{\xi} w,_{\theta} + \bar{w},_{\xi} w,_{\theta} + \bar{w},_{\theta} w,_{\xi}) \quad (2.23c)$$

Nondimensional Boundary Conditions

Simply Supported. The boundary conditions for the simply supported shell are expressed by (2.19). The corresponding conditions on the nondimensional displacements v and w are

$$v = 0 \quad (2.24)$$

$$w = 0 \quad \text{at } \xi = 0, 1 \quad (2.25)$$

The bending moment M_x is a function of the curvatures and was expressed by (2.5e) as

$$M_x = -D(\chi_x + v\chi_y) \quad (2.5e)$$

Expressing the curvatures in terms of the displacements by using (2.1d) and (2.1e) gives

$$M_x = -D(W_{,xx} + vW_{,yy})$$

At the ends of the shell $W = 0$ which implies that $W_{,yy} = 0$; hence, the condition that $M_x = 0$ at $x = 0$ and $x = L$ implies that $W_{,xx} = 0$ at $x = 0$ and $x = L$. In nondimensional form

$$w_{,\xi\xi} = 0 \quad \text{at } \xi = 0, 1 \quad (2.26)$$

Since $N_x = 0$ at $x = 0$ and $x = L$, it follows that $n_\xi = 0$ at $\xi = 0$ and $\xi = 1$. Hence, from (2.23a)

$$n_\xi = u_{,\xi} + \frac{1}{2}(w_{,\xi})^2 + \bar{w}_{,\xi}w_{,\xi} + v[v_{,\theta} - w + \frac{1}{2}(w_{,\theta})^2 + \bar{w}_{,\theta}w_{,\theta}] = 0$$
$$\text{at } \xi = 0, 1 \quad (2.27)$$

Clamped. The clamped boundary conditions (2.20) can also be expressed nondimensionally as

$$u = 0 \quad (2.28)$$

$$v = 0 \quad (2.29)$$

$$w = 0 \quad (2.30)$$

$$w,_{\xi} = 0 \quad \text{at } \xi = 0, 1 \quad (2.31)$$

Response Symmetric to Midspan. When the load, the initial imperfections, and the response are symmetric with respect to the midspan of the shell, only the portion of the shell between $\xi = 0$ and $\xi = 1/2$ needs to be considered. The nondimensional conditions that express symmetry at the midspan are

$$u = 0 \quad (2.32)$$

$$v,_{\xi} = 0 \quad (2.33)$$

$$w,_{\xi} = 0 \quad (2.34)$$

$$w,_{\xi\xi\xi} = 0 \quad \text{at } \xi = 1/2 \quad (2.35)$$

The three equations of motion, (2.22), together with the expressions for n_{ξ} , n_{θ} , and $n_{\xi\theta}$, (2.23), and the boundary conditions constitute a formulation of the problem under investigation. The next two chapters are devoted to their solution.

CHAPTER III

DEVELOPMENT OF THE NUMERICAL MODEL

I. INTRODUCTION

In this chapter the nondimensional, nonlinear governing partial differential equations derived in Chapter II are replaced by a set of difference-differential equations in which time is the only remaining independent variable. The difference-differential equations are henceforth referred to as the numerical model.

The model is developed by expanding the dependent variables in Fourier series in the circumferential coordinate. The Fourier coefficients in the series are functions of τ and the axial coordinate ξ . Products of Fourier series arise wherever there are nonlinear terms in the governing equations. The expansion of these products to single series generates products of the Fourier coefficients that couple the modes. The derivatives of the Fourier coefficients with respect to the axial coordinate are then approximated by modified finite differences, leading to the set of difference-differential equations.

II. FOURIER SERIES EXPANSIONS

During the early phases of the present study, consideration was given to a numerical model that approximated both the circumferential derivatives and the axial

derivatives by means of finite differences. To achieve good resolution of the strains and curvatures of the cylinder, the grid points must be close enough together so that there are several grid points covering the shortest wave length of the response. Based on the works of previous investigators [9, 10, 20], the parametrically excited modes are expected to have many waves around the circumference. Consequently, a very large number of points is needed for adequate resolution of the parametrically excited modes. For example, a flexural mode with sixteen waves around the circumference is not unreasonable to expect. Taking the number of axial stations to be twenty and assuming that eight node points per wave length are needed around the circumference, the total number of node points is approximately 2500. Satisfying axial, circumferential, and radial equilibrium at each node yields over 7500 simultaneous equations. The number of equations can be reduced by one half if the response is assumed to be symmetric with respect to some axial plane. Even so, the number of equations is still very large.

However, if the displacements are expanded in Fourier series in the circumferential coordinate, instead of using finite differences, the circumferential variation of the normal modes of the cylinder can be represented exactly. Furthermore, those modes which do not respond can be excluded. Thus, the number of equations can be kept small while retaining the significant features of the coupling

between modes. Expansions of the type employed here have been used previously by R. E. Ball [30] in a nonlinear analysis of statically loaded shells of revolution.

Form of the Series Expansions

The assumption is made that the initial imperfection of the cylinder can be expressed by the Fourier cosine series

$$\bar{w}(\xi, \theta) = \sum_{n=0}^{\infty} \bar{w}^n(\xi) \cos n\theta \quad (3.1)$$

This form somewhat limits the applicability of the analysis since the initial imperfection of most shells cannot be expressed by the cosine series alone. However, the form is still sufficiently general to permit the retention of coupling effects that hitherto have not been retained. There are no conceptual problems involved in using the complete Fourier series. Only the cosine series is used here because of limitations imposed by the practical considerations of computer storage space and computing time.

In order to correspond with the form of \bar{w} given by (3.1), the remaining dependent variables are expressed in trigonometric series as follows:

$$u(\xi, \theta, \tau) = \sum_{n=0}^{\infty} u^n(\xi, \tau) \cos n\theta \quad (3.2a)$$

$$v(\xi, \theta, \tau) = \sum_{n=1}^{\infty} v^n(\xi, \tau) \sin n\theta \quad (3.2b)$$

$$w(\xi, \theta, \tau) = \sum_{n=0}^{\infty} w^n(\xi, \tau) \cos n\theta \quad (3.2c)$$

$$n_{\xi}(\xi, \theta, \tau) = \sum_{n=0}^{\infty} n_{\xi}^n(\xi, \tau) \cos n\theta \quad (3.3a)$$

$$n_{\theta}(\xi, \theta, \tau) = \sum_{n=0}^{\infty} n_{\theta}^n(\xi, \tau) \cos n\theta \quad (3.3b)$$

$$n_{\xi\theta}(\xi, \theta, \tau) = \sum_{n=1}^{\infty} n_{\xi\theta}^n(\xi, \tau) \sin n\theta \quad (3.3c)$$

When these expressions for the displacements and in-plane forces are substituted into (2.22) and (2.23), the linear terms can be grouped together in one series. However, the nonlinear terms give rise to products of series and cannot be grouped with the linear terms until they are expanded into single series. The products of series are of three types; products of (1) two cosine series, (2) a sine series and a cosine series, and (3) two sine series. The details of the expansion of these types of products are described in Appendix B of Reference [30]. Employing (3.1), (3.2), and (3.3), the nonlinear terms contained in (2.22c) and (2.23) can be expressed by

$$\frac{1}{2}(w_{,\xi})^2 = \frac{1}{2} \left(\sum_{i=0}^{\infty} w_{,\xi}^i \cos i\theta \right) \left(\sum_{j=0}^{\infty} w_{,\xi}^j \cos j\theta \right) = \sum_{n=0}^{\infty} C_{XX}^n \cos n\theta \quad (3.4a)$$

$$\frac{1}{2}(w_{,\theta})^2 = \frac{1}{2} \left(\sum_{i=1}^{\infty} -iw_{,\theta}^i \sin i\theta \right) \left(\sum_{j=1}^{\infty} -jw_{,\theta}^j \sin j\theta \right) = \sum_{n=0}^{\infty} C_{TT}^n \cos n\theta \quad (3.4b)$$

$$w_{,\xi} w_{,\theta} = \left(\sum_{i=0}^{\infty} w_{,\xi}^i \cos i\theta \right) \left(\sum_{j=1}^{\infty} -jw_{,\theta}^j \sin j\theta \right) = \sum_{n=1}^{\infty} C_{XT}^n \sin n\theta \quad (3.4c)$$

$$\bar{w}_{,\xi} w_{,\xi} = \left(\sum_{i=0}^{\infty} \bar{w}_{,\xi}^i \cos i\theta \right) \left(\sum_{j=0}^{\infty} w_{,\xi}^j \cos j\theta \right) = \sum_{n=0}^{\infty} C_{IXX}^n \cos n\theta \quad (3.4d)$$

$$\bar{w}_{,\theta} w_{,\theta} = \left(\sum_{i=1}^{\infty} -i \bar{w}^i \sin i\theta \right) \left(\sum_{j=1}^{\infty} -j w^j \sin j\theta \right) = \sum_{n=0}^{\infty} C_{ITT}^n \cos n\theta \quad (3.4e)$$

$$\bar{w}_{,\xi} w_{,\theta} = \left(\sum_{i=0}^{\infty} \bar{w}_{,\xi}^i \cos i\theta \right) \left(\sum_{j=1}^{\infty} -j w^j \sin j\theta \right) = \sum_{n=1}^{\infty} C_{IXT}^n \sin n\theta \quad (3.4f)$$

$$\bar{w}_{,\theta} w_{,\xi} = \left(\sum_{i=1}^{\infty} -i \bar{w}^i \sin i\theta \right) \left(\sum_{j=0}^{\infty} w_{,\xi}^j \cos j\theta \right) = \sum_{n=1}^{\infty} C_{ITX}^n \sin n\theta \quad (3.4g)$$

$$n_{\xi}(w_{,\xi\xi} + \bar{w}_{,\xi\xi}) = \left(\sum_{i=0}^{\infty} n_{\xi}^i \cos i\theta \right) \left[\sum_{j=0}^{\infty} (\bar{w}_{,\xi\xi}^j + w_{,\xi\xi}^j) \cos j\theta \right] \quad (3.4h)$$

$$= \sum_{n=0}^{\infty} \eta_{\xi}^n \cos n\theta$$

$$2n_{\xi\theta}(w_{,\xi\theta} + \bar{w}_{,\xi\theta}) = \left(\sum_{i=1}^{\infty} 2n_{\xi\theta}^i \sin i\theta \right) \left[\sum_{j=1}^{\infty} -j (w_{,\xi\theta}^j + \bar{w}_{,\xi\theta}^j) \sin j\theta \right] \quad (3.4i)$$

$$= \sum_{n=0}^{\infty} \eta_{\xi\theta}^n \cos n\theta$$

$$n_{\theta}(w_{,\theta\theta} + \bar{w}_{,\theta\theta}) = \left(\sum_{i=0}^{\infty} n_{\theta}^i \cos i\theta \right) \left[\sum_{j=0}^{\infty} -j^2 (w_{,\theta\theta}^j + \bar{w}_{,\theta\theta}^j) \cos j\theta \right] \quad (3.4j)$$

$$= \sum_{n=0}^{\infty} \eta_{\theta}^n \cos n\theta$$

The products containing the initial imperfection, or derivatives of the initial imperfection, are not nonlinear since

$\bar{w}(\xi, \theta)$ is assumed to be known. However, the products containing \bar{w} expand in the same way as the nonlinear products; hence, they are included in the above list.

Reduction to Two Independent Variables

Equations of Motion. Expressions for the Fourier coefficients of the in-plane forces n_{ξ}^n , n_{θ}^n , and $n_{\xi\theta}^n$, can be obtained by substituting (3.2), (3.3) and (3.4a)-(3.4g) into (2.33), and equating coefficients of like values of n . Performing the operations yields

$$\begin{aligned} n_{\xi}^n = & u_{,\xi}^n + v(nv^n - w^n) + C_{XX}^n + C_{IXX}^n \\ & v(C_{TT}^n + C_{ITT}^n) \quad n = 0, 1, 2, \dots \end{aligned} \quad (3.5a)$$

$$\begin{aligned} n_{\theta}^n = & nv^n - w^n + vu_{,\xi}^n + C_{TT}^n + C_{ITT}^n \\ & + v(C_{XX}^n + C_{IXX}^n) \quad n = 0, 1, 2, \dots \end{aligned} \quad (3.5b)$$

$$\begin{aligned} n_{\xi\theta}^n = & \frac{1-v}{2}(v_{,\xi}^n - nu^n + C_{XT}^n + C_{IXT}^n + C_{ITX}^n) \\ & n = 1, 2, \dots \end{aligned} \quad (3.5c)$$

The equations of motion in the axial and circumferential directions can be expressed in terms of the Fourier coefficients by substituting (3.2) and (3.3) into (2.22a) and (2.22b), and by making use of (3.5). The result is

$$u_{,\xi\xi}^n + \frac{1+\nu}{2} n v_{,\xi}^n - \frac{1-\nu}{2} n^2 u^n + \lambda 1^n + \sum_{j=1}^{N_r} [C_4 n^4 u^n + C_4 n^2 (en^2 - 1) w_{,\xi}^n - C_5 n^2 (w_{,\xi}^n - u^n)]_j \delta(\xi - \xi_j) = 0$$

$$n = 0, 1, 2, \dots \quad (3.6)$$

$$-n^2 v^n - \frac{1+\nu}{2} n u_{,\xi}^n + \frac{1-\nu}{2} v_{,\xi\xi}^n + \lambda 2^n + \sum_{j=1}^{N_r} C_3 [n(en^2 - 1) w^n + n^2 v^n]_j \delta(\xi - \xi_j) = 0$$

$$n = 1, 2, \dots \quad (3.7)$$

where

$$\lambda 1^n = C_{XX,\xi}^n + C_{IXX,\xi}^n + \nu (C_{TT,\xi}^n + C_{ITT,\xi}^n) + \frac{1-\nu}{2} n (C_{XT}^n + C_{IXT}^n + C_{ITX}^n) - \nu w_{,\xi}^n$$

$$(3.8)$$

and

$$\lambda 2^n = -n [C_{TT}^n + C_{ITT}^n + \nu (C_{XX}^n + C_{IXX}^n)] + \frac{1-\nu}{2} (C_{XT,\xi}^n + C_{IXT,\xi}^n + C_{ITX,\xi}^n) + n w^n$$

$$(3.9)$$

All of the nonlinear terms are contained in $\lambda 1^n$ and $\lambda 2^n$. Examination of these two quantities reveals that the axial and circumferential equations are nonlinear in w^n only; there are no nonlinear terms which contain u^n or v^n .

By substituting (3.2c), (3.3b), and (3.4h)-(3.4j) into (2.22c), the equation of radial equilibrium is obtained in the form

$$\begin{aligned}
\frac{1}{12} \alpha^2 (w_{,\xi\xi\xi\xi}^n - 2n^2 w_{,\xi\xi}^n + n^4 w^n) &= \delta_{0n} p - [\ddot{w}^n + \\
\sum_{j=1}^{N_r} C_2 \ddot{w}_j^n \delta(\xi - \xi_j)] - \frac{c}{\alpha} \dot{w}^n + n_\theta^n & \\
+ \eta_\xi^n + \eta_{\xi\theta}^n + \eta_\theta^n + \sum_{j=1}^{N_r} R_j^n \delta(\xi - \xi_j) & \quad (3.10)
\end{aligned}$$

$$n = 0, 1, 2, \dots$$

where

$$\begin{aligned}
R_j^n &= -[C_4 n^2 + C_1 (n^2 - 1)^2 + C_3 (en^2 - 1)^2] w_j^n \\
&- [C_4 n^2 (1 - en^2) + C_5 n^2] (u_{,\xi}^n)_j - C_3 n (en^2 - 1) v_j^n \quad (3.11) \\
&- [C_4 en^2 (2 - en^2) - C_5 n^2] (w_{,\xi\xi}^n)_j
\end{aligned}$$

and

$$\delta_{0n} = \begin{cases} 1 & \text{if } n = 0 \\ 0 & \text{if } n \neq 0 \end{cases}$$

The number of independent variables has now been reduced from three (ξ , θ , and τ) to two (ξ and τ). However, now there are three equations to be solved for each value of n considered.

Boundary Conditions

The boundary conditions must also be expressed in terms of the Fourier coefficients of the displacements.

Simply Supported. Substitution of (3.2b)-(3.3a) into (2.24)-(2.27) yields the boundary conditions for a simply supported shell

$$v^n = 0 \quad (3.12a)$$

$$w^n = 0 \quad (3.12b)$$

$$w_{,\xi\xi}^n = 0 \quad (3.12c)$$

$$n_{\xi}^n = 0 \quad \text{at } \xi = 0, 1$$

With (3.5a), (3.12a), and (3.12b) the last of the above conditions reduces to

$$[u_{,\xi}^n + C_{XX}^n + C_{IXX}^n + v(C_{TT}^n + C_{ITT}^n)] = 0 \quad \text{at } \xi = 0, 1$$

From equations (3.12b), (3.4b), and (3.4e), it follows that C_{TT}^n and C_{ITT}^n are zero at the ends of the shell. Hence, the final boundary condition becomes

$$[u_{,\xi}^n + C_{XX}^n + C_{IXX}^n] = 0 \quad \text{at } \xi = 0, 1 \quad (3.12d)$$

Clamped. The boundary conditions for the clamped shell are obtained by substitution of (3.2) into (2.28)-(2.31). The result is

$$u^n = 0 \quad (3.13a)$$

$$v^n = 0 \quad (3.13b)$$

$$w^n = 0 \quad (3.13c)$$

$$w_{,\xi}^n = 0 \quad \text{at } \xi = 0, 1 \quad (3.13d)$$

Response Symmetric to the Midspan. Substitution of (3.2) into (2.32)-(2.35) gives

$$u^n = 0 \quad (3.14a)$$

$$v^n,_{\xi} = 0 \quad (3.14b)$$

$$w^n,_{\xi} = 0 \quad (3.14c)$$

$$w^n,_{\xi\xi\xi} = 0 \quad \text{at } \xi = 0, 1/2 \quad (3.14d)$$

III. MODIFIED FINITE DIFFERENCES

In this section a brief discription of the differencing procedure used to approximate the axial derivatives of (3.6)-(3.14) is presented. These finite differences have been called "modified" differences [31, 32] or "half station" differences [33].

As an alternative to the finite differences, the dependent variables could have been expanded in Fourier series in the axial coordinate. T. Wah and W. C. L. Hu [34] made use of expansions of this type in their linear vibration analysis of simply supported, ring-stiffened cylinders. The equations of motion of the shell and the equations of motion of the rings were satisfied simultaneously by enforcing the continuity of displacements, forces, and moments between the shell and the rings. However, the present problem is more complex than their problem due to nonlinearities in the equations of motion of the shell and due to the clamped boundary conditions. The use of the finite differences to approximate the axial derivatives appears

to facilitate the handling of both the boundary conditions and the effects of the discrete ring stiffeners. The use of series expansions in the axial coordinate was not investigated in detail; consequently, the advantages and disadvantages are not clear at the present time.

Modified differences are applicable to systems of equations in which only even or odd ordered derivatives of a given dependent variable appear in any one equation. As an example of equations that fall into this category, consider (3.6)-(3.10) with n_0^n replaced by (3.5b) and without the nonlinear terms and the terms associated with the rings, that is

$$u_{,\xi\xi}^n + \frac{1+\nu}{2} n v_{,\xi}^n - \frac{1-\nu}{2} n^2 u^n - \nu w_{,\xi}^n = 0 \quad (3.15a)$$

$$n = 0, 1, \dots$$

$$-n^2 v^n - \frac{1+\nu}{2} n u_{,\xi}^n + \frac{1-\nu}{2} v_{,\xi\xi}^n + n w^n = 0 \quad (3.15b)$$

$$n = 1, 2, \dots$$

$$\frac{1}{12} \alpha^2 (w_{,\xi\xi\xi\xi}^n - 2n^2 w_{,\xi\xi}^n + n^4 w^n) \quad (3.15c)$$

$$= \delta_{0n} p - \ddot{w}^n - \frac{c}{\alpha} \dot{w}^n + n v^n - w^n + \nu u_{,\xi}^n$$

$$n = 0, 1, \dots$$

Considering the spatial derivatives, note that only even derivatives of u^n appear in equation (3.15a); only odd derivatives of u^n appear in (3.15b) and (3.15c). Similarly, equation (3.15a) contains only odd derivatives of v^n and w^n ; and (3.15b) and (3.15c) contain only even derivatives of

v^n and w^n . For systems of equations having this property, a staggered finite difference mesh can be used advantageously. A staggered mesh, as illustrated in Figure 3.1, is one where half stations are interspaced between the whole stations, and the distance between consecutive whole or half stations is denoted by d . In the modified difference method, some of the dependent variables are defined only at whole stations and the remainder are defined only at half stations. For reasons which are not yet obvious, u^n will be defined at half stations; while v^n and w^n will be defined at whole stations as shown in Figure 3.1.

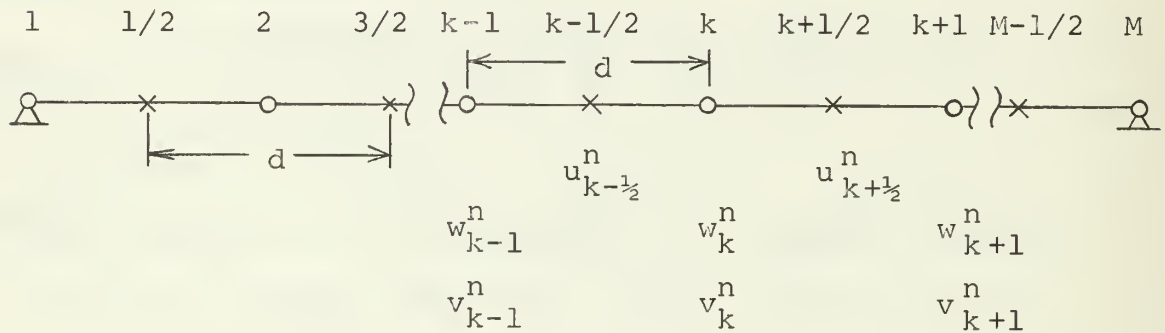


Figure 3.1

STAGGERED FINITE DIFFERENCE MESH

K. P. Chuang and A. S. Veletsos [31] were apparently the first to employ the modified differencing method in analyzing circular cylindrical shells. They proposed the fundamental modified central difference operator

$$[(\quad),_x]_k = \frac{1}{d} [(\quad)_{k+\frac{1}{2}} - (\quad)_{k-\frac{1}{2}}] \quad (3.16a)$$

for derivatives with respect to the independent variable x . Consistent applications of the operator yield a set of difference approximations for the higher order derivatives of the form

$$(f,_{xx})_k = \frac{1}{d^2} (f_{k+1} - 2f_k + f_{k-1}) \quad (3.16b)$$

$$(f,_{xxx})_k = \frac{1}{d^3} (f_{k+\frac{3}{2}} - 3f_{k+\frac{1}{2}} + 3f_{k-\frac{1}{2}} - f_{k-\frac{3}{2}}) \quad (3.16c)$$

$$(f,_{xxxx})_k = \frac{1}{d^4} (f_{k+2} - 4f_{k+1} + 6f_k - 4f_{k-1} + f_{k-2}) \quad (3.16d)$$

Returning now to (3.15), the difference equations are obtained by expressing (3.15a) at half stations and (3.15b) and (3.15c) at whole stations. The resulting difference equations are

$$\begin{aligned} \frac{1}{d^2} (u_{k+\frac{3}{2}}^n - 2u_{k+\frac{1}{2}}^n + u_{k-\frac{1}{2}}^n) + \frac{1+v}{2} n \frac{1}{d} (v_{k+1}^n - v_k^n) \\ - \frac{1-v}{2} n^2 u_{k+\frac{1}{2}}^n - v \frac{1}{d} (w_{k+1}^n - w_k^n) = 0 \quad n = 0, 1, \dots \end{aligned} \quad (3.17a)$$

$$\begin{aligned} -n^2 v_k^n - \frac{1+v}{2} n \frac{1}{d} (u_{k+\frac{1}{2}}^n - u_{k-\frac{1}{2}}^n) + \frac{1-v}{2} \frac{1}{d^2} (v_{k+1}^n - 2v_k^n + v_{k-1}^n) \\ + n w_k^n = 0 \quad n = 1, 2, \dots \end{aligned} \quad (3.17b)$$

$$\begin{aligned} \frac{1}{12} \alpha^2 \left[\frac{1}{d^4} (w_{k+2}^n - 4w_{k+1}^n + 6w_k^n - 4w_{k-1}^n + w_{k-2}^n) - 2n^2 \frac{1}{d^2} (w_{k+1}^n - 2w_k^n \right. \\ \left. + w_{k-1}^n) + n^4 w_k^n \right] = \delta_{0n} p_k - \ddot{w}_k^n - \frac{c}{\alpha} \dot{w}_k^n + n v_k^n - w_k^n + v \frac{1}{d} (u_{k+\frac{1}{2}}^n - u_{k-\frac{1}{2}}^n) \\ n = 0, 1, \dots \end{aligned} \quad (3.17c)$$

Observe that in the development of these three equations, it was not necessary to define u^n at whole stations. Likewise, w^n and v^n did not require definition at half stations. These circumstances prevail for two reasons: (1) the derivatives of any one variable are all odd or even ordered within a given equation, and (2) the equations are linear.

Superiority of Modified Differences over Conventional Differences

Chuang and Veletsos [31] showed that when the conventional central differences are used for all the derivatives, the difference equations obtained by discretization of the governing differential equations do not agree with those obtained by minimizing the finite difference form of the potential energy. On the other hand, when modified differences are used, the difference equations obtained by both procedures are identical. Consequently, the conventional and modified differencing of the differential equations gives rise to two different numerical models, a conventional difference model that approximates only the differential equations, and a modified difference model that approximately satisfies both the differential equations and the condition of minimum potential energy. In Appendix A, this inconsistency between the two schemes is shown to prevail even after the displacements have been expanded in Fourier series in the circumferential coordinate.

Chuang and Veletsos [31] compared the accuracy of the modified and conventional differences when used in the static analysis of cylindrical shell roofs. They found that the modified differences were far more accurate than the conventional differences for the same mesh spacing. Ball [32] used both the conventional and modified differences to compute the natural frequencies of circular rings and compared the numerically computed frequencies with the exact frequencies. The frequencies obtained using modified differences were considerably more accurate than those obtained with conventional differences for the same mesh spacing. N. J. Cyrus and R. E. Fulton [33] developed analytical representations of the errors associated with the modified and conventional differences when applied to beam and string problems. For a fixed number of stations, the errors in calculated deflections and curvatures resulting from the use of modified differences were, in general, smaller than those obtained by using conventional differences.

Adaptation to the Nonlinear Problem

The discussion of the modified differences has avoided applications to nonlinear problems until now.

Finite Difference Grid and Notation. In adapting the modified differences to the nonlinear equations, (3.6)-(3.14), the pattern used for the linear equations is followed. Difference equations are written which make use

of a staggered node system, and the displacements are defined at either half or whole stations. A convention is adopted whereby both half and whole station quantities are given integer subscripts. To distinguish whole station quantities from half station quantities, an upper case letter will be used for the whole station subscript, and a lower case letter, for the half station quantities. As shown in Figure 3.2, the k^{th} half station node is located between whole station nodes K and $K+1$. The distance between adjacent whole station nodes, as well as the distance between adjacent half station nodes, is equal to d . Let the radial and circumferential displacements w^n and v^n be defined at the whole stations; and, the axial displacement

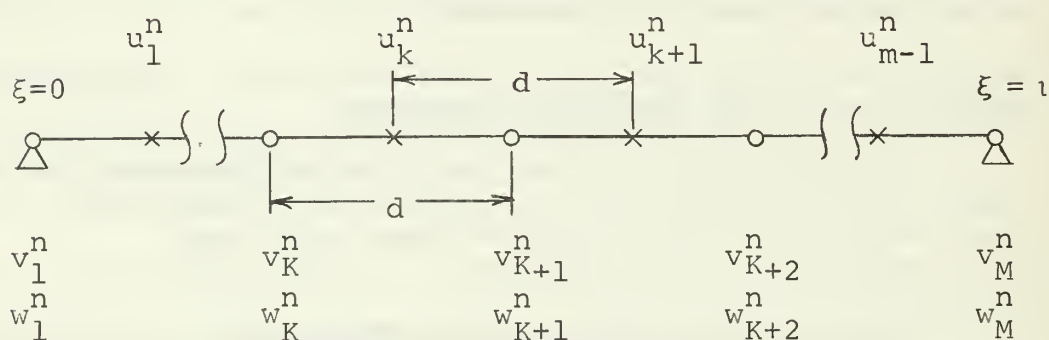


Figure 3.2

SPATIAL DISCRETIZATION USING MODIFIED DIFFERENCES

u^n , at half stations. At whole stations the difference operator of the modified differences becomes

$$[(\), \xi]_K = \frac{1}{d} [(\)_K - (\)_{K-1}]$$

and at half stations it becomes

$$[(\), \xi]_K = \frac{1}{d} [(\)_{K+1} - (\)_K]$$

Here, and in sequel, $k = K$ within a difference expression or equation.

Difference Expressions for Derivatives. Since the three displacements u^n , v^n , and w^n are not defined at every node point, the derivatives can be evaluated at either half stations or whole stations, but not at both. The derivatives that can be evaluated at the half stations are

$$(v_{,\xi}^n)_k = \frac{1}{d} (v_{K+1}^n - v_K^n) \quad (3.18a)$$

$$(w_{,\xi}^n)_k = \frac{1}{d} (w_{K+1}^n - w_K^n) \quad (3.18b)$$

$$(u_{,\xi\xi}^n)_k = \frac{1}{d^2} (u_{K+1}^n - 2u_K^n + u_{K-1}^n) \quad (3.18c)$$

$$(w_{,\xi\xi\xi}^n)_k = \frac{1}{d^3} (w_{K+2}^n - 3w_{K+1}^n + 3w_K^n - w_{K-1}^n) \quad (3.18d)$$

The derivatives that can be evaluated at the whole stations are

$$(u_{,\xi}^n)_K = \frac{1}{d} (u_{K+1}^n - u_K^n) \quad (3.18e)$$

$$(w'_{,\xi\xi})_K = \frac{1}{d^2} (w_{K+1}^n - 2w_K^n + w_{K-1}^n) \quad (3.18f)$$

$$(v'_{,\xi\xi})_K = \frac{1}{d^2} (v_{K+1}^n - 2v_K^n + v_{K-1}^n) \quad (3.18g)$$

$$(w'_{,\xi\xi\xi\xi})_K = \frac{1}{d^4} (w_{K+2}^n - 4w_{K+1}^n + 6w_K^n - 4w_{K-1}^n + w_{K-2}^n) \quad (3.18h)$$

Evaluation of Nonlinear Terms. The nonlinearities in the axial and circumferential equations (3.6) and (3.7) are embodied in the functions $\lambda 1^n$ and $\lambda 2^n$, given by (3.8) and (3.9); in the radial equation (3.10) the terms n_θ^n , η_θ^n , $\eta_{\xi\theta}^n$, and η_θ^n are nonlinear. The computation of these nonlinear quantities in terms of the discrete displacements presents difficulties not encountered with the linear equations.

To demonstrate the difficulty, assume that $\lambda 2^n$ must be computed at the whole station K. From (3.9), note that C_{XX}^n , along with several other quantities, must be computed at station K in order to get $\lambda 2_K^n$. Now, C_{XX}^n is defined by equation (3.4a), and is computed from¹

$$C_{XX}^n = \frac{1}{4} \sum_{i=0}^{\infty} w'_{,\xi}^i (\eta^c w'_{,\xi}^{i+n} + \mu^c w'_{,\xi}^{|i-n|})$$

where

$$\eta^c = \begin{cases} 1 & \text{if } n > 0 \\ 0 & \text{if } n = 0 \end{cases}$$

¹See Appendix B of Reference [30].

$$\mu^c = \begin{cases} 1 & \text{if } i \neq n \\ 2 & \text{if } i = n \end{cases}$$

Since C_{XX}^n must be computed at node K , $w_{,\xi}^n$ must be known at whole station K for each value of n . As evidenced by (3.18b), the first derivative of w^n can be expressed only at the half stations. Consequently, an interpolation of some form must be utilized in order to define $w_{,\xi}^n$ at a whole station in terms of w^n at nearby whole stations. The same situation exists for several of the other non-linear terms. The interpolations used to define the other derivatives falling in this category are developed in Appendix B. One example of these interpolations is the expression for $w_{,\xi}^n$ at whole station K

$$(w_{,\xi}^n)_K = \frac{1}{16d} [10 (w_{K+1}^n - w_{K-1}^n) - (w_{K+2}^n - w_{K-2}^n)]$$

Location of Rings

In the interest of simplicity, the assumption was made that rings could be located at whole stations, but not at half stations. As an aid in expressing the ring-associated terms, let the set H and the symbol δ_{KH_j} be defined as follows:

$$H = \{H_j \text{ such that } H_j = K, \text{ where } K \text{ is the whole station location of the } j^{\text{th}} \text{ ring; } j = 1, 2, \dots, N_r\}$$

(3.19a)

$$\delta_{KH_j} = \begin{cases} 1 & \text{if } K = H_j \\ 0 & \text{if } K \neq H_j \end{cases} \quad (3.19b)$$

IV. DIFFERENCE-DIFFERENTIAL EQUATIONS

Equations of Motion

In this section the difference-differential equations which constitute the numerical model are obtained by replacing the ξ -derivatives in the governing equations by the modified differences of (3.18).

When the response is not symmetric with respect to the midspan, the finite difference grid is arranged so that the whole stations $K = 1$ and $K = M$ are located at $\xi = 0$ and $\xi = 1$, respectively.² The total number of whole stations is thus equal to M . The half stations $k = 0$ and $k = m$ are imaginary points located a half mesh space from the ends of the shell. The whole stations $K = 0$ and $K = M+1$ are imaginary points located a full mesh space from the ends of the shell. Thus there are M whole stations and $m-1$ half stations on the shell.

When the motion of the shell is symmetric with respect to the midspan, the finite difference mesh is arranged so that there is a whole station at $\xi = 0$ and a half station at $\xi = 1/2$. The whole station at $\xi = 0$ is assigned the index $K = 1$, the half station at $\xi = 1/2$ is assigned the index $k = m$, and $m \equiv M$ is now the number of half stations

²See Figure 3.2.

as well as the number of whole stations located on the half of the shell between $\xi = 0$ and $\xi = 1/2$. Thus, the whole station $K = M$ is located at $\xi = \frac{1}{2}l - \frac{1}{2}d$.

By expressing (3.6) at the half stations, and (3.7) and (3.10) at whole stations, the difference-differential equations that govern the response can be obtained in the form³

$$\begin{aligned} u_{k+1}^n + dn \left(\frac{1+v}{2} \right) v_{k+1}^n - [2 + d^2 n^2 \left(\frac{1-v}{2} \right) - \sum_{j=1}^{N_r} d^2 n^2 (C_4 n^2 \\ + C_5) \delta_{KH_j}] u_k^n - dn \left(\frac{1+v}{2} \right) v_K^n + u_{k-1}^n = - d^2 \lambda l_K^n \quad (3.20) \\ - \sum_{j=1}^{N_r} dn^2 [C_4 (en^2 - 1) - C_5] \delta_{KH_j} (w_{K+1}^n - w_K^n) \end{aligned}$$

$$K=k=1, \dots, M-1 \text{ (or } M); n=0, 1, \dots$$

³The rings were assumed to be located only at whole stations. However, in equation (3.20), the term

$$- \sum_{j=1}^{N_r} d^2 n^2 (C_4 n^2 + C_5) \delta_{KH_j}$$

is multiplied by u_k^n , a displacement which is defined at a half station located one-half of a mesh space from the ring at station $K = H_j$. Since the axial displacements are generally small compared to the radial displacements, this inconsistency is probably not significant, especially if the grid points are close together. Alternatively, the above term could be replaced by

$$- \sum_{j=1}^{N_r} \frac{1}{2} d^2 n^2 (C_4 n^2 + C_5) (\delta_{KH_j} + \delta_{K+1 H_j})$$

Then half of the effect of a ring is felt at station k if there is a ring at station K or $K+1$.

$$\begin{aligned}
& \left(\frac{1-\nu}{2}\right) v_{K+1}^n - d n \left(\frac{1+\nu}{2}\right) u_K^n - [1-\nu+d^2 n^2 - \sum_{j=1}^{N_r} d^2 n^2 (C_3 \delta_{KH_j})] v_K^n \\
& + d n \left(\frac{1+\nu}{2}\right) u_{K-1}^n + \frac{1-\nu}{2} v_{K-1}^n = - d^2 \lambda_2^n \\
& - \sum_{j=1}^{N_r} d^2 n C_3 (e n^2 - 1) \delta_{KH_j} w_K^n \tag{3.21}
\end{aligned}$$

$K=k=1, \dots, M-1 \text{ (or } M); n=0, 1, \dots$

$$\begin{aligned}
d_1 \ddot{w}_K^n &= \delta_{0n} p_K + d_2 \dot{w}_K^n + d_3 w_{K+2}^n + d_4 w_{K+1}^n + d_5 w_K^n \\
& + d_4 w_{K-1}^n + d_3 w_{K-2}^n + n_{\theta_K}^n + \eta_{\xi_K}^n + \eta_{\xi\theta_K}^n \\
& + \eta_{\theta_K}^n + \sum_{j=1}^{N_r} \delta_{KH_j} R_j^n \tag{3.22}
\end{aligned}$$

$K=1, \dots, M; n=0, 1, \dots$

Here d_1, \dots, d_5 are known quantities which depend on n , c , α , and d . The terms λ_1^n , λ_2^n , $n_{\theta_K}^n$, $\eta_{\theta_K}^n$, $\eta_{\xi\theta_K}^n$, and $\eta_{\xi\theta_K}^n$ are calculated as explained in Appendix B. In (3.20) and (3.21), the upper limit M of the values assumed by K applies only when the response is symmetric with respect to the midspan. The ring term R_j^n , obtained from (3.11) and (3.18), is given by

$$\begin{aligned}
R_j^n &= d_6 w_{K+1}^n + d_7 w_K^n + d_6 w_{K-1}^n + d_8 (u_K^n - u_{K-1}^n) + d_9 v_K^n \\
& K=H_j; j=1, 2, \dots, N_r \tag{3.23}
\end{aligned}$$

Here d_6, \dots, d_9 are also known quantities that depend on n , d , and the ring coefficients C_1, \dots, C_5 , and e . The expressions for d_1, \dots, d_9 are given in Appendix C.

Boundary Conditions

Casting the boundary conditions in finite difference form is conceptually simple, but the process involves development of a few interpolations. The interested reader will find the development of the interpolations in Appendix B.

Simply Supported. The boundary conditions (3.12) allow an axisymmetric rigid-body translation along the ξ -coordinate. Consequently, when only the conditions of (3.12) are observed, the numerical solution is not unique. In order to obtain a unique solution, the axial displacement of the axisymmetric mode must be set to zero at some arbitrary axial station. To facilitate a numerical solution, the node at $\xi = 1$ where $K = M$ was chosen. Since the axial displacement is not defined at the whole stations, interpolation is required to express this condition. The interpolation is developed in Appendix B. Substituting the appropriate equations from (3.18) into (3.12) at $K = 1$ yields

$$w_1^n = 0 \quad (3.24a)$$

$$w_2^n - 2w_1^n + w_0^n = 0 \quad (3.24b)$$

$$v_1^n = 0 \quad (3.24c)$$

$$u_1^n - u_0^n + d(C_{XX_1}^n + C_{IXX_1}^n) = 0 \quad (3.24d)$$

and at $K = M$ yields

$$w_M^n = 0 \quad (3.25a)$$

$$w_{M+1}^n - 2w_M^n + w_{M-1}^n = 0 \quad (3.25b)$$

$$v_M^n = 0 \quad (3.25c)$$

$$u_m^n - u_{m-1}^n + d(C_{XX_M}^n + C_{IXX_M}^n) = 0 \quad (3.25d)$$

In order to tie down the axial displacement of the axisymmetric mode, the following expression is used at the end $\xi = 1$ ⁴

$$u_m^0 + 2u_{m-1}^0 - \frac{1}{3}u_{m-2}^0 = 0 \quad (3.26)$$

where the half station $k = m$ is located at $\xi = 1 - \frac{1}{2}d$.

Clamped. The finite difference formulation of boundary conditions (3.13b) and (3.13c) is straightforward requiring only the substitution of the appropriate expressions from (3.18). However, the discretization of (3.13a) and (3.13d) requires the utilization of interpolation formulas.⁴ The difference expressions for the clamped boundary conditions are

$$u_0^n + 2u_1^n - \frac{1}{3}u_2^n = 0 \quad (3.27a)$$

$$v_1^n = 0 \quad (3.27b)$$

$$w_1^n = 0 \quad (3.27c)$$

⁴See Appendix B.

$$w_0^n - 9w_2^n + w_3^n = 0 \quad \text{at } K = 1 \quad (3.27d)$$

and

$$u_m^n + 2u_{m-1}^n - \frac{1}{3} u_{m-2}^n = 0 \quad (3.28a)$$

$$v_M^n = 0 \quad (3.28b)$$

$$w_M^n = 0 \quad (3.28c)$$

$$w_{M-2}^n - 9w_{M-1}^n + w_{M+1}^n = 0 \quad \text{at } K = M \quad (3.28d)$$

Response Symmetric to the Midspan. Substitution of the appropriate expressions from (3.18) into (3.14) leads to

$$u_m^n = 0 \quad (3.29a)$$

$$v_M^n - v_{M+1}^n = 0 \quad (3.29b)$$

$$w_M^n - w_{M+1}^n = 0 \quad (3.29c)$$

$$w_{M-1}^n - w_{M+2}^n = 0 \quad (3.29d)$$

CHAPTER IV

SOLUTION OF THE NUMERICAL MODEL

I. SOLUTION PROCEDURE

There are various methods that could be used to solve the differential-difference equations that comprise the numerical model. Several of them are examined in this chapter. The algorithm that appears to be the most promising is a combination of the Gauss elimination method and the iterative Newmark beta-method. The solution procedure is carried out in the following manner. Suppose that w_K^n , \dot{w}_K^n , \ddot{w}_K^n , u_K^n , and v_K^n are known at time τ_1 for all values of K , k , and n . The solution is sought at time τ_2 , a small increment later than τ_1 . In the first iteration for the solution at τ_2 , \ddot{w}_K^n at τ_2 is taken equal to \ddot{w}_K^n at τ_1 . The quantities w_K^n and \dot{w}_K^n at τ_2 are then calculated for all K and n using the Newmark beta-method. Knowing w_K^n at τ_2 , the terms $\lambda 1_K^n$ and $\lambda 2_K^n$, which depend only on w_K^n , are computed; and u_K^n and v_K^n are obtained by solving equations (3.20) and (3.21) with the Gauss elimination method. Next, having computed estimates for w_K^n , \dot{w}_K^n , u_K^n , and v_K^n at time τ_2 , the acceleration \ddot{w}_K^n at τ_2 can be calculated from equation (3.22) for all K and n . The accelerations of the two consecutive iterations are compared to check for convergence. The iteration is continued until convergence is achieved.

This procedure is repeated for many time steps to compute the displacements as a function of time.

II. SOLUTION OF THE AXIAL AND CIRCUMFERENTIAL EQUATIONS

Applicable methods

The axial and circumferential ordinary differential equations, (3.6) and (3.7), constitute a linear boundary value problem in the two unknowns $u^n(\xi)$ and $v^n(\xi)$ when $\lambda 1^n$, $\lambda 2^n$, and w^n are known. In the development of the numerical model, these equations were replaced by a system of simultaneous algebraic equations (3.20) and (3.21). If $\lambda 1_k^n$, $\lambda 2_k^n$, and w_k^n are known, these equations can be solved independently of the radial equations (3.22). Either a direct elimination procedure or an iterative procedure is normally employed to solve systems of algebraic equations of this type [35, 36]. An example of the direct procedure is the Gauss elimination method. This method has been used by several investigators to solve static shell problems [23, 30, 37]. The Gauss-Siedel method is a popular iterative procedure.

The Gauss elimination method and the Gauss-Siedel iteration procedure were compared in an attempt to determine the best of the two methods for the problem under consideration. Computer routines using both methods were written to solve (3.20) and (3.21). Solutions to some simple linear problems were generated by both routines, and the computed solutions were compared with the exact solutions

to the differential equations. The Gauss elimination procedure required significantly less time on the computer than did the iterative procedure for the same degree of accuracy. When both methods used the same execution time, the elimination method provided a considerably more accurate solution. Consequently the Gauss elimination method was selected for the algorithm.

Gauss Elimination

To facilitate the development of the Gauss elimination procedure, the axial and circumferential equations are converted to matrix equations. First, let $\Lambda 1_K^n$ and $\Lambda 2_K^n$ be defined by

$$\Lambda 1_K^n = d^2 \lambda 1_K^n + \sum_{j=1}^{N_r} \delta_{KHj} d n^2 [C_4 (e n^2 - 1) - C_5] (w_{K+1}^n - w_K^n) \quad (4.1a)$$

$$\Lambda 2_K^n = d^2 \lambda 2_K^n + \sum_{j=1}^{N_r} \delta_{KHj} d^2 n C_3 (e n^2 - 1) w_K^n \quad (4.1b)$$

Equations (3.20) and (3.21) can now be written in the form

$$A^n z_{K+1}^n + B_K^n z_K^n + C^n z_{K-1}^n = g_K^n \quad (4.2)$$

where $n = 0, 1, \dots$; and $K = 1, 2, \dots, M-1$ or M , depending on whether the response is unsymmetric or symmetric with respect to the midspan. For the unsymmetric response, M is the number of whole stations between $\xi = 0$ and $\xi = 1$. If the response is symmetric with respect to the midspan, M is the number of whole stations located between $\xi = 0$ and

$\xi=1/2$. The matrices A^n , B_K^n , and C^n are 2×2 matrices whose elements are given in Appendix C, and z_K^n and g_K^n are defined by

$$z_K^n = \begin{bmatrix} u_K^n \\ v_K^n \end{bmatrix} \quad (4.3)$$

$$g_K^n = \begin{bmatrix} -\Lambda_{1K}^n \\ -\Lambda_{2K}^n \end{bmatrix} \quad (4.4)$$

For a fixed value of n , (4.2) represents a system of $2M-2$ (or $2M$) equations in $2M+2$ (or $2M+4$) unknowns for unsymmetric (or symmetric) response as shown in Figure 4.1. The boundary (or symmetry) conditions provide the remaining necessary equations

Recursion Relations. The Gauss elimination recursion relation for equations having the form of (4.2) is [30, 37]

$$z_K^n = -P_K^n z_{K+1}^n + x_K^n \quad (4.5a)$$

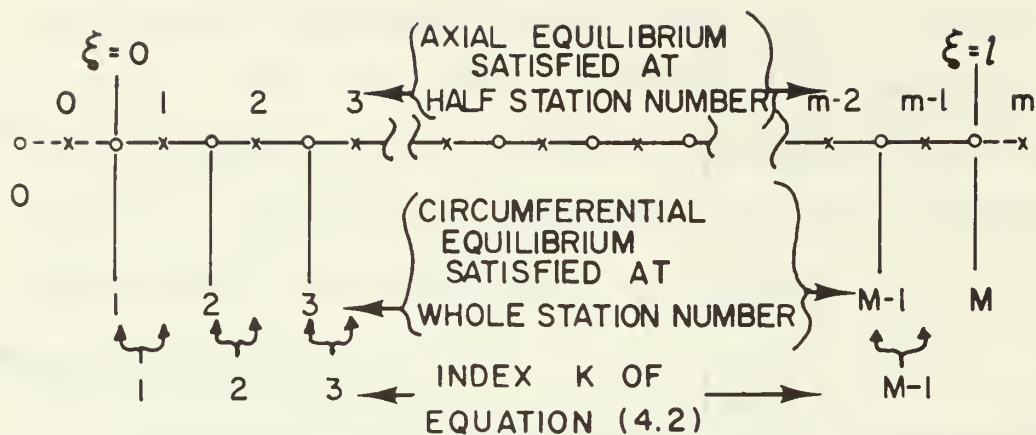
where P_K^n is a 2×2 square matrix, and x_K^n is a 2×1 vector.

Thus, the recursion relation for z_{K-1}^n is

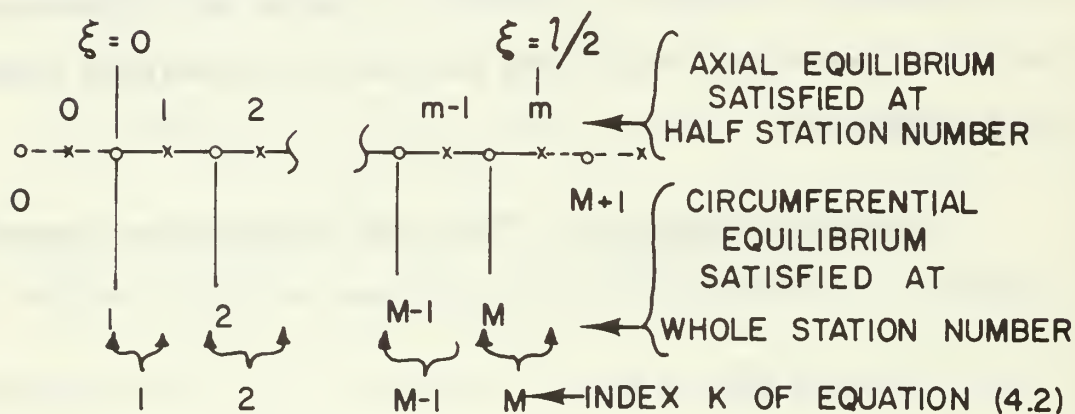
$$z_{K-1}^n = -P_{K-1}^n z_K^n + x_{K-1}^n \quad (4.5b)$$

Substitution of (4.5b) into (4.2) results in

$$z_K^n = -[B_K^n - C^n P_{K-1}^n]^{-1} A^n z_{K+1}^n + [B_K^n - C^n P_{K-1}^n]^{-1} [g_K^n - C^n x_{K-1}^n]$$



(a) UNSYMMETRIC RESPONSE



(b) SYMMETRIC RESPONSE

FIGURE 4.1
RELATIONSHIP BETWEEN MESH NODES
AND
INDEX K OF EQUATION (4.2)

Comparing the above equation with (4.5a) reveals that

$$P_K^n = [B_K^n - C^n P_{K-1}^n]^{-1} A^n \quad (4.6)$$

and

$$x_K^n = [B_K^n - C^n P_{K-1}^n]^{-1} [g_K^n - C^n x_{K-1}^n] \quad (4.7)$$

In solving (4.2), the following steps are performed:

- (1) the P_K^n matrices are computed by recursion relation (4.6);
- (2) the x_K^n vectors are calculated from (4.7); and
- (3) the solution vectors z_K^n are computed in a backward sweep by recursion relation (4.5a). Each of the steps will now be examined in more detail.

Computation of P_K^n Matrices. The general matrix P_K^n depends on P_{K-1}^n . Hence, P_1^n must be determined first. This matrix is determined from application of the boundary conditions. The boundary conditions which uniquely determine the P_1^n matrix are given by equations (3.24c) and (3.24d) when the shell is simply supported and by (3.27a) and (3.27b) when the shell is clamped. From the two appropriate boundary equations and the axial equilibrium equation at $K = 1$ an equation is obtained of the form

$$z_1^n = P_1^n z_2^n + x_1^n \quad (4.8)$$

The elements of the matrix P_1^n for both the simply supported and clamped shell are listed in Appendix C. By using the recursion formula (4.6), the remaining P_K^n matrices are

computed for all of the participating modes and for $K = 2, 3, \dots, M-2$. When the response is symmetric with respect to the midspan, $K = 2, 3, \dots, M-1$. These P matrices do not change with either the load or the response.

Computation of x_K^n Vectors. When the shell is simply supported the vector x_1^n of (4.8) is given by¹

$$x_1^n = \begin{bmatrix} \Lambda 1_1^n + d(C_{XX_1}^n + C_{IXX_1}^n) \\ 0 \end{bmatrix} / [1 + d^2 n^2 (\frac{1-\nu}{2})] \quad (4.9)$$

and when the shell is clamped, by

$$x_1^n = \begin{bmatrix} \Lambda 1_1^n \\ 0 \end{bmatrix} / [4 + d^2 n^2 (\frac{1-\nu}{2})] \quad (4.10)$$

Since in both cases x_1^n contains nonlinear terms in the radial deflection, x_1^n is not constant, but instead, varies with the load. The vector g_K^n , defined by (4.4), also changes with the load. Thus, the vectors x_K^n and g_K^n must be recomputed many times as a solution is generated; x_1^n from (4.9) or (4.10), and the other x_K^n vectors from (4.7).

¹The fact that the boundary condition on v_K^n is $v_1^n = 0$ makes it unnecessary to introduce v_0^n into the solution and to consider the circumferential equilibrium equation at point $K = 1$.

Back Substitution. The solution vectors z_K^n are obtained through back substitution, that is by sequential solution of equation (4.5a). However, relation (4.5a) requires a "starting" z-vector.

The boundary conditions at $\xi = 1$ provide the information necessary to compute this vector when the response is unsymmetric with respect to the midspan of the cylinder. The boundary conditions are given by (3.25c) and (3.25d) when the shell is simply supported and $n \neq 0$. When the shell is clamped, or when the shell is simply supported and $n = 0$, the corresponding boundary conditions are expressed by (3.28a) and (3.28b).² By substituting the boundary conditions into (4.2) with $K = M-1$ and by making use of (4.5a) at $K = M-2$, the following result is obtained for the solution at $K = M-1$.

$$z_{M-1}^n = [H^n - O^n P_{M-2}^n] [f^n - O^n x_{M-2}^n] \quad (4.11)$$

where H^n , O^n , and f^n are given in Appendix C for the simply supported and clamped boundary conditions.

When the response is symmetric with respect to the midspan, the starting vector z_M^n is determined by using the symmetry conditions given by (3.29a) and (3.29b). If (3.29a) and (3.29b) are substituted into the circumferential equilibrium equation at $K = M$ and the result combined with (4.5a) at $K = M-1$,³ the result is

²Equations (3.26) and (3.28a) are identical when $n=0$.

³The axial equilibrium equation is identically satisfied at the midspan.

$$z_M^n = [I + R^n P_{M-1}^n]^{-1} [R^n x_{M-1}^n + s^n] \quad (4.12)$$

where I is the identity matrix and R^n and s^n are given in Appendix C.

Once equations (4.11) or (4.12) have been evaluated for each n , the remaining z -vectors are computed in sequence using (4.5a).

III. TIME INTEGRATION

Four basic methods were considered for carrying out the time integration of the radial equations of motion. They were the Runge-Kutta methods, the explicit methods, the implicit methods, and the Newmark beta-method.

The Runge-Kutta method [38] has been used by several investigators to compute the nonlinear dynamic response of cylindrical shells [11, 20, 22]. However, they included only a few modes in the response and did not employ finite differences along the axial coordinate. Consequently, their systems of equations were much smaller than the system to be solved here. For the large system of equations of the present analysis, the Runge-Kutta method would require prohibitively large amounts of computer storage space and excessive computing time.

The explicit methods [39, 40] all have the common feature that the unknowns can be calculated explicitly without solving a large system of simultaneous equations each time the solution is advanced one time increment.

Nonlinear equations can be solved without iteration since the nonlinear terms contain only products of previously computed quantities. However, the explicit methods are numerically unstable if the time increment is too large. While the largest permissible time increment can be predicted theoretically for linear equations, the permissible time increment for nonlinear equations has not been established as yet. Since a numerical instability might easily be mistaken for a physically unstable response, the explicit methods were ruled out.

The implicit methods [39, 40, 41] all utilize time averaged finite difference approximations of the spatial derivatives. As a result, the difference equation at any spatial location contains several unknowns. The advancement of the solution by one time increment is accomplished by solving a system of simultaneous algebraic equations. If the differential equations are nonlinear in the spatial derivatives of the dependent variables, as in the case for the equations under study, the simultaneous algebraic equations are usually nonlinear. These nonlinear equations must be solved by an iterative procedure that solves a sequence of linear equations. The implicit methods have the advantage of being numerically stable when applied to linear problems. However, since an iterative procedure must be used in the implicit methods to solve the nonlinear equations, the decision was made to use an iterative integration procedure.

The iterative integration procedure selected as the most suitable for carrying out the time integration is the Newmark beta-method. References [42] and [43] contain a detailed description of the method and a theoretical determination of the stability and convergence limits. A typical application of the method, as well as references to several other investigations that employed the method may be found in Reference [44].

Integration Procedure

The numerical integration procedure begins with the assumption that the displacements, u_K^n , v_K^n , and w_K^n ; the velocities, \dot{w}_K^n ; and the accelerations, \ddot{w}_K^n , are known at time τ_1 . The corresponding physical quantities may be computed at time $\tau_2 = \tau_1 + \Delta\tau$, where $\Delta\tau$ is the time increment, by repetition of the following steps:

1. Assume that $\ddot{w}_K^n(\tau_2) = \ddot{w}_K^n(\tau_1)$ for the first iteration. For subsequent iterations, assume that $\ddot{w}_K^n(\tau_2) = \ddot{w}_1^n(\tau_2)$ where \ddot{w}_1^n is computed in step 6.
2. Calculate the radial displacements and velocities at time τ_2 by the relations

$$\dot{w}_K^n(\tau_2) = \dot{w}_K^n(\tau_1) + \frac{1}{2}[\ddot{w}_K^n(\tau_1) + \ddot{w}_K^n(\tau_2)] \Delta\tau \quad (4.13)$$

$$w_K^n(\tau_2) = w_K^n(\tau_1) + \dot{w}_K^n(\tau_1)\Delta\tau + (\frac{1}{2}-\beta) \ddot{w}_K^n(\tau_1)(\Delta\tau)^2 + \beta \ddot{w}_K^n(\tau_2)(\Delta\tau)^2 \quad (4.14)$$

The significance of the parameter β will be discussed in a later paragraph.

3. Evaluate the nonlinear terms $\Lambda 1_K^n$ and $\Lambda 2_K^n$ from (4.1).
4. Compute u_K^n and v_K^n by Gauss elimination.
5. Evaluate $n_{\theta_K}^n$, $\eta_{\xi_K}^n$, $\eta_{\xi\theta_K}^n$, and $\eta_{\theta_K}^n$.
6. Compute the radial accelerations from equation (3.22). Let $\ddot{w}_K^n(\tau_2)$ denote the values computed here to distinguish them from $\ddot{w}_K^n(\tau_2)$ of step 1.
7. Compare $\ddot{w}_K^n(\tau_2)$ with $\ddot{w}_K^n(\tau_2)$. If their relative difference is larger than a prescribed value ϵ , the convergence criterion, repeat steps 1-7. If the difference is smaller than ϵ , the solution is said to have converged.

This procedure can be repeated as often as desired in order to determine the response of the shell as a function of time.

The Parameter Beta. Equations (4.13) and (4.14) are the quadrature relations of the Newmark beta-method. Newmark [43] has shown that the choice of a particular value of β is related to the shape of the acceleration-time curve during the time increment $\Delta\tau$. Acceleration-time curves associated with $\beta = 1/4$, $1/6$, and $1/8$ are shown in Figure 4.2. For this study, β was taken equal to $1/6$ corresponding to a linear variation of the acceleration during the time increment.

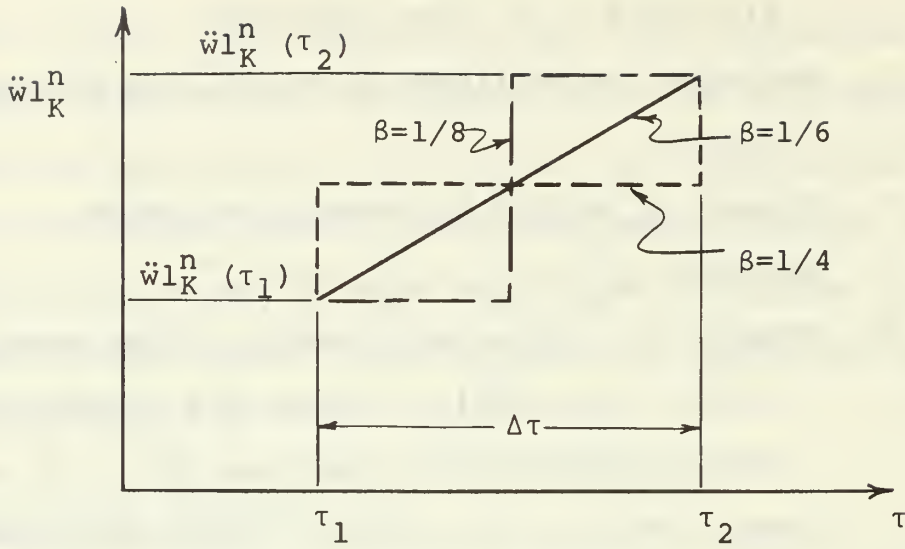


Figure 4.2

ACCELERATION VS. TIME FOR $\beta = 1/4, 1/6$, AND $1/8$

The stability and convergence limits of the Newmark beta-method are given by critical values of the ratio of the time increment $\Delta\tau$ to the shortest natural period T of the finite difference model. If the ratio $\Delta\tau/T$ is larger than the stability or convergence limit, the procedure is unstable or does not converge. The stability limits, derived by Newmark [43] for a linear oscillator, are given in Table I for several values of β . When β is larger than one-eighth, the convergence limit is more stringent than the stability limit.

The problem under study is governed by a set of non-linear equations, and the shortest natural period is not easily obtained since the natural frequencies of a non-linear system vary with the amplitude of the motion.

Nevertheless, the shortest natural frequency of an unstiffened shell, as predicted by the linear theory, will serve as a useful guide.

TABLE I
STABILITY AND CONVERGENCE LIMITS

β	0	1/12	1/8	1/6	1/4
Stability Limit, $\Delta\tau/T =$	0.318	0.389	0.450	0.551	infinite
Convergence Limit, $\Delta\tau/T =$	infinite	0.551	0.450	0.389	0.318

For the Fourier modes of interest, the linear equations reveal that the axisymmetric mode ($n=0$) has the shortest period.⁴ If the shell is simply supported, $n_{\xi}^0 = n_{\xi\theta}^0 = 0$ and $n_{\theta}^0 = -(1-\nu^2)w^0$. Hence, from (3.10), the linear differential equation for the axisymmetric mode is seen to be

$$\frac{1}{12} \alpha^2 w_{,\xi\xi\xi\xi}^0 + (1-\nu^2) w^0 = -\ddot{w}^0 \quad (4.15)$$

Approximation of the spatial derivatives by central differences leads to

$$\begin{aligned} \frac{1}{12} \frac{\alpha^2}{d^4} (w_{K+2}^0 - 4w_{K+1}^0 + w_K^0 - 4w_{K-1}^0 + w_{K-2}^0) \\ + (1-\nu^2) w_K^0 = -\ddot{w}_K \end{aligned} \quad (4.16)$$

⁴In Chapter V, it will be shown that this is true.

Assume a solution to (4.15) of the form

$$w^0 = \sin (\Omega_{0q} \tau) \sin \left(\frac{q\pi \xi}{l} \right) \quad (4.17)$$

where Ω_{0q} is the natural frequency of the axisymmetric mode with wavelength $\frac{q\pi}{2l}$. If the shell is divided into $M-1$ intervals of length d , it follows that

$$\xi = (K-1) d$$

$$l = (M-1) d$$

Thus equation (4.17) may be written

$$w^0 = \sin (\Omega_{0q} \tau) \sin \left[\frac{q\pi (K-1)}{M-1} \right] \quad (4.18)$$

The natural frequency Ω_{0q} is now the frequency associated with the difference-differential equations. Substituting (4.18) into (4.16) and performing several algebraic and trigonometric manipulations yield

$$\Omega_{0q}^2 = \frac{1}{12} \frac{\alpha^2}{d^4} \left[2 \cos \left(\frac{2q\pi}{M-1} \right) - 8 \cos \left(\frac{q\pi}{M-1} \right) + 6 \right] + (1-\nu^2)$$

The maximum value of Ω_{0q}^2 occurs when $\frac{q}{M-1} = 1$. Hence, the highest frequency is given by

$$\Omega_{0 \ M-1}^2 = \frac{4}{3} \frac{\alpha^2}{d^4} + 1-\nu^2 \quad (4.19)$$

Consequently, the shortest natural period of the finite difference model is

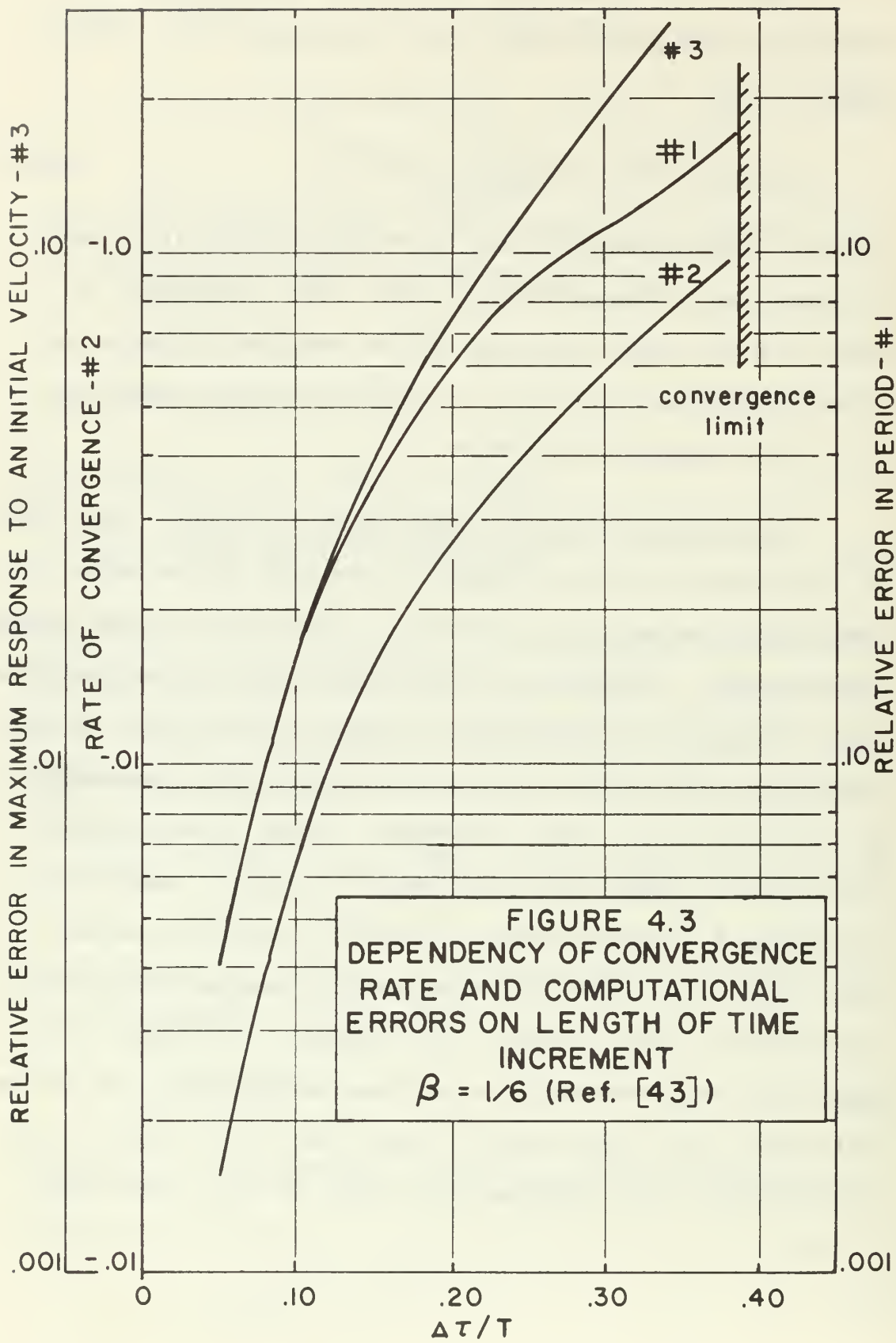
$$T = 2\pi \left(\frac{4}{3} \frac{\alpha^2}{d^4} + 1-\nu^2 \right)^{-\frac{1}{2}} \quad (4.20)$$

With T given by (4.20), $\Delta\tau$ for convergence and stability is given in Table I as a function of β . Thus taking β equal to $1/6$,

$$\Delta\tau \leq (0.389)(2\pi) \left(\frac{4}{3} \frac{\alpha^2}{d^4} + 1 - \nu^2 \right)^{-\frac{1}{2}} \quad (4.21)$$

insures both convergence and stability of the algorithm in computing a linearized solution. The assumption is made that the same reasoning can be applied to the non-linear equations; that is, if the calculation converges, it is also numerically stable.

Convergence Rate and Computational Errors. The rate of convergence used by Newmark is defined as the error in the derived acceleration divided by the error in the assumed acceleration. Newmark has shown that for a linear oscillator, the rate of convergence, as well as the error in the amplitude and frequency of the computed motion, depends on the size of the time increment. These relationships are shown in Figure 4.3 for β equal to $1/6$. Inspection of Figure 4.3 reveals that in order to keep the errors small, the time increment must be much shorter than the convergence limit permits. For example, if errors in amplitude and frequency larger than two percent can not be tolerated, then $\Delta\tau/T$ must be less than 0.12, whereas the convergence limit requires only that $\Delta\tau/T$ be less than 0.389.



Newmark [42] has suggested that when β is equal to $1/6$, a stable integration procedure for nonlinear equations can be obtained by requiring that the assumed acceleration and the derived acceleration agree to within one percent, or less, by the end of the fourth iteration. If convergence is not obtained by the fourth iteration, the time increment should be reduced. On the other hand, if the accelerations converge in one or two iterations, the time step should be increased to ensure optimum computing efficiency.

V. COMPUTER PROGRAM

A computer program was written for the IBM 360 Model 67 computer to generate a solution to the governing difference-differential equations developed in Chapter II and Chapter III. Appendix D contains a description and complete documentation of the program, including instructions for the preparation of input data cards and other information necessary for the operation of the program. The program is dimensioned to accommodate twenty equally spaced axial stations ($M \leq 20$) and fifteen Fourier modes. It will handle up to three ring stiffeners located so as to divide the shell into segments of equal length. Both simple and clamped supports can be handled. The basic output consists of the displacements and in-plane forces at specified time steps. The axial location, time, and

magnitude of the maximum circumferential stress at $\theta = 0^\circ$ are also printed.

The program adjusts the size of the time increment so that the number of iterations always falls within a range specified by the user. The number of iterations required to obtain a converged solution depends on the convergence criterion, ϵ . Convergence is assumed to have occurred when

$$\epsilon \geq \frac{|\ddot{w}_K^n^{I+1} - \ddot{w}_K^n^I|}{\text{Max} \left\{ |\ddot{w}_K^n^{I+1}|, |\ddot{w}_K^n^I| \right\}} \quad \begin{array}{l} n = 0, 1, \dots \\ K = 0, \dots, M \end{array}$$

where I is the iteration number

Calculation of the Circumferential Stress at a Typical Location

A structure designed for repeated use may experience low cycle fatigue cracking and even total failure if the stresses repeatedly exceed the yield point stress of the material. Therefore, one criterion for a safe load is that the stresses which develop during the response must never exceed the yield stress. For the problem at hand, only radial loads are considered; and the load is carried principally by circumferential stresses. Thus, the circumferential stress is a close approximation to the maximum principal stress. In the present program the circumferential stresses are computed at $\theta = 0^\circ$.⁵

⁵At a fixed axial location, the circumferential stress is not necessarily largest at $\theta = 0^\circ$; but since the assumed imperfection modes are in phase at $\theta = 0^\circ$, it is a reasonable indication of the state of maximum stress in the shell.

At a point on the midsurface of the shell, the circumferential stress σ_θ is given by

$$\sigma_\theta = \frac{E}{1-\nu^2} n_\theta \quad (4.22)$$

At either the inner or the outer surface the magnitude of the circumferential stress is larger than the stress at the midsurface, the additional stress being due to bending of the shell. The circumferential surface stress due to the circumferential curvature change, denoted $\sigma_{\theta B}$, is given by

$$\sigma_{\theta B} = \pm \frac{1}{2} \frac{Eh}{a^2} \frac{d^2 w}{d\theta^2} \quad (4.23)$$

The influence of the meridional curvature change on the circumferential bending stress is neglected. The magnitude of the largest surface stress, denoted $|\sigma_{\theta s}|$, is given by

$$|\sigma_{\theta s}| = |\sigma_\theta| + |\sigma_{\theta B}| \quad (4.24)$$

Substituting (4.22) and (4.23) into (4.24) leads to

$$|\sigma_{\theta s}| = \frac{E}{1-\nu^2} |n_\theta| + \frac{1}{2} E \frac{h}{a^2} \left| \frac{d^2 w}{d\theta^2} \right| \quad (4.25)$$

On substituting (3.2c) and (3.3b) into (4.25), the result is

$$|\sigma_{\theta s}| = \frac{E}{1-\nu^2} \left| \sum_{n=0}^{\infty} n_\theta^n \cos n\theta \right| + \frac{1}{2} E \alpha \left| \sum_{n=0}^{\infty} n^2 w^n \cos n\theta \right| \quad (4.26)$$

When $\theta = 0^\circ$

$$|\sigma_{\theta s}|_{\theta=0^\circ} = \frac{E}{1-\nu^2} \left| \sum_{n=0}^{\infty} n_{\theta}^n \right| + \frac{1}{2} E \alpha \left| \sum_{n=0}^{\infty} n^2 w^n \right| \quad (4.27)$$

Let \bar{n}_{θ} be defined by the relationship

$$|\sigma_{\theta s}|_{\theta=0^\circ} = \frac{E}{1-\nu^2} \bar{n}_{\theta} \quad (4.28)$$

Then from (4.27) and (4.28)⁶

$$\bar{n}_{\theta} = \left| \sum_{n=0}^{\infty} n_{\theta}^n \right| + \frac{1}{2} \alpha (1-\nu^2) \left| \sum_{n=0}^{\infty} n^2 w^n \right| \quad (4.29)$$

At a given axial station, the value of \bar{n}_{θ} is thus proportional to the stress at $\theta = 0^\circ$. Equation (4.29) can also be expressed in finite difference form as

$$\bar{n}_{\theta_K} = \left| \sum_{n=0}^{\infty} n_{\theta_K}^n \right| + \frac{1}{2} \alpha \left| \sum_{n=0}^{\infty} n^2 w_K^n \right| \quad (4.30)$$

The maximum circumferential stress at $\theta=0^\circ$, $\bar{n}_{\theta_{MAX}}$, occurs at some grid point K. Hence

$$\bar{n}_{\theta_{MAX}} = \text{Max} \left\{ \bar{n}_{\theta_K}, K = 2, 3, \dots, M-1 \text{ (or } M) \right\} \quad (4.31)$$

For convenience, we will refer to this as the maximum circumferential stress.

⁶In the computer program, the quantity $1-\nu^2$ in (4.29) was taken equal to unity. The error introduced is certainly no greater than the errors involved with the other approximations. If the program is revised to compute the exact stresses, this factor should be reinserted.

Verification of Computer Program

As indicated in Chapter I, there apparently are no previous solutions for the nonlinear dynamic response of a cylindrical shell that can be used to check all of the features of the present computer program. Furthermore, the program cannot be readily simplified or altered to correspond with the previous analyses. Consequently, only a linearized version of the program was verified through comparison with other solutions known to be correct. It might be argued that some of the new features of the program are of minor significance, and that the results of some of the earlier analyses could be used to test the program. However, if discrepancies were discovered, it would be difficult to decide whether to attribute them to an error in the program or to differences in the analyses.

To check the capability of the program to compute a fully nonlinear, nonaxisymmetric solution, a typical problem was run through several time steps, and a complete sequential printout of the program variables was obtained. The printout was then checked against a hand calculated solution.

To date, those features of the program that compute the contributions from the rings have been checked in a cursory manner. One computer run was made for which the shell was assumed to have ring stiffeners. The computed displacements appeared to be correct. The parts of the

program that compute the ring contributions are isolated and do not affect results obtained for unstiffened shells.

The results presented in the next chapter also serve to verify the analysis and the program in that many of the results agree very favorably with those obtained by other investigators.

Linear Test Cases

Under an axisymmetric load, the response of the shell, as governed by linearized equations, is also axisymmetric. The correctness of the program in computing a nonaxisymmetric response was checked in conjunction with the verification of the nonlinear features of the program.

Moving Step Load. The transient, axisymmetric response of a simply supported shell subjected to a moving step pressure discontinuity has been determined earlier by P. G. Bhuta [45] using a series solution to the linear Donnell equations. A subroutine was assembled to compute $p(\xi, \tau)$ for this loading condition, and a numerical solution for the axisymmetric response was computed using the program with all nonlinear terms set equal to zero. Twenty-one axial stations were used,⁷ and convergence to one per cent in a maximum of four and a minimum of three iterations was specified. A comparison of the radial

⁷The present program is dimensioned to handle a maximum of twenty axial points.

displacements at the quarter-span station is shown in Figure 4.4. The constants for the example are also given in Figure 4.4. The computed results agree fairly well with the series solution. However, by the end of the calculation a detectable error has developed.

The computed displacements are given in Figure 4.4 at every tenth time step. During the time that the load discontinuity was on the shell, the time increment remained small, and approximately one hundred and seventy time steps were taken to compute the first cycle of the motion. Shortly before the discontinuity moved off the shell, the time increment increased, and approximately thirty time steps were required to compute the second cycle. The ratio $\Delta\tau/T$, where T is defined by equation (4.20), reached a maximum value of .05. From Figure 4.3, it is seen that the computational errors should be very small for this value. The numerical errors are apparently accumulative and may reach significant magnitudes in lengthy computations. In subsequent computations, the parameter ϵ was set equal to .001 to reduce the accumulative error.

Uniform Harmonic Load. The axisymmetric transient response of a simply supported shell subjected to a loading given by

$$p(\xi, \tau) = p_0 \cos \Omega \tau$$

was computed and compared to the series solution. The response predicted by the linear theory is

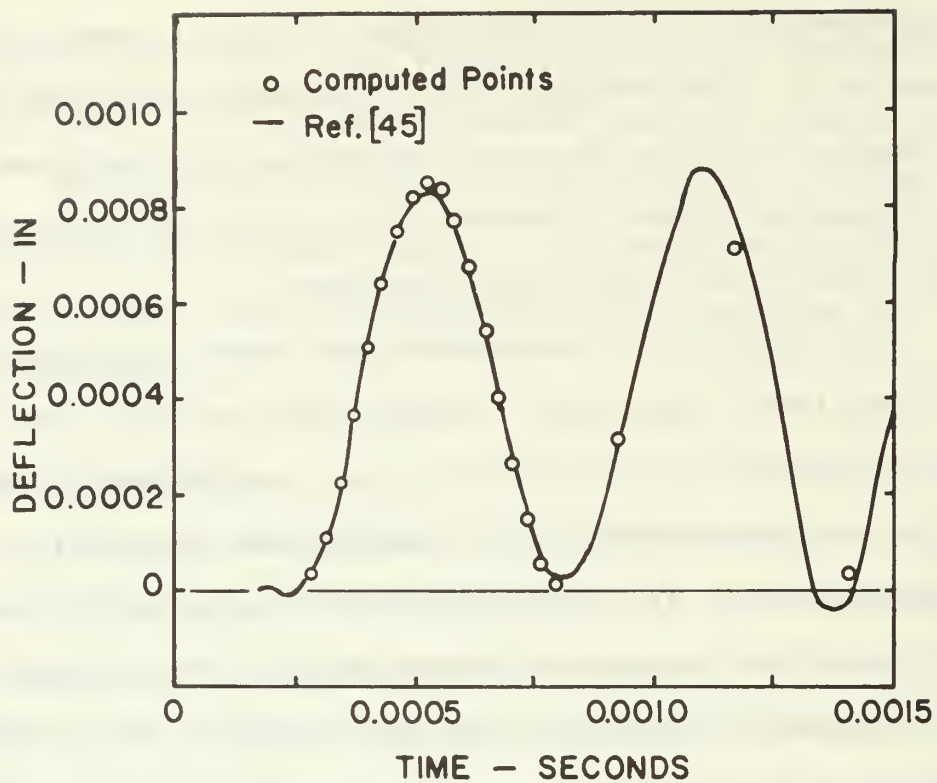


FIGURE 4.4
QUARTER-SPAN RESPONSE TO A MOVING
STEP LOAD

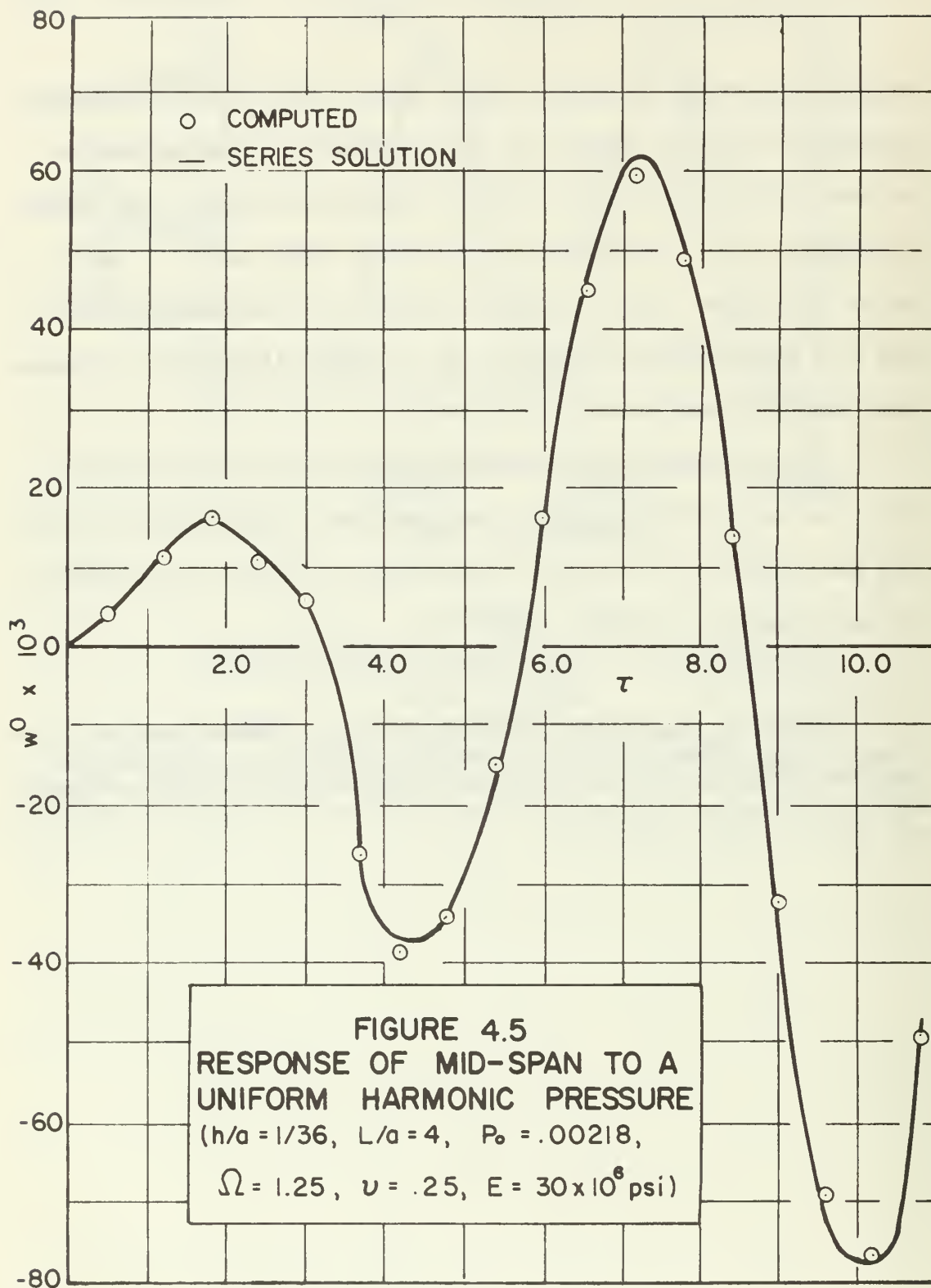
($a=18\text{in}$, $h=1/2\text{in}$, $L=72\text{in}$, $P_0=20\text{psi}$, $E=30\times 10^6$
 $\rho=7.332\times 10^{-4}\text{lb-sec in}^{-2}$, $\nu=0.3$, velocity = 72,000 in/sec)

$$w(\xi, \tau) = \sum_{q=1,3,5,\dots}^{31} \frac{4p_o}{\pi q (\Omega_q^2 - \Omega^2)} (\cos \Omega \tau - \cos \Omega_q \tau) \sin \left(\frac{q\pi \xi}{l} \right)$$

Thirty-one axial stations were used,⁸ and the convergence parameter was set equal to .001. The computed solution at every 10th time step and the series solution are shown in Figure 4.5. As with the previous test case, a small error developed after several cycles of the oscillation and was manifested primarily as a phase difference between the computed and exact responses.

On the basis of the above tests, it was concluded that the algorithm provides an adequate representation of the axisymmetric transient response of a shell subjected to axisymmetric loads.

⁸During the initial phases of the investigation, the program was dimensioned to accomodate 31 axial stations. The dimensions of the computer program were later reduced, and the program listed in Appendix D will handle a maximum of twenty axial stations.



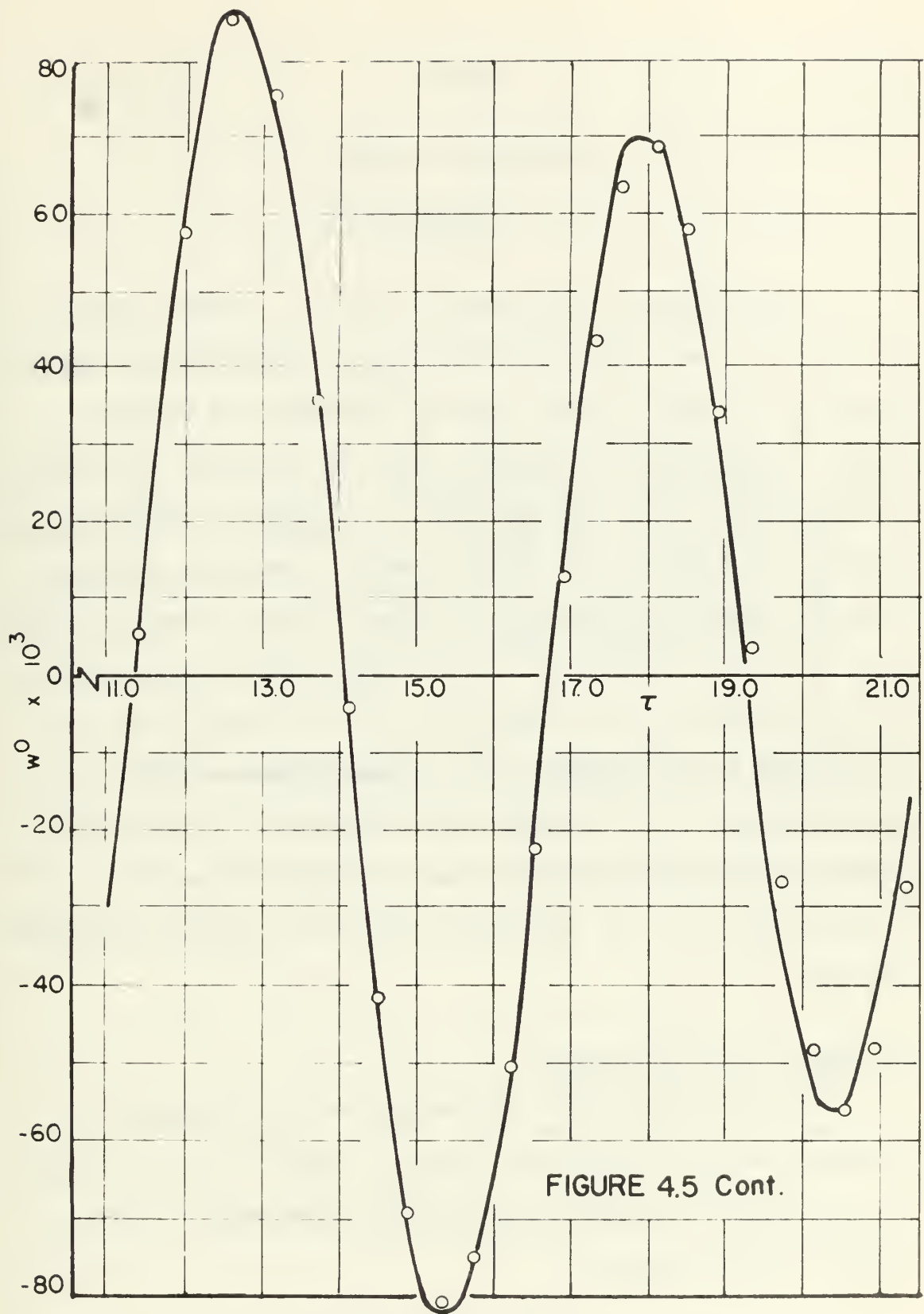


FIGURE 4.5 Cont.

CHAPTER V

NUMERICAL RESULTS

I. INTRODUCTION

The analysis, the numerical model, and the method of solution developed in the preceding chapters are applicable to a rather broad class of problems. A complete study to determine the significance of the many features incorporated in the analysis and the computer program is beyond the scope of the present work. Hence, a problem that has been considered in two very recent investigations [19, 20] was selected for an in-depth study. Treatment of the problem by the algorithm of this dissertation accomplished three things: (1) increased understanding of the solution to the problem was developed; (2) the feasibility and practicality of the new approach were established; and (3) deficiencies of the program were disclosed.

Statement of the Problem

The problem is the determination of the dynamic response of an unstiffened, simply supported cylindrical shell subjected to an exponentially decaying, uniform, radial pressure pulse.

Shell Properties. The shell was assumed to be made from 6061-T6 aluminum and to have the following properties:

$$a = 3.0 \text{ in}$$

$$L/a = 2$$

$$h/a = 1/100$$

$$\rho = 2.54 \times 10^{-4} \text{ lb} - \text{sec}^2 - \text{in}^{-4}$$

$$E = 10^7 \text{ psi}$$

$$\nu = 0.3$$

$$\sigma_{yp} = 42 \text{ ksi}$$

$$c = 3.416 \times 10^{-5}$$

where σ_{yp} is the yield point stress of the material. The nondimensional damping coefficient c corresponds to a value determined experimentally by Fung, Sechler, and Kaplan [46]. Yao [6] used the same coefficient in his dynamic stability study.

Initial Imperfection. The existence of a small, but finite, initial imperfection in each mode was postulated. The Fourier coefficients of the initial imperfection were assumed to be of the form

$$\bar{w}^n = w_i^n \sin \left(\frac{\pi \xi}{l} \right) \quad (5.1)$$

where w_i^n is the amplitude of the imperfection in mode n . Except for one special case, the amplitudes of the imperfection were all taken equal to 1/1000th of the shell thickness. The corresponding nondimensional amplitudes were thus

$$w_i^n = 1.0 \times 10^{-5}$$

For the one special case, the imperfection amplitudes were taken from a table of random numbers.

Load. The loading was assumed to be

$$P(x,t) = \begin{cases} 0 & \text{for } t < 0 \\ P_0 e^{-\frac{t}{t_0}} & \text{for } t \geq 0 \end{cases} \quad (5.2)$$

where P_0 is the peak pressure and t_0 is a time constant. The loading is expressed nondimensionally by

$$p(\xi,\tau) = \begin{cases} 0 & \text{for } \tau < 0 \\ p_0 e^{-\frac{\tau}{\tau_0}} & \text{for } \tau \geq 0 \end{cases} \quad (5.3)$$

For this study, $\tau_0 \gg 1$. By integrating the load from $t = -\infty$ to $t = +\infty$, the impulse per unit area is found to be

$$I = P_0 t_0 \quad (5.4)$$

II. PREVIOUS INVESTIGATIONS OF THE PROBLEM

Certain aspects of the problem outlined above have been the topic of two very recent articles. Anderson and Lindberg [19] investigated dynamic buckling under an exponentially decaying, uniform, radial pressure, given by (5.2). McIvor and Lovell [20] computed the dynamic response for a uniform radial impulse, a limiting case of the loading considered here and in Reference [19]. In the following

two sections, these investigations are reviewed in some detail in order to lay the foundation for later comparisons. The simplified equations used by Anderson and Lindberg are examined in considerable detail as they illustrate many of the essential features of the problem.

Anderson and Lindberg's Investigation

Anderson and Lindberg's analysis identified the peak pressure and the total impulse as the important load parameters for determining whether dynamic buckling will occur. When the total impulse was relatively small, they found that buckling occurred at very high pressures; in fact, so high that buckling took place only after the onset of plastic flow. A tangent modulus model was developed for predicting buckling loads in this regime. For loads of large total impulse, buckling occurred at much lower pressures and was governed by an elastic model. Both of these models were developed for the prediction of dynamic buckling loads and were not intended to predict the dynamic response under sub-critical loads. Their elastic model is of interest here and will be used as a standard of comparison.

For their elastic model, they assumed the motion to consist of a uniform radial displacement plus an infinite number of nonaxisymmetric flexural modes. The flexural modes were required to satisfy simply supported boundary conditions, and the axial variation of both the flexural

modes and the initial imperfections was taken to be a half sine wave. These assumptions were satisfied by

$$w = w^0 + \sum_{n=1}^{\infty} w^n \sin \left(\frac{\pi \xi}{l} \right) \cos n\theta$$

for the radial displacement and

$$\bar{w} = \sum_{n=1}^{\infty} w_i^n \sin \left(\frac{\pi \xi}{l} \right) \cos n\theta$$

for the initial imperfection. Finally, the coupling between the flexural modes plus the nonlinear terms in the equations of the axisymmetric mode were neglected. The resulting equations for the undamped motion were

$$\ddot{w}^0 + w^0 = p_0 e^{-\frac{\tau}{\tau_0}} \quad (5.5)$$

$$\frac{\ddot{w}^n}{w_i^n} + \left[\frac{1}{12} \alpha^2 \left(n^2 + \frac{\pi^2}{l^2} \right)^2 + \frac{(1-\nu^2) \left(\frac{\pi}{l} \right)^4}{\left(n^2 + \frac{\pi^2}{l^2} \right)^2} - n^2 w^0 \right] \frac{w^n}{w_i^n} = n^2 w^0$$

$$n = 1, 2, \dots \quad (5.6)$$

Equation (5.6) can be written in the form

$$\frac{\ddot{w}^n}{w_i^n} + n^2 (p_{cr}^n - w^0) \frac{w^n}{w_i^n} = n^2 w^0 \quad n = 1, 2, \dots \quad (5.7)$$

where

$$p_{cr}^n = \frac{1}{n^2} \left[\frac{1}{12} \alpha^2 \left(n^2 + \frac{\pi^2}{l^2} \right)^2 + \frac{(1-\nu^2) \left(\frac{\pi}{l} \right)^4}{\left(n^2 + \frac{\pi^2}{l^2} \right)^2} \right] \quad (5.8)$$

The nondimensional static pressure which will cause classical buckling of the n^{th} mode is equal to p_{cr}^n given by (5.8). The natural frequency of the n^{th} mode, Ω_n , is obtained from (5.7) by equating w^0 to zero, from which

$$\Omega_n^2 = n^2 p_{\text{cr}}^n \quad (5.9)$$

Table II contains the natural frequencies, the natural periods $T_n = 2\pi/\Omega_n$, and the buckling pressures of several of the modes of the shell under consideration. Note that the axisymmetric mode has the highest natural frequency, as was assumed in Chapter IV. Also, mode 6 has the lowest buckling pressure and, thus, is the static buckling mode.¹

Hyperbolic Response. Anderson and Lindberg [19] pointed out that whenever $w^0 > p_{\text{cr}}^n$, the solution of (5.7) is hyperbolic in nature, and the amplitude of the displacement grows in an exponential manner with time. The closed form solution of equation (5.5) is

$$w^0(\tau) = \frac{p_o \tau_o^2}{1 + \tau_o} \left[e^{-\frac{\tau}{\tau_o}} - \cos \tau + \frac{1}{\tau_o} \sin \tau \right] \quad (5.10)$$

when \dot{w}^0 and w^0 are initially zero. As seen from Table II, the frequencies of modes four through eleven are considerably less than Ω_0 , the frequency of the uniform radial mode. Consequently, these modes will not respond

¹Mode 6 is the mode for which $n = 6$. In the sequel, the modes will be referred to in this manner.

TABLE II
NATURAL FREQUENCIES, NATURAL PERIODS,
AND BUCKLING PRESSURES PREDICTED BY
EQUATIONS OF ANDERSON AND LINDBERG [19]^a

n	Ω_n	T_n	$p_{cr}^n \times 10^4$
0	1.0000	6.28	
4	0.1382	45.48	11.93
5	0.1168	53.82	5.45
6	0.1268	49.56	4.47
7	0.1561	40.25	5.08
8	0.1951	32.20	5.95
9	0.2426	25.90	7.27
10	0.2968	21.17	8.81
11	0.3569	17.60	10.53
12	0.4231	14.85	12.43
13	0.4952	12.69	14.51
14	0.5731	10.96	16.75
15	0.6567	9.56	19.17

^aAll quantities are nondimensional.

appreciably to the harmonic oscillation of the axisymmetric motion.² Discarding the harmonic terms gives

$$w^0(\tau) = \frac{p_o \tau_o^2}{1 + \tau_o} e^{-\frac{\tau}{\tau_o}}$$

Since $\tau_o \gg 1$ for the loadings of interest to the present study, the above equation reduces to

$$w^0(\tau) = p_o e^{-\frac{\tau}{\tau_o}}$$

which represents the quasi-static response of the axisymmetric mode to the applied load. Substituting this result into (5.7) yields

$$\frac{\ddot{w}^n}{w_i^n} + n^2 (p_{cr} - p_o e^{-\frac{\tau}{\tau_o}}) \frac{w^n}{w_i^n} = n^2 p_o e^{-\frac{\tau}{\tau_o}} \quad (5.11)$$

As pointed out earlier, the solution of (5.11) is hyperbolic in nature when $p_o e^{-\frac{\tau}{\tau_o}} > p_{cr}^n$. Hence, as long as the pressure $p_o e^{-\frac{\tau}{\tau_o}}$ exceeds the critical pressure of any one of the modes, that mode will grow in an exponential manner. Such modes will be referred to as "hyperbolic" modes.

By virtue of their simplified analysis, Anderson and Lindberg [19] were able to express the response of the n^{th} mode in terms of the amplification ratio w^n/w_i^n , as can be

²The results of McIvor and Lovell [20] show this to be true.

seen in (5.6). They showed that an amplification of 1000 is tantamount to permanent buckling. The equations of the present analysis can not be solved directly for the amplification due to the nonlinear terms in the equations. However, once a solution is obtained, the amplification of each mode can be computed, based upon the values given to w_i^n ; and direct comparisons can be made with the results of Reference [19].

Mathieu Instability. A mode can also be excited to large amplitude through the mechanism of parametric resonance, or Mathieu instability. For $\tau_0 \gg 1$, the essential features of the mechanism are present when (5.10) is reduced to

$$w^0(\tau) = p_0 (e^{-\tau/\tau_0} - \cos \tau) \quad (5.12)$$

Substituting (5.12) into (5.7) and making use of (5.9) lead to

$$\ddot{w}^n + (\Omega_n^2 - n^2 p_0 e^{-\tau/\tau_0} + n^2 p_0 \cos \tau) w^n = n^2 p_0 (e^{-\tau/\tau_0} - \cos \tau) w_i^n \quad (5.13)$$

If $\tau \gg \tau_0$ and $w_i^n = 0$,³ (5.13) reduces to Mathieu's equation

$$\ddot{w}^n + (\Omega_n^2 + n^2 p_0 \cos \tau) w^n = 0 \quad (5.14)$$

³The assumption that $\tau \gg \tau_0$ is not valid for the present problem. Consequently, the stability chart of (5.14) does not adequately identify the Mathieu modes.

There are two possible solutions to (5.14), both of them oscillatory. However, one of them grows unbounded with increasing time, while the other remains bounded. The unbounded growth is known as parametric resonance or dynamic instability. The name Mathieu mode, as used in the sequel, is given to any mode that grows to large amplitude in an oscillatory manner.

The stability boundaries for the solutions of (5.14) are well documented [7, 47] and are shown by Figure 5.1. If a point $(\Omega_n^2, n^2 p_0)$ falls in the unstable region, the solution for that mode will grow without bound. The stability chart shows that when the frequency of a flexural mode is approximately one-half of the axisymmetric natural frequency ($\Omega_0 = 1.0$), the response of that flexural mode will be unstable, even for a very small peak pressure. The points corresponding to modes 12, 13, 14, and 15 for the shell considered here are shown in Figure 5.1.

Anderson and Lindberg [19] were interested in predicting the critical buckling loads. From experimental results, they knew that dynamic buckling occurs as the result of very rapid growth of the buckling mode accompanied by very little oscillatory motion. However, the Mathieu instability occurs in an oscillatory manner requiring several cycles before the displacements become large. Furthermore, when the amplitude of a Mathieu mode becomes large enough to cause plastic flow, energy will be dissipated, the axisymmetric oscillations will decay,

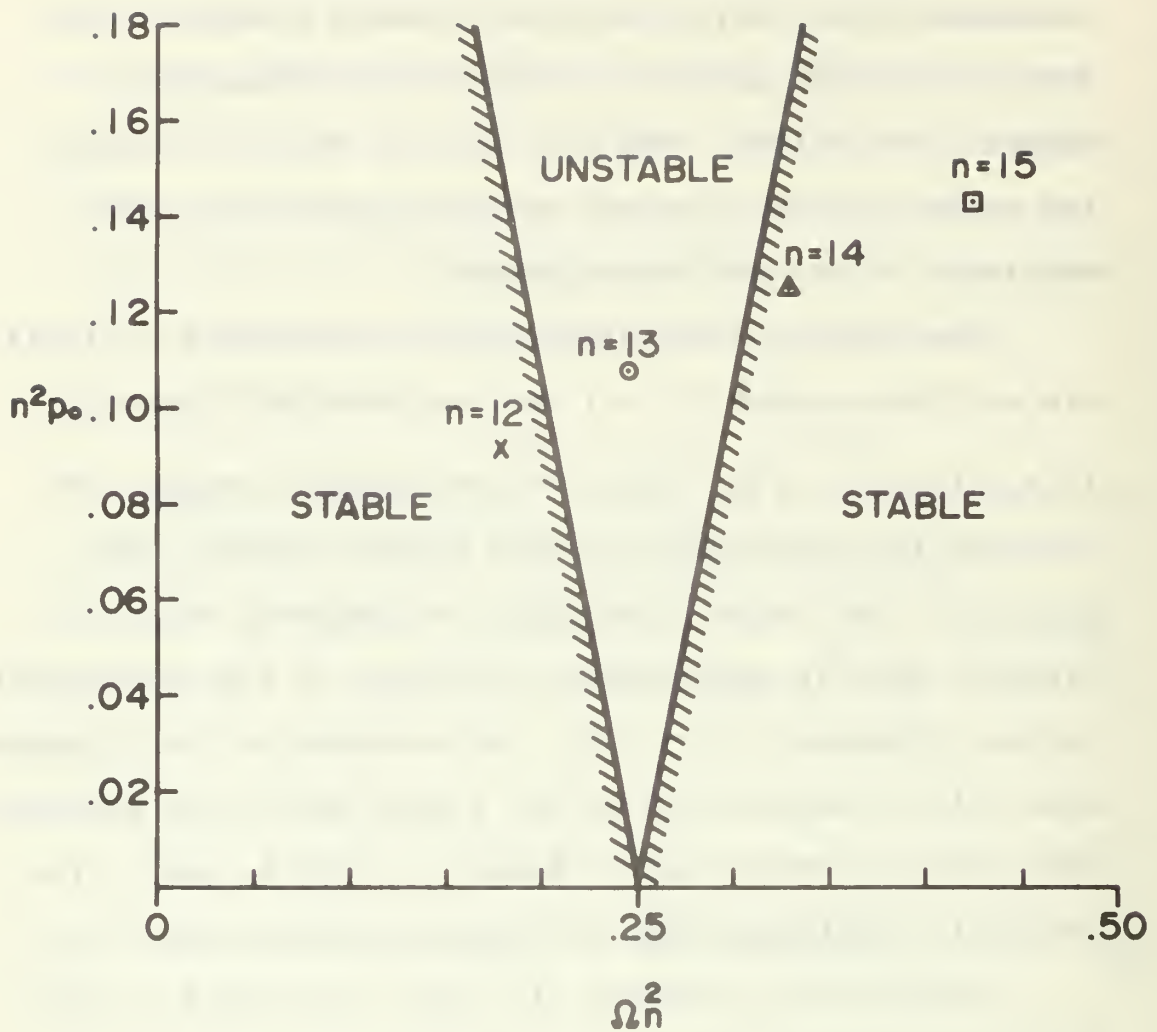


FIGURE 5.1
MATHIEU STABILITY CHART FOR HARMONIC
UNIFORM PRESSURE

and subsequent growth of the Mathieu mode would most likely not occur.⁴ Consequently, they were able to disregard the response of the Mathieu modes.

McIvor and Lovell's Contribution

Under impulsive loads, the initial growth of the flexural modes is governed by the Mathieu equation. The impulsive response of the axisymmetric mode can be obtained from (5.10) by taking the limit as τ_0 goes to zero while the product $p_0 \tau_0$ remains constant. The result is

$$w^0(\tau) = p_0 \tau_0 \sin \tau \quad (5.15)$$

Substituting (5.15) into (5.7) and making use of (5.9) lead to

$$\ddot{w}^n + (\Omega_n^2 - n^2 p_0 \tau_0 \sin \tau) w^n = w_i^n n^2 p_0 \tau_0 \sin \tau \quad (5.16)$$

If $w_i^n = 0$, (5.16) reduces to the Mathieu equation

$$\ddot{w}^n + (\Omega_n^2 - n^2 p_0 \tau_0 \sin \tau) w^n = 0 \quad (5.17)$$

McIvor and Lovell's investigation [20] was concerned with the undamped response to purely impulsive loads. With an equation similar to (5.17), they identified the Mathieu modes from a stability chart. The total deflection was assumed to consist of the Mathieu modes plus the axisymmetric mode. An energy balance revealed that the

⁴The axisymmetric oscillations are due to the initial conditions. Thus, there is a limited amount of energy in them. Once this energy is dissipated, they will no longer exist; and the mechanism for dynamic instability is removed.

response of the neglected modes was, in fact, negligible. All of the nonlinear coupling between the modes was retained. During the response, the modes underwent beat-like oscillations accompanied by a cyclic exchange of energy between the modes. The maximum amplitude of a mode did not always occur during the first beat, sometimes occurring during the second beat. The stresses developed during the response to an impulse were several times higher than the stresses of an axisymmetric response to the same impulse. Furthermore, the largest stress usually did not occur during the first significant exchange of energy, but occurred later when several modes were nearly in phase. The maximum amplitudes attained by the flexural modes were nearly independent of the magnitudes of the perturbation in each mode; however, the phasing between the modes was affected by the magnitudes of the perturbation.

III. INVESTIGATION OF THE PROBLEM BY THE METHODS DEVELOPED IN THIS STUDY

Preliminaries

Minimum Number of Axial Grid Points. In order to minimize the computing time, the number of axial stations was kept as small as reasonable accuracy permitted. The criteria used for assessing the adequacy of a given number of stations were: (1) the accuracy of the circumferential in-plane forces, (2) the accuracy of the amplification

factors, and (3) the accuracy of the representation of the axial variation of the radial displacements.

Since the load and the initial imperfection were assumed to be symmetric with respect to the midspan of the shell, it would not be unreasonable to expect the response to also be symmetric with respect to the midspan. If true, this would effect a considerable savings in the computing time. Two fully nonlinear solutions were computed to determine whether or not the response was indeed symmetric. The first run employed the simple support conditons at both ends of the shell and fourteen axial stations. The second run used the midspan symmetry conditons and seven axial stations. The displacements of the two solutions were identical to at least four significant figures. Therefore, the response for this problem was assumed to be symmetric with respect to the midspan of the shell.

A series of computer runs was made using a different number of axial stations over the half-length of the shell for each run. There were no significant differences in the results when nine, eleven, or thirteen axial stations were used along one-half of the shell. However, when the number of stations was reduced to seven, the error in the circumferential in-plane force was approximately 7 per cent near the end of shell; and smaller errors were noted in the radial displacements and the amplification factors.

Consequently, nine stations over the half-span of the shell were used for the solutions presented in the following sections of this chapter.

Selection of the Participating Modes. Since the computer program is dimensioned to accomodate a maximum of fifteen Fourier modes,⁵ the series expansions for the displacements had to be truncated. However, the truncated series was not restricted to the first fifteen modes, modes 0 through 14. Instead, the participating modes were selected to include only those expected to respond to the particular loading condition. The procedure used for selecting the responding modes can best be explained by an example.

Consider the loading

$$P(t) = 70 e^{-t/.003} \quad (5.18)$$

Comparing the 70 psi ($p_0 = 6.37 \times 10^{-4}$) peak pressure with the buckling pressures listed in Table II reveals that modes 5 through 8 should exhibit hyperbolic behavior during the early phases of the response. Hence, these modes were included in the series.

Identifying the Mathieu modes is a little more difficult. As a result of the assumptions made to arrive at (5.14), the stability chart of Figure 5.1 is not sufficient

⁵The number of modes is limited primarily by computing time.

to identify the Mathieu modes. Consequently, a procedure was used that investigated the stability of each of the possible Mathieu modes. For example, Table II shows that modes 12 through 15 are possible Mathieu modes since they have frequencies lying in the neighborhood of one-half the frequency of the axisymmetric mode. To determine which of these modes were Mathieu modes, the series was truncated so that only modes 0 and 12 through 15 were retained. As a result of this choice of Fourier indices, each of the flexural modes couples only with mode zero.⁶ Finally, the coupling terms in the equations of mode 0 were equated to zero by a simple alteration of the computer program. This eliminated the mechanism for the extraction of energy from the mode zero oscillation. The resulting equations of motion of the flexural modes resembled Mathieu's equation, and any mode that grew to a large amplitude under these circumstances was assumed to be a Mathieu mode. A computer run was carried out based on this procedure using the pressure given by (5.18). The

⁶The modes which couple are determined by forming all combinations of sums and differences of the Fourier numbers in the series. If any sum or difference equals any of the Fourier numbers in the series, then the two Fourier numbers contributing to that sum or difference are said to couple with the third mode. For example, modes 3 and 5 couple to influence modes 2 and 8 since $3 + 5 = 8$ and $5 - 3 = 2$. Mode 13 couples with itself to influence modes 0 and 26 since $13 - 13 = 0$ and $13 + 13 = 26$. For a more detailed explanation see Appendix B, Reference [30].

results are given in Table III. The maximum amplification listed in the table is defined as the maximum value of the ratio

$$\frac{|w_i^n|}{|\bar{w}_i^n|} \quad (5.19)$$

where station i is the whole station nearest to the midspan of the shell. From Table III, mode 14 can be readily identified as a Mathieu mode. However, as shown in Figure 5.1, the Mathieu stability chart of (5.14) indicates that mode 13 should be the unstable mode.

A possible explanation of this discrepancy can be surmised by considering (5.13). When w_i^n is equal to zero, (5.13) reduces to

$$\ddot{w}^n + (\Omega_n^2 - n^2 p_o e^{-\tau/\tau_o} + n^2 p_o \cos \tau) w^n = 0 \quad (5.20)$$

TABLE III
RESPONSE OF INDIVIDUAL MODES WITHOUT
EXTRACTION OF ENERGY FROM AXISYMMETRIC MODE

$$p_o = 6.37 \times 10^{-4}, \tau_o = 208$$

Mode	Maximum Amplification Attained During Interval $\tau = 0$ to 140
12	1.8
13	1.8
14	1990.0
15	3.4

This equation is similar to the Mathieu equation, except that Ω_n^2 has been replaced by

$$\Omega_n^2 = n^2 p_0 e^{-\tau/\tau_0} \quad (5.21)$$

The quantity expressed by (5.21) can be thought of as a time varying frequency of the n^{th} mode. If this quantity is plotted along the abscissa of the Mathieu stability chart instead of Ω_n^2 , as in Figure 5.2, the points associated with the flexural modes 12, 13, 14 and 15 move horizontally across the chart as τ increases.

Examination of Figure 5.2 reveals that at $\tau = 0$, modes 12 and 13 are in the stable regions, and modes 14 and 15 are unstable. In computing the amplifications listed in Table III, the integration was terminated at $\tau = 140$. During that time interval, modes 12 and 13 grew very little; mode 14 was amplified nearly two thousand times; and mode 15 was amplified 3.4 times. These results can be correlated with the trajectories of the corresponding points in Figure 5.2. During the interval of integration, modes 12 and 13 remained in a stable region, but mode 14 remained in the unstable region. Mode 15, which was initially in an unstable region, quickly moved into a stable region. Since growth to a large amplitude requires several oscillations of the axisymmetric mode, mode 15 moved into a stable region before having time to grow appreciably. Had the integration continued, mode 13 would have entered the unstable region; but mode 12 would have remained stable.

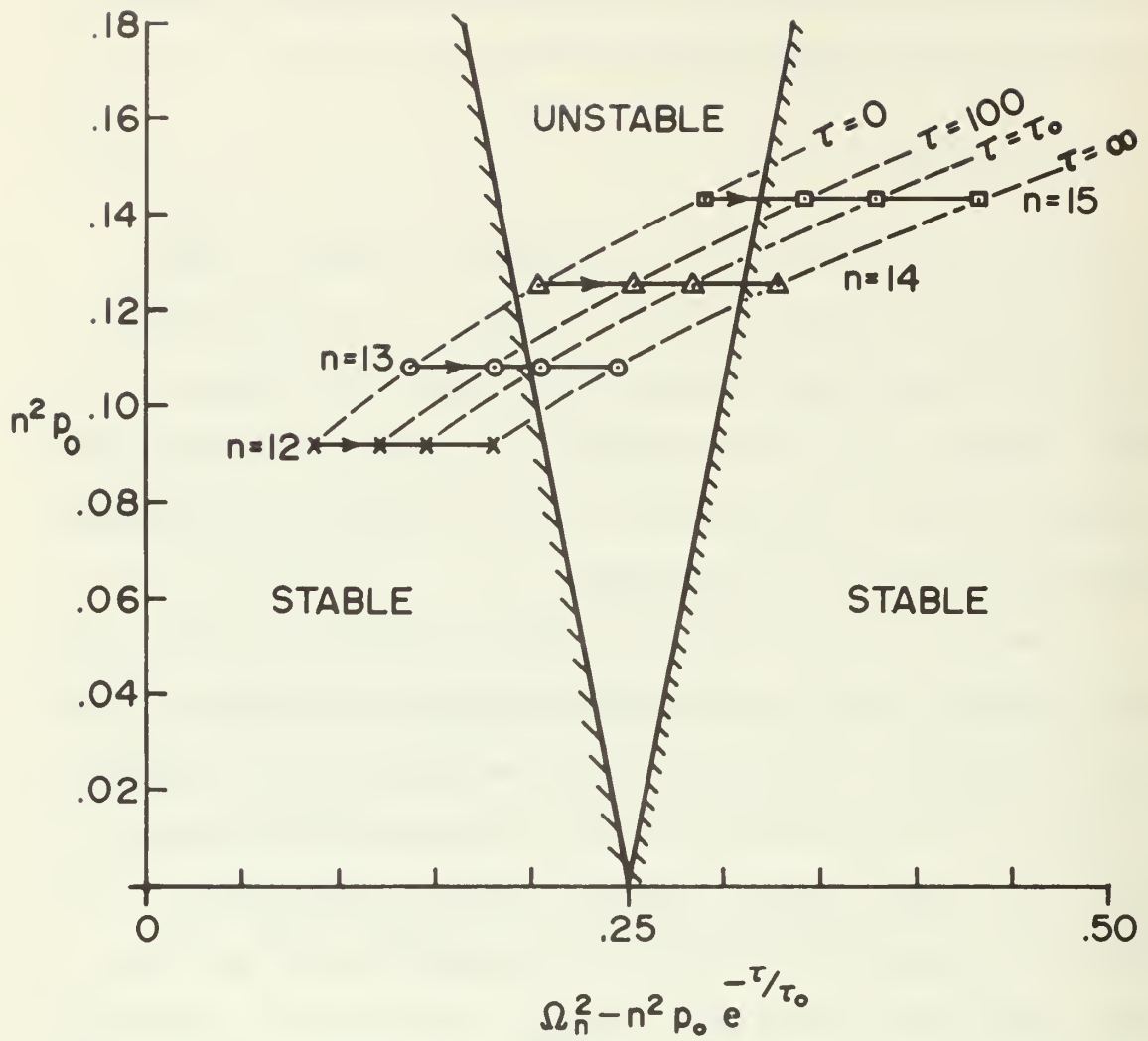


FIGURE 5.2
 MATHIEU STABILITY CHART FOR EXPONENTIALLY
 DECAYING UNIFORM PRESSURE
 $P_0 = 70 \text{ psi}$ ($p_0 = 6.37 \times 10^{-4}$), $t_0 = 3.0 \text{ msec}$ ($\tau_0 = 208$)

As a consequence of this correlation the stability chart of Figure 5.2, which is based on the simplified equations of Reference [19], was considered to be adequate for identifying the Mathieu modes for the problem under consideration. To identify the Mathieu modes for a problem with different loading conditions, it might be necessary to make several preliminary computer runs similar to the one described above.

When computing a fully coupled nonlinear solution for the loading given by (5.18), modes 0, 1, 4, 5, 6, 7, 8, 9, 10, 13, 14, and 15 were retained in the Fourier expansions. Note that modes 4, 9, and 10, modes in the neighborhood of the hyperbolic modes, were retained. The Mathieu modes that were retained included all modes whose trajectories in Figure 5.2 passed through the unstable region. Finally, mode 1 was also included because it becomes involved in the coupling of all the modes whose wave numbers differ by unity.⁷ The adequacy of this choice of modes was established by computing a solution in which modes 0 through 14 were retained. The extra modes, 2, 3, 11, and 12, did not respond appreciably; and including them did not alter the response of the other modes.

⁷In the Donnell theory mode 1 is inaccurately described for many classes of shells. However, if the shell is thin and $L/a \leq 2$, as is the case here, the representation of mode 1 is reasonably accurate [48].

Results

Computer solutions were generated for four specific cases, hereafter referred to as A, B, C, and D.⁸ In cases A and B, the damping coefficient c was taken equal to zero, while in cases C and D, $c = 3.416 \times 10^{-5}$. Cases A and C were each composed of three runs with $t_0 = 3.0$ msec ($\tau_0 = 208$) and P_0 equal to 60 psi ($p_0 = 5.46 \times 10^{-4}$), 70 psi ($p_0 = 6.37 \times 10^{-4}$), and 77 psi ($p_0 = 7.01 \times 10^{-4}$). Cases B and D were also composed of three runs each, but at three different peak pressures with $t_0 = 1.0$ msec ($\tau_0 = 69.3$). The results for these cases will be compared with the results obtained by Anderson and Lindberg [19] and McIvor and Lovell [20].

The significance of the amplitudes of the initial imperfection modes was also investigated by computing a solution in which the amplitudes w_i^n were taken from a table of random numbers. Finally, some results are presented to show the importance of the nonlinear coupling between the modes

Case A. The results for this series of runs are summarized in Table IV. The first column shows the Fourier indices of the modes included in the solution. The second column shows the maximum amplification of each flexural mode, as given by (5.19). The third column contains the

⁸A typical solution required approximately 45 minutes on the IBM 360/67.

TABLE IV

CASE A, AMPLIFICATIONS AND STRESSES

 $t_0 = 3.0$ msec ($\tau_0 = 208$), ZERO DAMPING $P_0 = 60$ psi $: p_0 = 5.46 \times 10^{-4}$

Maximum circumferential stress = 21,600 psi

Maximum circumferential stress occurred at $\tau = 116$ Integration terminated at $\tau = 118$

mode	maximum amp.	τ for maximum amp.
0		
1	.72	110.4
4	1.53	27.83
5	11.22	52.67
6	41.02	72.05
7	24.15	52.79
8	9.18	33.77
9	4.60	20.13
13	1.94	117.6
14	97.39	116.4
15	1.56	116.6

 $P_0 = 70$ psi $: p_0 = 6.37 \times 10^{-4}$

Maximum circumferential stress = 32,200 psi

Maximum circumferential stress occurred at $\tau = 165$ Integration terminated at $\tau = 198$

mode	maximum amp.	τ for maximum amp.
0		
1	7.93	190.6
4	2.22	88.35
5	26.70	71.71
6	222.3	97.35
7	101.7	72.23
8	22.02	40.37
9	7.84	26.41
10	4.15	19.43
13	3.80	193.8
14	229.2	164.6
15	4.06	162.8

TABLE IV Continues

$P_O = 77 \text{ psi}$	$: p_O = 7.01 \times 10^{-4}$
------------------------	-------------------------------

Maximum circumferential stress = 64,300 psi

Maximum circumferential stress occurred at $\tau = 125$

Integration terminated at $\tau = 166$
--

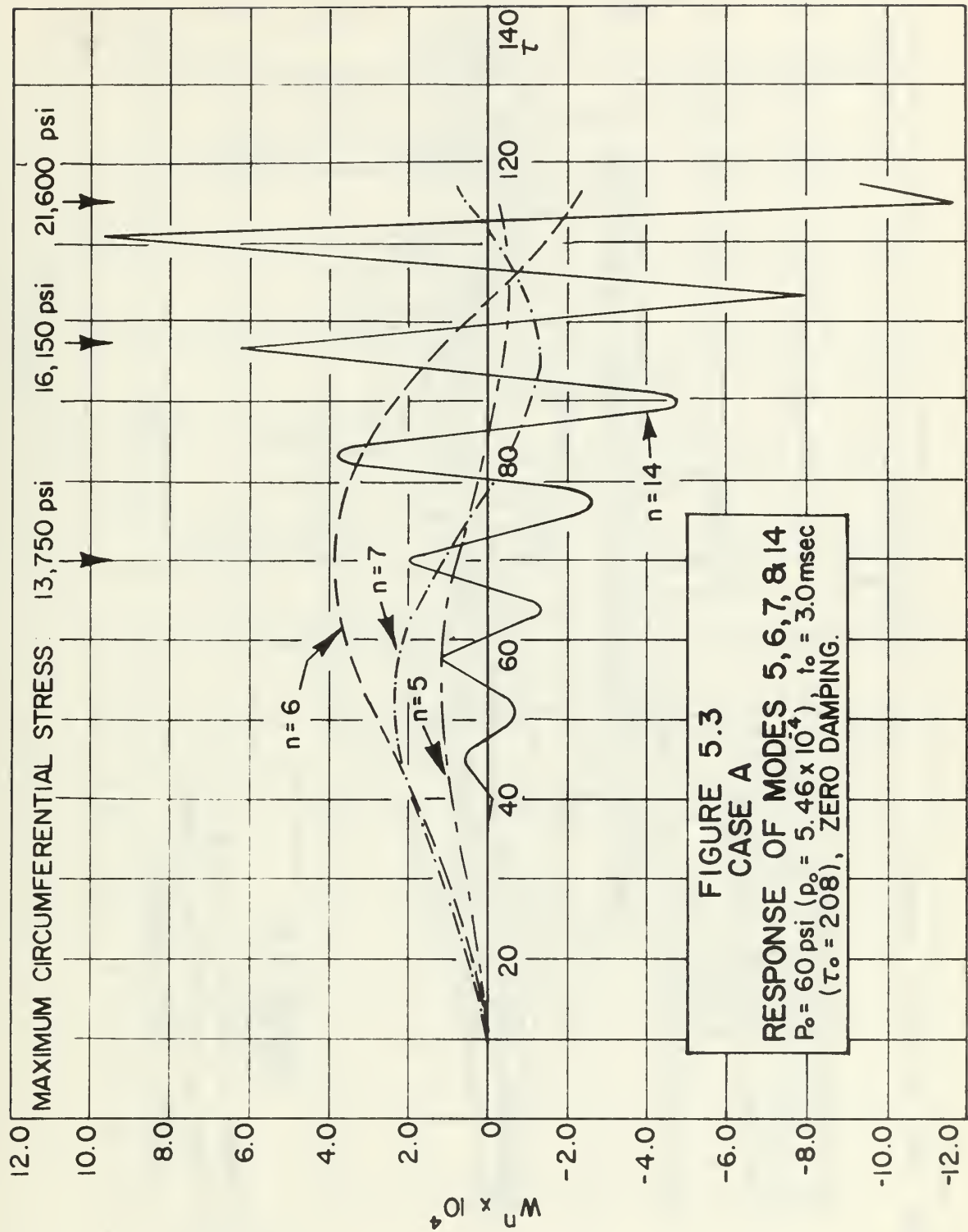
mode	maximum amp.	τ for maximum amp.
------	--------------	-------------------------

0		
1	126.8	116.7
4	10.90	159.7
5	134.7	135.0
6	1411.	127.4
7	423.8	90.96
8	97.20	118.3
9	25.80	118.9
10	7.79	145.3
13	116.6	145.4
14	239.5	144.1
15	41.17	157.7

nondimensional time at which the maximum amplification occurred. The magnitude of the maximum circumferential stress at $\theta = 0^\circ$, as given by (4.31), and the nondimensional time of its occurrence are also listed. Finally, the nondimensional time at which the run was terminated is indicated.⁹

The time histories of the radial displacements at the whole station nearest to the midspan are shown in Figures 5.3-5.5 for the four or five modes that attained the largest amplifications. In addition, the Figures are

⁹The nondimensional period of the axisymmetric mode is approximately equal to 2π .



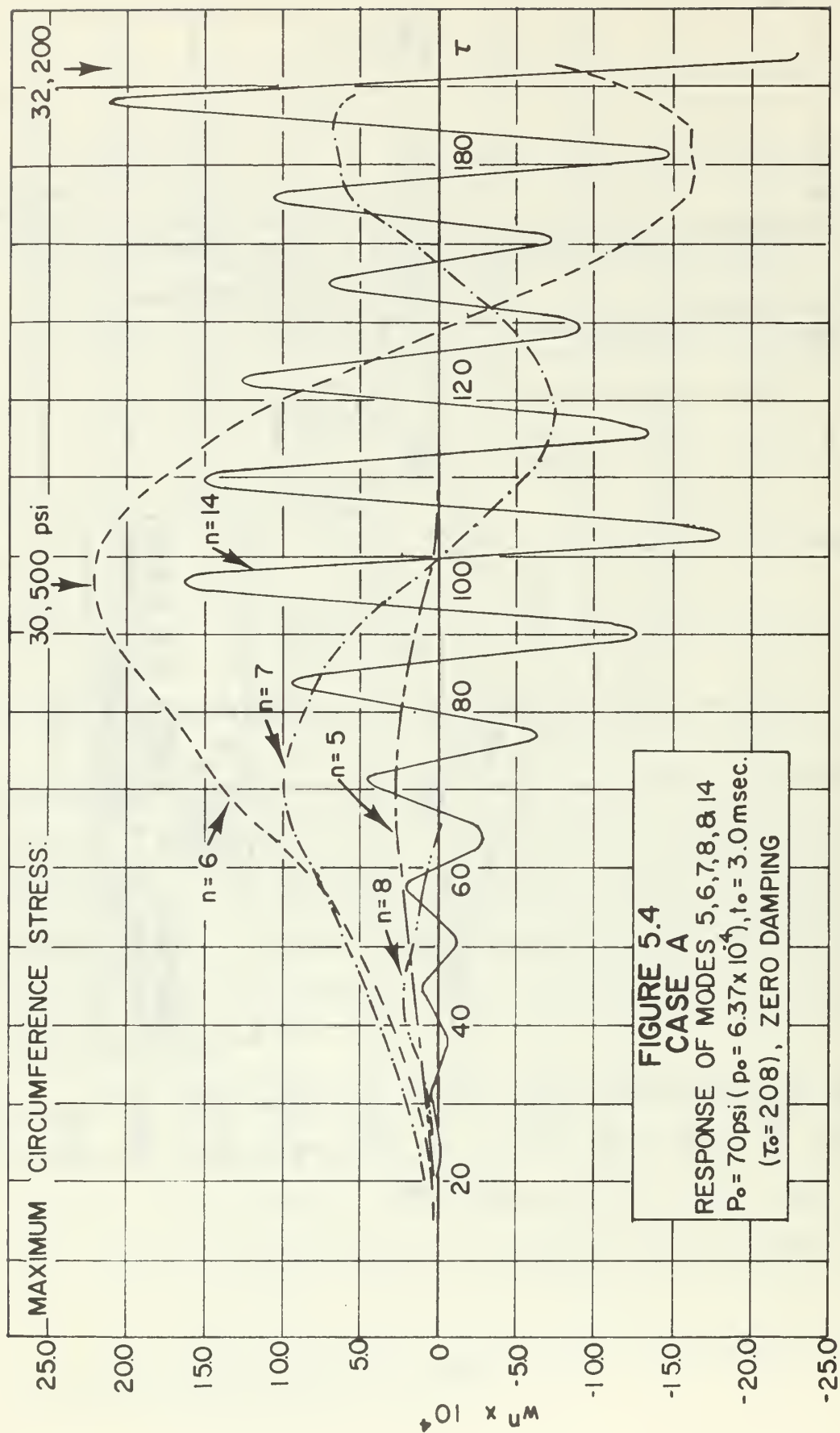


FIGURE 5.4
CASE A
 RESPONSE OF MODES 5, 6, 7, 8, & 14
 $P_0 = 70 \text{ psi}$ ($p_0 = 6.37 \times 10^4$), $t_0 = 3.0 \text{ msec.}$
 ($\tau_0 = 208$), ZERO DAMPING

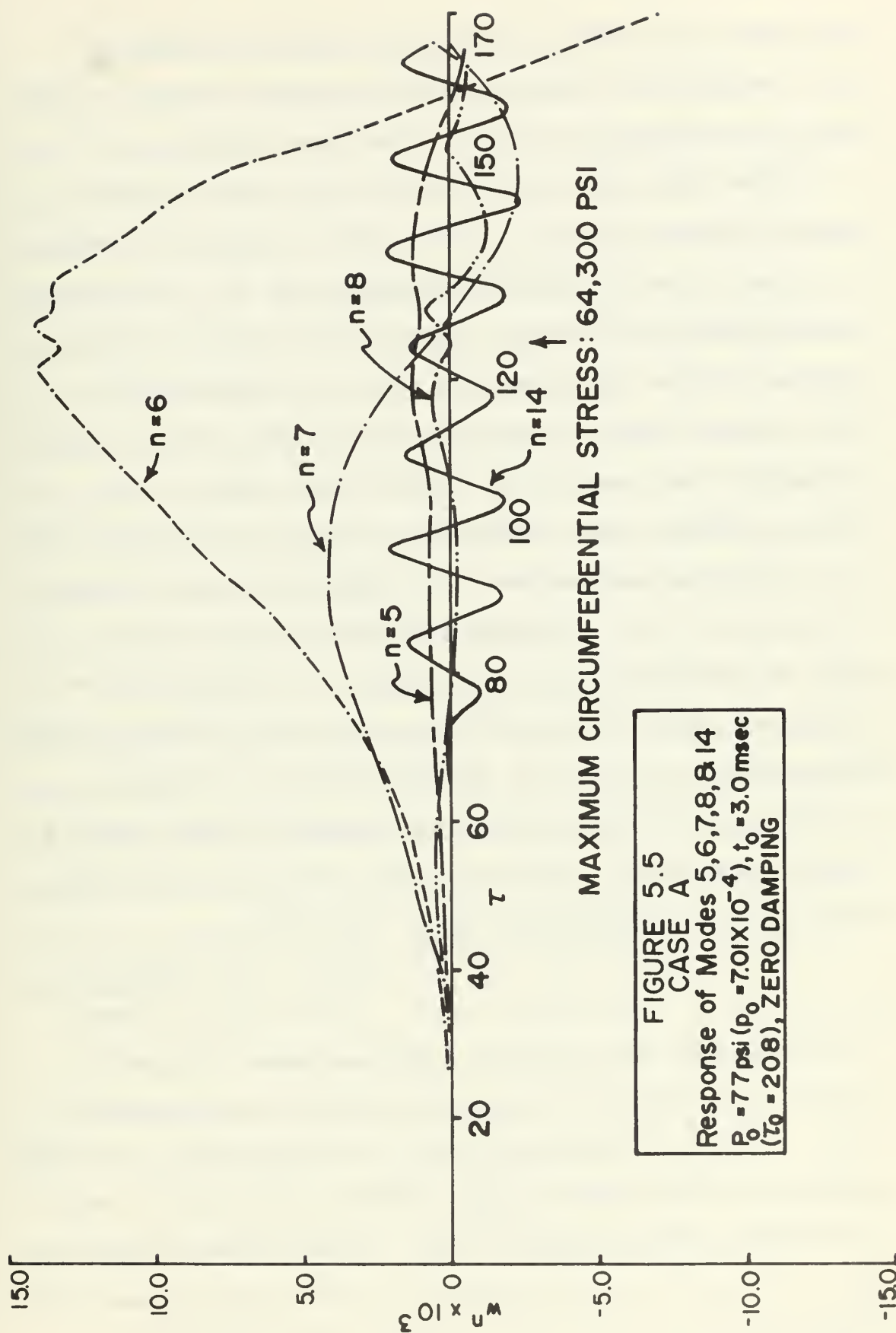


FIGURE 5.5
CASE A
Response of Modes 5, 6, 7, 8, & 14
 $P_0 = 7.7 \text{ psi}$ ($p_0 = 7.01 \times 10^{-4}$), $t_0 = 3.0 \text{ msec}$
($\tau_0 = 208$), ZERO DAMPING

annotated with values of the circumferential stress to show the times at which a relative maximum occurred. Note the different scales for w^n in the three Figures.

From Table IV, it can be seen that when the peak pressure was 60 psi ($p_0 = 5.46 \times 10^{-4}$), hyperbolic modes 5, 6, and 7 grew to large amplitudes, and that the growth occurred during the early phases of the response. Examination of Table II shows that these are precisely the modes having static buckling pressures less than the peak pressure of the load pulse. Furthermore, mode 6, the static buckling mode, attained a larger amplification than the other hyperbolic modes. If comparisons are made for the other two runs, similar observations can be made.

In the third run, mode 1 grew to an amplification of 126.8 just prior to the peaking out of the hyperbolic modes. This growth of mode 1 was very likely due to coupling between the hyperbolic modes that produced large coupling terms in the mode 1 equations. The reason for including mode 1 in the truncated series is now clear.

In all three runs, mode 14 attained the largest amplification of the Mathieu modes. Inspection of Figures 5.3-5.5 reveals that mode 14 underwent beat-like oscillations requiring several cycles to attain a maximum amplitude. However, it was not clear in any run that the largest amplitude of the Mathieu modes had occurred prior to the termination of the computer run. In fact, the information shown in Figure 5.2 indicates that mode 13 would have grown large for $\tau > \tau_0$.

Comparison of the time histories for the three runs reveals that at the lower peak pressures, the Mathieu mode dominated the response. As shown in Figure 5.3, the amplification attained by mode 14 was more than twice as large as the amplification of any of the hyperbolic modes. Furthermore, the largest stresses occurred as a result of the growth of the Mathieu mode. As the peak pressure and the total impulse $P_0 t_0$ were increased, the amplifications of both the Mathieu mode and hyperbolic modes were of about equal magnitude, as shown in Figure 5.4. Figure 5.5 shows that at the highest pressure and impulse, the hyperbolic modes dominated, and the maximum stresses occurred as a result of their growth.

In Figure 5.6, the maximum amplification of the hyperbolic mode 6 is plotted against the peak pressure and, equivalently, the total impulse. Assuming an amplification of 1000 to be the dynamic buckling limit,¹⁰ Figure 5.6 shows that the buckling pressure is 76 psi when the total impulse is 228 psi-msec. Note the logarithmic scale for the amplification factor.

Case B. For the runs of case B, the time constant of the decaying load was reduced to 1.0 msec ($\tau_0 = 69.3$); and the pressures for the three runs were 100 psi ($p_0 = 9.10 \times 10^{-4}$), 110 psi ($p_0 = 10.01 \times 10^{-4}$), and 120 psi ($p_0 = 10.92 \times 10^{-4}$). The hyperbolic modes were 5, 6,

¹⁰Anderson and Lindberg [19] also used this criterion.

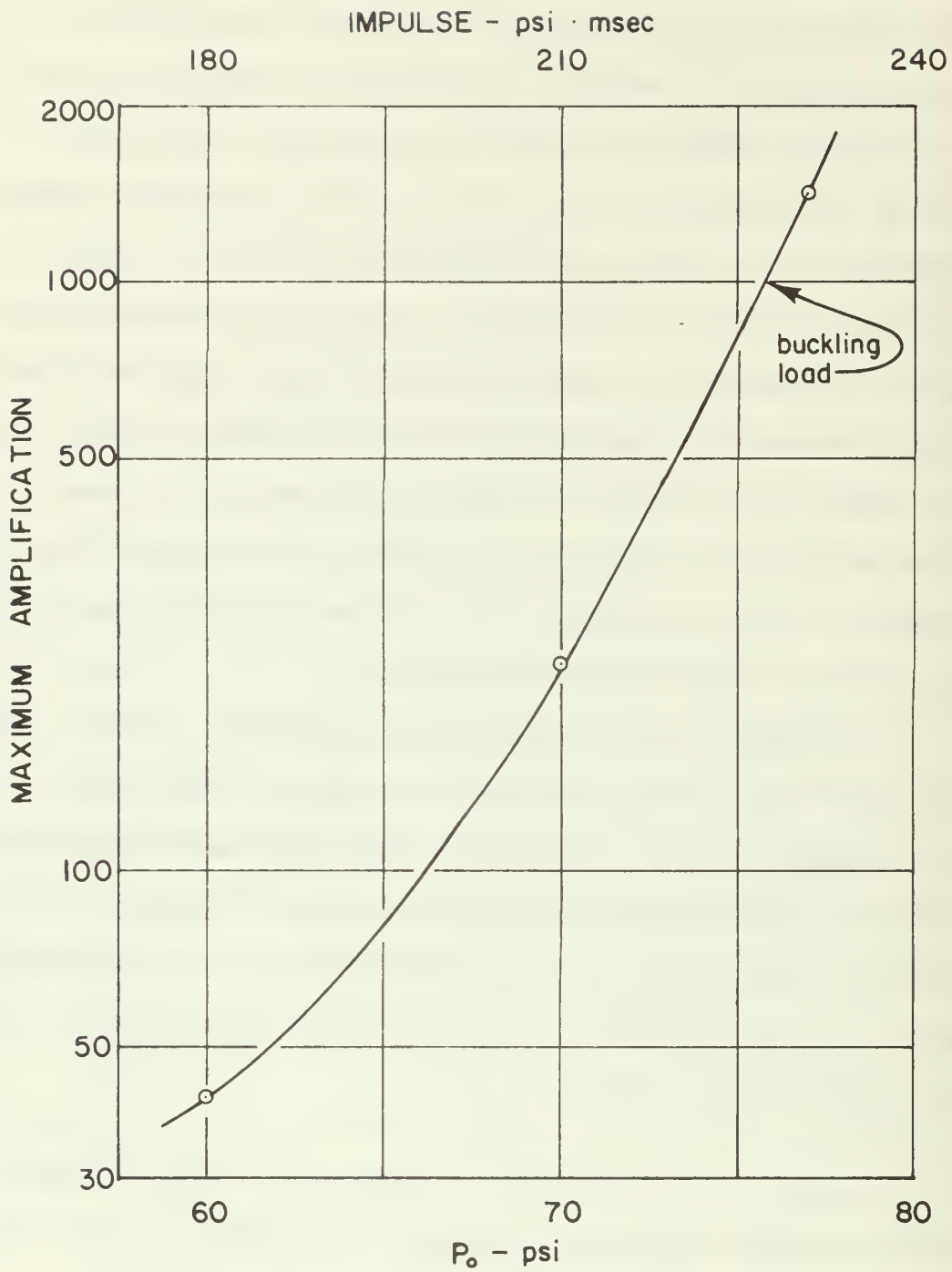


FIGURE 5.6
CASE A
MAXIMUM AMPLIFICATION OF HYPERBOLIC
MODES

7, 8, and 9, all of which have buckling pressures less than the peak pressures of the loads. In addition, modes 4 and 10 were included. The Mathieu modes were identified from a stability chart similar to Figure 5.2 and included modes 13, 14, and 15 at the lowest peak pressure plus mode 12 at the two higher peak pressures. As with case A, the damping coefficient was set to zero. Two of the runs were computed out to $\tau = 200$; and the third, to $\tau = 150$. The results are summarized in Table V.

As in Case A, the character of the response changed considerably as the peak pressure and the total impulse were increased. When $P_0 = 100$ psi ($p_0 = 9.10 \times 10^{-4}$), the maximum amplifications of the Mathieu modes were roughly twice as large as the amplifications of the hyperbolic modes. For the second solution, the peak pressure was equal to 110 psi; and the maximum amplifications of the hyperbolic and Mathieu modes were approximately equal. The loading of the final run was near the critical dynamic buckling limit and boosted the hyperbolic mode 6 to an amplification of 832.6. The largest amplification of the Mathieu modes was 340.6. The maximum stress occurred well after the hyperbolic modes had passed their peak amplifications in the first and second runs. On the other hand, the largest stress occurred in conjunction with the large response of the hyperbolic modes in the last run.

TABLE V

CASE B, AMPLIFICATIONS AND STRESSES

 $t_o = 1.0$ msec ($\tau_o = 69.3$), ZERO DAMPING

$P_o = 100 \text{ psi}$		$: p_o = 9.10 \times 10^{-4}$
Maximum circumferential stress = 55,000 psi		
Maximum circumferential stress occurred at $\tau = 199$		
Integration terminated at $\tau = 200$		
mode	maximum amp.	τ for maximum amp.
0		
1	96.15	197.7
4	5.34	185.6
5	32.85	58.55
6	134.2	65.44
7	119.7	52.72
8	51.77	40.24
9	20.38	156.6
10	9.64	19.79
11	13.85	182.9
13	331.0	196.2
14	245.1	77.09
15	73.04	193.9

$P_o = 110 \text{ psi}$		$: p_o = 10.01 \times 10^{-4}$
Maximum circumferential stress = 65,500 psi		
Maximum circumferential stress occurred at $\tau = 117$		
Integration terminated at $\tau = 200$		
mode	maximum amp.	τ for maximum amp.
0		
1	77.55	125.1
4	14.82	179.6
5	57.19	63.56
6	291.5	71.22
7	256.7	59.28
8	106.1	46.52
9	54.66	172.8
10	17.88	131.4
11	51.86	195.6
12	226.5	184.2
13	273.2	184.1
14	258.7	112.5
15	138.6	169.6

TABLE V Continued

$p_o = 120 \text{ psi}$		$: p_o = 10.92 \times 10^{-4}$
Maximum circumferential stress = 76,200 psi		
Maximum circumferential stress occurred at $\tau = 57$		
Integration terminated at $\tau = 150$		
mode	maximum amp.	τ for maximum amp.
0		
1	148.6	78.31
3	36.77	100.3
4	34.58	136.3
5	160.5	81.54
6	832.6	82.50
7	656.4	66.93
8	218.2	52.06
9	70.54	77.54
10	45.48	128.4
11	30.94	135.7
12	152.8	114.2
13	274.4	141.0
14	340.6	113.6
15	250.3	98.83

The behavior of the Mathieu modes reflected the shorter time constant and the higher peak pressures. In all three runs, all of the included Mathieu modes grew to significant amplitudes. Again this can be explained by the stability chart of Figure 5.2. As $n^2 p_o$ is increased, the trajectories of the Mathieu modes are shifted upward and extended in length to the left; the reduced time constant causes the points corresponding to the modes to move across the chart at a faster rate. The net result was that modes 12, 13, and 15, as well as 14, were in the unstable region sufficiently long to respond.

Note that in all three runs, the stress exceeded 42 ksi, the yield point stress of the shell material, while the amplifications of the hyperbolic modes never exceeded 1000, the dynamic buckling limit used by Anderson and Lindberg [19].

The maximum amplification of the hyperbolic modes as a function of the peak pressure and the total impulse is shown in Figure 5.7. An amplification of 1000 corresponds to a pressure of approximately 122 psi.

Comparison with Anderson and Lindberg's Findings.

Anderson and Lindberg [19] identified the peak pressure P_0 and the total impulse $P_0 t_0$ as the significant parameters in the dynamic buckling problem. Their dynamic buckling curve, along which the maximum amplification of the hyperbolic modes was 1000, is shown in Figure 5.8. The sharp break in the curve divides the regime of the elastic model, on the lower right, from the regime of the tangent modulus model, at the upper left. As the impulse of the load goes to infinity, corresponding to a step load, the dynamic buckling curve approaches the static buckling pressure line. The dynamic curve shows that the shell can endure a pulse having a peak pressure larger than the static buckling pressure, with the critical peak pressure depending on the total impulse of the load. While Anderson and Lindberg's model gives the dynamic buckling curve, it does not predict the response in the region lying below the

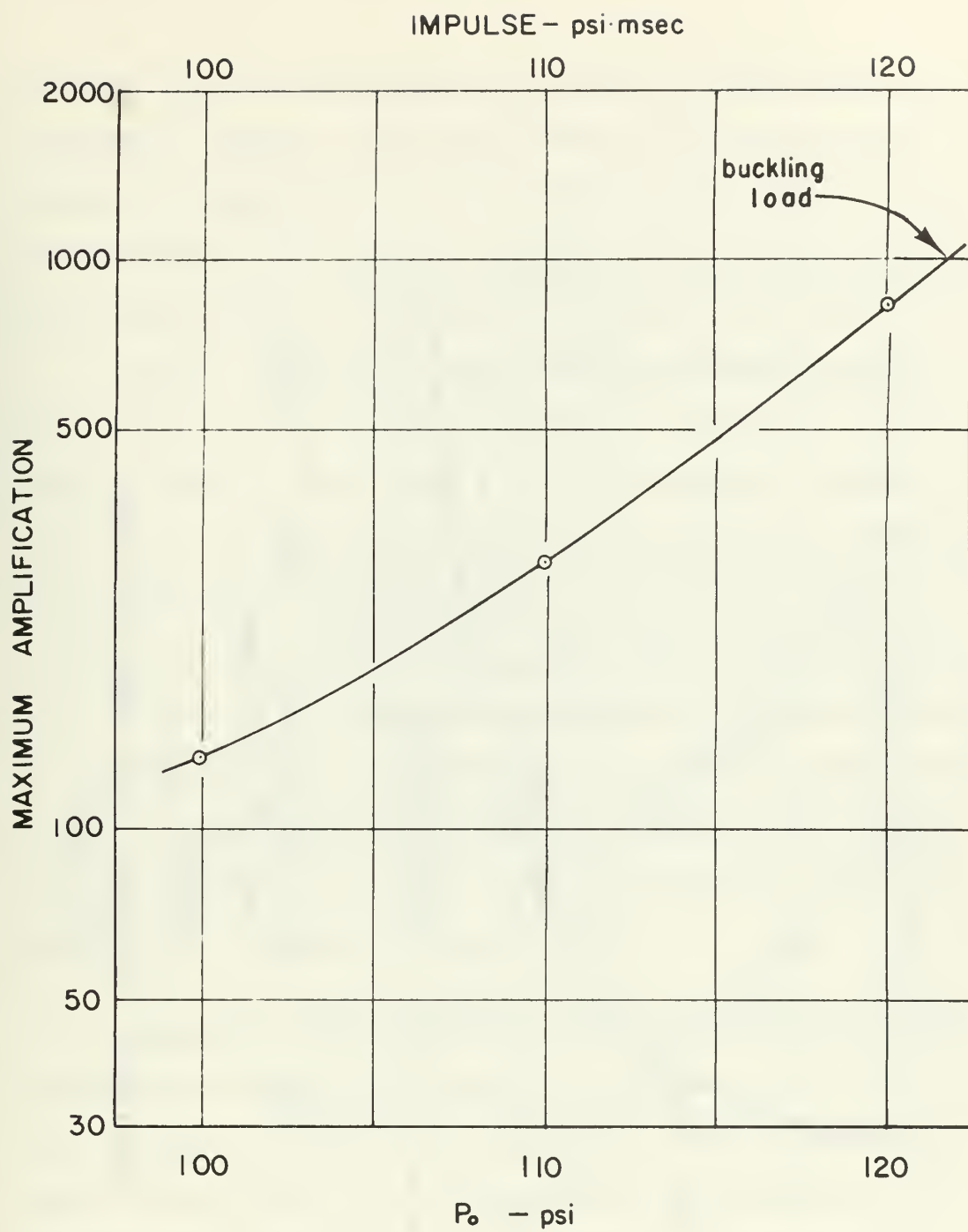


FIGURE 5.7
CASE B
MAXIMUM AMPLIFICATION OF HYPERBOLIC MODES

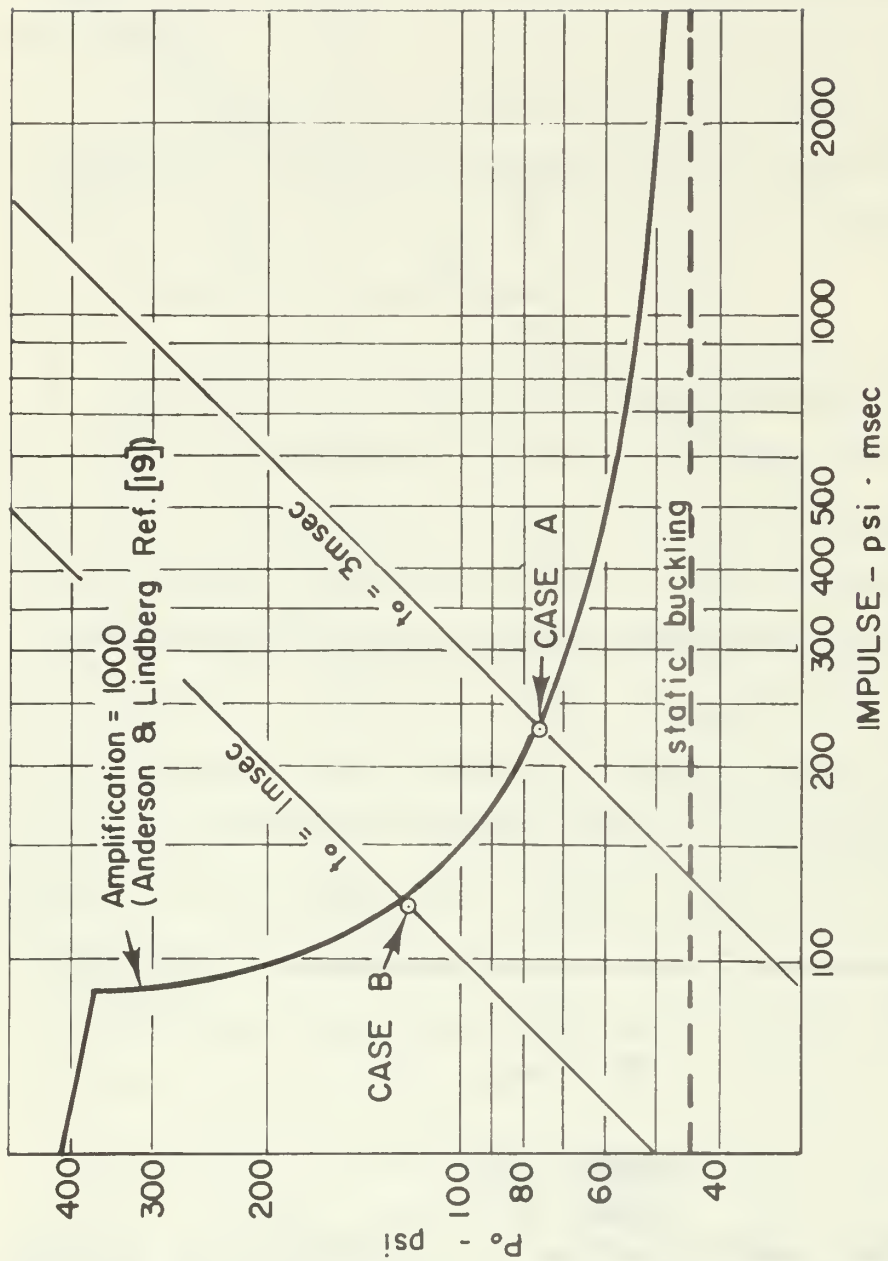


FIGURE 5.8
CRITICAL LOADING FOR AMPLIFICATION
OF 1000

dynamic buckling curve since the Mathieu modes were not included. However, the algorithm of this dissertation is capable of computing the displacements and the stresses in the subcritical region, notably, in the region between the static buckling line and the dynamic buckling curve.

The two straight lines running diagonally across the Figure are lines along which t_0 is equal to 3.0 msec, case A, and 1.0 msec, case B. The two points labeled CASE A and CASE B are the buckling pressures and impulses which were obtained from Figures 5.6 and 5.7. They are based on an amplification of 1000. Note that the points fall very close to Anderson and Lindberg's buckling curve. Therefore, Anderson and Lindberg's treatment of the boundary conditions and their neglecting of certain nonlinear coupling terms do not lead to any significant errors in predicting the amplification of 1000.

Comparison with McIvor and Lovell's Findings. Under an impulsive load, as considered by McIvor and Lovell [20], the axisymmetric mode oscillates about its unloaded static equilibrium state, and the quasi-static response of the axisymmetric mode is zero. Therefore, the hyperbolic modes, which respond primarily to the quasi-static motion of the axisymmetric, are not excited. In cases A and B, the amplitudes of the hyperbolic modes were small at the lower pressures and impulses, because the quasi-static response of the axisymmetric mode was very small; yet the

high frequency oscillation of the axisymmetric mode was sufficient to excite the Mathieu modes. The observed behavior of the Mathieu modes agrees qualitatively with McIvor and Lovell's findings.¹¹ For instance, in Figure 5.4, the Mathieu mode responded in a beat-like manner requiring several cycles to attain the first peak. Furthermore, the peak amplitude of the Mathieu mode was larger in the second beat than in the first, leading to a large stress.

Maximum Stresses. Although the theory of Reference [19] appears to be very adequate for computing buckling thresholds, the results for cases A and B, contained in Tables IV and V, indicate that the stresses may exceed the yield point stress at peak pressures and total impulses well below the buckling threshold. When the load was subcritical, maximum stress occurred well after the lower frequency, buckling modes had attained their maximum amplitudes. However, at loads near critical the maximum stress occurred at about the time the dominant hyperbolic mode was at its largest amplitude.

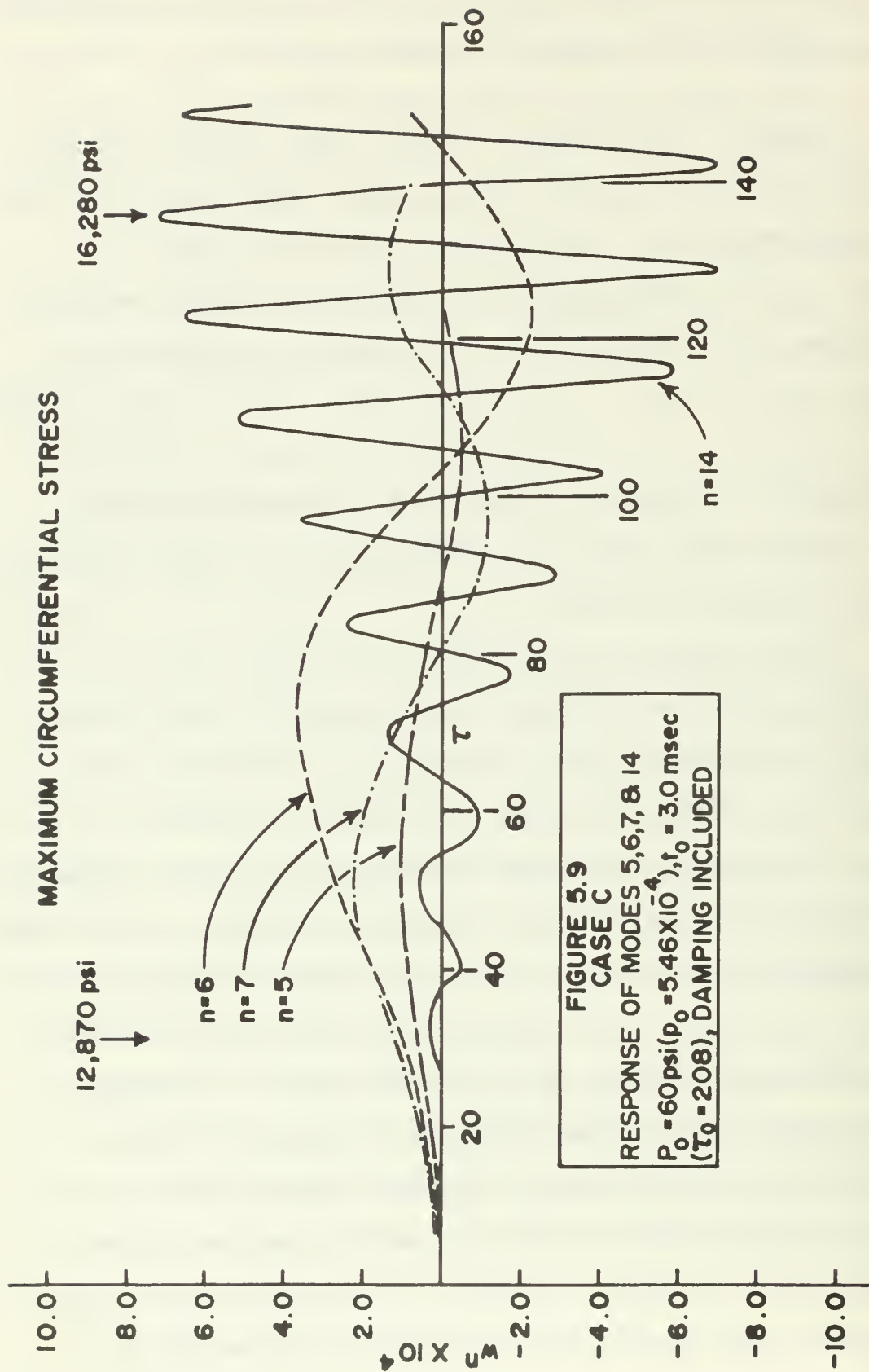
Since a structure designed for repeated use, such as the NWL shock tube, would experience fatigue weakening if the stresses exceed the yield point stress, one might ask whether a normal amount of viscous damping would

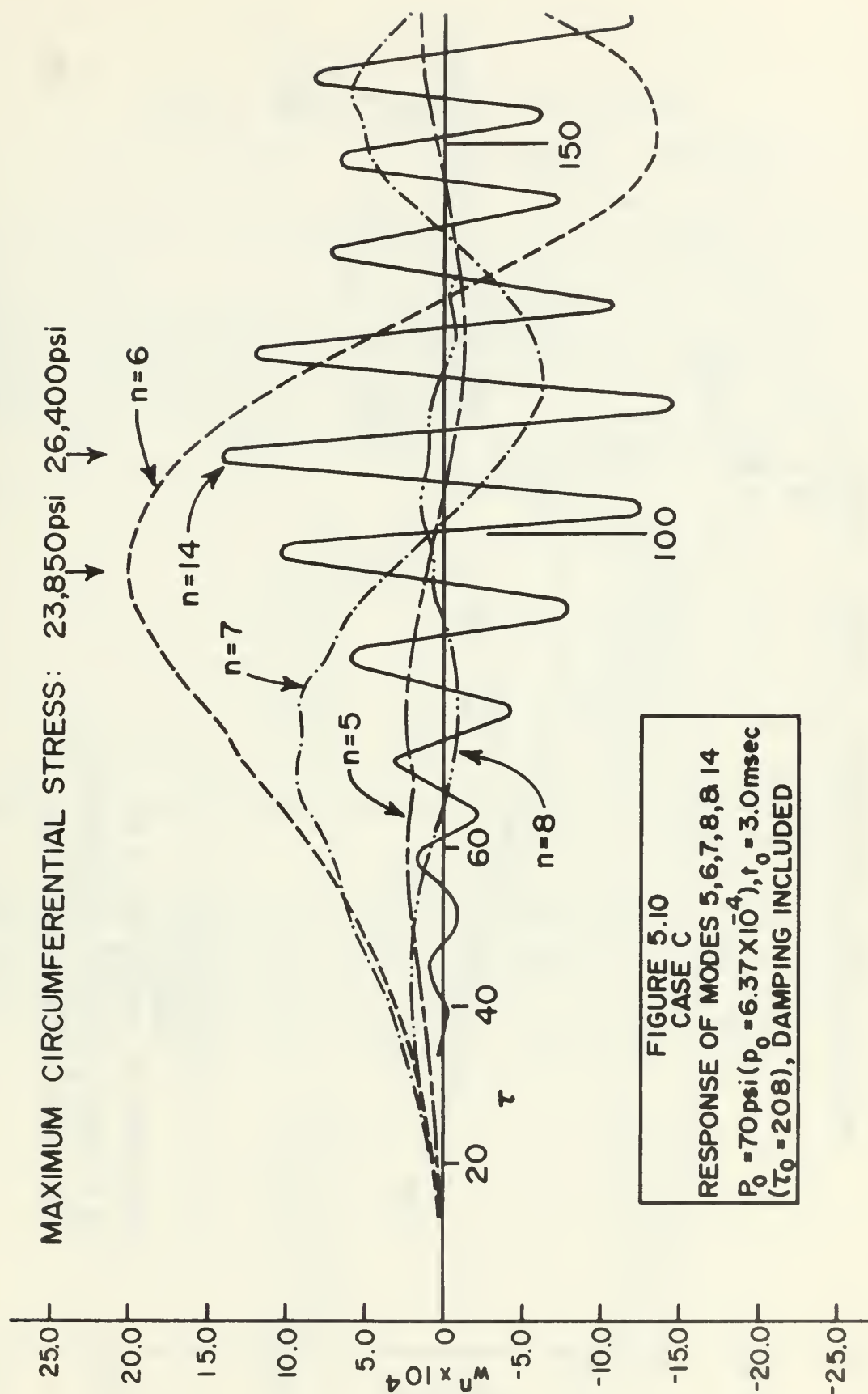
¹¹A quantitative comparison can not be made due to the differences in the analyses.

attenuate the Mathieu response, thus reducing the stresses. This aspect is considered in cases C and D.

Case C. The loading of case C was the same as the loading of case A except that viscous damping was included. The nondimensional coefficient c was taken equal to 3.416×10^{-5} . The maximum amplification of each mode and the time of its occurrence, the maximum circumferential stress and the time of its occurrence, and the time at which the integration was terminated are contained in Table VI. In addition, Figures 5.9-5.11 show the time histories of the active modes, annotated to indicate the times at which large stresses occurred.

The computer runs of case C were carried out for longer periods of time than were the runs of case A in order to include any significant growth of mode 13 that might lead to high stresses. The amplifications of Table VI indicate that mode 13 had moved into the unstable region of the Mathieu chart of Figure 5.2 prior to the end of each run. On the first two runs, mode 13 became unstable only after the damping effects had extracted much of the energy from the motion of the shell. Consequently, mode 13 did not grow sufficiently to generate a higher stress than had previously occurred. Due to the higher peak pressure of the third run, mode 13 became unstable much sooner. However, the mode 13 response was not responsible for the maximum stress since the motion of the





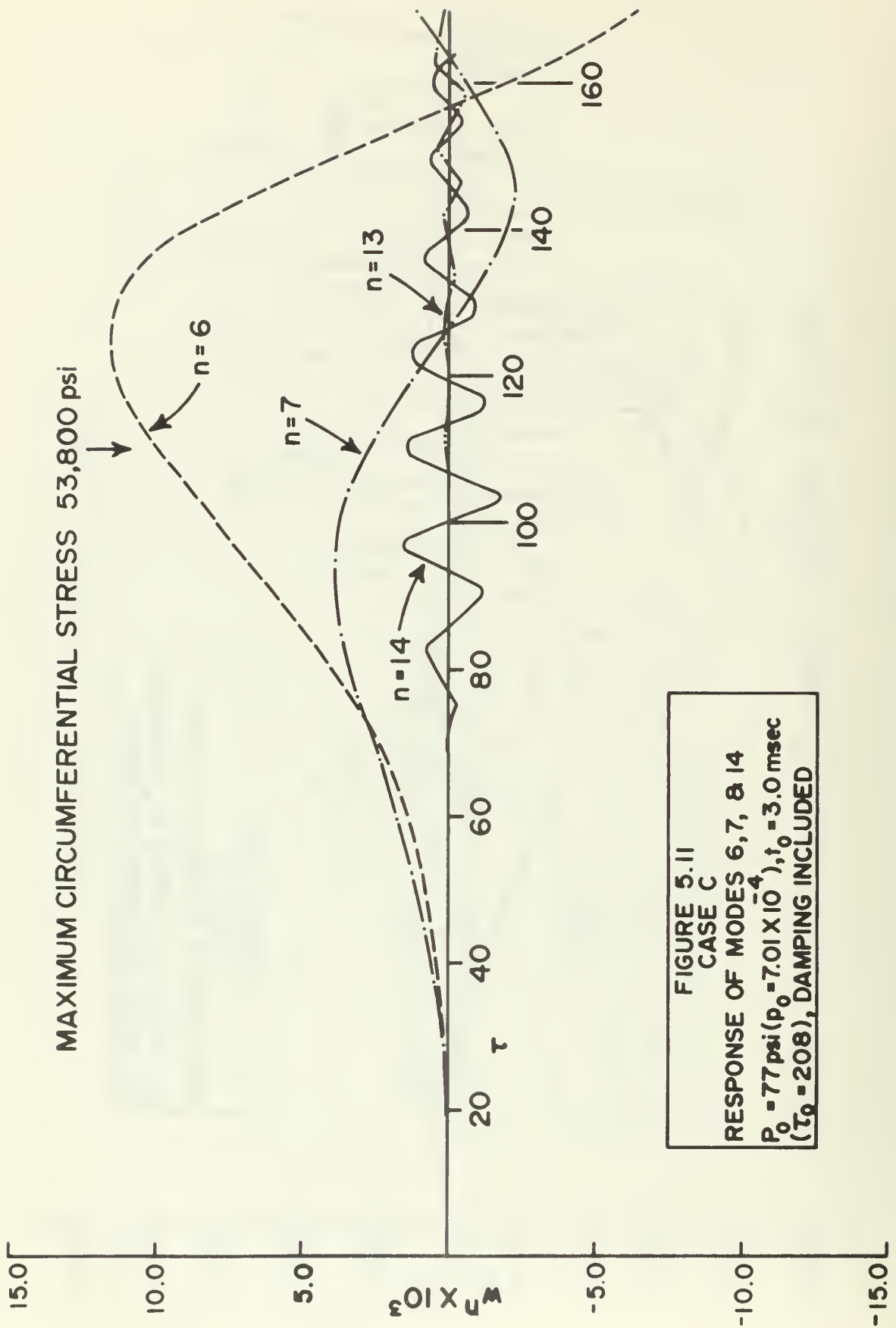


FIGURE 5.11
CASE C
RESPONSE OF MODES 6, 7, & 14
 $P_0 = 77 \text{ psi} (p_0 = 7.01 \times 10^{-4})$, $t_0 = 3.0 \text{ msec}$
($\tau_0 = 208$), DAMPING INCLUDED

TABLE VI

CASE C, AMPLIFICATIONS AND STRESSES

 $t_o = 3.0$ msec ($\tau_o = 208$), DAMPING INCLUDED $P_o = 60$ psi $: p_o = 5.46 \times 10^{-4}$

Maximum circumferential stress = 16,250

Maximum circumferential stress occurred at $\tau = 136$ Integration terminated at $\tau = 300$

mode	maximum amp.	τ for maximum amp.
0		
1	.94	287.5
4	1.49	27.65
5	10.61	52.78
6	38.24	72.01
7	22.98	52.78
8	8.93	33.86
9	4.52	20.21
13	22.86	296.0
14	71.96	135.7
15	1.45	84.41

 $P_o = 70$ psi $: p_o = 6.37 \times 10^{-4}$

Maximum circumferential stress = 26,400 psi

Maximum circumferential stress occurred at $\tau = 110$ Integration terminated at $\tau = 257$

mode	maximum amp.	τ for maximum amp.
0		
1	4.53	85.72
4	1.99	33.57
5	24.79	71.78
6	202.0	97.66
7	95.82	72.14
8	21.26	46.44
9	7.68	26.54
10	4.09	19.41
13	4.98	252.1
14	147.5	177.3
15	3.09	36.32

TABLE VI Continued

$P_o = 77 \text{ psi}$	$: p_o = 7.01 \times 10^{-4}$	
Maximum circumferential stress = 53,800 psi		
Maximum circumferential stress occurred at $\tau = 110$		
Integration terminated at $\tau = 198$		
mode	maximum amp.	τ for maximum amp.
0		
1	91.06	103.9
4	5.33	196.5
5	87.00	119.6
6	1154.	127.3
7	396.2	91.54
8	69.72	118.1
9	17.71	119.0
10	6.54	168.1
13	155.8	197.0
14	174.1	103.5
15	9.92	183.0

Mathieu modes was greatly overshadowed by the early growth of the hyperbolic modes.

The effectiveness of the damping in attenuating the Mathieu modes can be ascertained by comparing the mode 14 amplifications of the damped and undamped responses. Comparison of the amplifications of mode 14 contained in Table IV with those contained in Table VI reveals that the maximum amplification of mode 14 was reduced by 25 to 30 per cent by the inclusion of damping.

Assuming that the damping would have extracted sufficient energy to preclude the development of stresses higher than those computed in Table VI, a critical pressure and impulse based on the yield point stress can be

determined. In Figure 5.12 the maximum circumferential stress is shown as a function of the peak pressure. The critical pressure and impulse corresponding to a maximum stress of 42 ksi are 75 psi and 225 psi-msec, respectively. Note that the yield stress occurs at a pressure where the hyperbolic modes have much larger amplifications than the Mathieu modes. However, the bending stress, given by the second term of (4.29), depends on n^2 ; consequently, the Mathieu modes with their higher mode numbers can make significant contributions to the stress even though their amplitudes may be small.

Case D. In case D, the time constant t_0 was taken equal to 1.0 msec ($\tau_0 = 69.3$), the time constant used in case B. The nondimensional damping coefficient was again taken equal to 3.416×10^{-5} ; and three computer runs were carried out at peak pressures of 90 psi, 100 psi, and 110 psi. The results are summarized in Table VII. Note that for all three runs, the integration was carried out long enough to include the maximum amplification of mode thirteen.

Comparison of the amplifications of the first run of case B (Table V) with the second run of case D (Table VII) shows that the amplifications of the Mathieu modes were again reduced approximately 25 to 35 per cent. However, a similar comparison of the third run results of case D with the second run results of case B reveals that at the higher

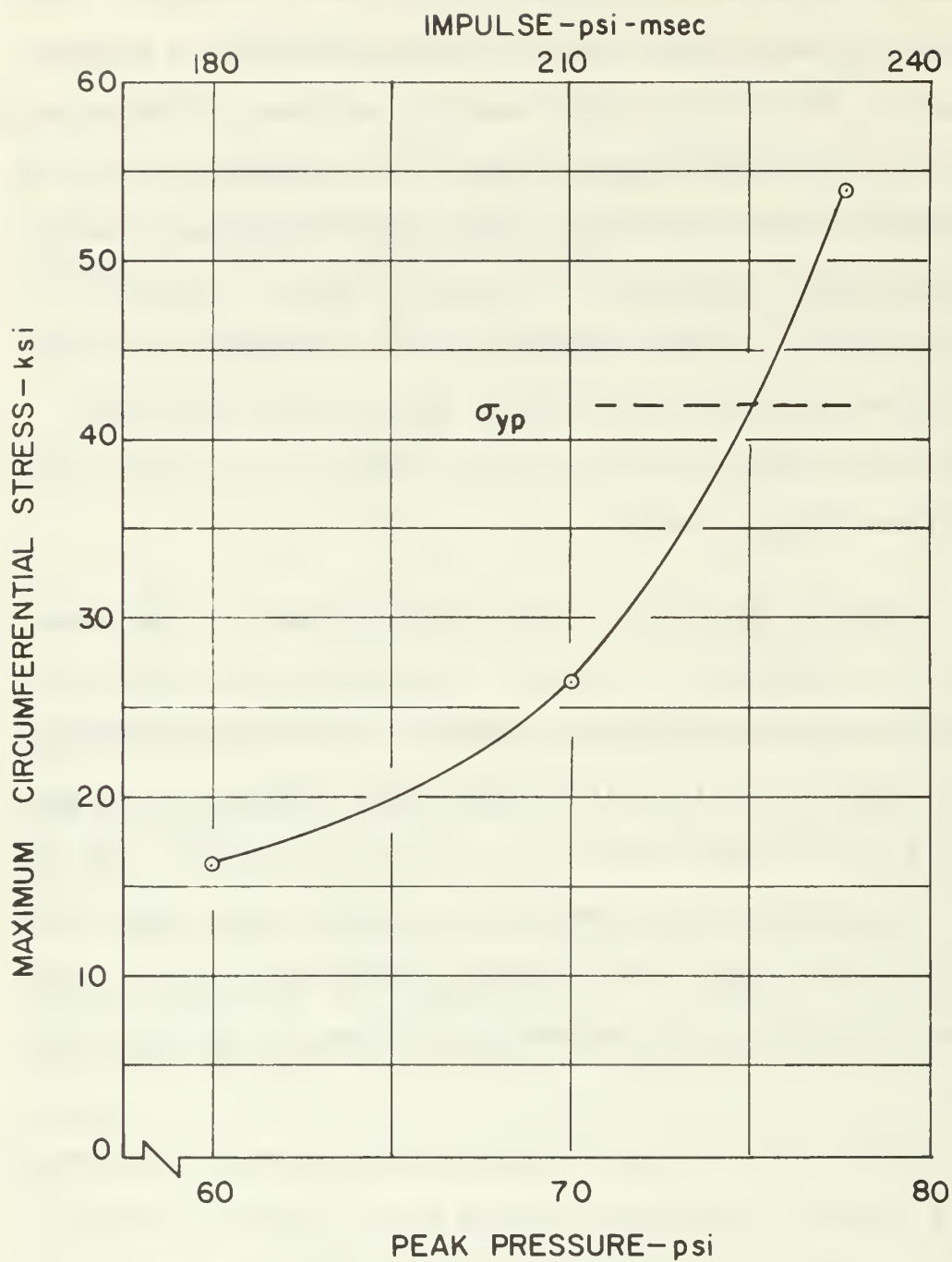


FIGURE 5.12
CASE C

MAXIMUM CIRCUMFERENTIAL STRESS vs.
PEAK PRESSURE

$t_0 = 3.0$ msec ($\tau_0 = 20.8$), Damping Included

TABLE VII

CASE D, AMPLIFICATIONS AND STRESSES

 $t_0 = 1.0$ msec ($\tau_0 = 69.3$), DAMPING INCLUDED $P_0 = 90$ psi $: p_0 = 8.19 \times 10^{-4}$

Maximum circumferential stress = 32,100 psi

Maximum circumferential stress occurred at $\tau = 187$ Integration terminated at $\tau = 224$

mode	maximum amp.	τ for maximum amp.
0		
1	26.14	221.5
4	2.44	28.71
5	19.15	52.59
6	61.94	58.95
7	53.41	46.70
8	24.94	40.03
9	11.76	26.39
10	6.47	19.56
11	4.66	214.7
13	199.9	158.2
14	155.5	89.83
15	10.75	49.03

 $P_0 = 100$ psi $: p_0 = 9.10 \times 10^{-4}$

Maximum circumferential stress = 37,900 psi

Maximum circumferential stress occurred at $\tau = 182$ Integration terminated at $\tau = 193$

mode	maximum amp.	τ for maximum amp.
0		
1	37.87	150.2
4	3.74	162.2
5	30.82	58.60
6	125.6	65.44
7	113.6	52.68
8	50.01	40.28
9	18.98	26.93
10	9.46	19.84
11	6.23	182.4
13	236.5	152.5
14	208.3	83.39
15	34.67	56.14

TABLE VII Continued

$P_o = 110 \text{ psi}$		$: p_o = 10.01 \times 10^{-4}$
Maximum circumferential stress = 45,400		
Maximum circumferential stress occurred at $\tau = 120$		
Integration terminated at $\tau = 188$		
mode	maximum amp.	τ for maximum amp.
0		
1	56.98	144.0
4	7.57	185.9
5	52.84	63.71
6	267.9	71.32
7	245.8	59.19
8	103.1	46.47
9	33.80	33.52
10	13.54	20.08
11	9.88	176.5
12	68.58	183.6
13	257.4	146.5
14	252.1	118.8
15	100.5	62.52

peak pressure damping was not nearly so effective in reducing the amplifications of the Mathieu modes.

In Figure 5.13 the maximum circumferential stress is plotted against the peak pressure. Assuming that the yield point stress is 42 ksi, the critical peak pressure is approximately 106.5 psi. At this pressure the amplitudes of both types of modes are approximately the same. Thus the Mathieu modes play a dominant part in the stress state of the cylinder for this loading condition.

Critical Loading Based on Maximum Stress. A critical loading curve based on the maximum circumferential stress

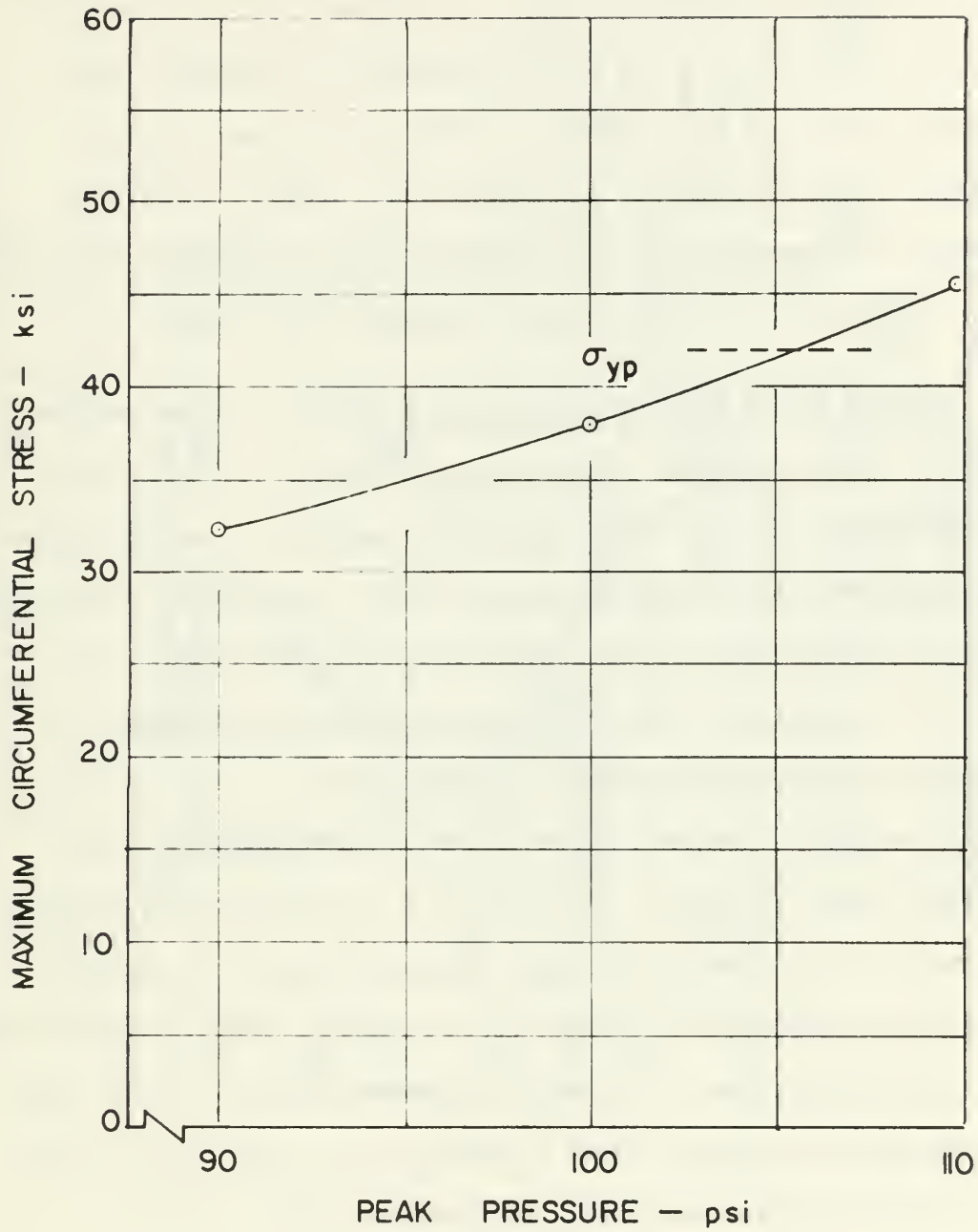


FIGURE 5.13
CASE D

MAXIMUM CIRCUMFERENTIAL STRESS vs.
 $t_0 = 1.0 \text{ msec}$ ($\tau_0 = 69.3$), Damping Included

at $\theta = 0^\circ$ being equal to the yield point stress is plotted in the pressure-impulse plane in Figure 5.14. The curve for an amplification of 1000 obtained by Anderson and Lindberg [19] is also shown. Although cases C and D provide only two points to define the curve, clearly, critical stresses occur at pressures and impulses less than those required to produce amplifications of 1000.

Axial Wave Form of Responding Modes. Anderson and Lindberg [19] assumed the axial variation of the radial displacements of the flexural modes and the initial imperfection modes to be a half sine wave. The axial variation of the displacements was completely unspecified in the present analysis. For the solutions of this chapter, the initial imperfection modes were assumed to vary as a half sine wave in the axial direction, corresponding with Anderson and Lindberg. In Figure 5.15, the axial distributions of the computed radial displacements in modes 6 and 14 are plotted at arbitrarily chosen times. Note that the axial variation of mode 6 is essentially a sine wave as assumed by Anderson and Lindberg. On the other hand, the radial displacement of the Mathieu mode is not a single half sine wave.

The axial variation of the Mathieu mode shown in Figure 5.15 appears to contain a component of the form $\sin(3\pi\xi/l)$ as well as a component of the form $\sin(\pi\xi/l)$. The natural frequency Ω_{qn} of a mode of the form

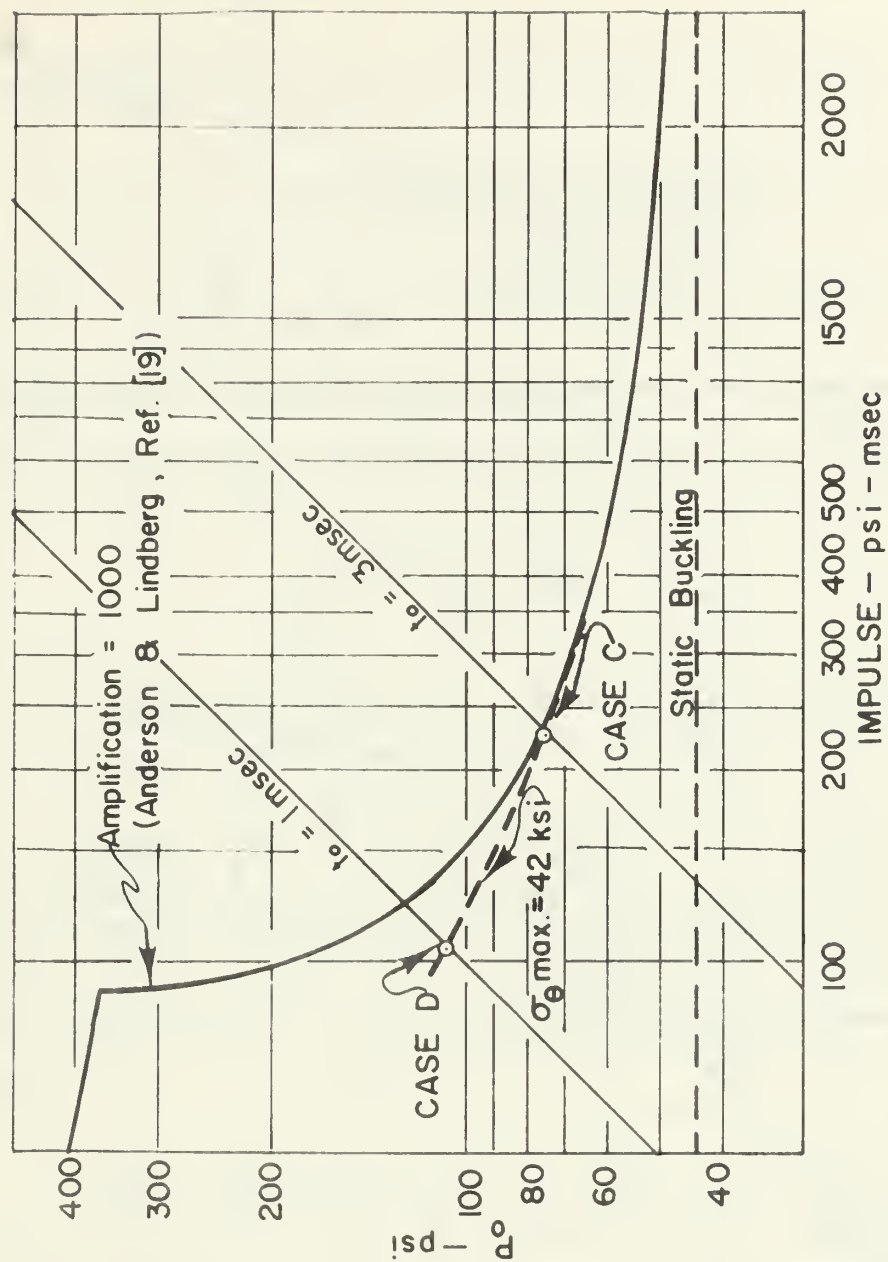


FIGURE 5.14
CRITICAL LOADING BASED ON STRESS
($\sigma_{yp} = 42 \text{ ksi}$, Damping Included)

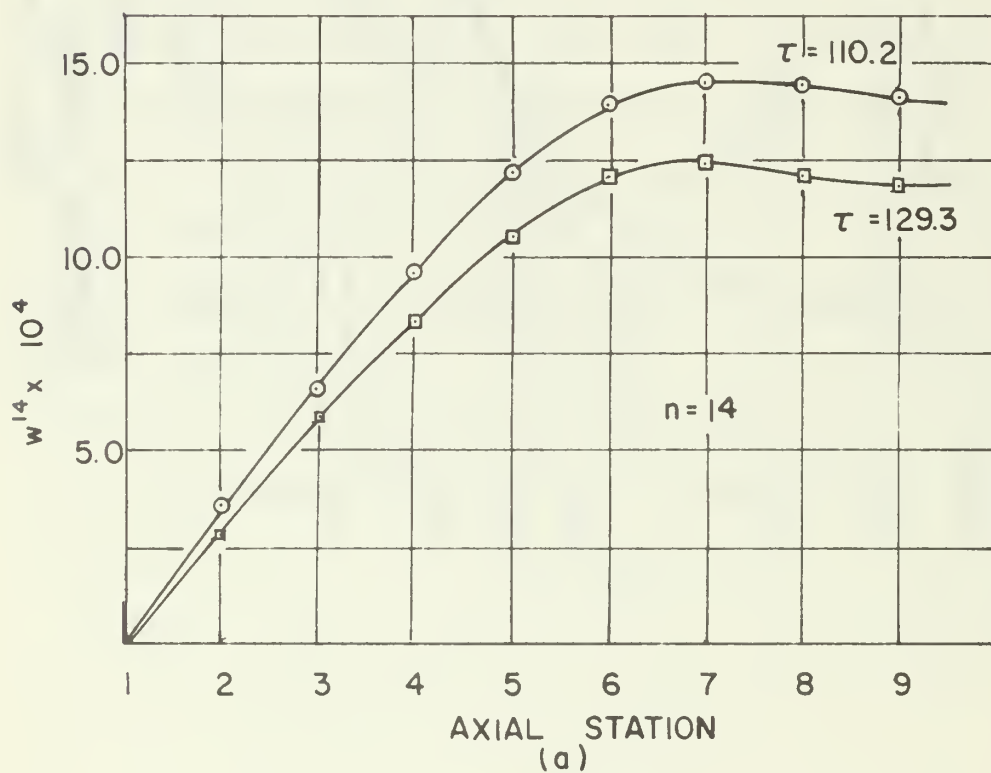
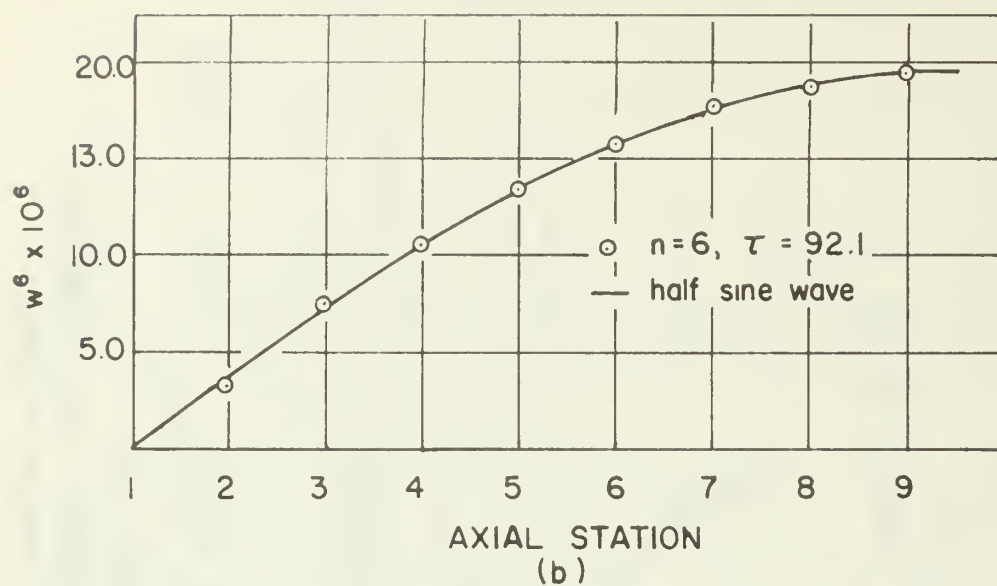


FIGURE 5.15
 AXIAL VARIATION OF
 (a) HYPERBOLIC MODES
 (b) MATHIEU MODES
 $\rho_0 = 6.37 \times 10^{-4}, \tau_0 = 208$

$$w^{qn} \sin\left(\frac{q\pi\xi}{l}\right) \cos n\theta$$

is given by

$$\Omega_{qn}^2 = \frac{1}{12} \alpha^2 \left(n^2 + \frac{q^2 \pi^2}{l^2} \right) + \frac{(1-\nu^2) \left(\frac{q\pi}{l} \right)^4}{\left(n^2 + \frac{q^2 \pi^2}{l^2} \right)^2} \quad (5.19)$$

A few quick calculations show that when q is equal to three, the natural frequencies are equal to

$\frac{n}{l}$	$\frac{\Omega_{3n}}{l}$
10	.3931
11	.4391
12	.4964
13	.5630
14	.6373

The frequency for $n = 12$ is very close to one-half, and the possibility exists that this mode might be parametrically excited by the oscillation of the axisymmetric mode.¹²

Random Imperfections. In practice, the engineer does not know the magnitude of the initial imperfection until after the shell has been constructed. This leads one to examine the sensitivity of the solution to the magnitudes of the initial imperfections. One computer run was made at $P_0 = 70$ psi, $t_0 = 3$ msec, and $w_i^n \leq 1.0 \times 10^{-5}$.

¹²McIvor and Lovell [20] recognized this possibility and included similar Mathieu modes in their calculations.

The magnitude of the imperfection in each mode was selected from a table of random numbers. The results obtained for uniform imperfections and random imperfections are shown in Table VIII for purposes of comparison.

Note that the amplifications of modes four through ten are nearly the same in both cases. However, the displacements are significantly different. On the other hand, the magnitude of the displacement, instead of the amplification, remains approximately constant for modes 13, 14, and 15. Thus, it appears that the hyperbolic modes are very sensitive to the magnitude of the initial imperfection, whereas the response of the Mathieu modes is largely independent of the initial imperfection. This is in agreement with the conclusions of Anderson and Lindberg [19] and McIvor and Lovell [20]. Anderson and Lindberg considered the hyperbolic modes to be directly proportional to the imperfection; while McIvor and Lovell found that the maximum amplitude of a Mathieu mode was rather insensitive to the initial imperfection.

Since the stresses depend on the magnitude of the displacements, the stresses are very sensitive to the magnitude of the initial imperfection when the hyperbolic modes play a dominant role.

Significance of Intermodal Coupling of the Flexural Modes. The maximum amplifications of the hyperbolic modes obtained by Anderson and Lindberg [19] agree well with the

TABLE VIII
EFFECT OF MAGNITUDE OF INITIAL IMPERFECTION^a

$$P_0 = 70 \text{ psi}, t_0 = 3.0$$

ZERO DAMPING

Mode	w_i^n	Maximum Amp.	$ w^n _{\max} \times 10^4$
0	0.0	-	-
1	1.0×10^{-5}	7.93	.79
4	1.0×10^{-5}	2.22	.22
5	1.0×10^{-5}	26.70	2.67
6	1.0×10^{-5}	222.3	22.23
7	1.0×10^{-5}	101.7	10.17
8	1.0×10^{-5}	22.02	2.20
9	1.0×10^{-5}	7.84	.78
10	1.0×10^{-5}	4.15	.42
13	1.0×10^{-5}	3.80	.38
14	1.0×10^{-5}	229.2	22.92
15	1.0×10^{-5}	4.06	.41

Mode	w_i^n	Maximum Amp.	$ w^n _{\max} \times 10^4$
0	0.0	-	-
1	1.05×10^{-6}	15.87	.02
4	4.66×10^{-6}	2.02	.09
5	2.25×10^{-6}	26.53	.60
6	6.17×10^{-6}	217.2	13.40
7	6.10×10^{-7}	102.1	.623
8	5.35×10^{-6}	22.0	1.18
9	7.12×10^{-6}	7.83	.56
10	5.69×10^{-6}	4.15	.24
13	2.53×10^{-6}	16.70	.42
14	1.80×10^{-6}	1089.0	19.6
15	1.55×10^{-6}	3.57	.06

^aIntegration terminated at $\tau = 197$.

amplifications computed by the fully coupled nonlinear theory. Since their analysis neglects, among other things, the intermodal coupling of the flexural modes, the possibility arises that the coupling between the flexural modes is of negligible importance. Neglecting intermodal coupling of the flexural modes is equivalent to retaining only those nonlinear products which contain the Fourier coefficient of the axisymmetric mode. Motion in the axisymmetric mode affects the motion of each of the other modes, and conversely each mode couples back to the axisymmetric mode. However, modes i and j do not affect each other if neither i nor j is equal to zero.

The computer program can be altered very readily to effect this limited coupling. A run was made for the parameters of case A, $P_0 = 70$ psi, using the altered program. The maximum amplifications for both complete and limited nonlinear coupling are presented in Table IX. The integration was terminated at $\tau = 200$ so that mode 13 did not have time to grow. The magnitudes and times of the maximum amplification of all of the modes are nearly the same for both cases. On the basis of this one solution, it appears that the intermodal coupling of the flexural modes for this problem is quite weak and can be neglected.

Additional computer runs should be made in the future to cover a larger spectrum of loading conditions. If it can be shown that the intermodal coupling of the flexural modes

TABLE IX

AMPLIFICATIONS WITH TOTAL
AND LIMITED INTERMODAL COUPLING

$$P_0 = 70 \text{ psi}, t_0 = 3.0 \text{ msec}, w_i^n = 1.0 \times 10^{-5}$$

ZERO DAMPING

Mode	Total Coupling		Limited Coupling	
	Maximum Amplification	τ For Max. Amp.	Maximum Amplification	τ For Max. Amp.
0				
1	7.933	190.6	.039	198.1
4	2.220	88.35	1.974	33.53
5	26.70	71.71	26.20	71.78
6	222.3	97.35	219.6	97.48
7	101.7	72.23	101.3	72.15
8	22.02	40.37	21.98	40.37
9	7.838	26.41	7.827	26.56
10	4.147	19.43	4.143	19.45
13	3.796	193.8	8.854	199.9
14	229.2	164.6	229.3	164.6
15	4.064	162.8	3.795	191.4
Max. Stress	30,000 psi	@ $\tau = 197$	32,900 psi	@ $\tau = 165$

is indeed negligible for all loadings of interest, the analysis and the computer program can be simplified very substantially.

Significance of Coupling Terms in Mode Zero Equations.

The coupling terms in the equations of mode 0, the axisymmetric mode, provide the mechanism for the extraction of energy from that mode. A natural question to ask is whether the response of the flexural modes would be affected if this mechanism were removed. If this coupling, as well as the intermodal coupling of the flexural modes, is unimportant, then the response of all of the flexural modes could be computed one mode at a time, using equations (5.5) and (5.6), or similar equations. Three computer runs were made to study this question. In all three runs, the coupling terms in the mode 0 equations were equated to zero. Run one included the flexural modes 5 through 8, run two included the flexural modes 12 through 15, and run three included the flexural modes 16 through 18. The choice of these flexural modes rules out any intermodal coupling of the flexural modes. The loading had a peak pressure of 70 psi and a time constant of 3.0 msec, the same as the loading of the second run of case A. The maximum amplification of each mode from both solutions is contained in Table X. Comparison of the appropriate amplifications from Table IV with those contained in Table X reveals that the amplifications of the hyperbolic modes,

TABLE X

RESPONSE OF INDIVIDUAL MODES WITHOUT

ENERGY EXTRACTION FROM THE AXISYMMETRIC MODE

$$P_0 = 70 \text{ psi } (p_0 = 6.37 \times 10^{-4}), t_0 = 3.0 \text{ msec } (\tau_0 = 208)$$

Run	Mode	Maximum Amplification Attained at $\tau = 140$
1	5	26.8
	6	228.0
	7	104.0
	8	21.4
2	12	1.8
	13	1.8
	14	1990.0
	15	3.4
3	16	1.7
	17	1.7
	18	2.7

modes 5 through 8, were not changed appreciably when the coupling terms in the mode 0 equation were neglected. On the other hand, the amplification of the Mathieu mode, mode 14, was drastically larger. This is reasonable since the initial conditons rather than the loading cause the oscillations of the axisymmetric mode. Thus, the oscillatory energy of the axisymmetric mode is limited. If this limited energy can not be removed by coupling, then the Mathieu mode will grow very large as if an oscillatory load were being applied.

Although the results are somewhat limited in number, they indicate that the response of a particular flexural mode has little direct effect on the response of another flexural mode; that is the intermodal coupling of the flexural modes is weak. However, all of the flexural modes have a very significant indirect influence on the response of the Mathieu modes, since they extract energy from the axisymmetric mode. Consequently the response of all the modes must be computed simultaneously in order to obtain the total response of the cylindrical shell.

CHAPTER VI

SUMMARY, FINDINGS, AND RECOMMENDATIONS FOR FUTURE WORK

I. SUMMARY

A numerical algorithm was developed for computing the dynamic response of a ring-stiffened, nearly circular cylindrical shell under transient axisymmetric loads. The governing equations, which are based on the nonlinear Donnell theory, account for the class of radial imperfections whose circumferential variation can be expressed in a Fourier cosine series. The equations for the rings and shell structure were derived by using Hamilton's principle and include the radial inertia and a viscous damping term. The analysis accounts for the discrete location and eccentricity of a set of identical rings.

Elimination of the circumferential variable was achieved by assuming a Fourier sine or cosine series for the displacements. The nonlinear terms generated products of Fourier series which were expanded to single series, yielding modal coupling terms. The series were truncated for the actual computations, with a maximum of fifteen participating modes. The retained modes were not limited to the first fifteen, but were selected to include those modes most responsive to the particular load. The partial differential equations were replaced with difference-differential equations by approximating the axial

derivatives with finite differences. A nonconventional differencing procedure, commonly called "modified" or "half station" differencing, was used. Provisions were made for both the clamped and simply supported end conditions. The iterative Newmark beta-method was employed for the time integration of the radial difference-differential equations. The axial and circumferential equilibrium equations were solved by Gauss elimination during each iteration.

The algorithm was used to compute the response of a simply supported shell under a uniform, exponentially decaying, radial pressure. This particular shell and similar loading conditions have been considered in the earlier investigations of Anderson and Lindberg [19] and McIvor and Lovell [20]. The load parameters were selected so as to fall in the regime where dynamic buckling is governed by an elastic model, and the peak pressures and total impulses considered were between the static buckling limit and the dynamic buckling limit. Several response histories were computed, both with and without viscous damping; and comparisons were made with the results of References [19, 20]. The significance of the intermodal coupling of the flexural modes and the feedback coupling to the axisymmetric mode was also investigated. Finally, the role played by the imperfection magnitudes was briefly considered.

A potential user of the computer program, or one interested in pursuing this work further, should be aware of the following limitations of the program:

1. The analysis employs the Donnell shell theory which is not valid for many classes of shells [48].
2. The circumferential variation of the initial imperfections is expressed in a Fourier cosine series, instead of a complete series containing both sines and cosines.
3. The axial, circumferential, and rotatory inertia of the rings and the shell are neglected.
4. The portions of the computer program that calculate ring effects have been verified in only a cursory manner.
5. A maximum of three rings can be accommodated by the computer program. The rings must be identical in geometry and material properties and spaced so as to divide the shell into segments of equal length. A principal axis of the ring cross sections must be parallel to the axis of the cylinder.
6. The imperfection of the shell must not distort the rings.
7. The rotations of the rings must be small, and restrictive warping is not accounted for in the expression for the strain energy of the rings.

8. The distance between the midsurface of the shell and the centroids of the ring cross sections must be small compared to the radius of the cylinder.
9. The circumferential stress is computed only at $\theta = 0^\circ$. The meridional curvature change is not included in the calculation of the circumferential stress; in addition, $1 - \nu^2$ is taken equal to unity.
10. In the axial equilibrium equation, the effect of a ring is felt at a station which is located one-half of the mesh spacing from the ring.

II. FINDINGS

The exponentially decaying pressure pulses were found to excite flexural modes belonging to two families, herein referred to as hyperbolic and Mathieu modes. The hyperbolic modes are the buckling modes, and they grow to their maximum amplitude in an exponential manner with little accompanying oscillation. On the other hand, the Mathieu modes grow in an oscillatory manner requiring several cycles to attain their maximum amplitude.

The hyperbolic modes grow primarily as a result of the quasi-static displacement of the axisymmetric mode. The loads considered in the present study were on the shell for a period of time much longer than the natural period

of the axisymmetric mode. Hence, the quasi-static response of the axisymmetric mode was nearly proportional to the instantaneous magnitude of the pressure. A given hyperbolic mode was found to respond as long as the instantaneous magnitude of the pressure exceeded the static buckling pressure of the mode.

The Mathieu modes were found to be those modes whose natural frequencies were approximately one-half of the axisymmetric natural frequency and usually much higher than the frequencies of the hyperbolic modes. The Mathieu modes were identified through the use of a modified Mathieu stability chart. The modification replaced the natural frequency of the flexural mode by a pseudo frequency which accounted for the instantaneous value of the pressure. Hence the susceptibility of a given flexural mode to parametric excitation depended not only on the peak pressure and frequencies of the flexural and axisymmetric modes, but also on the instantaneous value of the pressure. Thus, as the pressure pulse decayed, the points corresponding to the flexural modes moved across the Mathieu diagram. Some modes moved from an unstable region into a stable region, while other modes moved from a stable region into an unstable region. The response of the Mathieu modes could be characterized as beat-type oscillations during which energy was cyclically exchanged between modes.

Anderson and Lindberg [19] investigated the dynamic pulse buckling of cylindrical shells subjected to axisymmetric loadings. They showed that dynamic buckling occurs as a result of the rapid growth of the hyperbolic modes, and that the Mathieu modes are of little importance.

McIvor and Lovell [20] studied the nonlinear dynamic response of shells under purely impulsive loads. Their results show that for such loads only the Mathieu modes respond since the quasi-static response of the axisymmetric mode is zero. However, the stresses developed during the response were found to be several times larger than stresses of an axisymmetric response to the same impulsive load.

The results of the present work consolidate the findings of these two previous investigations. At the lower peak pressures and total impulses, for which the quasi-static response of the axisymmetric mode was small, the Mathieu modes dominated; and the computed motion was qualitatively similar to the motion computed by McIvor and Lovell. As the peak pressure and total impulse were increased, a gradual transition occurred; and the hyperbolic modes played an increasingly significant role. Near the dynamic buckling threshold, the hyperbolic modes completely dominated the Mathieu modes. The dynamic buckling loads predicted by the fully coupled nonlinear analysis agreed very closely with Anderson and Lindberg's results.

However, at peak pressures and total impulses well below the dynamic buckling threshold, stresses in excess of the yield point stress occurred due to the combined response of the Mathieu and hyperbolic modes.

For those solutions in which a small amount of damping was assumed, the maximum amplitudes of both the dominant hyperbolic and Mathieu modes were reduced by 10 to 30 per cent in comparison to the zero damping case. Generally, the Mathieu modes were attenuated more than the hyperbolic modes. A critical pressure-impulse curve based on the yield point stress was determined for the damped response. This curve shows that stresses in excess of the yield point stress can occur at total impulses and peak pressures less than those required for dynamic buckling even when damping is accounted for.

The intermodal coupling of the flexural modes and the feedback coupling to the axisymmetric mode did not significantly affect the response of the hyperbolic modes. Furthermore, the maximum amplitude attained by a given hyperbolic mode was found to be linearly proportional to shape and magnitude of the imperfection in that mode. These findings are in complete agreement with the assumptions made by Anderson and Lindberg [19].

However, the feedback coupling to the axisymmetric mode very significantly affected the response of the Mathieu modes. This coupling is the mechanism by which energy is exchanged between the axisymmetric mode and the flexural

modes. On the other hand, the maximum amplitudes attained by the Mathieu modes were unaffected by both the inter-modal coupling of the flexural modes and the magnitude of the imperfections.

The findings presented here apply to one specific simply supported shell and loading condition. The buckling mode shape of this shell is $\sin\frac{\pi x}{L}\cos 6\theta$, and the dominant Mathieu mode is $\sin\frac{\pi x}{L}\cos 14\theta$. For other shells with different loading conditions, hyperbolic modes, and Mathieu modes, the coupling may be more significant; and these conclusions would not apply. This remains to be seen.

The algorithm developed in this dissertation is capable of computing the fully coupled, nonlinear dynamic response of cylindrical shells under transient pressures. However, the practicality of the method is somewhat limited by the execution time of the computer program. For example, approximately forty-five minutes are required on the IBM 360 model 67 to compute a solution through thirty cycles of the axisymmetric mode when fifteen Fourier modes are retained. When the pressure pulse decays rather slowly, as it did in cases B and D of Chapter V, the solution must be computed through as many as fifty cycles of the axisymmetric mode in order to encompass the response of all of the Mathieu modes.

III. RECOMMENDATIONS FOR FUTURE WORK

The computer program has yet to be fully exploited; and, as previously pointed out, the correctness of those portions of the program which compute the ring contributions have not been fully confirmed. Consequently, the following studies should be conducted using the program:

1. Additional solutions carried out to longer times are needed to establish the significance of the intermodal coupling to the response of the Mathieu modes. If part of the coupling terms could be eliminated, the computing time could be reduced appreciably, thus, extending the usefulness of the program.
2. Solutions should be generated for shorter shells with $L/a \doteq 1$. For shells of this geometry, the static buckling mode and the Mathieu mode coincide. The dynamic buckling loads might turn out to be significantly different from those predicted by Reference [19].
3. Solutions should be computed for shells with clamped ends and compared with the results for the simply supported shell.
4. The stabilizing or destabilizing effects of ring stiffeners should be studied. For example, if the stiffeners are too close together, it is possible that coincidence of the Mathieu modes

and the hyperbolic modes may render the structure unstable.

5. The program should be used to study the dynamic stability of shells under moving loads.
6. An effort should be made to improve the Fortran coding of the program. It is believed that a professional programmer could improve the coding and, thus, reduce the running time.

LIST OF REFERENCES

1. Culbertson, D. W., "Conical Shock Tube Blast Simulator Facility Description and Capabilities," NWL-TM No. T-15/67, U.S. Naval Weapons Laboratory, Dahlgren, Virginia.
2. Bolotin, V. V., The Dynamic Stability of Elastic Systems, translation from the Russian (1956), Holden-Day, Inc., San Francisco, London, Amsterdam. 1964.
3. Agamirov, V. L. and Vol'mir, A. S., "Behavior of Cylindrical Shells Under Dynamic Loading by Hydrostatic Pressure or by Axial Compression," translation from the Russian (1959), ARS Journal, Vol. 31, No. 1, Jan. 1961, pp. 98-102.
4. Yao, J. C., "Stability of a Cylinder Under Dynamic Radial Pressure," ARS Journal, Vol. 31, No. 12, Dec. 1961, pp. 1705-1708.
5. Kadashevich, Y. I. and Pertsev, A. K., "Loss of Stability of a Cylindrical Shell Under Dynamic Loads," translation from the Russian (1960), ARS Journal, Vol. 32, No. 1, Jan. 1962, pp. 140-143.
6. Yao, J. C., "Dynamic Stability of Cylindrical Shells Under Static and Periodic Axial and Radial Loads," AIAA Journal, Vol. 1, No. 6, Jun. 1963, pp. 1391-1396.
7. McLachlan, N. W., Theory and Application of Mathieu Functions, Oxford University Press, New York, London, 1947.
8. Wood, J. D. and Koval, L. R., "Buckling of Cylindrical Shells under Dynamic Loads," AIAA Journal, Vol. 1, No. 11, Nov. 1963, pp. 2576-2582.
9. Goodier, J. N. and McIvor, I. K., "The Elastic Cylindrical Shell Under Nearly Uniform Radial Impulse," Journal of Applied Mechanics, Transactions of the ASME, Vol. 31, No. 2, Jun. 1964, pp. 259-266.
10. Lindberg, H. E., "Buckling of a Very Thin Cylindrical Shell Due to an Impulsive Pressure," Journal of Applied Mechanics, Transactions of the ASME, Vol. 31, No. 2, Jun. 1964, pp. 267-272.

11. Roth, R. S. and Klosner, J. M., "Nonlinear Response of Cylindrical Shells Subjected to Dynamic Axial Loads," AIAA Journal, Vol. 2, No. 10, Oct. 1964, pp. 1788-1794.
12. Evan-Iwanowski, R. M., "On the Parametric Response of Structures," Applied Mechanics Reviews, Vol. 18, No. 9, Sept. 1965, pp. 699-702.
13. Bienick, M. P., Fan, T. C., and Lackman, L. M., "Dynamic Stability of Cylindrical Shells," AIAA Journal, Vol. 4, No. 3, Mar. 1966, pp. 495-500.
14. Hegemeir, G. A., "Instability of Cylindrical Shells Subjected to Axisymmetric Moving Loads," Journal of Applied Mechanics, Transactions of the ASME, Vol. 33, No. 2, Jun. 1966, pp. 289-296.
15. Hegemeir, G. A., "Stability of Cylindrical Shells Under Moving Loads by the Direct Method of Liapunov," Journal of Applied Mechanics, Transactions of the ASME, Vol. 34, No. 4, Dec. 1967, pp. 991-998.
16. Fan, T. C., "Dynamic Stability of a Thin Cylinder Under Radial Pressure," Memorandum RM-4583-PR, Jun. 1966, The Rand Corp.
17. Lock, M. H., "The Nonlinear Response of a Thin Circular Ring Under a Uniform Step Pressure Load," TR-1001(2240-30)-1, Nov. 1966, Aerospace Corp.
18. Lindberg, H. E., Anderson, D. L., Firth, R. D., and Parker, L. V., "Response of Reentry Vehicle-Type Shells to Blast Loads," Final Report to Lockheed Missiles and Space Co., Contract P.O. 24-14517 under AF 04(694) - 655, 1965, Stanford Research Institute.
19. Anderson, D. L. and Lindberg, H. E. "Dynamic Pulse Buckling of Cylindrical Shells Under Transient Lateral Pressures," AIAA Journal, Vol. 6, No. 4, Apr. 1968, pp. 589-598.
20. McIvor, I. K. and Lovell, E. G., "Dynamic Response of Finite-Length Cylindrical Shells to Nearly Uniform Radical Impulse," AIAA Journal, Vol. 6, No. 12, Dec. 1968, pp. 2346-2351.
21. Dietz, W. K., "On the Dynamic Stability of Eccentrically Reinforced Circular Cylindrical Shells," Ph.D. dissertation, Jan. 1967, Syracuse University.

22. Klosner, J. M. and Franklin, H. N., "A Note on the Dynamic Instability of Stiffened Cylindrical Shells," PIBAL Report No. 68-1, Jan. 1968, Polytechnic Institute of Brooklyn, Department of Aerospace Engineering and Applied Mechanics.
23. Block, D. L., "Influence of Discrete Ring Stiffeners and Prebuckling Deformations on the Buckling of Eccentrically Stiffened Orthotropic Cylinders," NASA TN D-4283, Jan. 1968.
24. Donnell, L. H., "Stability of Thin-walled Tubes Under Torsion," NACA Report No. 479, 1933.
25. Donnell, L. H., "A New Theory for the Buckling of Thin Cylinders Under Axial Compression and Bending," Transactions of the American Society of Mechanical Engineers, Vol. 56, 1934, pp. 795-806.
26. Galletly, G. D., "On the In-vacuo Vibrations of Simply Supported, Ring-Stiffened Cylindrical Shells," Proceedings of the U.S. National Congress of Applied Mechanics, 2nd., 1954, pp. 225-231.
27. Goldstein, H., Classical Mechanics, Addison-Wesley, Reading, Massachusetts, 1950, pp. 38-44.
28. Timoshenko, S. and Goodier, J. N., Theory of Elasticity, 2nd ed., McGraw-Hill, New York, Toronto, London, 1951, pp. 275-280.
29. Hurty, W. C. and Rubinstein, M. F., Dynamics of Structures, Prentice Hall, Englewood Cliffs, New Jersey, 1964, pp. 80-90.
30. Ball, R. E., "A Geometrically Nonlinear Analysis of Arbitrarily Loaded Shells of Revolution," NASA CR-909, Jan. 1968.
31. Chuang, K. P. and Veletsos, A. S., "A Study of Two Approximate Methods of Analyzing Cylindrical Shell Roofs," Civil Engineering Studies, Structural Research Series, No. 258, University of Illinois, Oct. 1962.
32. Ball, R. E., "Dynamic Analysis of Rings by Finite Differences," Journal of the Engineering Mechanics Division, Proceedings of the ASCE, Vol. 93, No. EM1, Mar. 22, 1966, pp. 1-10.
33. Cyrus, N. J. and Fulton, R. E., "Finite Difference Accuracy in Structural Analysis," Journal of the Structural Division, Proceedings of the ASCE, Vol. 92, No. ST6, Dec. 1966, pp. 459-471.

34. Wah, T. and Lu, W. C. L., "Vibration Analysis of Stiffened Cylinders including Inter-Ring Motion," The Journal of the Acoustical Society of America, Vol. 43, No. 5, 1968, pp. 1005-1016.
35. Smith, G. D., Numerical Solutions of Partial Differential Equations, Oxford University Press, New York, London, 1965, pp. 143-161.
36. Forsythe, G. E. and Wasow, W. R., Finite-Difference Methods for Partial Differential Equations, John Wiley & Sons, New York, London, Sydney, 1960, pp. 208-220.
37. Budiansky, B. and Radkowski, P. P., "Numerical Analysis of Unsymmetrical Bending of Shells of Revolution," AIAA Journal, Vol. 1, No. 8, Aug. 1963, pp. 1833-1842.
38. Jennings, W., First Course in Numerical Methods, Macmillan, New York, 1964, p. 149.
39. Crandall, S. H., Engineering Analysis, McGraw-Hill, New York, Toronto, London, 1956, pp. 376-396.
40. Johnson, D. E. and Grief, R., "Dynamic Response of a Cylindrical Shell: Two Numerical Methods," AIAA Journal, Vol. 4, No. 3, Mar. 1966, pp. 486-494.
41. Forsythe and Wasow, op. cit., pp. 101-107.
42. Newmark, N. M., "Computation of Dynamic Structural Response in the Range Approaching Failure," Proceedings of the Symposium on Earthquake and Blast Effects on Structures, Earthquake Engineering Institute, Los Angeles, 1952.
43. Newmark, N. M., "A Method of Computation for Structural Dynamics," Journal of the Engineering Mechanics Division, Proceedings of the ASCE, Vol. 85, No. EM 3, Jul. 1959, pp. 67-94.
44. Chang, G. C. and Ang, A. H. S., "Numerical Analysis of Plane Structure-Medium Interaction in Elastic Perfectly Plastic Media," Civil Engineering Studies, Structural Research Series No. 307, University of Illinois, Jun. 1966.
45. Bhuta, P. G., "Transient Response of a Thin Elastic Cylindrical Shell to a Moving Shock Wave," The Journal of the Acoustical Society of America, Vol. 35, No. 1, Jan. 1963, pp. 25-30.

46. Fung, Y. C., Sechler, E. E., and Kaplan, A., "On the Vibration of Thin Cylindrical Shells under Internal Pressure," Journal of the Aeronautical Sciences, Vol. 24, No. 9, Sep. 1957, pp. 650-660.
47. Stoker, J. J., Nonlinear Vibrations, Interscience Publishers, Inc., New York, 1950, pp. 202-213.
48. Krauss, H., Thin Elastic Shells, John Wiley & Sons, Inc., New York, London, Sydney, 1967, pp. 221-229.

APPENDIX A

INCONSISTENCY OF THE CONVENTIONAL DIFFERENCES

We will first show that the difference equations obtained by discretization of the governing differential equations do not agree with the difference equations obtained by minimizing the finite difference form of the potential energy when conventional central differences are used for approximating the derivatives. We will then show that the two sets of difference equations are identical when modified differences are used. Chuang and Veletsos [31] presented a very similar proof of this inconsistency of the conventional differences, but they did not expand the displacements in Fourier series as has been done here.

Consider the static equilibrium of a cylindrical shell under a uniform radial pressure. For the purpose of the present discussion, the linear shell equations will be used. After deleting the acceleration and velocity terms, equations (3.15) become

$$\begin{aligned}
 u_{,\xi\xi}^n + \frac{1+\nu}{2} n v_{,\xi}^n - \frac{1-\nu}{2} n^2 u^n - \nu w_{,\xi}^n &= 0 \\
 -n^2 v^n - \frac{1+\nu}{2} n u_{,\xi}^n + \frac{1-\nu}{2} v_{,\xi\xi}^n + n w^n &= 0 \\
 \frac{1}{12} \alpha^2 (w_{,\xi\xi\xi\xi}^n - 2n^2 w_{,\xi\xi}^n + n^4 w^n) &= \\
 \delta_{0n} p + n v^n - w^n + \nu u_{,\xi}^n &
 \end{aligned} \tag{A.1}$$

The conventional central differences for the first, second, and fourth derivatives of a function $f(\xi)$ are

$$\begin{aligned}(f,_{\xi})_K &= \frac{1}{2d} (f_{K+1} - f_{K-1}) \\(f,_{\xi\xi})_K &= \frac{1}{d^2} (f_{K+1} - 2f_K + f_{K-1}) \\(f,_{\xi\xi\xi\xi})_K &= \frac{1}{d^4} (f_{K+2} - 4f_{K+1} + 6f_K - 4f_{K-1} + f_{K-2})\end{aligned}\tag{A.2}$$

where d is spacing of the node points.

Using the conventional central differences given by (A.2) to approximate the derivatives in equations (A.1) leads to

$$\begin{aligned}\frac{1}{d^2} (u_{K+1}^n - 2u_K^n + u_{K-1}^n) + \frac{1+v}{2} n \frac{1}{2d} (v_{K+1}^n - v_{K-1}^n) - \frac{1-v}{2} n^2 u_K^n \\ - v \frac{1}{2d} (w_{K+1}^n - w_{K-1}^n) = 0 \\ -n^2 v_K^n - \frac{1+v}{2} n \frac{1}{2d} (u_{K+1}^n - u_{K-1}^n) + \frac{1-v}{2} \frac{1}{d^2} (v_{K+1}^n - 2v_K^n + v_{K-1}^n) + n w_K^n = 0 \\ \frac{1}{12} \alpha^2 \left[\frac{1}{d^4} (w_{K+2}^n - 4w_{K+1}^n + 6w_K^n - 4w_{K-1}^n + w_{K-2}^n) \right. \\ \left. - 2n^2 \frac{1}{d^2} (w_{K+1}^n - 2w_K^n + w_{K-1}^n) + n^4 w_K^n \right] = \\ \delta_{0n} p_K + n v_K^n - w_K^n + v \frac{1}{2d} (u_{K+1}^n - u_{K-1}^n)\end{aligned}\tag{A.3}$$

A set of difference equations can also be derived by minimizing the potential energy. The potential energy Π , for the linear shell under consideration here, is given by

$$\begin{aligned} \Pi = \frac{1}{2} \int_0^L \int_0^{2\pi a} & (N_x \epsilon_x + N_{xy} \gamma_{xy} + N_y \epsilon_y \\ & - M_x \chi_x + 2M_{xy} \chi_{xy} - M_y \chi_y - 2PW) dy dx \end{aligned} \quad (A.4)$$

The strain-displacement relations of the linear theory are

$$\begin{aligned} \epsilon_x &= U_{,x} & \chi_x &= W_{,xx} \\ \epsilon_y &= V_{,y} - \frac{W}{a} & \chi_y &= W_{,yy} \\ \gamma_{xy} &= U_{,y} + V_{,x} & \chi_{xy} &= W_{,xy} \end{aligned} \quad (A.5)$$

The in-plane forces and moments are related to the displacements by

$$\begin{aligned} N_x &= B[U_{,x} + \nu(V_{,y} - \frac{W}{a})] \\ N_y &= B(V_{,y} - \frac{W}{a} + \nu U_{,x}) \\ N_{xy} &= (\frac{1-\nu}{2})B(U_{,y} + V_{,x}) \\ M_x &= -D(W_{,xx} + \nu W_{,yy}) \\ M_y &= -D(W_{,yy} + \nu W_{,xx}) \\ M_{xy} &= (1-\nu)DW_{,xy} \end{aligned} \quad (A.6)$$

As before, the displacements are expanded in Fourier series

$$U(x, \theta) = \sum_{n=0}^{\infty} U^n(x) \cos n\theta \quad (\text{A.7a})$$

$$V(x, \theta) = \sum_{n=1}^{\infty} V^n(x) \sin n\theta \quad (\text{A.7b})$$

$$W(x, \theta) = \sum_{n=0}^{\infty} W^n(x) \cos n\theta \quad (\text{A.7c})$$

The terms comprising the integrand of (A.4) can be expressed in terms of the displacements by means of (A.5) and (A.6), leading to

$$\begin{aligned} N_x \epsilon_x &= B [U_x^2 + \nu (V_y - \frac{W}{a}) U_x] \\ N_y \epsilon_y &= B [(V_y - \frac{W}{a})^2 + \nu (V_y - \frac{W}{a}) U_x] \\ N_{xy} \gamma_{xy} &= \frac{1-\nu}{2} B (U_y + V_x)^2 \\ M_x \chi_x &= -D (W_{xx}^2 + \nu W_{xx} W_{yy}) \\ M_y \chi_y &= -D (W_{yy}^2 + \nu W_{yy} W_{xx}) \\ M_{xy} \chi_{xy} &= (1-\nu) D W_{xy}^2 \end{aligned} \quad (\text{A.8})$$

Replacing the displacements in (A.8) by the series of (A.7) yields

$$\begin{aligned} N_x \epsilon_x &= B \sum_{n=0}^{\infty} \sum_{m=0}^{\infty} [U_x^n U_x^m + \frac{\nu}{a} (nV^n - W^n) U_x^m] \cdot \\ &\quad \cos n\theta \cos m\theta \end{aligned} \quad (\text{A.9a})$$

$$N_Y \epsilon_Y = B \sum_{n=0}^{\infty} \sum_{m=0}^{\infty} \left[\frac{1}{2} (nV^n - W^n) (mV^m - W^m) + \frac{\nu}{a} U_{,x}^n (mV^m - W^m) \right] \cos n\theta \cos m\theta \quad (A.9b)$$

$$N_{xy} \gamma_{xy} = \frac{1-\nu}{2} B \sum_{n=1}^{\infty} \sum_{m=1}^{\infty} (V_{,x}^n - \frac{n}{a} U^n) (V_{,x}^m - \frac{m}{a} U^m) \cdot \sin n\theta \sin m\theta \quad (A.9c)$$

$$M_x \chi_x = -D \sum_{n=0}^{\infty} \sum_{m=0}^{\infty} (W_{,xx}^n W_{,xx}^m - \frac{\nu}{a^2} n^2 W^n W_{,xx}^m) \cdot \cos n\theta \cos m\theta \quad (A.9d)$$

$$M_y \chi_y = -D \sum_{n=0}^{\infty} \sum_{m=0}^{\infty} (\frac{n^2 m^2}{a^4}) W^n W^m - \nu \frac{n^2}{a^2} W^n W_{,xx}^m) \cdot \cos n\theta \cos m\theta \quad (A.9e)$$

$$M_{xy} \chi_{xy} = (1-\nu) D \sum_{n=1}^{\infty} \sum_{m=1}^{\infty} \frac{mn}{a^2} W_{,x}^n W_{,x}^m \sin n\theta \sin m\theta \quad (A.9f)$$

The potential energy of each mode is obtained by substituting (A.7c) and (A.9) into (A.4) and performing the circumferential integration. When $m, n \neq 0$, the potential energy of the n^{th} mode reduces to

$$\begin{aligned}
\Pi^n = & \frac{\pi a}{2} \int_0^L \{ B[(U, \frac{n}{x})^2 + \frac{v}{a} (nV^n - W^n) U, \frac{n}{x}] + \\
& \frac{1-v}{2} B(V, \frac{n}{x} - \frac{n}{a} U^n)^2 + B[\frac{1}{2} (nV^n - W^n)^2 + \\
& \frac{v}{a} U, \frac{n}{x} (nV^n - W^n)] + D[(W, \frac{n}{xx})^2 - \frac{v}{a^2} n^2 W, \frac{n}{xx}] \\
& + 2(1-v) D \frac{n^2}{a^2} (W, \frac{n}{x})^2 \\
& + D[\frac{n^4}{4} (W^n)^2 - v \frac{n^2}{a^2} W^n W, \frac{n}{xx}] \} dx
\end{aligned} \tag{A.10}$$

When $m = n = 0$, the potential energy is

$$\begin{aligned}
\Pi^0 = & \pi a \int_0^L \{ B[(U, \frac{0}{x})^2 - \frac{v}{a} W^0 U, \frac{0}{x} + \frac{1}{a^2} (W^0)^2] \\
& + D(W, \frac{0}{xx})^2 + 2PW^0 \} dx
\end{aligned} \tag{A.11}$$

The total potential energy is given by

$$\Pi = \sum_{n=0}^{\infty} \Pi^n$$

The principle of Minimum Potential Energy applies to each mode individually as well as to the collective sum of the potential energies of all the modes. Furthermore, the potential energy of a mode may be multiplied by an arbitrary constant without changing the conditions necessary for its

minimization. Accordingly, Π^0 is multiplied by one-half. This allows us to write a general expression for the potential energy which is valid for all values of n . For convenience the terms are grouped into two integrals, leading to

$$\begin{aligned}
 \Pi^n = & \frac{\pi a}{2} \int_0^L \{ B[(U_{,x}^n)^2 + \frac{2v}{a} (nV^n - W^n) U_{,x}^n \\
 & + \frac{1}{a^2} (nV^n - W^n)^2] + D[(W_{,xx}^n)^2 - 2\frac{v}{a^2} n^2 W^n W_{,xx}^n \\
 & + \frac{n^4}{a^4} (W^n)^2] + 2\delta_{0n} P W^n \} dx \\
 & + \frac{\pi a}{2} \int_0^L \{ \frac{1-v}{2} B(V_{,x}^n - \frac{n}{a} U^n)^2 \\
 & + 2(1-v) D \frac{n^2}{a^2} (W_{,x}^n)^2 \} dx
 \end{aligned} \tag{A.12}$$

where $\delta_{0n} = 1$ when $n = 0$ and $\delta_{0n} = 0$ when $n \neq 0$.

Let $\bar{\Pi}^n$ be defined by

$$\bar{\Pi}^n = \frac{2}{\pi a B} \Pi^n \tag{A.13}$$

Expressing (A.12) in terms of the nondimensional variables of (2.21) and using (A.13) give

$$\begin{aligned}
 \bar{\Pi}^n = & \int_0^1 \{ (u_{,\xi}^n)^2 + 2v(nV^n - W^n) u_{,\xi}^n + (nV^n - W^n)^2 \\
 & + \frac{1}{12} \alpha^2 [(w_{,\xi\xi}^n)^2 - 2vn^2 W^n w_{,\xi\xi}^n + n^4 (W^n)^2] + 2\delta_{0n} P W^n \} d\xi \\
 & + \int_0^1 \frac{1-v}{2} [v_{,\xi}^n - n u^n]^2 + \frac{1}{6} (1-v) \alpha^2 n^2 (w_{,\xi}^n)^2 \} d\xi
 \end{aligned} \tag{A.14}$$

Conventional differences will now be used in conjunction with equation (A.14) to derive a set of difference equations. In order to discretise the potential energy integral, let the ξ - coordinate of the n^{th} mode be divided into M elements each of length d . At the center of each element, locate a node point K . Then $\bar{\Pi}^n$ may be expressed by the following series.

$$\begin{aligned} \bar{\Pi}^n = & \lim_{M \rightarrow \infty} \sum_{K=1}^M \left\{ (u, \xi_K^n)^2 + 2\nu (nv_K^n - w_K^n) (u, \xi_K^n) \right. \\ & + (nv_K^n - w_K^n)^2 + \frac{1}{12} \alpha^2 [(w, \xi_K^n)^2 - 2\nu n^2 w_K^n (w, \xi_K^n) \\ & + n^4 (w_K^n)^2] + 2\delta_{0n} p_K w_K^n + \frac{1-\nu}{2} [(v, \xi_K^n) - \\ & \left. nu_K^n]^2 + \frac{1}{6} (1-\nu) \alpha^2 n^2 (w, \xi_K^n)^2 \right\} d \end{aligned} \quad (\text{A.15})$$

where $d = 1/M$. The potential energy $\bar{\Pi}^n$ can be approximated by taking M to be finite and using central differences to express the derivatives.

The principle of minimum potential energy demands that the displacements $u_1^n, v_1^n, w_1^n, u_2^n, v_2^n, w_2^n, \dots, u_M^n, v_M^n, w_M^n$ minimize the potential energy $\bar{\Pi}^n$, i.e.

$$\delta \bar{\Pi}^n = \sum_{K=1}^M \left\{ \frac{\partial \bar{\Pi}^n}{\partial u_K^n} \delta u_K^n + \frac{\partial \bar{\Pi}^n}{\partial v_K^n} \delta v_K^n + \frac{\partial \bar{\Pi}^n}{\partial w_K^n} \delta w_K^n \right\} = 0 \quad (\text{A.16})$$

Since the virtual displacements $\delta u_1^n, \delta v_1^n, \delta w_1^n, \dots, \delta u_M^n, \delta v_M^n, \delta w_M^n$ are arbitrary, it follows that

$$\frac{\partial \bar{\Pi}^n}{\partial (u_K^n)} = 0$$

$$\frac{\partial \bar{\Pi}^n}{\partial (v_K^n)} = 0 \quad (\text{A.17})$$

$$\frac{\partial \bar{\Pi}^n}{\partial (w_K^n)} = 0 \quad K = 1, \dots, M$$

When the derivatives in (A.15) are replaced by their conventional central difference approximations (A.2), the potential energy becomes

$$\begin{aligned} \bar{\Pi}^n = & \{ \dots + (\frac{u_{K+2}^n - u_K^n}{2d})^2 + \dots + (\frac{u_K^n - u_{K-2}^n}{2d})^2 + \dots \\ & + 2v(nv_{K+1}^n - w_{K+1}^n)(\frac{u_{K+2}^n - u_K^n}{2d}) + 2v(nv_K^n - w_K^n) \cdot \\ & (\frac{u_{K+1}^n - u_{K-1}^n}{2d}) + 2v(nv_{K-1}^n - w_{K-1}^n)(\frac{u_K^n - u_{K-2}^n}{2d}) + \dots \\ & + (nv_K^n - w_K^n)^2 + \dots \frac{1}{12} \alpha^2 [(\frac{w_{K+2}^n - 2w_{K+1}^n + w_K^n}{d^2})^2 \\ & + (\frac{w_{K+1}^n - 2w_K^n + w_{K-1}^n}{d^2})^2 + (\frac{w_K^n - 2w_{K-1}^n + w_{K-2}^n}{d^2})^2 + \dots \\ & - 2vn^2 w_{K+1}^n (\frac{w_{K+2}^n - 2w_{K+1}^n + w_K^n}{d^2}) - 2vn^2 w_K^n (\frac{w_{K+1}^n - 2w_K^n + w_{K-1}^n}{d^2}) \\ & - 2vn^2 w_{K-1}^n (\frac{w_K^n - 2w_{K-1}^n + w_{K-2}^n}{d^2}) + \dots + n^4 (w_K^n)^2] + \dots + 2\delta_{0n} p_K w_K^n \\ & + \dots + \frac{1-v}{2} [(\frac{v_{K+2}^n - v_K^n}{2d} - nu_{K+1}^n)^2 + (\frac{v_{K+1}^n - v_{K-1}^n}{2d} - nu_K^n)^2 + \\ & (\frac{v_K^n - v_{K-2}^n}{2d} - nu_{K-1}^n)^2 + \dots + \frac{1}{6} (1-v) \alpha^2 n^2 [(\frac{w_{K+2}^n - w_K^n}{2d})^2 + \dots + \\ & (\frac{w_K^n - w_{K-2}^n}{2d})^2] + \dots \} d \end{aligned} \quad (\text{A.18})$$

Only the terms containing u_K^n , v_K^n , and w_K^n have been displayed since the displacements at the other stations, $K+1$, $K-1$, etc., do not enter into the variation of u_K^n , v_K^n , and w_K^n .

The axial, circumferential, and radial difference equations are obtained by equating to zero $\frac{\partial \Pi^n}{\partial (u_K^n)}$, $\frac{\partial \Pi^n}{\partial (v_K^n)}$, $\frac{\partial \Pi^n}{\partial (w_K^n)}$. The resulting equations are

Axial:

$$\frac{u_{K+2}^n - 2u_K^n + u_{K-2}^n}{4d^2} + \frac{1+\nu}{2} n \left(\frac{v_{K+1}^n - v_{K-1}^n}{2d} \right) \quad (A.19a)$$

$$- \frac{1-\nu}{2} n^2 u_K^n - \nu \left(\frac{w_{K+1}^n - w_{K-1}^n}{2d} \right) = 0$$

Circumferential:

$$-n^2 v_K^n - \frac{1+\nu}{2} n \left(\frac{u_{K+1}^n - u_{K-1}^n}{2d} \right) + \frac{1-\nu}{2} \left(\frac{v_{K+2}^n - 2v_K^n + v_{K-2}^n}{4d^2} \right)$$

$$+ n^2 w_K^n = 0 \quad (A.19b)$$

Radial:

$$\frac{1}{12} \alpha^2 \left[\left(\frac{w_{K+2}^n - 4w_{K+1}^n + 6w_K^n - 4w_{K-1}^n + w_{K-2}^n}{d^4} \right) \right.$$

$$- 2n^2 \left(\frac{w_{K+2}^n - 2w_K^n + w_{K-2}^n}{4d^2} \right) + n^4 w_K^n +$$

$$\left. \frac{\nu}{2} n^2 d^2 \left(\frac{w_{K+2}^n - 4w_{K+1}^n + 6w_K^n - 4w_{K-1}^n + w_{K-2}^n}{d^4} \right) \right] =$$

$$\delta_{0n} p_K + n v_K^n - w_K^n - w_K^n + \nu \left(\frac{u_{K+1}^n - u_{K-1}^n}{2d} \right)$$

Let us compare the above difference equations with (A.3) which were derived directly from the differential equations. Note that the second derivatives in equations (A.19) are represented by expressions of the form

$$(f, \xi \xi)_K = \frac{1}{4d^2} (f_{K+2} - 2f_K + f_{K-2})$$

as opposed to the conventional central differences of the second derivatives in (A.3).

In addition, (A.19c) contains a term which has no counterpart in (A.3c) namely

$$\frac{\nu}{24} \alpha^2 d^2 n^2 \left(\frac{w_{K+2}^n - 4w_{K+1}^n + 6w_K^n - 4w_{K-1}^n + w_{K-2}^n}{d^4} \right)$$

Were it not for the presence of n^2 , this term might be discarded as a higher order term. However, the problem under investigation encompasses response modes having several circumferential waves; and the term may not be small compared to other quantities which appear in the radial equilibrium equation.

Consider now the modified central differences. A set of difference equations will be derived by minimizing the potential energy in modified difference form. Consequently, a series representation of (A.14) must replace the integral formulation. The right side of (A.14) was written as the sum of two integrals for reasons which will now become apparent. In order to obtain a series which is

equivalent to the first integral, let the ξ -coordinate be subdivided such that a whole station node is located at the center of each segment. This procedure is schematically illustrated in Figure A.1a. In approximating the first integral, the half station at each end is neglected. Doing so does not affect the difference equations that must hold at the interior points. Hence, the first integral can be written in the form

$$\begin{aligned} \text{1st Integral} = & \sum_{K=2}^{M-1} \{ (u, \xi)_K^n^2 + 2v(nv_K^n - w_K^n)(u, \xi)_K^n + (nv_K^n - w_K^n)^2 \\ & + \frac{1}{12} \alpha^2 [(w, \xi\xi)_K^n^2 - 2vn^2 w_K^n (w, \xi\xi)_K^n + n^4 (w_K^n)^2] + 2\delta_{0n} p_K w_K^n \} d \end{aligned}$$

The second integral of (A.14) is approximated by using finite elements which are centered at half station nodes, as shown in Figure A.1b. The series approximation of this integral is given by

$$\begin{aligned} \text{2nd Integral} = & \sum_{K=1/2, 3/2, \dots}^{M-1/2} \{ \frac{1-v}{2} [(v, \xi)_K^n^2 - nu_K^n]^2 \\ & + \frac{1}{6} (1-v) \alpha^2 n^2 (w, \xi)_K^n^2 \} d \end{aligned}$$

Combining these two series leads to the equation for the potential energy. Replacing the derivatives by modified central differences of (3.16) and minimizing the potential energy lead to the governing difference equations

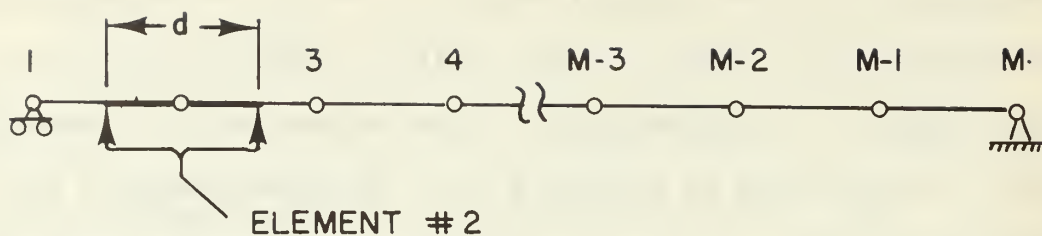


FIGURE A.1a

"WHOLE" STATION MESH-MODIFIED DIFFERENCES

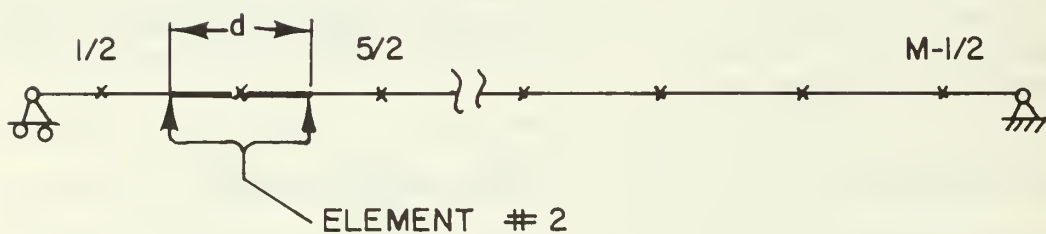


FIGURE A.1b

"HALF" STATION MESH-MODIFIED DIFFERENCES

$$\begin{aligned}
& \frac{1}{d^2} (u_{K+3/2}^n - 2u_{K+1/2}^n - u_{K+1/2}^n) + \frac{1-\nu}{2} n \frac{1}{d} (v_{K+1}^n - v_K^n) \\
& - \frac{1-\nu}{2} n^2 u_{K+1/2}^n - \nu \frac{1}{d} (w_{K+1}^n - w_K^n) = 0 \\
& -n^2 \frac{1}{d} v_K^n + \frac{1-\nu}{2} n \frac{1}{d} (u_{K+1/2}^n - u_{K-1/2}^n) + \frac{1-\nu}{2} \frac{1}{d^2} (v_{K+1}^n - 2v_K^n + v_{K-1}^n) \\
& + n w_K^n = 0 \tag{A.20}
\end{aligned}$$

$$\begin{aligned}
& \frac{1}{12} \alpha^2 \left[\frac{1}{d^4} (w_{K+2}^n - 4w_{K+1}^n + 6w_K^n - 4w_{K-1}^n + w_{K-2}^n) \right. \\
& \left. - 2n^2 \frac{1}{d^2} (w_{K+1}^n - 2w_K^n + w_{K-1}^n) + n^4 w_K^n \right] \\
& = \delta_{0n} p_K - n v_K^n - w_K^n + \nu \frac{1}{d} (u_{K+1/2}^n - u_{K-1/2}^n)
\end{aligned}$$

These equations are identical to the static version of (3.17), equations obtained by applying the modified differences to the governing differential equations (3.15).

When the modified differences are used to approximate the derivatives, the set of difference equations obtained by satisfying the differential equations at a finite number of points are the same as the difference equations obtained by satisfying the condition of minimum potential energy. On the other hand, when conventional central differences are used, the difference equations obtained from the differential equations do not agree with those obtained by the energy method. Consequently, the

modified differences should yield more accurate solutions than conventional differences for the same mesh length.

APPENDIX B

ADAPTATION OF MODIFIED DIFFERENCES TO THE NONLINEAR EQUATIONS

I. EVALUATION OF NONLINEAR TERMS

In-plane Forces, λ_1 , and λ_2

The in-plane forces were expressed in Chapter III by (3.5). Let n_ξ^n and n_θ^n be defined as whole station quantities, and let $n_{\xi\theta}^n$ be a half station quantity. Replacing the derivatives in (3.5) with the appropriate modified difference expressions from (3.18) leads to

$$\begin{aligned} (n_\xi^n)_K &= \frac{1}{d}(u_K^n - u_{K-1}^n) + v(nv_K^n - w_K^n) \\ &\quad + C_{xx_K}^n + C_{IT_T_K}^n + v(C_{TT_K}^n + C_{ITT_K}^n) \end{aligned} \tag{B.1a}$$

$$\begin{aligned} (n_\theta^n)_K &= nv_K^n - w_K^n + \frac{v}{d}(u_K^n - u_{K-1}^n) \\ &\quad + C_{TT_K}^n + C_{ITT_K}^n + v(C_{XX_K}^n + C_{IXX_K}^n) \end{aligned} \tag{B.1b}$$

$$\begin{aligned} (n_{\xi\theta}^n)_K &= \frac{1-v}{2} \left[\frac{1}{d}(v_{K+1}^n - v_K^n) - nu_K^n + C_{XT_K}^n \right. \\ &\quad \left. + C_{IXT_K}^n + C_{ITX_K}^n \right] \end{aligned} \tag{B.1c}$$

The nonlinear terms in the axial and circumferential equations are contained in λ_1^n and λ_2^n , defined by (3.8) and (3.9). Equation (3.20) requires that λ_1^n be defined

at half stations, and equation (3.21) requires that $\lambda 2^n$ be defined at whole stations. Approximating (3.8) at the half station k and (3.9) at the whole station K results in

$$\begin{aligned} \lambda 1_k^n = & \frac{1}{d}(C_{XX_{K+1}}^n - C_{XX_K}^n) + \frac{1}{d}(C_{IXX_{K+1}}^n - C_{IXX_K}^n) + \\ & v[\frac{1}{d}(C_{TT_{K+1}}^n - C_{TT_K}^n) + \frac{1}{d}(C_{ITT_{K+1}}^n - C_{ITT_K}^n)] \quad (B.2a) \\ & + \frac{1-v}{2}n(C_{XT_k}^n + C_{IXT_k}^n + C_{ITX_k}^n) - \frac{v}{d}(w_{K+1}^n - w_K^n) \end{aligned}$$

$$\begin{aligned} \lambda 2_K^n = & -n[C_{TT_K}^n + C_{ITT_K}^n + v(C_{XX_K}^n + C_{IXX_K}^n)] + \\ & \frac{1-v}{2} [\frac{1}{d}(C_{XT_k}^n - C_{XT_{k-1}}^n) + \frac{1}{d}(C_{IXT_k}^n - C_{IXT_{k-1}}^n)] \quad (B.2b) \\ & + \frac{1}{d}(C_{ITX_k}^n - C_{ITX_{k-1}}^n) + nw_K^n \end{aligned}$$

Examination of (B.1) and (B.2) shows that C_{TT}^n , C_{ITT}^n , C_{XX}^n , and C_{IXX}^n must be defined at whole stations while C_{IXT}^n , C_{XT}^n , and C_{ITX}^n must be defined at half stations. As seen from (3.4a) and (3.4d), C_{XX}^n and C_{IXX}^n are obtained by summing appropriate products of the form

$$w_{\xi}^i w_{\xi}^j$$

and

$$\bar{w}_{\xi}^i w_{\xi}^j$$

Since C_{XX}^n and C_{IXX}^n are defined at a whole station, $w_{,\xi}^n$ and $\bar{w}_{,\xi}^n$ must be calculated at whole stations. However, w^n is defined at whole stations only; and the modified difference form defines $w_{,\xi}^n$ at half stations, not whole stations. A similar situation exists for the half station nonlinear terms C_{XT}^n and C_{IXT}^n , terms which can be evaluated only if w^n is known at half stations. This creates some difficulty when utilizing the modified finite differences to solve the nonlinear equations numerically. The difficulty is overcome through the use of interpolation formulas or simple averaging.

Consider the problem of determining $w_{,\xi}^n$ at a whole station. With reference to Figure B.1, let w_{k-1}^n and w_k^n be the radial displacements at half stations $k-1$ and k , respectively. The required derivative of w^n , which we shall denote $(w_{,\xi}^n)_K$, is given by

$$(w_{,\xi}^n)_K = \frac{1}{d}(w_k^n - w_{k-1}^n) \quad (B.3)$$

By expanding w^n in Taylor series, the quantity $(w_k^n - w_{k-1}^n)$ can be expressed as a linear combination of w_{K-2}^n , w_{K-1}^n , w_{K+1}^n , and w_{K+2}^n . Using the Taylor series to express w_K^n , we have

$$w_K^n = w_k^n - \frac{d}{2}(w_{,\xi}^n)_K + \frac{1}{2}\left(\frac{d}{2}\right)^2 (w_{,\xi\xi}^n)_K + O(d^3) \quad (B.4)$$

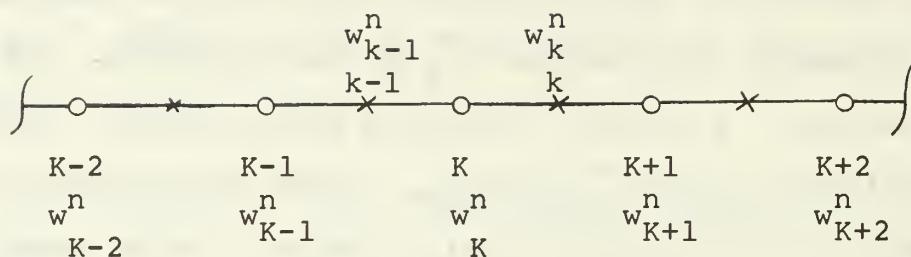


FIGURE B.1
FINITE DIFFERENCE STATIONS

where $(w_{,\xi}^n)_k$ and $(w_{,\xi\xi}^n)_k$ are the first and second derivatives of w^n at half station k . The notation $O(d^3)$ means that the truncated terms are of order d^3 . The second derivative $(w_{,\xi\xi}^n)_k$ can be expressed in terms of $(w_{,\xi\xi}^n)_K$ or $(w_{,\xi\xi}^n)_{K+1}$ as

$$(w_{,\xi\xi}^n)_k = (w_{,\xi\xi}^n)_K + \frac{d}{2}(w_{,\xi\xi\xi}^n)_K + O(d^2) \quad (B.5a)$$

$$(w_{,\xi\xi}^n)_k = (w_{,\xi\xi}^n)_{K+1} - \frac{d}{2}(w_{,\xi\xi\xi}^n)_K + O(d^2) \quad (B.5b)$$

Adding the above two equations yields

$$\begin{aligned} (w_{,\xi\xi}^n)_k &= \frac{1}{2}[(w_{,\xi\xi}^n)_K + (w_{,\xi\xi}^n)_{K+1}] + O(d^2) \\ &= \frac{1}{2d^2}(w_{K+2}^n - w_{K+1}^n - w_K^n + w_{K-1}^n) + O(d^2) \end{aligned} \quad (B.6)$$

Also, we have that

$$(w_{,\xi}^n)_k = \frac{1}{d}(w_{K+1}^n - w_K^n) + O(d^2) \quad (B.7)$$

Substituting (B.6) and (B.7) into (B.4) leads to

$$w_K^n = \frac{9}{16}(w_K^n + w_{K+1}^n) - \frac{1}{16}(w_{K-1}^n + w_{K+2}^n) + O(d^3) \quad (B.8)$$

It follows immediately from (B.8) that

$$w_{K-1}^n = \frac{9}{16}(w_{K-1}^n + w_K^n) - \frac{1}{16}(w_{K+1}^n + w_{K-2}^n) + O(d^3) \quad (B.9)$$

Finally, the interpolation formula for the derivative is obtained by substituting (B.8) and (B.9) into (B.3), resulting in

$$(w'_{,\xi})_K = \frac{1}{16d}[10(w_{K+1}^n - w_K^n) - (w_{K+2}^n - w_{K-2}^n)] + O(d^2) \quad (B.10a)$$

When it is necessary to calculate w^n at a half station, either (B.8) or (B.9) may be used.

At the boundaries the first derivative of w^n may be approximated by using a forward or backward difference with (B.8) or (B.9). Since $w_1^n = w_M^n = 0$, the result is

$$(w'_{,\xi})_{K=1} = \left(\frac{2}{d}\right)\left[\frac{9}{16}w_2^n - \frac{1}{16}(w_0^n + w_3^n)\right] + O(d) \quad (B.10b)$$

and

$$(w'_{,\xi})_{K=M} = -\left(\frac{2}{d}\right)\left[\frac{9}{16}w_{M-1}^n - \frac{1}{16}(w_{M+1}^n + w_{M-2}^n)\right] + O(d) \quad (B.10c)$$

The procedures for evaluating the Fourier coefficients of the nonlinear terms defined by equations (3.4a) - (3.4g) are described in Appendix B of Reference [30]. For example, C_{XX}^n at whole station K is given by

$$(C_{XX}^n)_K = \frac{1}{4} \sum_{i=0}^{\infty} (w_{,\xi}^n)_K [\eta^C(w_{,\xi}^{i+n})_K + \mu^C(w_{,\xi}^{|i-n|})_K] \quad (B.11)$$

where

$$\eta^C = \begin{cases} 1 & \text{if } n > 0 \\ 0 & \text{if } n = 0 \end{cases}$$

$$\mu^C = \begin{cases} 1 & \text{if } i \neq n \\ 2 & \text{if } i = n \end{cases}$$

The terms of the series can be evaluated by utilizing

(3.18), (B.8), (B.9), or (B.10). The other nonlinear terms $C_{IXX_K}^n$, $C_{TT_K}^n$, $C_{ITT_K}^n$, $C_{XT_K}^n$, $C_{IXT_K}^n$, and $C_{ITX_K}^n$ can be evaluated from equations similar to (B.11).¹

Nonlinear Terms η_{ξ}^n , $\eta_{\xi\theta}^n$, and η_{θ}^n

The nonlinear terms in the radial equation, (3.22), are embodied in the terms $\eta_{\theta_K}^n$, $\eta_{\xi_K}^n$, $\eta_{\xi\theta_K}^n$, and $\eta_{\theta_K}^n$. Equation (B.1b) is used to compute the first of these terms. The nonlinear terms η_{ξ}^n and η_{ξ}^n are defined by (3.4h) and (3.4j). The calculation of $(\eta_{\xi}^n)_K$ involves the summation of products of the form

$$(n_{\xi}^i)_K [(w_{,\xi\xi}^j)_K + (\bar{w}_{,\xi\xi}^j)_K]$$

¹The coefficients $C_{IXX_K}^n$, $C_{ITT_K}^n$, $C_{IXT_K}^n$, and $C_{ITX_K}^n$ are not truly nonlinear since they are sums of products that contain derivatives of the initial imperfection. However they are computed in the same manner as the nonlinear terms.

for appropriate values of i and j , and the calculation of $(\eta_{\theta}^n)_K$ requires summing products of the form

$$(\eta_{\theta}^i)_K [-j^2 (w^j + \bar{w}^j)_K]$$

The summations are defined by expressions similar to (B.11). The terms in the products can be computed from (B.1a), (B.1c), and the difference approximations of (3.18).

The remaining nonlinear term $(\eta_{\xi\theta}^n)_K$ requires the use of a simple average. Equation (3.4i) expresses $(\eta_{\xi\theta}^n)_K$ as

$$\left(\sum_{i=1}^{\infty} 2n_{\xi\theta_K}^i \sin i\theta \right) \left[\sum_{j=1}^{\infty} -j (w_{\xi_K}^j + \bar{w}_{\xi_K}^j) \sin j\theta \right] = \sum_{n=0}^{\infty} \eta_{\xi\theta_K}^n \cos n\theta \quad (3.4i)$$

However, (B.1c) defines $\eta_{\xi\theta}^n$ as a half station quantity. We take $\eta_{\xi\theta_K}^n$ as the average of $\eta_{\xi\theta_K}^n$ and $\eta_{\xi\theta_{K-1}}^n$; thus, (3.4i) can be written as

$$\sum_{n=0}^{\infty} \eta_{\xi\theta_K}^n \cos n\theta = \left[\sum_{i=1}^{\infty} (n_{\xi\theta_K}^i + n_{\xi\theta_{K-1}}^i) \sin i\theta \right] \left[\sum_{j=1}^{\infty} -j (w_{\xi_K}^j + \bar{w}_{\xi_K}^j) \sin j\theta \right] \quad (B.12)$$

where, as before, $w_{\xi_K}^n$ is the first derivative of w^n at whole station K and can be evaluated by using equation (B.10). From (B.1c) it follows that

$$\begin{aligned} n_{\xi\theta_K}^n + n_{\xi\theta_{K-1}}^n &= \frac{1-v}{2} [v_{K+1}^n - v_{K-1}^n - n(u_K^n + u_{K-1}^n)] \\ &+ C_{XT_K}^n + C_{XT_{K-1}}^n + C_{IXT_K}^n + C_{IXT_{K-1}}^n + C_{ITX_K}^n + C_{ITX_{K-1}}^n \end{aligned} \quad (B.13)$$

Finally $(\eta_{\xi\theta}^n)_K$ can be evaluated by using a formula from Appendix B of Reference [30], similar to (B.11).

II. Boundary Conditions on Displacements

Consider the case in which the axial displacements are zero at the ends. Since u^n is not defined at the whole stations $K=1$ and $K=M$ at the ends of the shell, interpolation formulae are required. The finite difference stations near the end $\xi = 0$ are shown in Figure B.2. The displacement $u_{K=1}^n$ can be expressed by the Taylor series

$$u_{K=1}^n = u_{K=1}^n + \frac{d}{2}(u_{,\xi}^n)_{K=1} + \frac{1}{2}\left(\frac{d}{2}\right)^2(u_{,\xi\xi}^n)_{K=1} + O(d^2) \quad (B.14)$$

Now

$$u_{,\xi}^n_{K=1} = \frac{u_{K=1}^n - u_{K=2}^n}{d} + O(d^2) \quad (B.15)$$

and using forward differences gives

$$(u_{,\xi\xi}^n)_{K=1} = \frac{(u_{,\xi}^n)_{K=2} - (u_{,\xi}^n)_{K=1}}{d} + O(d) \quad (B.16)$$

We also have

$$(u_{,\xi}^n)_{K=2} = \frac{u_{K=2}^n - u_{K=1}^n}{d} + O(d^2) \quad (B.17)$$

To obtain the desired boundary condition, (B.15) and (B.17) are substituted into (B.16), (B.15) and (B.16) are substituted into (B.14), and $(u^n)_{K=1}$ is equated to zero. The result is

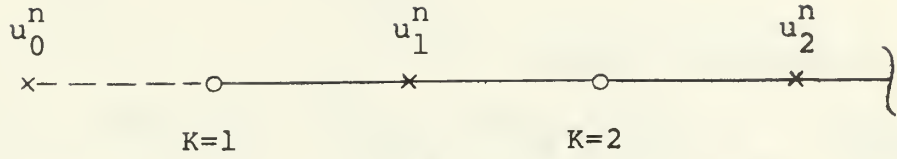


FIGURE B.2

FINITE DIFFERENCE STATIONS
AT THE END $\xi = 0$

$$u_0^n + 2u_1^n - \frac{1}{3} u_2^n + O(d^3) = 0 \quad (\text{B.18})$$

Similarly, the condition that $u^n = 0$ at $\xi = 1$ can be expressed by

$$u_m^n + 2u_{m-1}^n - \frac{1}{3} u_{m-2}^n + O(d^3) = 0 \quad (\text{B.19})$$

When the shell is clamped at $K=1$ and $K=M$, the slopes, $(w_{,\xi}^n)_{K=1}$ and $(w_{,\xi}^n)_{K=M}$ must be zero. Equating (B.10b) and (B.10c) to zero yields

$$w_0^n - 9w_2^n + w_3^n = 0 \quad (\text{B.20})$$

$$w_{M-2}^n - 9w_{M-1}^n + w_{M-1}^n = 0 \quad (\text{B.21})$$

APPENDIX C

DEFINITIONS OF CONSTANTS AND MATRICES

In equation (3.22)

$$d_1 = 1 + \sum_{j=1}^{N_r} \delta_{KH_j} C_2$$

$$d_2 = - \frac{c}{\alpha}$$

$$d_3 = - \frac{1}{12} \frac{\alpha^2}{d^4}$$

$$d_4 = - \frac{1}{6} \frac{\alpha^2}{d^2} (n^2 + \frac{2}{d^2})$$

$$d_5 = - \frac{1}{12} \frac{\alpha^2}{d^4} (6 + 4n^2 d^2 + n^4 d^4)$$

In equation (3.23)

$$d_6 = - \frac{n^2}{d^2} [C_4 e^{(2-en^2)} - C_5]$$

$$d_7 = - C_4 n^2 - C_1 (n^2 - 1)^2 - C_3 (en^2 - 1)^2 - 2d_6$$

$$d_8 = - \frac{n^2}{d} [C_4 (1 - en^2) + C_5]$$

$$d_9 = nC_3 (1 - en^2)$$

In equation (4.2)

$$A^n = \begin{bmatrix} 1 & \operatorname{dn}\left(\frac{1+\nu}{2}\right) \\ 0 & \frac{1-\nu}{2} \end{bmatrix}$$

$$B_K^n = \begin{bmatrix} -2 - d^2 n^2 \left(\frac{1-\nu}{2}\right) + \sum_{j=1}^{N_r} \delta_{KH_j} d^2 n^2 (C_4 n^2 + C_5) & -\left(\frac{1+\nu}{2}\right) \operatorname{dn} \\ -\left(\frac{1+\nu}{2}\right) \operatorname{dn} & -1(1-\nu) - d^2 n^2 + \sum_{j=1}^{N_r} \delta_{KH_j} d^2 n^2 C_3 \end{bmatrix}$$

$$C^n = \begin{bmatrix} 1 & 0 \\ \operatorname{dn}\left(\frac{1+\nu}{2}\right) & \frac{1-\nu}{2} \end{bmatrix}$$

In equation (4.8), P_1^n is given by the following expressions.

Simply supported ends:

$$P_1^n = \begin{bmatrix} \frac{-1}{1 + d^2 n^2 \left(\frac{1-\nu}{2}\right)} & \frac{-\operatorname{dn}\left(\frac{1+\nu}{2}\right)}{1 + d^2 n^2 \left(\frac{1-\nu}{2}\right)} \\ 0 & 0 \end{bmatrix}$$

Clamped ends:

$$P_1^n = \begin{bmatrix} \frac{-4/3}{4 + d^2 n^2 \left(\frac{1-\nu}{2}\right)} & \frac{-\operatorname{dn}\left(\frac{1+\nu}{2}\right)}{4 + d^2 n^2 \left(\frac{1-\nu}{2}\right)} \\ 0 & 0 \end{bmatrix}$$

In equation (4.11) matrices H^n and 0^n are given by the following expressions.

Simply supported ends:

$$H^n = - \begin{bmatrix} 1 + d^2 n^2 \left(\frac{1-\nu}{2}\right) & dn \left(\frac{1+\nu}{2}\right) \\ dn \left(\frac{1+\nu}{2}\right) & 1-\nu + d^2 n^2 \end{bmatrix}$$

$$0^n = \begin{bmatrix} 1 & 0 \\ dn \left(\frac{1+\nu}{2}\right) & \frac{1-\nu}{2} \end{bmatrix}$$

$$f^n = g_{M-1}^n + \begin{bmatrix} d(c_{XX}^n + c_{IXX}^n) \\ 0 \end{bmatrix}_M$$

Clamped ends:

$$H^n = - \begin{bmatrix} 4 + d^2 n^2 \left(\frac{1-\nu}{2}\right) & dn \left(\frac{1+\nu}{2}\right) \\ dn \left(\frac{1+\nu}{2}\right) & 1-\nu + d^2 n^2 \end{bmatrix}$$

$$0^n = \begin{bmatrix} 4/3 & 0 \\ \operatorname{dn}(\frac{1+v}{2}) & \frac{1-v}{2} \end{bmatrix}$$

$$f_K^n = g_{M-1}^n$$

In equation (4.12)

$$R^n = \begin{bmatrix} 0 & 0 \\ \frac{\operatorname{dn}(\frac{1+v}{2})}{\frac{1-v}{2} + d^2 n^2} & \frac{(\frac{1-v}{2})}{(\frac{1-v}{2}) + d^2 n^2} \end{bmatrix}$$

$$s^n = \begin{bmatrix} 0 \\ \frac{\Lambda 2_m^n}{\frac{1-v}{2} + d^2 n^2} \end{bmatrix}$$

APPENDIX D

COMPUTER PROGRAM

I. FORTRAN VARIABLES

Table XI lists the major Fortran variables and their algebraic counterparts from the main body of the dissertation, if such a counterpart exists. The equation in which the algebraic counterpart was first defined is indicated in the remarks column. The more important program control variables are also briefly described.

II. DESCRIPTION OF THE PROGRAM

The computer program has been written in FORTRAN IV language for operation with the IBM 360 MODEL 67 Computer. The program was compiled by the FORTRAN IV G Level 1, Mod 3 compiler. The program is dimensioned to accommodate twenty equally spaced axial stations and fifteen arbitrary Fourier modes. The program will handle up to three identical ring stiffeners, located so as to divide the shell into segments of equal length. The memory requirements and the execution time are contained in part IV of this appendix.

The program solves a set of three nondimensional, nonlinear equations by an iterative procedure. The dependent variables are expanded in Fourier sine or cosine series in the circumferential coordinate. The nonlinear

TABLE XI
DESCRIPTION OF FORTRAN VARIABLES

FORTRAN VARIABLE	ALGEBRAIC COUNTERPART	DEFINING EQUATION AND/OR DESCRIPTION
A(I,J)	A^n	(4.2)
ALPHA	α	(2.21)
AMP(L)	$ w_1^n / \bar{w}_1^n $	(5.19)
B(I,J)	B_K^n	(4.2) B_K^n matrix without ring terms
BC3(I,J)	H^n or R^n	(4.11) or (4.12)
BC4(I,J)	O^n	(4.11)
BETA	β	(4.14)
BR(I,J)	B_K^n	(4.2) B_K^n matrix with ring terms
BSTRES	$\frac{1}{2}\alpha \mid \Sigma n^2 w_K^n \mid$	(4.30)
C(I,J)	C^n	(4.2)
C1,...,C5	C1,...,C5	(2.21)
CDAMP	c	(2.21)
CITT(K,L)	$C_{ITT_K}^n$	(3.4e)

TABLE XI Continued

FORTAN VARIABLE	ALGEBRAIC COUNTERPART	DEFINING EQUATION AND/OR DESCRIPTION
CITX(K,L)	$C_{ITX_K}^n$	(3.4g)
CIXT(K,L)	$C_{IXT_K}^n$	(3.4f)
CIXX(K,L)	$C_{IXX_K}^n$	(3.4d)
CTT(K,L)	$C_{TT_K}^n$	(3.4b)
CXT(K,L)	$C_{XT_K}^n$	(3.4c)
D	d	nondimensional spacing of finite difference mesh
D1,...,D11		dummy floating point variables
DEE(I,J,K,L)	$[B_K^n - C^n P_{K-1}^n]^{-1}$	(4.7)
DM1(I,J) DM2(I,J) DM3(I,J)		dummy 2x2 floating point arrays
DST(I,J,K,L)	$[B_K^n - C^n P_{K-1}^n]^{-1} C^n$	(4.7)
DT	$\Delta\tau$	(4.13)
DTMAX		maximum permissible $\Delta\tau$

TABLE XI Continued

FORTAN VARIABLE	ALGEBRAIC COUNTERPART	DEFINING EQUATION AND/OR DESCRIPTION
E	e	(2.21)
EPS	ϵ	convergence parameter
ETAX(K,L)	$\eta_{\xi K}^n$	(3.22)
ETAXTH(K,L)	$\eta_{\xi \theta K}^n$	(3.22)
ETATH(K,L)	$\eta_{\theta K}^n$	(3.22)
FN	n	
GEE	g_K^n	(4.2)
GNU	ν	Poisson's ratio
I1,...,I4		Dummy integer variables
ICORFL		Indicates whether or not more modes are to be added
ID(L,J)		Fourier numbers N(ID) that combine through differences to produce a coupling term in equations of mode N(L)
IJS(L)		Fourier number N(IJS) that combines with itself to produce a coupling term in equation of mode N(L)

TABLE XI Continued

FORTRAN VARIABLE	ALGEBRAIC COUNTERPART	DEFINING EQUATION AND/OR DESCRIPTION
INMAX		Total number of Fourier coefficients in the series representation of the initial imperfection
IPASS		Indicates whether or not all combinations of sums and differences of Fourier numbers have been computed for all modes
IS(L,J)		Fourier numbers N(IS) that combine through sums to produce a coupling term in equation of mode N(L)
JD(L,J)		Fourier numbers N(JD) that combine through differences to produce a coupling term in equations of mode N(L)
JS(L,J)		Fourier numbers N(JS) that combine through sums to produce a coupling term in equations of mode N(L)
K		Subscript corresponding to axial station number
KMAX	M-1	Where M is the number of axial stations
KP		Printout control parameter
KPRINT		Printout occurs every KPRINT time steps
KR(K)		Axial station at which K th ring is located

TABLE XI Continued

FORTAN VARIABLE	ALGEBRAIC COUNTERPART	DEFINING EQUATION AND/OR DESCRIPTION
KSUM	M-1 or M	(4.2) where M is the number of axial stations
KSTRES		Axial station where max stress occurred
L		Subscript used in summing over the Fourier numbers N(L)
LAM1(K,L)	$\Lambda 1_K^n$	(4.1a)
LAM2(K,L)	$\Lambda 2_K^n$	(4.1b)
MAXD(L)		Number of combinations of differences of Fourier numbers that equal N(L)
MAXM		Maximum number of Fourier modes in the solution
MAXS(L)		Number of combinations of sums of Fourier numbers that equal N(L)
MAXSTP		Maximum number of time steps to be computed
MAXSY(L)		Number of combinations of sums of Fourier numbers with themselves that equal N(L)
MM	M	Number of axial stations
MNMAXO		Number of Fourier modes in solution prior to calling subroutine MODES

TABLE XI Continued

FORTRAN VARIABLE	ALGEBRAIC COUNTERPART	DEFINING EQUATION AND/OR DESCRIPTION
N(L)	n	Fourier numbers
NBC		Boundary condition parameter
NCONV		Indicates whether or not solution has converged
NIT		Iteration number
NITMAX		Maximum number of iterations per time step
NITMIN		Minimum number of iterations per time step
NN		Number of modes in solution after return from subroutine MODES
NR	N_r	(2.11) Number of ring-stiffeners
NSTEP		Time step number
NSYM		Indicates whether response is symmetric or unsymmetric with respect to midspan shell
P(I,J,K,L)	P_K^n	(4.5a)
PLOAD(K)	P_K	(3.22)

TABLE XI Continued

FORTAN VARIABLE	ALGEBRAIC COUNTERPART	DEFINING EQUATION AND/OR DESCRIPTION
PO	P_O	(5.3)
R	$1/\tau_O$	(5.3)
STPAM(L)		τ for maximum amplification of mode N(L)
STRESM	$\bar{n}_\theta \text{ max}$	(4.31)
T	τ	
TFINAL		τ at which solution is to be terminated
TMS		τ for maximum stress
TSTRES	$\bar{n}_{\theta K}$	(4.30)
TX(L)	$(n_\xi^n)_K$	(B.1a)
TXA(K)	n_ξ	(2.23a) evaluated $\theta=0^\circ$ and at each axial station
TXY(K,L)	$n_{\xi\theta K}^n + n_{\xi\theta K-1}^n$	(B.13)
TXYA(K,L)	$n_{\theta\xi}$	(2.23c) evaluated at increments of 10° and at each axial station
TY(K,L)	$(n_\theta^n)_K$	(B.1b)

TABLE XI Continued

FORTRAN VARIABLE	ALGEBRAIC COUNTERPART	DEFINING EQUATION AND/OR DESCRIPTION
TYA(K)	n_θ	(2.23b) evaluated at $\theta=0^\circ$ and at each axial station
U(K,L)	u_K^n	(3.20)
V(K,L)	v_K^n	(3.21)
VD1(I),...,VD3(I)		Dummy 2x1 floating point arrays
W(K,L)	$w_K^n(\tau_1)$	(4.14)
W1(K,L)	$w_K^n(\tau_2)$	(4.14)
WDOT(K,L)	$\dot{w}_K^n(\tau_1)$	(4.14)
WDOT1(K,L)	$\dot{w}_K^n(\tau_2)$	(4.13)
WDDOT(K,L)	$\ddot{w}_K^n(\tau_1)$	(4.14)
WDDOT1(K,L)	$\ddot{w}_K^n(\tau_2)$	(4.14)
WI(L)	w_i^n	(5.1)
WIXH(K,L)	$(\bar{w}, \xi)_K^n$	Derivatives of the initial imperfection at half station k or whole station K
WIXW(K,L)	$(\bar{w}, \xi)_K^n$	
WIXX(K,L)	$(\bar{w}, \xi\xi)_K^n$	
WIXY(K,L)	$-n(\bar{w}, \xi)_K^n$	

TABLE XI Continued

FORTRAN VARIABLE	ALGEBRAIC COUNTERPART	DEFINING EQUATION AND/OR DESCRIPTION
WIYH(K,L)	$-n \bar{w}_k^n$	Derivatives of the initial imperfection at half station k or whole station K.
WIYW(K,L)	$-n \bar{w}_K^n$	
WIYY(K,L)	$-n^2 \bar{w}_K^n$	
WWTH(L)	$-n^2 \bar{w}_k^n$	evaluated by using (B.8)
WWX(L)	$(w, \xi \xi)_K^n$	(3.18)
WWXTH(L)	$-n (w, \xi)_K^n$	evaluated by using (B.10a)
WXH(K,L)	$(w, \xi)_K^n$	(3.18)
WXW(K,L)	$(w, \xi)_K^n$	(B.10a)
WYH(K,L)	$-nw_k^n$	evaluated by using (B.8)
WYW(K,L)	$-nw_K^n$	
X(I,K)	x_K^n	(4.7)

terms are thus converted to products of Fourier series. The products are expanded to obtain a single series for each such product. Derivatives with respect to the axial coordinate are evaluated numerically by using a set of modified staggered node, central differences.

The radial equation of motion for each mode is integrated in the time domain by using Newmark's beta-method. After determining the radial displacements, the nonlinear terms in the axial and circumferential equations are evaluated. The axial and circumferential displacements are then computed by Gauss elimination. Finally, the radial accelerations are computed from the radial equilibrium equations; and a convergence test is made. The process is repeated until convergence is achieved or until a specified maximum number of iterations have been completed. If the solution fails to converge in the maximum allowable number of iterations, the time increment is multiplied by two-thirds and the procedure is repeated. Whenever convergence occurs in less than some specified minimum number of iterations, the time increment is increased by 15 per cent.

The output consists of the maximum circumferential stress at $\theta = 0^\circ$ attained during the solution together with the time and station at which the maximum stress occurred. In addition, the displacements and in-plane stress resultants are printed at specified intervals.

Main Program

The main program performs the following functions:

1. Controls the logical connections between the subroutines.
2. Adjusts the length of the time increment.
3. Sums the Fourier coefficients in the series for the in-plane stress resultants.
4. Computes the circumferential stress due to bending.
5. Computes the maximum circumferential stress together with the location and time of its occurrence.
6. Prints out the solution at specified time steps and after completion of the solution.

Subroutine START

This subroutine performs the following functions:

1. Reads in the data cards.
2. Prints the problem description and program control parameters.
3. Sets the initial values of all array elements to zero.
4. Calls subroutines WIDER 1 and WIDER 2, or WILSIN and WI2SIN, which compute and store derivatives of the initial imperfection.
5. Sets certain program control parameters to proper initial values.

Subroutine WDEF

This subroutine performs the time integration by Newmark's beta-method.

Subroutine MODES

Subroutine MODES was taken directly from Reference [30] with the permission of its author.

In MODES, the arrays that define those sets of indices that combine to equal each value of n in the problem are determined. They are IS, JS, ID, JD, IJS, MAXS, MAXD, and MAXSY. MODES is called during the first iteration of the first time step and during each subsequent iteration until the number of Fourier terms reaches a specified number. The arrays computed here are used as control parameters by subroutines LAM1N2 and TNETA in evaluating the nonlinear terms.

Subroutine LAM1N2

The quantities LAM1 and LAM2, the terms which comprise the load vector in the Gauss elimination, are computed in Subroutine LAM1N2. The derivatives of the radial displacement that appear in LAM1 and LAM2 are first evaluated. A multiplying and summing procedure is then carried out to evaluate CXX, CIXX, CTT, CITT, CXT, CIXT, and CITX, the Fourier coefficients of the expanded products of series. Arrays IS, JS, ID, JD, IJS, MAXS, MAXD, and MAXSY, which were generated in MODES, are used as control parameters in the multiplications and summations.

Subroutine PMATRX

PMATRX serves as a control program for the computation and storage of the matrices P, DEE, and DST, matrices used in the Gauss elimination solution for the displacements u_k^n and v_k^n . The subroutine is called by the main program during the first iteration and whenever the expansion of the products of series introduces new Fourier modes. The boundary conditions at the first axial station are incorporated into the submatrices of P associated with the first station. Subroutines ABC and PANDD are then called to compute the rest of the P matrix and the matrices DEE and DST.

Subroutine ABC

This subroutine computes the elements of the A, B, and C matrices for a given Fourier number. These matrices are used in subroutine PANDD to compute the elements of P, DEE, and DST. At stations having rings, the matrix BR is used in place of B.

Subroutine PANDD

The matrices P, DEE, and DST are computed by PANDD. Subroutine MATMAT and INVMAT are called to perform elementary matrix operations.

Subroutine UVDEF

Subroutine UVDEF computes the displacements u_k^n and v_k^n , which correspond to the new radial displacement, w_l .

UVDEF first computes the new vector GEE, then performs row operations on the vector GEE to generate the X vectors, and finally computes u_k^n and v_k^n by back substitution. Subroutines MATMAT, INVMAT, and MATVEC are called for elementary matrix operations.

Subroutine TNETA

This subroutine performs the following functions.

1. Computes TX, TXY, and TY, the Fourier coefficients of the in-plane stress resultants.

2. Computes WWX, WWXTH, and WWTTH, the Fourier coefficients of the ξ -curvature, the twist, and the circumferential curvature, respectively.

3. Carries out a multiplication and summation procedure to compute ETAX, ETATH, and ETAXTH, the Fourier coefficients of the nonlinear terms in the radial equilibrium equations. The arrays IS, JS, ID, JD, IJS, MAXS, MAXD, and MAXSY, which were prepared in subroutine MODES, are used as control parameters in the multiplication and summation process.

Subroutine ACELR8

This subroutine solves the radial equilibrium equation of each mode for the radial acceleration WDDOT1. The convergence test is performed as the new accelerations are computed. The parameter NCONV is set to zero when the solution converges, or to one, if the convergence test fails.

The program stops checking for convergence as soon as a test fails.

Subroutines INVMAT, MATMAT, and MATVEC

These subroutines perform elementary matrix operations on 2 x 2 matrices and 2 x 1 vectors. INVMAT inverts a matrix, MATMAT forms the product of two matrices, and MATVEC multiplies a vector by a matrix.

Subroutines WIDER 1 and WIDER 2

These subroutines compute and store the derivatives of the initial imperfection required in subroutines LAM1N2 and TNETA. The subroutines are based on the assumptions that the imperfection in mode n is equal to

$$w_1^n \{1 - \cos [2\pi(N_r + 1)\xi/l]\} \cos n\theta$$

and that the rings are located such that the shell is divided into $N_r + 1$ segments of equal length. This means that the imperfection and its first derivatives are zero at the ring stations and do not produce any strains in the rings, as assumed in the analysis. Accordingly, there is a finite number of compatible ring stations. They are tabulated in the program listing of subroutine WIDER1. The program listed calls these routines. If another form of the imperfection is desired, a separate routine must be written.

Subroutines WILSIN and WI2SIN

These subroutines are substitutes for WIDER1 and WIDER2 and were used in computing the solutions presented in Chapter V. These subroutines are based on the assumption that the initial imperfection in mode n is given by

$$w_i^n \sin(\pi \xi / l) \cos n\theta$$

Subroutine PLOAD

This subroutine computes PLOAD at each station for a uniform time decaying external pressure, i.e.

$$PLOAD(K) = PO \exp (-RT)$$

The subroutine may be replaced by the user for other pressure time histories. The variables PO , R , S , and $OMEGA$, in labeled common block A1, are read from data card number ten. These, variables are not used anywhere else in the program and are available to the user in developing an alternate subroutine for the loading.

Subroutine AMPMAX

Subroutine AMPMAX is not an integral part of the program. It was, however, employed in computing the solutions presented in Chapter V. It should be used only in conjunction with WILSIN and WI2SIN. AMPMAX computes the amplification of those Fourier modes for which an initial imperfection was specified. If the magnitude of

the initial imperfection for some mode is set identically to zero by the input data, the subroutine will compute an amplification of zero even though the response of that mode may not be zero. The amplification is computed at the midspan of the shell or at the whole station nearest to the modspan. In computing the amplification, the initial imperfection is assumed to be equal to

$$w_i^n \sin\left(\frac{\pi \xi}{l}\right) \cos n\theta$$

III. INPUT REQUIREMENTS

The layout of each data card is shown in Figure D.1. The first three cards will be referred to as TITLE 1, 2, 3; and the remaining cards, as DATA 1 - 13.

The program uses nondimensional variables throughout and the user must supply the data in nondimensional form. The contents of each card are listed below.

Data Cards

TITLE 1 - 3: The description of the problem is placed on these three cards and will be printed at top of the first page of output.

DATA 1:

MM - The number of axial stations, including the stations at the ends of the shell;
MM ≤ 20

TITLE 1,2,3 FORMAT (9A8) IDENTIFICATION

1 TITLE 1 2 3 4 5 6 7 8 9 10 11 12 13 14 15 16 17 18 19 20 21 22 23 24 25 26 27 28 29 30 31 32 33 34 35 36 37 38 39 40 41 42 43 44 45 46 47 48 49 50 51 52 53 54 55 56 57 58 59 60 61 62 63 64 65 66 67 68 69 70 71 72 73 74 75 76 77 78 79 80 81 82 83 84 85 86 87 88 89 90 91 92 93 94 95 96 97 98 99 100

DESCRIPTION OF PROBLEM

DATA 1: FORMAT (8X,I2, 9X,I1, 2(8X,I2))

10 20 30 40 50 60 70 80
MM NR INMAX MAXM DATA 1

DATA 2: FORMAT(2(9X,I1), 2(8X,I5), 3F10.6)

10 20 30 40 50 60 70 80
NITMAX NITMIN MAXSTP KPRINT TFINAL BETA EPS DATA 2

DATA 3: FORMAT (2(9X,I1))

10 20 30 40 50 60 70 80
NBC NSYM DATA 3

DATA 4: FORMAT (6F10.6)

10 20 30 40 50 60 70 80
C1 C2 C3 C4 C5 E DATA 4

FIGURE D.1
INPUT FORMAT

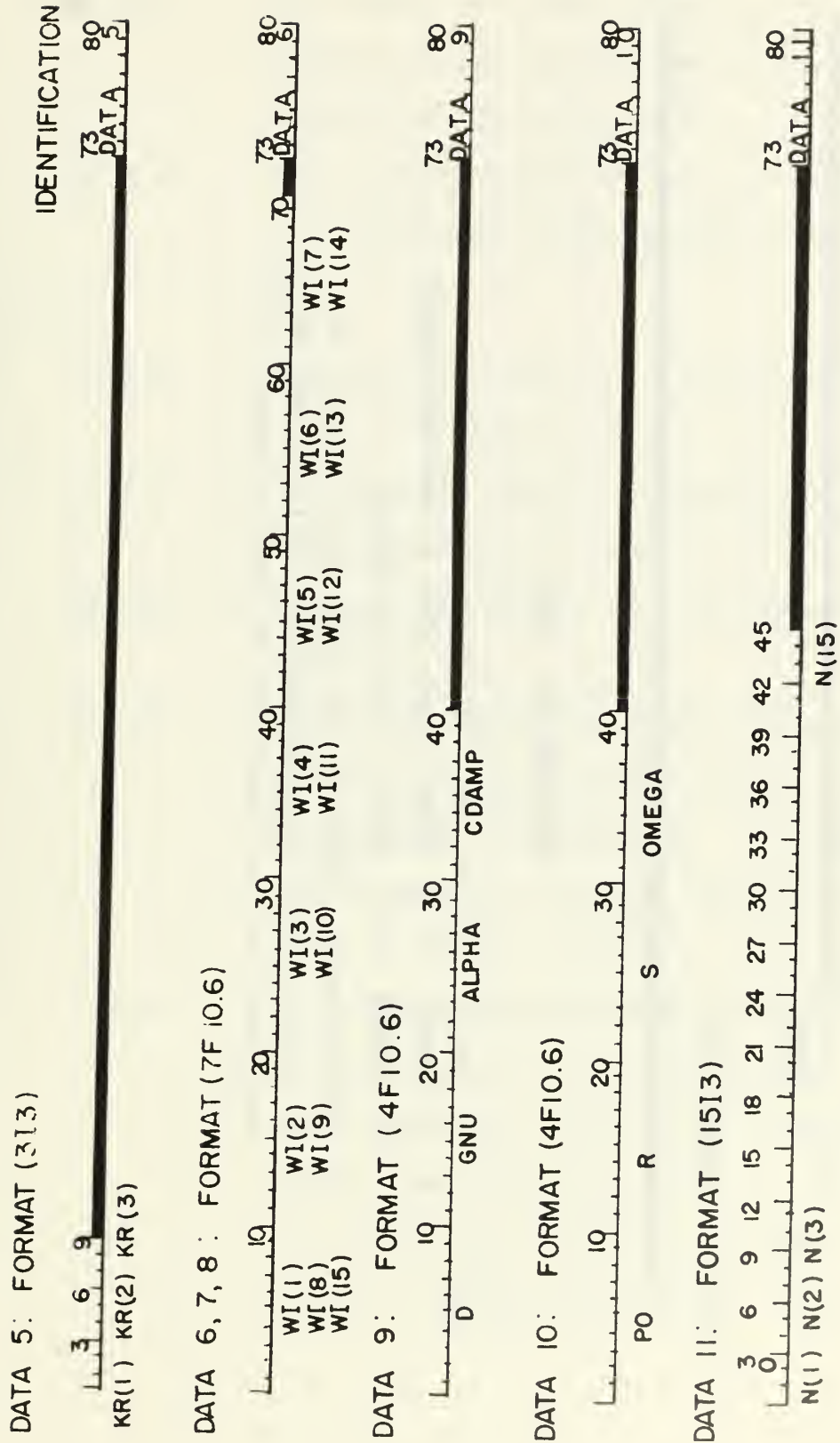


FIGURE D.1 Cont.

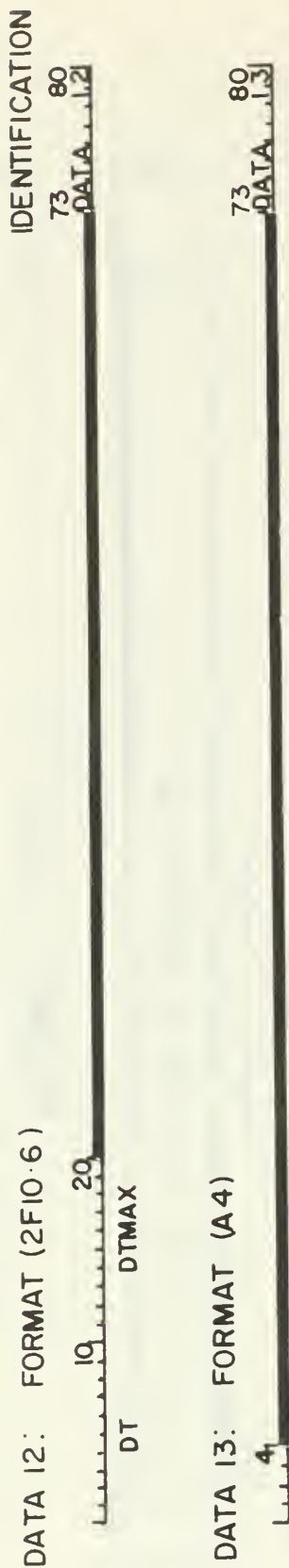


FIGURE D.1 Cont.

- NOTES:
1. If $NR=0$, DATA 4 and DATA 5 must be omitted.
 2. If $INMAX < 8$, DATA 7 and DATA 8 must be omitted.
If $INMAX < 15$, DATA 8 must be omitted.
 3. Information on DATA 6, 7, 8 and DATA 11 must be in one-to-one correspondence, i.e. $W1(L)$ is the Fourier coefficient of the mode with the Fourier number $N(L)$.

- NR - The number of stiffening rings; $NR \leq 3$
- INMAX - The number of modes with an initial imperfection, including the axisymmetric mode ($n = 0$); $INMAX \leq 15$
- MAXM - The maximum number of Fourier modes to be considered; $INMAX \leq MAXM \leq 15$

DATA 2:

- NITMAX - The maximum number of iterations per time step (recommended value = 4)
- NITMIN - The minimum number of iterations per time step (Recommended value = 3)
- MAXSTP - The maximum number of time steps to be computed
- KPRINT - Time step intervals at which the displacements, stress resultants, and maximum stress are to be printed. If $KPRINT = 50$, print out will occur at the end of time step 50, 100, 150, etc.
- TFINAL - The nondimensional time at which the calculation is to be terminated. (The nondimensional period of the axisymmetric mode is approximately 2π)
- BETA - Integration parameter of Newmark's beta-method (Recommended value - .1666667)

EPS - Convergence test parameter. Convergence is assumed when the magnitude of the change in the acceleration for two successive iterations is less than or equal to EPS times the magnitude of the larger acceleration. (Recommended value - .001)

DATA 3:

NBC - The boundary condition parameter. When the shell:

1. Has simple boundary conditions,
NBC = 1.
2. Has clamped boundary conditions,
NBC = 2.

NSYM - Symmetry parameter. When the motion:

1. Is assumed to be symmetric with respect to the midspan, NSYM = 1.
2. Otherwise, NSYM = 2.

DATA 4: This data card contains nondimensional parameters representing the stiffness and geometric properties of the stiffening rings. This card must be omitted if the shell does not have stiffening rings.

$$\begin{array}{ll}
C1 & - \frac{E_r}{E} \frac{I_x (1-v^2)}{a^2 h \Delta X} \\
C2 & - \frac{\rho_r}{\rho} \frac{A_r}{h \Delta X} \\
C3 & - \frac{E_r}{E} \frac{A_r (1-v^2)}{h \Delta X} \\
C4 & - \frac{E_r}{E} \frac{I_z (1-v^2)}{a^2 h \Delta X} \\
C5 & - \frac{E_r}{E} \frac{C_T (1-v^2)}{2 a^2 h \Delta X} \\
E & - \frac{\bar{e}}{a}, \text{ the eccentricity of the rings}
\end{array}$$

where

$$X = \frac{L}{2MM-1} \text{ when NSYM} = 1, \text{ and}$$

$$X = \frac{L}{MM-1} \text{ when NSYM} = 2.$$

DATA 5: KR(1), KR(2), and KR(3) are the axial stations at which the rings are located. (See the FORTRAN listing of Subroutine WIDER1.) If there are no rings, omit DATA 5.

DATA 6, DATA 7, and DATA 8: The nondimensional magnitudes of the initial imperfection are placed on these cards. For example, if the magnitude of the imperfection in each mode is one one-thousandth of the shell thickness

and the Fourier number $n = N(L)$, then

$$WI(L) = \frac{1}{1000} \times \frac{h}{a}.$$

WI(1) - The Fourier coefficient of the initial imperfection in the axisymmetric mode, $n = 0$. Normally, $WI(1) = 0$.

WI(2) - The Fourier coefficient of the initial imperfection in the mode whose Fourier number is $n = N(2)$. (See explanation of DATA 12)

WI(INMAX) - The Fourier coefficient of the initial imperfection in the mode whose Fourier number is $n = N(INMAX)$

If INMAX:

1. Is less than 15, DATA 8 must be omitted.
2. Is less than 8, DATA 7 must be omitted.

DATA 9:

D - The nondimensional length $= L/a$. Subroutine START sets D equal to the nondimensional spacing of the finite difference stations.

GNU - Poisson's ratio

ALPHA - h/a

CDAMP - the nondimensional viscous damping coefficient $CDAMP = C \left[\frac{(1-\nu^2)}{E\rho} \right]^{\frac{1}{2}}$, where C is the viscous damping coefficient.

DATA 10: (As required by subroutine PRLOAD)

PO - The maximum pressure

R - The decay rate

In dimensional units,

$$P(t) = P_O e^{-rt} = P_O e^{-t/t_O}$$

Then

$$P_O = P_O \frac{a(1-v^2)}{Eh}$$

$$R = ra \left[\frac{\rho(1-v^2)}{E} \right]^{\frac{1}{2}} = \frac{a}{t_O} \left[\frac{\rho(1-v^2)}{E} \right]^{\frac{1}{2}}$$

S,OMEGA - blank. S and OMEGA are available to the user in preparing a subprogram to replace PRLOAD.

DATA 12:

N(1) = 0

N(2) The Fourier numbers of the initial imperfection. These numbers must be in one

N(INMAX) to one correspondence with

WI(1),...,WI(INMAX) on DATA 6, DATA 7, and DATA 8. N(1) must always be equal to zero.

DATA 13:

DT - The time increment to be used for the first time step (value used in calculations of Chapter V = .05)

DTMAX - The upper limit on the time increment.
When $BETA = 1/6$, DTMAX should not be larger than one-fifth of the shortest period of any mode in the problem. Normally, the axisymmetric mode has the shortest period. (value used in calculations of Chapter V = 0.7)

DATA 14: This data card provides the capability of solving several problems during a single computer run.

LAST - 1. LAST = , , , , if one or more problem data sets follow.
2. LAST = if the present data set is the last one

Truncation of the Series

The user prescribes which modes are in the truncated Fourier series by the values given to INMAX, MAXM and N(L). Coefficients having the same Fourier numbers as $N(1), \dots, N(INMAX)$ are included in the truncated series for the displacements; and if MAXM is equal to INMAX, no other modes will be considered in the solution. If MAXM is greater than INMAX, subroutine MODES will add additional modes to the series for the displacements until the total number of modes is equal to MAXM. For example, if $INMAX = 2$, $MAXM = 4$ and $N(1) = 0$, and $N(2) = 3$, subroutine

MODES will add modes six and nine to the series for the displacements with zero taken as the initial imperfection in modes six and nine.

IV. USER ALTERATIONS TO OBTAIN UNCOUPLED SOLUTIONS

Elimination of Nonlinear Feedback to Axisymmetric Mode

In Chapter V a procedure was outlined for identifying the Mathieu modes. The procedure involves computing the response of the flexural modes whose frequencies are close to one-half the frequency of the axisymmetric mode. In setting up the program for such an identifying run, the nonlinear terms in the equations of the axisymmetric mode are set equal to zero. The following alterations of the program will eliminate the appropriate nonlinear terms.

In subroutine IAMLN2:

After the statement

```
11  D $\phi$  12  L = 1, MNMAX $\phi$ 
```

insert

```
G $\phi$   T $\phi$  20
```

```
100 C $\phi$ NTINUE
```

The second inserted statement is necessary to avoid an error message from the Fortran compiler.

In subroutine TNETA:

After the statement

```
9  D $\phi$  10  L = 1, MNMAX $\phi$ 
```

insert

GØ TØ 11

100 CØNTINUE

The second inserted statement is necessary to avoid an error message from the Fortran compiler.

Elimination of Nonlinear Coupling Between the Flexural Modes

In Chapter V a comparison was made between a fully coupled nonlinear solution and one with limited coupling. To eliminate the intermodal coupling between the flexural modes, but yet retain the coupling between each flexural mode and the axisymmetric mode, the following alterations are required:

In subroutine LAM1N2:

After the statements

IF(N(M).EQ.0) GØ TØ 11

MAXL = MAXS(M)

insert

MAXL = 1

After the statement

8 MAXL = MAXD(M)

insert

MAXL = 1

After the statement

10 IF (MAXSY(M).EQ.0) GØ TØ 13

insert

GØ TØ 13

100 CØNTINUE

The second inserted statement is necessary to avoid an error message from the Fortran compiler.

In subroutine TNETA:

After the statements

```
IF (N(M).EQ.O) GØ TØ 9
```

```
MAXL = MAXS(M)
```

insert

```
MAXL = 1
```

After the statement

```
6 MAXL = MAXD(M)
```

insert

```
MAXL = 1
```

After the statement

```
8 IF(MAXSY(M).EQ.O) GØ TØ 11
```

insert

```
GØ TØ 11
```

```
100 CØNTINUE
```

The second inserted statement is necessary to avoid an error message from the Fortran compiler.

V. STORAGE REQUIREMENTS AND EXECUTION TIME

The program requires approximately 125K bytes of storage space in the IBM 360 Model 67 memory when subroutines AMPMAX, WI1SIN, and WI2SIN, or WIDER1 and WIDER2 are removed from the deck. This figure includes the space required for the execution of the required input and output routines.

The approximate execution time for calculating a completely coupled nonlinear solution until τ equal two-hundred is shown in Figure D.2 as a function of the number of modes in the Fourier series.

VI. PROGRAM LISTING

The listing of the program is contained on pages 244 - 279.

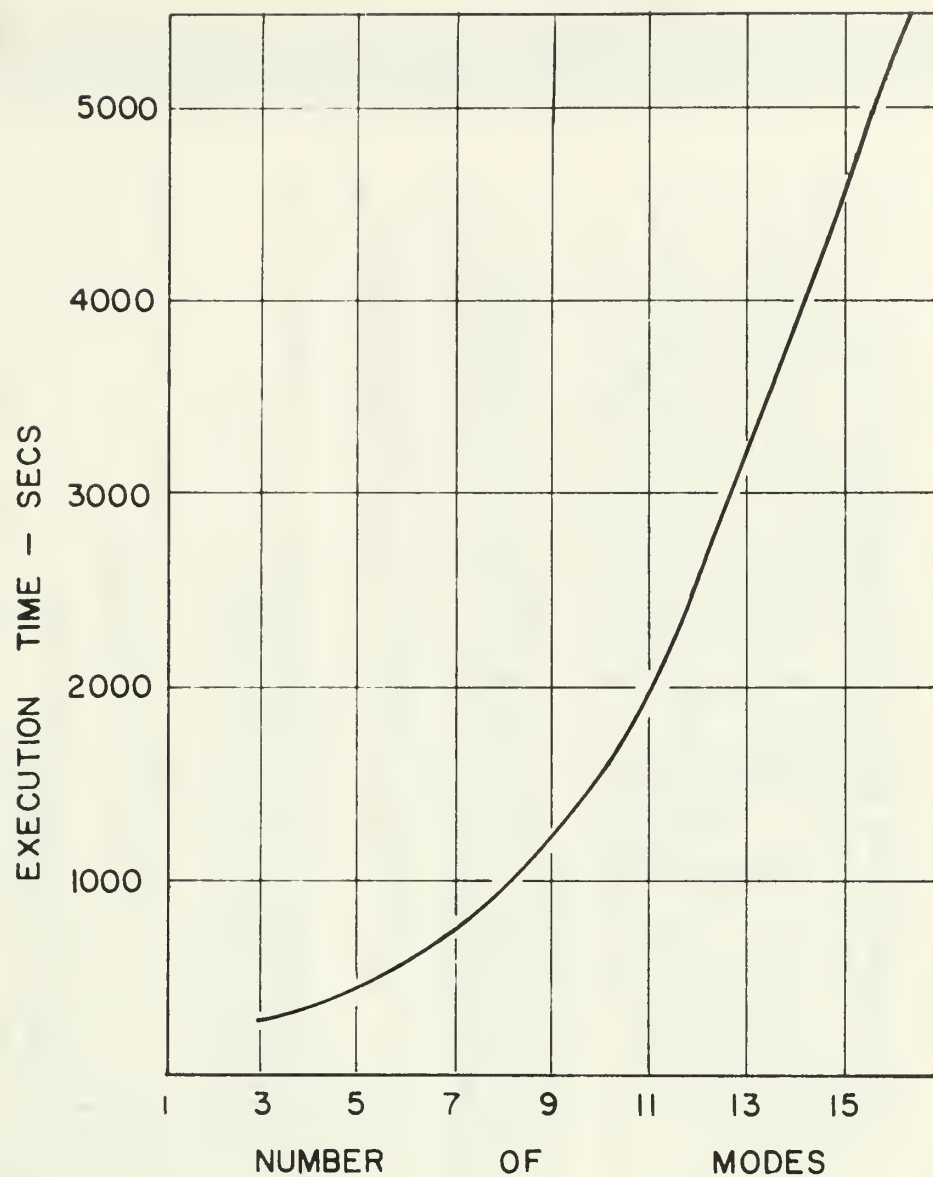


FIGURE D.2
EXECUTION TIME, $\tau = 0$ to 200


```

COMMON/P7/ WIXY(20,15),WIXX(20,15),WIYY(20,15)
COMMON/R9/ LAM1(20,15),LAM2(20,15)
REAL LAM1,LAM2
COMMON/Z0/ WI(15)
COMMON/Y0/ WWX(15),WWTH(15),WWXTH(15),TX(15)

REMOVE C FROM COLUMN 1 OF NEXT CARD IF SUBROUTINE AMPMAX IS USED
COMMON/Y1/ MMHALF,AMP(15),STPAM(15)
COMMON/Z1/ CIXX(20,15),CIXT(20,15),CITT(20,15),CITX(20,15),CXX(20,
115),CCT(20,15),CXT(20,15)
COMMON/Z2/ ETAX(20,15),ETATH(20,15),ETAXTH(20,15),TY(20,15),TX(20
1,15)
COMMON/Z3/ U(20,15),V(20,15),W(20,15),W1(20,15),WDOT(20,15),WDOT1
1(20,15),WDDOT(20,15),WDDOT1(20,15)
COMMON/Z4/ GNU
COMMON/Z8/ WXH(15),WXW(15),WYH(15),WYW(15)
COMMON/Z5/ P(2,2,20,15),DEE(2,2,20,15),DST(2,2,20,15)
COMMON/Z6/ MAXSTP,NITMAX,NITMIN,TFINAL,KPRINT
COMMON/Z7/ TXA(20),TYA(20),TXYA(20,18)
COMMON/Z9/ NSTEP,KP
DATA ILAST/...../
DATA JLAST/...../
STRESM=0.
99 CALL START

      COMPUTE INITIAL RADIAL PRESSURE.
      CALL PRLCAD
      COMPUTE INITIAL ACCELERATION.
      CALL ACELR8
      T=DT
      COMPUTE RADIAL PRESSURE AT END OF FIRST TIME STEP.
      CALL PRLOAD
      BEGIN FIRST ITERATION.

10 NIT=1

      UPDATE RADIAL DISPLACEMENT, VELOCITY, AND ACCELERATION.
      DO 1 K=2,KSUM
      DO 1 L=1,NN
      W(K,L)=WI(K,L)
      WDOT(K,L)=WDDOT1(K,L)

```

```

0048
0049
0050
0051
0052
0053
0054
0055
0057
0058
0059
0060
0061
0062
0063
0064
0065
0066
0067
0068
0069
0070
0071
0072
0073
0074
0075
0076
0077
0078
0079
0080
0081
0082
0083
0084
0085
0086
0087
0088
0089
0090
0091
0092
0093
0094
0095
0096

```

1	WDDOT(K,L)=WDDOT1(K,L)	0097
	COMPUTE VELOCITY AND DISPLACEMENT AT END OF CURRENT TIME STEP.	0098
20	CALL WDEF	0099
	COMPUTE FOURIER NUMBERS OF NEW MODES GENERATED BY NONLINEAR TERMS.	0100
	IF(IPASS.LT.2) GO TO 4	0101
	COMPUTE NONLINEAR TERMS IN AXIAL AND CIRCUMFERENTIAL EQUATIONS.	0102
	CALL LAMIN2	0103
11	COMPUTE AND STORE P,DEE, AND DST MATRICES FOR NEW MODES. P,DEE, AND DST ARE USED IN SOLVING FOR U AND V BY GAUSS ELIMINATION.	0104
	IF(NINIT.LE.MAXM) GO TO 5	0105
	CALL UVDEF	0106
	COMPUTE NONLINEAR TERMS IN THE RADIAL EQUILIBRIUM EQUATION.	0107
	CALL INETA	0108
	COMPUTE AXIAL AND CIRCUMFERENTIAL DISPLACEMENTS. TIME STEP AND RECOMPUTE RADIAL ACCELERATION AT END OF CURRENT TIME STEP AND CHECK FOR CONVERGENCE.	0109
	CALL ACELR8	0110
	IF(NCONV.EQ.0) GO TO 8	0111
	CONVERGENCE TEST FAILED.	0112
	NIT=NIT+1	0113
	IF(NIT.GT.NITMAX) GO TO 9	0114
	BEGIN NEXT ITERATION.	0115
	GO TO 20	0116
4	MNMAXC=NN	0117
	CALL MODES	0118
	GO TO 11	0119
	SOLUTION HAS CONVERGED.	0120
	EVALUATE HOOP FORCE AND ADDITIONAL HOOP BENDING STRESS.	0121
8	DO 22 K=2,KSUM	0122
		0123
		0124
		0125
		0126
		0127
		0128
		0129
		0130
		0131
		0132
		0133
		0134
		0135
		0136
		0137
		0138
		0139
		0140
		0141
		0142
		0143
		0144

```

TYA(K)=0.
BSTRES=0.
DO 24 L=1,NN
FN=N(L)
24 TYA(K)=TY(K,L)+TY(K,L)+ALPHA*FN**2*W1(K,L)
   BSTRES=BSTRES+BSTRES
   TSTRES=ARS(TYA(K))+ARS(BSTRES)
   IF(TSTRES.LE.STRESM) GO TO 22
   STRESM=TSTRES
   KSTRES=K
   TMS=T
22 CONTINUE

      COMPUTE AMPLIFICATION OF MODES HAVING INITIAL IMPERFECTIONS.
      REMOVE ENERGY COLUMN 1 OF NEXT CARD IF AMPMAX IS USED.
      CALL AMPLX
25 IF(NSTEP.NE.KP) GO TO 15

      WRITE SOLUTION AT SPECIFIED INTERVALS.

      KP=KP+KPRINT
      WRITE(6,1020)T,NSTEP
26 WRITE(6,1005)
   WRITE(6,1004)(K,PLQAD(K),K=2,KSUM)
   WRITE(6,101)NIT
   WRITE(6,1006)(N(L),L=1,NN)
   I1=10
   I2=10
   IF(MM.LT.10) I1=MM
   WRITE(6,1023)
   WRITE(6,1024)
   WRITE(6,1025)(K,K=1,I1)
   DO 31 L=1,NN
31 WRITE(6,1015)(N(L),(W1(K,L),K=1,I1))
   IF(MM.LT.I1) GO TO 33
   WRITE(6,1024)
   WRITE(6,1025)(K,K=1,I,MM)
   DO 32 L=1,NN
32 WRITE(6,1015)(N(L),(W1(K,L),K=1,I,MM))
33 WRITE(6,1024)
   IF(KSUM.LT.10) I2=KSUM
   WRITE(6,1025)(K,K=1,I2)
   DO 34 L=1,NN
34 WRITE(6,1015)(N(L),(U(K,L),K=1,I2))
   IF(KSUM.LT.I1) GO TO 36

```

C
C
C
C
C
C
C

0145
0146
0147
0148
0149
0150
0151
0152
0153
0154
0155
0156
0157
0158
0159
0160
0161
0162
0163
0164
0165
0166
0167
0168
0169
0170
0171
0172
0173
0174
0175
0176
0177
0178
0179
0180
0181
0182
0183
0184
0185
0186
0187
0188
0189
0190
0191
0192


```

C      NUMBER OF ITERATIONS REQUIRED FOR CONVERGENCE WAS LESS THAN
C      'NITMIN'...INCREASE THE TIME INCREMENT.
C
16  D1=1.15*DT
27  IF(D1.LE.DTMAX) GO TO 21
28  IF(DT-DTMAX)28,17,30
30  DT=DTMAX
30  GO TO 29
30  WRITE(6,1021)
30  STOP
21  DT=D1
29  WRITE(6,106) NSTEP,DT
30  GO TO 17
C
C      REQUIRED EXCESSIVE NUMBER OF ITERATIONS...REDUCE TIME INCREMENT
C      AND RECOMPUTE CURRENT TIME STEP.
C
9   DT=.6666667*DT
   WRITE(6,107)NSTEP,DT
   T=T-.3333333*DT
   IF(DT.LT.1.E-05) TFINAL=T
   CALL PRLOAD
   DO 19 K=2,KSUM
   DO 19 L=1,NN
   WDDOT1(K,L)=WDDOT(K,L)
   WDDOT1(K,L)=WDDOT(K,L)
19  W1(K,L)=W(K,L)
   GO TO 10
5   CALL PMATRIX
   GO TO 6
18  CONTINUE
   REMOVE C FROM COLUMN 1 OF NEXT CARD IF SUBROUTINE AMPMAX IS USED.
   WRITE(6,1008)(N(L),STPAM(L),L=1,INMAX)
   WRITE(6,1002) STRESM,KSTRES,TMS
C
C      SOLUTION COMPLETED...CHECK DATA FOR ANOTHER PROBLEM.
C
   READ(5,1003) LAST
   IF(LAST.EQ.JLAST) GO TO 99
   IF(LAST.EQ.ILAST) GO TO 999
   WRITE(6,1014)
999  CONTINUE
101  FORMAT(/5X,'SOLUTION CONVERGED AFTER',I3,' ITERATIONS')
106  FORMAT(/10X,'TIME INCREMENT INCREASED AFTER COMPLETION OF TIME STEP',I6/10X,'TIME INCREMENT NOW EQUALS',IPE14.4)
107  FORMAT(/10X,'TIME INCREMENT DECREASED DURING TIME STEP',I6/10X,'TIME INCREMENT NOW EQUALS',IPE14.4)
1002 FORMAT(/10X,'THE MAXIMUM HOOP STRESS=',IPE14.4,' OCCURRED AT STAT

```



```

1003 ION, I3, AT TIME=, IPE11.4)
1004 FORMAT(A4)
1005 FORMAT(I4X, I2, I4X, IPE11.4)
1006 FORMAT(/10X, 'EXTERNAL PRESSURES'/13X, 'AXIAL'/12X, 'STATION', 13X,
1007 'PRESSURE')
1008 FORMAT(/10X, 'MODES NOW IN PROBLEM ARE', I5I3)
1009 FORMAT(/10X, 'MAXIMUM IN-PLANE NORMAL FORCES', /5X, 'AXIAL', 15X, 'X',
1010 '119X, 'Y', /5X, 'GRID', 12X, 'NORMAL', 14X, 'NORMAL', /5X, 'POINT', 12X, 'FORCE',
1011 '2, 15X, 'FORCE')
1012 FORMAT(/10X, 'MAX AMPLIFICATION ATTAINED DURING SOLUTION', /10X,
1013 '1, MODE', 10X, 'AMPLIFICATION', 10X, 'TIME', /11X, I2, 13X, IPE10.3,
1014 '28X, IPE10.3')
1015 FORMAT(7X, I2, 11X, IPE10.3, 10X, IPE10.3)
1016 FORMAT(/10X, 'IN PLANE SHEAR FORCES AT EACH AXIAL STATION AND AT TE
1017 '20X, '20, '9X, '30, '9X, '40, '9X, '50, '9X, '60, '9X, '70, '9X, '80, '1X, 'GRID',
1018 '3, '9(4X, 'DEGREES', /1X, 'POINT')
1019 FORMAT(2X, I2, 7X, '0.0', 3X, IPE11.3)
1020 FORMAT(/1X, 'AXIAL', 5X, '90, '8X, '100, '8X, '110, '8X, '120, '8X, '130, '8X,
1021 '1, 140, '8X, '150, '8X, '160, '8X, '170, '8X, '180, '1X, 'GRID', 10(4X, 'DEGREES
1022 '2, '1X, 'POINT')
1023 FORMAT(2X, I2, 3X, IPE11.3)
1024 FORMAT(10X, I2, 6X, IPE10.2)
1025 FORMAT(11X, 5X, 'TIME=, IPE11.4, 10X, 'TIME STEP NUMBER', I6)
1026 FORMAT(/10X, 'TIME STEP IS GREATER THAN DTMAX')
1027 FORMAT(/20X, 'RADIAL DISPLACEMENT...', )
1028 FORMAT(1X, 'MODE', /2X, 'NO.', 49X, 'AXIAL STATION')
1029 FORMAT(6X, 10(8X, I2))
1030 FORMAT(/20X, '...AXIAL DISPLACEMENT...')
1031 FORMAT(/20X, '...CIRCUMFERENTIAL DISPLACEMENT...')
1032 STOP
1033 END

```

```

SUBROUTINE START
SUBROUTINE START ZEROES ALL ARRAYS, READS THE PARAMETERS FOR THE
PROBLEM FROM DATA CARDS, COMPUTES DERIVATIVES OF THE INITIAL
IMPERFECTION, AND INITIALIZES PROGRAM CONTROL PARAMETERS.

COMMON/A1/ PO,R,S,OMEGA
COMMON/A4/ C1,C2,C3,C4,C5,E
COMMON/A5/ NR,KR( 3)

SUBROUTINE START
SUBROUTINE START ZEROES ALL ARRAYS, READS THE PARAMETERS FOR THE
PROBLEM FROM DATA CARDS, COMPUTES DERIVATIVES OF THE INITIAL
IMPERFECTION, AND INITIALIZES PROGRAM CONTROL PARAMETERS.

COMMON/A1/ PO,R,S,OMEGA
COMMON/A4/ C1,C2,C3,C4,C5,E
COMMON/A5/ NR,KR( 3)

```


COMMON/A6/	PLCAD(20)	0333
COMMON/A7/	MM,NN,D,FN,NBC,N(15),KMAX,NSYM,KSUM	0334
COMMON/A8/	DT,RETA	0335
COMMON/A9/	T,DTMAX	0336
COMMON/B0/	A(2,2),B(2,2),C(2,2),BR(2,2),NINIT	0337
COMMON/B2/	INMAX	0338
COMMON/B3/	MNMAXO	0339
COMMON/B4/	MAXD(15),MAXS(15),MAXSY(15),ID(15,15),JD(15,15),IS(8,15	0340
1),JS(8,15),IJS(15)		0341
COMMON/B5/	MAXM,MNINIT,ICORFL,IPASS	0342
COMMON/B6/	NCONV,ALPHA,EPS,CDAMP	0343
COMMON/B7/	WIXY(20,15),WIXX(20,15),WIYY(20,15)	0344
COMMON/B8/	WIXH(20,15),WIXW(20,15),WIYH(20,15),WIYW(20,15)	0345
REAL LAM1,LAM2		0346
COMMON/B9/	LAM1(20,15),LAM2(20,15)	0347
COMMON/YO/	WWX(15),WWTH(15),WWXTH(15),TX(15)	0348
		0349
REMOVE C FROM COLUMN 1 OF NEXT CARD IF SUBROUTINE AMPMAX IS USED.		0350
COMMON/Y1/	MMHALF,AMP(15),STPAM(15)	0351
COMMON/Z0/	WI(15)	0352
COMMON/Z1/	CIXX(20,15),CIXT(20,15),CITT(20,15),CITX(20,15),CXX(20,	0353
115),CTT(20,15),CXT(20,15)		0354
COMMON/Z2/	ETAX(20,15),ETATH(20,15),ETAXTH(20,15),TY(20,15),TX(20	0355
1,15)		0356
COMMON/Z3/	U(20,15),V(20,15),W(20,15),W1(20,15),WDOT(20,15),WDOT1	0357
1(20,15),WDDCT(20,15),WDDOT1(20,15)		0358
COMMON/Z4/	GNU	0359
COMMON/Z5/	P(2,2,20,15),DEE(2,2,20,15),DST(2,2,20,15)	0360
COMMON/Z6/	MAXSTP,NITMAX,NITMIN,TFINAL,KPRINT	0361
COMMON/Z7/	TXA(20),TYA(20),TXYA(20,18)	0362
COMMON/Z8/	WXH(15),WXW(15),WYH(15),WYW(15)	0363
COMMON/Z9/	NSTEP,KP	0364
REAL*8 TITLE(27)		0365
READ(5,509)(TITLE(I),I=1,27)		0366
WRITE(6,1000)(TITLE(I),I=1,27)		0367
READ(5,501) MM,NR,INMAX,MAXM		0368
WRITE(6,1001)		0369
WRITE(6,1002) MM,NR,INMAX,MAXM		0370
REMOVE C FROM COLUMN 1 OF NEXT 3 CARDS IF SUBROUTINE AMPMAX		0371
IS USED.		0372
MMHALF=0		0373
DO 14 K=1,MM,2		0374
MMHALF=MMHALF+1		0375
14		0376
ZERO ALL ARRAYS.		0377
DO 1 K=1,20		0378
		0379
		0380
		0381

```

PLOAD(K)=0.
TYA(K)=0.
TXA(K)=0.
DO 1 L=1,15
  U(K,L)=0.
  V(K,L)=0.
  W(K,L)=0.
  WI(K,L)=0.
  WDOT(K,L)=0.
  WDOT1(K,L)=0.
  WDDOT(K,L)=0.
  WDDOT1(K,L)=0.
  CIXX(K,L)=0.
  CXX(K,L)=0.
  CIT(K,L)=0.
  CIT1(K,L)=0.
  CXT(K,L)=0.
  CXT1(K,L)=0.
  CITX(K,L)=0.
  ETAX(K,L)=0.
  ETATH(K,L)=0.
  ETY(K,L)=0.
  TXY(K,L)=0.
  LAM1(K,L)=0.
  LAM2(K,L)=0.
  WIXW(K,L)=0.
  WIXH(K,L)=0.
  WIYH(K,L)=0.
  WIXX(K,L)=0.
  WIYY(K,L)=0.
  WIXY(K,L)=0.
  DO 1 I=1,2
    DO 1 J=1,2
      P(I,J,K,L)=0.
      DEE(I,J,K,L)=0.
      DST(I,J,K,L)=0.
1 CONTINUE
DO 2 L=1,15
  REMOVE C FROM COLUMN 1 OF NEXT TWO CARDS IF SUBROUTINE AMPMAX
  IS USED.
  AMP(L)=0.
  STPAM(L)=0.
  N(L)=0.
  WI(L)=0.
  WXW(L)=0.

```

C
C
C
C
C

0382
0383
0384
0385
0386
0387
0388
0389
0390
0391
0392
0393
0394
0395
0396
0397
0398
0399
0400
0401
0402
0403
0405
0406
0407
0408
0409
0410
0411
0412
0413
0414
0415
0416
0417
0418
0419
0420
0421
0422
0423
0424
0425
0426
0427
0428
0429
0430

```

WXH(L)=0.
WYW(L)=0.
WYH(L)=0.
WWX(L)=0.
WWTH(L)=0.
WWXTH(L)=0.
TX(L)=0.
2 CONTINUE
12 DO 12 I=1,3
DO 9 I=1,15
DO 7 J=1,15
1D(I,J)=0
7 JD(I,J)=0
CO 8 J=1,8
IS(J,I)=0
8 JS(J,I)=0
MAXD(I)=0
MAXSY(I)=0
9 IJS(I)=0
C1=0.
C2=0.
C3=0.
C4=0.
C5=0.
E=0.
DO 3 K=1,20
DO 3 J=1,18
TXYA(K,J)=0.
3 READ(5,502)NITMAX,NITMIN,MAXSTP, KPRINT,TFINAL,BETA,EPS
WRITE(6,1003) NITMAX,NITMIN,BETA,MAXSTP,KPRINT,TFINAL,EPS
READ(5,508) NBC,NSYM
KSUM=MM-1
IF(NSYM.EQ.2) GO TO 10
WRITE(6,1013)
KSUM=MM
10 IF(NRC.EQ.1) GO TO 4
WRITE(6,1004)
GO TO 13
WRITE(6,1012)
4 IF(NR.EQ.0) GO TO 11
13 READ(5,503)C1,C2,C3,C4,C5,E
WRITE(6,1005) C1,C2,C3,C4,C5,E
READ(5,504)(KR(I),I=1,NR)
WRITE(6,1006)(KR(I),I=1,NR)
11 READ(5,505)(WI(L),L=1,INMAX)
READ(5,503)D,GNU,ALPHA,CDAMP

```

0431
0432
0433
0434
0435
0436
0437
0438
0439
0440
0441
0442
0443
0444
0445
0446
0447
0448
0449
0450
0451
0452
0453
0454
0455
0456
0457
0458
0459
0460
0461
0462
0463
0464
0465
0466
0467
0468
0469
0470
0471
0472
0473
0474
0475
0476
0477
0478

```

0479 WRITE(6,1011)D,GNU,ALPHA,CDAMP
0480 DUM=2*MM-1
0481 IF(NSYM.EQ.2) DUM=MM-1
0482 D=D/DUM
0483 READ(5,591) PO,R,S,OMEGA
0484 WRITE(6,1008) PO,R,S,OMEGA
0485 READ(5,506)(N(I),I=1,INMAX)
0486 WRITE(6,1007)
0487 WRITE(6,1009)(N(I),I=1,INMAX)
0488 READ(5,507)DT,DTMAX
0489 WRITE(6,1010) DT,DTMAX
0490
0491 COMPUTE DERIVATIVES OF INITIAL IMPERFECTION.
0492
0493 DO 6 L=1,INMAX
0494 DO 6 K=1,MM
0495
0496 REMOVE C FROM COLUMN 1 OF NEXT 2 CARDS IF WI1SIN AND WI2SIN
0497 ARE USED.
0498 CALL WI1SIN(K,L)
0499 CALL WI2SIN(K,L)
0500
0501 REMOVE C FROM COLUMN 1 OF NEXT 2 CARDS IF WIDER1 AND WIDER2
0502 ARE USED.
0503 CALL WIDER1(K,L)
0504 CALL WIDER2(K,L)
0505 CONTINUE
0506
0507 INITIALIZE PROGRAM CONTROL PARAMETERS
0508
0509 NN=INMAX
0510 NSTEP=1
0511 T=0.
0512 MNINIT=1
0513 NINIT=1
0514 IPASS=0
0515 ICORFL=0
0516 KP=KPRINT
0517 KMAX=MM-1
0518 IF(NN.EQ.MAXM) GO TO 5
0519 RETURN
0520 ICORFL=1
0521 IPASS=1
0522 FORMAT(8X,I2,9X,I1,8X,I2,8X,I2)
0523 FORMAT(4(5X,I5),3F10.6)
0524 FORMAT(6F10.6)
0525 FORMAT(3I3)
0526 FORMAT(7F10.6)
0527

```

```

506 FORMAT(15I3)
507 FORMAT(2F10.6)
508 FORMAT(9X,I1,9X,I1)
509 FORMAT(9A8)
591 FORMAT(4F10.6)
1000 FORMAT(1H1/(20X,9A8))
1001 FORMAT(/10X,'PROGRAM CONTROL PARAMETERS AND SHELL SPECIFICATIONS
1002 FORMAT(/10X,'NUMBER OF AXIAL STATIONS=',I2//10X,'NUMBER OF RINGS=',
1003 FORMAT(/10X,'NUMBER OF MODES COMPRISING INITIAL IMPERFECTION=',I2//10
1004 FORMAT(/10X,'MAXIMUM/MINIMUM NUMBER OF ITERATIONS PER TIME STEP=',
1005 FORMAT(/10X,'NEWMARK'S BETA PARAMETER=',F10.8//10X,'MAXIMUM NU
1006 FORMAT(/10X,'PRINT EVERY',I6,'TH TIME STEP',F10.4//10X,
1007 FORMAT(/10X,'CONVERGENCE PARAMETER=',F6.4)
1008 FORMAT(/10X,'BOUNDARY CONDITIONS',C1,C2,C3,C4,C5,F//10X,1P6E14.4)
1009 FORMAT(/10X,'RING PARAMETERS',C1,C2,C3,C4,C5,F//10X,1P6E14.4)
1010 FORMAT(/10X,'WHOLE STATIONS AT WHICH RINGS ARE LOCATED',I3I4)
1011 FORMAT(/10X,'INITIAL IMPERFECTION',F10.6//10X,'MODE',5X,'MAGNITUDE',
1012 FORMAT(/10X,'PO,R,S,OMEGA',RESPECTIVELY//10X,1P4E14.4)
1013 FORMAT(/10X,'DTMAX=',1PE11.3//10X,'DT=',1PE11.3//10X,'POISSON'S RATIO=',F4.2//
1014 FORMAT(/10X,'LENGTH/RADIUS=',F4.2//10X,'DAMPING COEFFICIENT=',F10.6)
1015 FORMAT(/10X,'THICKNESS/RADIUS=',F4.2//10X,'SIMPLE')
1016 FORMAT(/10X,'BOUNDARY CONDITIONS',C1,C2,C3,C4,C5,F//10X,1P6E14.4)
1017 FORMAT(/10X,'RESPONSE IS SYMMETRIC WITH RESPECT TO A PLANE PERPEND
1018 ICULAR',F10.6//10X,'TO SHELL AXIS & PASSING THROUGH MIDSPAN')
1019 RETURN
1020 END

```

```

SUBROUTINE WDEF
SUBROUTINE WDEF COMPUTES THE RADIAL DISPLACEMENT AND VELOCITY AT
END OF CURRENT TIME STEP BY NEWMARK'S BETA METHOD.

COMMON/A7/ MM,NN,D,FN,NBC,N(15),KMAX,NSYM,KSUM
COMMON/A8/ DT,BETA
COMMON/Z3/ U(20,15),V(20,15),W(20,15),W1(20,15),WDOT1
1(20,15),WDDOT1(20,15),WDDOT1(20,15)
DO 1 K=2,KSUM
DO 1 L=1,NN
WDOT1(K,L)=W(K,L)+5*DT*(WDDOT(K,L)+WDDOT1(K,L))
1 W1(K,L)=W(K,L)+DT*WDOT(K,L)+DT**2*(.5-BETA)*WDDOT(K,L)+DT**2*BETA*

```



```

IWDDOI(K,L)
RETURN
END

```

0573
0574
0575

SUBROUTINE MODES

```

SUBROUTINE MODES CALCULATES THE NEW MODES GENERATED BY THE
NONLINEAR QUANTITIES AND SETS UP THE PROPER MODE NUMBER
COMBINATIONS

```

0576
0577
0578
0579
0580
0581
0582
0583
0584
0585
0586
0587
0588
0589
0590
0591
0592
0593
0594
0595
0596
0597
0598
0599
0600
0601
0602
0603
0604
0605
0606
0607
0608
0609
0610
0611
0612
0613
0614
0615
0617

```

COMMON/A7/ MM,NN,D,FN,NBC,N(15),KMAX,NSYM,KSUM
COMMON/B3/ MNMAXO
COMMON/B4/ MAXD(15),MAXS(15),MAXSY(15),ID(15,15),JD(15,15),IS(8,15)
1) JS(8,15),IJS(15)
COMMON/B5/ MAXM,MNINIT,ICCRFL,IPASS
IF (MAXM.EQ.1) RETURN
DO 1 MN=1,MNMAXO
NMN=N(MN)
NNS=MN
IF (MNINIT.GT.MN) NNS=MNINIT
DO 1 MD=NNS,MNMAXO
NMM=N(MD)
NTEST=IABS(NMN-NMM)
DO 2 MMFT=1,NN
IF (NTEST.EQ.N(MMFT)) GO TO 10
2 CONTINUE
IF (ICCRFL .EQ.1) GO TO 1
NN=NN+1
N(NN)=NTEST
MMFT=NN
IF (NN.EQ.MAXM) ICCRFL=1
10 IF ((NMN-NMM).EQ.0) GO TO 1
IF ((NMN-NMM).GT.0) GO TO 12
LOCD=MAXD(MMFT)+1
MAXD(MMFT)=LOCD
ID(LOCD,MMFT)=MD
JD(LOCD,MMFT)=MN
GO TO 1
12 LOCD=MAXD(MMFT)+1
MAXD(MMFT)=LOCD
ID(LOCD,MMFT)=MN
JD(LOCD,MMFT)=MD
1 CONTINUE

```

C
C
C
C
C
C


```

DO 301 MN=1, MNMAXD
  MN=N(MN)
  NNS=MN
  IF(MNINIT.GT.MN) NNS=MNINIT
DO 301 MD=NNS, MNMAXD
  MM=N(MD)
  NTEST=NMN+NMN
DO 302 MMFT=1, NN
  IF(NTEST.EQ.N(MMFT)) GO TO 310
CONTINUE
302 IF(ICORFL.EQ.1) GO TO 301
  NN=NN+1
  N(NN)=NTEST
  MMFT=NN
  IF(NN.EQ.MAXM) ICORFL=1
  IF(NMN.EQ.NMN) GO TO 360
  LOCS=MAXS(MMFT)+1
  MAXS(MMFT)=LOCS
  IS(LOCS, MMFT)=MN
  JS(LOCS, MMFT)=MD
GO TO 301
360 IF(NMN.EQ.0) GO TO 301
  MAXSY(MMFT)=1
  IJS(MMFT)=MN
301 CONTINUE
  MNINIT=MNMAXC+1
  IF(ICORFL.GT.0) IPASS=IPASS+1
  RETURN
END

```

```

SUBROUTINE LAMIN2
SUBROUTINE LAMIN2 COMPUTES LAM1 AND LAM2, THE NONLINEAR TERMS IN
THE AXIAL AND CIRCUMFERENTIAL EQUILIRPIUM EQUATIONS.

COMMON/A2/ D1,D2,D3,D4,D5,D6,D7,D8,D9,D10,D11
COMMON/A3/ I1,I2,I3,I4
COMMON/A4/ C1,C2,C3,C4,C5,E
COMMON/A5/ NR,KR( 3)
COMMON/A7/ MM,NN,D,FN,NBC,N(15),KMAX,NSYM,KSUM
COMMON/R1/ DM1(2,2),DM2(2,2),DM3(2,2)
COMMON/R3/ MNMAXD
COMMON/B4/ MAXD(15),MAXS(15),ID(15,15),JD(15,15),IS(8,15)

```

C
C
C
C
C

```

1),JS(8,15),IJS(15)
COMMON/B8/ WIXH(20,15),WIXW(20,15),WIYH(20,15),WIYW(20,15)
COMMON/B9/ LAM1(20,15),LAM2(20,15)
REAL LAM1,LAM2
COMMON/Z0/ WI(15)
COMMON/Z1/ CIXX(20,15),CIXT(20,15),CITT(20,15),CITX(20,15),CXX(20,
115),CTT(20,15),CXT(20,15)
COMMON/Z3/ U(20,15),V(20,15),W(20,15),W1(20,15),WDOT(20,15),WDOT1
1(20,15),WDDOT(20,15),WDDOT1(20,15)
COMMON/Z4/ GNU
COMMON/Z8/ WXH(15),WXW(15),WYH(15),WYW(15)

C
C
C
SET UP BOUNDARY CONDITIONS.
DO 14 K=1,MM
D1=1.
D2=1.
D3=1.
D4=1.
I1=K+1
I2=K+2
I3=K-1
I4=K-2
IF(K.EQ.1) GO TO 1
IF(K.EQ.2) GO TO 2
IF(NSYM.EQ.2) GO TO 21
IF(K.EQ.KMAX) GO TO 3
GO TO 5
1 I4=K+2
I3=K+1
IF(NBC.EQ.2) GO TO 5
D4=-1.
D3=-1.
GO TO 5
2 I4=K
IF(NBC.EQ.1) D4=-1.
GO TO 5
3 I2=MM
GO TO 5
4 I2=MM-1
I1=MM
GO TO 5
21 IF(K.EQ.KMAX) GO TO 22
IF(K.EQ.MM) GO TO 23
GO TO 5
22 I2=K
IF(NBC.EQ.1) D2=-1.

```

0663
0664
0665
0666
0667
0668
0669
0670
0671
0672
0673
0674
0675
0676
0677
0678
0679
0680
0681
0682
0683
0684
0685
0686
0687
0688
0689
0690
0691
0692
0693
0694
0695
0696
0697
0698
0699
0700
0701
0702
0703
0704
0705
0706
0707
0708
0710

```

0711 GO TO 5
0712 I2=K-2
0713 I1=K-1
0714 IF(NBC.EQ.2) GO TO 5
0715 D1=-1.
0716 D2=-1.
0717 5 CONTINUE
0718
0719 COMPUTE THE HALF AND WHOLE STATION DERIVATIVES OF THE RADIAL
0720 DISPLACEMENT.
0721
0722 DO 6 L=1,NN
0723   WXH(L)=(D1*W1(I1,L)-W1(K,L))/D
0724   WXW(L)=.625*D1*W1(I1,L)-.625*D3*W1(I3,L)-.0625*D2*W1(I2,L)+
0725   1.0625*D4*W1(I4,L)
0726   WXW(L)=WXW(L)/D
0727   FN=N(L)
0728   WYH(L)=-FN*(9.*(D1*W1(I1,L)+W1(K,L)) -D2*W1(I2,L)-D3*W1(I3,L))/16.
0729   WYW(L)=-FN*W1(K,L)
0730 6 CONTINUE
0731
0732 EVALUATE NONLINEAR TERMS.
0733
0734 DO 14 M=1,NA
0735   SUMA=0.
0736   SUMB=0.
0737   SUMC=0.
0738   SUMD=0.
0739   SUME=0.
0740   SUMF=0.
0741   SUMG=0.
0742   IF(N(M).EQ.0) GO TO 11
0743   MAXL=MAXS(M)
0744   IF(MAXL.EQ.0) GO TO 8
0745   DO 7 L=1,MAXL
0746     I=IS(L,M)
0747     J=JS(L,M)
0748     SUMB=SUMB+WXW(I)*WXW(J)
0749     SUMC=SUMC-WYW(I)*WYW(J)
0750     SUME=SUME+WXH(I)*WYH(J)+WXH(J)*WYH(I)
0751     SUMA=SUMA+WXW(I)*WXW(J)+WXW(J)*WXW(I)
0752     SUMD=SUMD-WYW(I)*WYW(J)-WYW(J)*WYW(I)
0753     SUMF=SUMF+WIXH(I)*WYH(J)+WYH(J)*WIXH(I)
0754     SUMG=SUMG+WYH(I)*WXH(J)+WXH(J)*WYH(I)
0755   MAXL=MAXD(M)
0756   IF(MAXL.EQ.0) GO TO 10
0757   DO 9 L=1,MAXL
0758     I=ID(L,M)

```

```

J=JD(L,M)
SUMB=SUMC+WXW(I)*WXW(J)
SUMC=SUMC+WYW(I)*WYW(J)
SUME=SUME+WXH(I)*WYH(J)+WXH(J)*WYH(I)
SUMA=SUMA+WXW(I)*WIXW(K,J)+WXW(J)*WIXW(K,I)
SUMD=SUMD+WYW(I)*WIYW(K,J)+WYW(J)*WIYW(K,I)
SUMF=SUMF+WIXH(K,I)*WYH(J)+WIXH(J)*WYH(I)
SUMG=SUMG-WXW(I)*WIYH(K,J)+WXH(J)*WIYH(K,I)
CONTINUE
9 IF(MAXSY(M).EQ.0) GO TO 13
I=IJS(M)
SUMB=SUMB+WXW(I)**2/2.
SUMC=SUMC+WYW(I)**2/2.
SUME=SUME+WXH(I)*WYH(I)
SUMA=SUMA+WIXW(K,I)*WXW(I)
SUMD=SUMD-WIYW(K,I)*WYW(I)
SUMF=SUMF+WIXH(K,I)*WYH(I)
SUMG=SUMG+WIYH(K,I)*WXH(I)
GO TO 13
10
11 DO 12 L=1,MNMAXO
SUMB=SUMB+WXW(L)**2
SUMC=SUMC+WYW(L)**2
SUMA=SUMA+WIXW(K,L)*WXW(L)
SUMD=SUMD+WYW(L)*WIYW(K,L)
IF(M.GT.MNMAXO) GO TO 20
SUMA=SUMA+WIXW(K,M)*WXW(M)
SUMB=SUMB+WXW(M)**2
CONTINUE
20 CIXX(K,M)=.5*SUMA
CXX(K,M)=.25*SUMB
CTT(K,M)=.25*SUMC
CITT(K,M)=.5*SUMD
CXT(K,M)=0.
CXT(K,M)=0.
CITX(K,M)=0.
GO TO 14
13 CIXX(K,M)=0.5*SUMA
CXX(K,M)=0.5*SUMB
CTT(K,M)=0.5*SUMC
CITT(K,M)=0.5*SUMD
CXT(K,M)=0.5*SUME
CXT(K,M)=0.5*SUMF
CITX(K,M)=0.5*SUMG
CONTINUE
14 DNU=D*GNU

```

COMPUTE LAM1 AND LAM2 WITHOUT CONTRIBUTIONS OF RING STIFFENERS.

C
C
C

```

0807 DO 15 L=1,NA
0808 FN=N(L)
0809 CSQN=D**2*FN
0810 DO 16 K=2, KSUM
0811 IF(K.EQ.MM.AND.NSYM.EQ.1) I1=MM
0812 LAM1(K,L)=-DNU*(W1(I1,L)-W1(K,L))+D*(CXX(I1,L)-CXX(K,L))+D*
0813 1(CIXX(I1,L)-CIXX(K,L))+DNU*(CIT(I1,L)-CIT(K,L))+CIT(I1,L)-
0814 2CIT(K,L))+ (1.-GNU)*DSQN*(CXT(K,L)+CIX(K,L)+CIT(K,L))/2.
0815 16 LAM2(K,L)=DSQN*W1(K,L)-DSQN*(CIT(K,L)+CIT(K,L))-DSQN*GNU*
0816 1(CXX(K,L)+CIX(K,L))+ (1.-GNU)*(CXT(K,L)-CXT(K-1,L)+CIX(K,L)-
0817 2CIX(K-1,L)+CIT(K,L)-CIT(K-1,L))*D/2.
0818 15 LAM1(1,L)=-DNU*(W1(2,L)-W1(1,L))+D*(CXX(2,L)+D*(CIXX(2,
0819 1L)-CIXX(1,L))+DNU*(CIT(2,L)-CIT(1,L))+CIT(1,L))+ (1.-GNU
0820 2)*DSQN*(CXT(1,L)+CIX(1,L)+CIT(1,L))/2.
0821 IF(NR.EQ.0) GO TO 18
0822 CSQ=D**2
0823
0824
0825
0826
0827
0828
0829
0830
0831
0832
0833
0834
0835
0836
0837
0838
0839
0840

```

ADD CONTRIBUTIONS OF RING STIFFENERS.

```

0841 DO 17 M=1,NR
0842 DO 17 L=1,NA
0843 K=KR(M)
0844 FN=N(L)
0845 FNSQ=FN**2
0846 RING1=D*(C4*FNSQ*(E*FNSQ-1.)-C5*FNSQ)*(0.625*(W1(K+1,L)-W1(K-1,L))
0847 1-(W1(K+2,L)+W1(K-2,L))*0.625)
0848 RING2=DSQ*FN*(E*FNSQ-1.)*W1(K,L)
0849 LAM1(K,L)=LAM1(K,L)+RING1
0850 LAM2(K,L)=LAM2(K,L)+RING2
0851 17 CONTINUE
0852 RETURN
0853 END

```

SUBROUTINE PMATRIX

SUBROUTINE PMATRIX COMPUTES MATRICES P, DEE, AND DST. THESE MATRICES ARE NEEDED TO COMPUTE U AND V BY GAUSS ELIMINATION.

```

COMMON/A2/ D1,D2,D3,D4,D5,D6,D7,D8,D9,D10,D11
COMMON/A4/ C1,C2,C3,C4,C5,E
COMMON/A5/ NR,KP(3)
COMMON/A7/ MM,NN,D,FN,NBC,N(15),KMAX,NSYM,KSUM

```



```

COMMON/RO/ A(2,2),B(2,2),C(2,2),AR(2,2),NINIT
COMMON/RI/ DM1(2,2),DM2(2,2),DM3(2,2)
COMMON/Z4/ GNU
COMMON/Z5/ P(2,2,20,15),DEE(2,2,20,15),DST(2,2,20,15)
P4=1.
DO 1 L=NINIT,NN
FN = N(L)
CALL ABC
D1=D*FN*(1.+GNU)/2.
D2=D**2*FN**2*(1.-GNU)/2.
D3=1.+D2
IF(NBC.EQ.2) GO TO 2
3 P(1,1,1,L)=-D4/D3
P(1,2,1,L)=-D1/D3
CALL PANDD(L)
1 CONTINUE
GO TO 4
2 P4=1.333333
D3=4.*D2
GO TO 3
4 NINIT=NINIT+1
RETURN
END

```

0852
0853
0854
0855
0856
0857
0858
0859
0860
0861
0862
0863
0864
0865
0866
0867
0868
0869
0870
0871
0872
0873
0874

SUBROUTINE PANDD(L)

SUBROUTINE PANDD COMPUTES P, DEE, AND DST.

C
C
C
C
C

```

COMMON/A5/ NR,KR( 3)
COMMON/A7/ MM,NN,D,FN,NBC,N(15),KMAX,NSYM,KSUM
COMMON/RO/ A(2,2),B(2,2),C(2,2),BR(2,2),NINIT
COMMON/RI/ DM1(2,2),DM2(2,2),DM3(2,2)
COMMON/Z5/ P(2,2,20,15),DEE(2,2,20,15),DST(2,2,20,15)
MR=1
KK=KMAX
IF(NSYM.EQ.2) KK=MM
DO 1 K=2,KK
DO 2 I=1,2
DO 2 J=1,2
DM1(I,J)=P(I,J,K-1,L)
CALL MATMAT(C,DM1,DM2)
IF(K.EQ.KR(MR))GO TO 3
DO 4 I=1,2

```

0875
0876
0877
0878
0879
0880
0881
0882
0883
0884
0885
0886
0887
0888
0889
0890
0891
0892
0893
0894
0895


```

      DO 4 J=1,2
      4 DM1(I,J)=B(I,J)
      DO 5 I=1,2
      5 GO TO 5
      DO 6 I=1,2
      6 DM1(I,J)=BR(I,J)
      MR=MR+1
      DO 7 I=1,2
      7 DO 7 J=1,2
      7 DM3(I,J)=DM1(I,J)-DM2(I,J)
      CALL INVMAT(DM3)
      CALL MATMAT(DM3,A,DM1)
      DO 8 I=1,2
      8 DO 8 J=1,2
      8 P(I,J,K,L)=DM1(I,J)
      DEE(I,J,K,L)=DM3(I,J)
      CALL MATMAT(DM3,C,DM2)
      DO 9 I=1,2
      9 DO 9 J=1,2
      9 DST(I,J,K,L)=DM2(I,J)
      I CONTINUE
      RETURN
      END

```

```

0896
0897
0898
0899
0900
0901
0902
0903
0904
0905
0906
0907
0908
0909
0910
0911
0912
0913
0914
0915
0916
0917
0918

```

SUBROUTINE ABC

SUBROUTINE ABC COMPUTES MATRICES A, B, AND C.

```

COMMON/A2/ C1,D2,D3,D4,D5,D6,D7,D8,D9,D10,D11
COMMON/A4/ C1,C2,C3,C4,C5,E
COMMON/A7/ MM,NN,D,FN,NBC,N(15),KMAX,NSYM,KSUM
COMMON/B0/ A(2,2),B(2,2),C(2,2),BR(2,2),NINIT
COMMON/Z4/ GNU
D2=(1.+GNU)/2.
D3=(1.-GNU)/2.
A(1,1)=1.
A(1,2)=D2*D*FN
A(2,1)=0.
A(2,2)=D3
B(1,1)=-2.-D3*D**2*FN**2
B(1,2)=-A(1,2)
B(2,1)=B(1,2)
B(2,2)=-D**2*FN**2-2.*D3

```

```

0919
0920
0921
0922
0923
0924
0925
0926
0927
0928
0929
0930
0931
0932
0933
0934
0935
0936
0937
0938
0939

```

C
C
C
C

0940
0941
0942
0943
0944
0945
0946
0947
0948
0949

```
C(1,1)=1.0
C(1,2)=0.
C(2,1)=A(1,2)
C(2,2)=A(2,2)
BR(1,1)=B(1,1)+D**2*(C4*FN**4-C5*FN**2)
BR(2,2)=B(2,2)+D**2*C3*FN**2
BR(1,2)=B(1,2)
BR(2,1)=B(2,1)
RETURN
END
```

0950
0951
0952
0953
0954
0955
0956
0957
0958
0959
0960
0961
0962
0963
0964
0965
0966
0967
0968
0969
0970
0971
0972
0973
0974
0975
0976
0977
0978
0979
0980
0981
0982
0983

```
SUBROUTINE UVDEF
SUBROUTINE UVDEF COMPUTES THE AXIAL AND CIRCUMFERENTIAL DISPLACEMENTS BY GAUSS ELIMINATION. THE ELEMENTS OF THE LOAD VECTOR, GEE, ARE LAM1 AND LAM2.
```

```
COMMON/A2/ D1,D2,D3,D4,D5,D6,D7,D8,D9,D10,D11
COMMON/A7/ MM,NN,D, FN,NBC,N(15),KMAX,NSYM,KSUM
COMMON/B1/ CM1(2,2),DM2(2,2),DM3(2,2)
COMMON/B9/ LAM1(20,15),LAM2(20,15)
REAL LAM1,LAM2
COMMON/Z1/ CIXX(20,15),CIXT(20,15),CITT(20,15),CITX(20,15),CXX(20,15),CXT(20,15),CXT(20,15)
COMMON/Z3/ U(20,15),V(20,15),W(20,15),W1(20,15),WDOT(20,15),WDOT1(20,15),WDDCT(20,15),WDDOT1(20,15)
COMMON/Z4/ GNU
COMMON/Z5/ P(2,2,20,15),DEE(2,2,20,15),DST(2,2,20,15)
DIMENSION X(2,20),VD1(2),VD2(2),VD3(2),GEE(2),BC3(2,2),BC4(2,2)
D1=(1.-GNU)/2.
D2=(1.+GNU)/2.
DO 17 L=1,NN
FN=N(L)
```

```
INCORPORATE BOUNDARY CONDITIONS AT X=0.
```

```
IF(NBC.EQ.1) GO TO 1
X(1,1)=LAM1(1,L)/(4.+D**2*FN**2*D1)
X(2,1)=0.
GO TO 2
1 X(1,1)=(LAM1(1,L)+D*(CXX(1,L)+CIXX(1,L)))/(1.+D**2*FN**2*D1)
X(2,1)=0.
```

PERFORM ELIMINATION OPERATIONS ON THE NEW LOAD VECTOR.

```

C
C
2 KK=KMAX
  IF(NSYM.EQ.2) KK=MM-2
  DO 4 K=2, KK
    GEE(1)=-LAM1(K,L)
    GEE(2)=-LAM2(K,L)
    DO 3 I=1,2
      VD1(I)=0.
      VD3(I)=0.
    DO 3 J=1,2
      VD1(I)=VD1(I)+DEE(I,J,K,L)*GEE(J)
3    VD3(I)=VD3(I)+DST(I,J,K,L)*X(J,K-1)
4    X(1,K)=VD1(1)-VD3(1)
  X(2,K)=VD1(2)-VD3(2)
  IF(NSYM.EQ.2) GO TO 13

RESPONSE ASSUMED TO BE SYMMETRIC WITH RESPECT TO MIDSPAN.
INCORPORATE BOUNDARY CONDITIONS AT MIDSPAN.
C
C
BC3(1,1)=0.0
BC3(1,2)=0.0
BC3(2,1)=D*FN*D2/(D1+FN**2*D**2)
BC3(2,2)=D1/(D1+FN**2*D**2)
VD3(1)=0.0
VD3(2)=LAM2(MM,L)/(D1+FN**2*D**2)
DO 10 I=1,2
  VD1(I)=X(I,KMAX)
10 CALL MATVEC(BC3,VD1,VD2)
DO 11 I=1,2
  VD1(I)=VD2(I)+VD3(I)
DO 12 I=1,2
  DO 12 J=1,2
    DM1(I,J)=P(I,J,KMAX,L)
12 CALL MATMAT(BC3,DM1,DM2)
DM2(1,1)=DM2(1,1)+1.0
DM2(2,2)=DM2(2,2)+1.0
CALL INVMAT(DM2)

SOLVE FOR U AND V BY BACK SUBSTITUTION.
C
C
U(MM,L)=0.
V(MM,L)=0.
DO 8 I=1,2
  U(MM,L)=U(MM,L)+DM2(1,I)*VD1(I)
8  V(MM,L)=V(MM,L)+DM2(2,I)*VD1(I)
  K=MM
DO 9 I=1,KMAX

```

```

C
C
C
C
      K=K-1
      U(K,L)=X(1,K)-P(1,1,K,L)*U(K+1,L)-P(1,2,K,L)*V(K+1,L)
      V(K,L)=X(2,K)-P(2,1,K,L)*U(K+1,L)-P(2,2,K,L)*V(K+1,L)
      GO TO 17
1032
1034
1035
1036
1037
1038
1039
1040
1041
1042
1043
1044
1045
1046
1047
1048
1049
1050
1051
1052
1053
1054
1055
1056
1057
1058
1059
1060
1061
1062
1063
1064
1065
1066
1067
1068
1069
1070
1071
1072
1073
1074
1075
1076
1077
1078
1079
1080

      NO ASSUMPTICN MADE REGARDING SYMMETRY WITH RESPECT TO MIDSPAN.
      INCORPORATE BOUNDARY CONDITIONS AT X=L.

13  RC3(1,1)=-4.-D**2*FN**2*D1
      BC3(1,2)=-D*FN*D2
      BC3(2,1)=BC3(1,2)
      RC3(2,2)=-2.*D1-FN**2*D**2
      RC4(1,1)=1.333333
      RC4(1,2)=0.
      RC4(2,1)=D*FN*D2
      RC4(2,2)=D1
      IF(NBC.EQ.1.AND.N(L).NE.0) GO TO 14
15  DO 5 I=1,2
      DO 5 J=1,2
      DM1(I,J)=0.
      DO 5 K=1,2
      DM1(I,J)=DM1(I,J)+RC4(I,K)*P(K,J,MM-2,L)
      DO 6 I=1,2
      DO 6 J=1,2
      DM2(I,J)=BC3(I,J)-DM1(I,J)
      CALL INVMAT(DM2)
      SOLVE FOR U AND V BY BACK SUBSTITUTION.
C
C
C
      DO 7 I=1,2
      VD1(I)=0.
      DO 7 J=1,2
      VD1(I)=VD1(I)+BC4(I,J)*X(J,MM-2)
      VD1(1)=-VD1(1)-LAM1(MM-1,L)
      VD1(2)=-VD1(2)-LAM2(MM-1,L)
      IF(NBC.EQ.1.AND.N(L).NE.0) VD1(1)=VD1(1)+D*CIXX(MM,L)+D*CIXX(MM,L)
      U(MM-1,L)=0.
      V(MM-1,L)=0.
      DO 18 I=1,2
      U(MM-1,L)=U(MM-1,L)+DM2(1,I)*VD1(I)
      V(MM-1,L)=V(MM-1,L)+DM2(2,I)*VD1(I)
      K=MM-1
      IMAX=MM-2
      DO 19 I=1,IMAX
      K=K-1
      U(K,L)=X(1,K)-P(1,1,K,L)*U(K+1,L)-P(1,2,K,L)*V(K+1,L)
      V(K,L)=X(2,K)-P(2,1,K,L)*U(K+1,L)-P(2,2,K,L)*V(K+1,L)
      GO TO 17
19

```

```

14 BC3(1,1)=BC3(1,1)+3.
   RC4(1,1)=1.
   GO TO 15
17 CONTINUE
   RETURN
   END

```

1081
1082
1083
1084
1085
1086

SUBROUTINE TNETA

SUBROUTINE TNETA COMPUTES THE STRESS RESULTANTS, THE CURVATURES
AND THE NONLINEAR TERMS IN THE RADIAL EQUILIBRIUM EQUATION.

```

COMMON/A2/ D1,D2,D3,D4,D5,D6,D7,D8,D9,D10,D11
COMMON/A3/ I1,I2,I3,I4
COMMON/A5/ NR,KR( 3)
COMMON/A7/ MM,NN,D,FN,NBC,N(15),KMAX,NSYM,KSUM
COMMON/B2/ INMAX
COMMON/B3/ MNMAXO
COMMON/B4/ MAXD(15),MAXS(15),MAXSY(15),ID(15,15),JD(15,15),IS(8,15
1),JS(8,15),IJS(15)
COMMON/B7/ WIXY(20,15),WIXX(20,15),WIYY(20,15)
COMMON/B9/ LAM1(20,15),LAM2(20,15)
PEAL LAM1,LAM2
COMMON/Z0/ WI(15)
COMMON/Z1/ CIXX(20,15),CIXT(20,15),CITT(20,15),CITX(20,15),CXX(20,
115),CTT(20,15),CXT(20,15)
COMMON/Z2/ ETAX(20,15),ETATH(20,15),ETAXTH(20,15),TY(20,15),TX(20
1,15)
COMMON/Z3/ U(20,15),V(20,15),W(20,15),W1(20,15),WDOT(20,15),WDOT1
1(20,15),WDDOT(20,15),WDDOT1(20,15)
COMMON/Z4/ GNU
COMMON/Y0/ WWX(15),WWTH(15),WWXTH(15),TX(15)
COMMON/Z7/ TXA(20),TYA(20),TYA(20),TYA(20,18)
COMMON/Z9/ NSTEP,KP
DO 12 K=2,KSUM

```

1087
1088
1089
1090
1091
1092
1093
1094
1095
1096
1097
1098
1099
1101
1102
1103
1104
1105
1106
1107
1108
1109
1110
1111
1112
1113
1114
1115
1116
1117
1118
1119
1120
1121
1122
1123
1124
1125

SET UP BOUNDARY CONDITIONS.

```

I1=K+1
I2=K+2
I4=K-2

```

C
C
C


```

D2=1.
D4=1.
IF(K.EQ.2) GO TO 1
IF(NSYM.EQ.2) GO TO 20
IF(K.EQ.MM) GO TO 2
IF(K.EQ.KMAX) GO TO 15
GO TO 3
1 I4=K
IF(NBC.EQ.1) D4=-1.
GO TO 3
2 I2=MM-1
I1=MM
GO TO 3
15 I2=MM
GO TO 3
20 IF(K.EQ.KMAX) GO TO 21
GO TO 3
21 I2=K
IF(NBC.EQ.1) D2=-1.
3 CONTINUE

      COMPUTE INPLANE FORCES AND CURVATURES.

DO 4 L=1,NN
FN=N(L)
IF(N(L).EQ.0) GO TO 19
TX(L)=(U(K,L)-U(K-1,L))/D+GNU*FN*V(K,L)-GNU*W1(K,L)+CXX(K,L)+
1 CIXX(K,L)+GNU*(CIT(K,L)+CITT(K,L))
1 CXY(K,L)=((1.-GNU)/4.)*((V(I1,L)-V(K-1,L))/D+CXT(K,L)+CXT(K-1,L)+
1 CIXT(K,L)+CIXT(K-1,L)+CITX(K,L)+CITX(K-1,L)-FN*(U(K,L)+U(K-1,L)))
GO TO 16
19 TX(K,L)=0.
TXY(K,L)=0.
16 TY(K,L)=FN*V(K,L)-W1(K,L)+GNU*(U(K,L)-U(K-1,L))/D+CIT(K,L)+
1 CITT(K,L)+GNU*(CXX(K,L)+CIXX(K,L))
WXXTH(L)=-FN*(.625*(W1(I1,L)-W1(K-1,L))-0.0625*(D2*W1(I2,L)-D4*
1 W1(I4,L)))/D+WIXY(K,L)
WWT(L)=-FN**2*W1(K,L)+W1YY(K,L)
WXX(L)=(W1(I1,L)-2*W1(K,L)+W1(K-1,L))/D**2+WIXX(K,L)
IF(ABS(WWT(L)).LT.1.E-15) WWT(L)=0.0
IF(ABS(WXXTH(L)).LT.1.E-15) WXXTH(L)=0.0
IF(ABS(WWT(L)).LT.1.E-15) WWT(L)=0.0
4 IF(INSTEP.LT.KP) GO TO 13

      COMPUTE AXIAL STRESS RESULTANT AT THETA=0 FOR SUBSEQUENT PRINTOUT.

TXA(K)=0.
DO 14 L=1,NN

```



```

14 TXA(K)=TXA(K)+TX(L)
C
C
C
EVALUATE NONLINEAR TERMS.
13 DO 12 M=1,NN
SUMA=0.
SUMB=0.
SUMC=0.
IF(N(M).EQ.0) GO TO 9
MAXL=MAXS(M)
IF(MAXL.EQ.0) GO TO 6
DO 5 L=1,MAXL
I=IS(L,M)
J=JS(L,M)
SUMA=SUMA+TX(I)*WWX(J)+TX(J)*WWX(I)
SUMB=SUMB+TY(K,I)*WWTH(J)+TY(K,J)*WWTH(I)
SUMC = SUMC-TXY(K,I)*WWXTH(J)-TXY(K,J)*WWXTH(I)
5 SUMC=MAXD(M)
6 IF(MAXL.EQ.0) GO TO 8
DO 7 L=1,MAXL
I=ID(L,M)
J=JD(L,M)
SUMA=SUMA+TX(I)*WWX(J)+TX(J)*WWX(I)
SUMB=SUMB+TY(K,I)*WWTH(J)+TY(K,J)*WWTH(I)
SUMC = SUMC+TXY(K,I)*WWXTH(J) + TXY(K,J)*WWXTH(I)
7 SUMC=MAXSY(M).EQ.0) GO TO 11
8 I=IJS(M)
SUMA=SUMA+TX(I)*WWX(I)
SUMB=SUMB+TY(K,I)*WWTH(I)
SUMC = SUMC -TXY(K,I)*WWXTH(I)
GO TO 11
9 DO 10 L=1,MNMAXO
SUMA=SUMA+TX(L)*WWX(L)
SUMB=SUMB+TY(K,L)*WWTH(L)
SUMC = SUMC + TXY(K,L)*WWXTH(L)
10 IF(M.GT.MNMAXO) GO TO 11
SUMA=SUMA+TX(M)*WWX(M)
SUMB=SUMB+TY(K,M)*WWTH(M)
11 ETAX(K,M)=.5*SUMA
ETATH(K,M)=.5*SUMB
12 ETAXTH(K,M)= SUMC
C
C
C
COMPUTE AXIAL AND CIRCUMFERENTIAL FORCES AT ENDS OF SHELL.
IF(NSTEP.NE.KP) GO TO 17
D5=D*(1.+GNU)/2.
D6=D**2*(1.-GNU)/2.
TXA(1)=0.

```

1174
1175
1176
1177
1178
1179
1180
1181
1182
1183
1184
1185
1186
1187
1188
1189
1190
1191
1192
1193
1194
1195
1196
1197
1198
1199
1200
1201
1202
1203
1204
1205
1206
1207
1208
1209
1210
1211
1212
1213
1214
1215
1216
1217
1218
1219
1220
1221

```

C
C
C
IF(NSYM.EQ.2) GO TO 23
COMPUTE AXIAL AND CIRCUMFERENTIAL STRESS RESULTANTS AT ENDS OF
SHELL AND FOR THETA=0.
DO 18 L=1,NN
FN=N(L)
D7=FN*D5
D8=2.*FN**2*D6
UL=LAM1(1,L)+U(2,L)+D7*V(2,L)-D8*U(1,L)
D1=(U(1,L)+UL)/D+CXX(1,L)+CIXX(1,L)
TXA(1)=TXA(1)+D1
18 CONTINUE
TYA(1)=GNU*TXA(1)
GO TO 17
23 TXA(MM)=0.
DO 24 L=1,NN
FN=N(L)
D7=FN*D5
D8=2.*FN**2*D6
UL=LAM1(1,L)+U(2,L)+D7*V(2,L)-D8*U(1,L)
D1=(U(1,L)+UL)/D+CXX(1,L)+CIXX(1,L)
TXA(1)=TXA(1)+D1
UR=-LAM1(KMAX,L)+D8*U(KMAX,L)+D7*V(KMAX,L)-U(MM-2,L)
D2=(UR-U(KMAX,L))/D+CXX(MM,L)+CIXX(MM,L)
TXA(MM)=TXA(MM)+D2
24 CONTINUE
TYA(1)=GNU*TXA(1)
TYA(MM)=GNU*TXA(MM)
17 CONTINUE
END

```

```

SUBROUTINE ACELR8
SUBROUTINE ACELR8 SOLVES THE RADIAL EQUILIBRIUM EQUATION FOR THE
RADIAL ACCELERATION AND COMPARES THE PRESENT VALUES TO THOSE
COMPUTED DURING THE PRECEDING ITERATION.
COMMON/A2/ D1,D2,D3,D4,D5,D6,D7,D8,D9,D10,D11
COMMON/A3/ I1,I2,I3,I4
COMMON/A4/ C1,C2,C3,C4,C5,E
COMMON/A5/ NR,KR( 3)

```

```

COMMON/A6/ PLCAD(20)
COMMON/A7/ MM,NN,D, FN,NBC,N(15),KMAX,NSYM,KSUM
COMMON/B6/ NCONV,ALPHA,EPS,CDAMP
COMMON/Z2/ ETAX(20,15),ETATH(20,15),ETAXTH(20,15),TY(20,15),TX(20
1,15)
COMMON/Z3/ U(20,15),V(20,15),W(20,15),WDOT(20,15),WDOT1
1(20,15),WDDOT(20,15),WDDOT1(20,15)
NCONV=0
ALPHSQ=ALPHA**2
D4TH=C**4
DSQ=C**2
DI1=1.+C2
ZERO =1.E-15
DO 8 L=1,NN
FN=N(L)**2
FNSQ=FNSQ*(FNSQ+2./DSQ)/(6.*DSQ)
D5=ALPHSQ*(FNSQ+2./DSQ)/(6.*DSQ)
C6=- (6.+4.*FNSQ*DSQ+FNSQ**2*D4TH)*ALPHSQ/(12.*D4TH)
C7=- (C4*E*(2.-E*FNSQ)-C5)*FNSQ/DSQ
D8=-C4*FNSQ-C1*(FNSQ-1.)*2-C3*(E*FNSQ-1.)*2-2.*D7
D9=- (C4*(1.-E*FNSQ)+C5)*FNSQ/D
D10=FN*(1.-E*FNSQ)*C3
NR=1
DO 8 K=2,KSUM
SET UP BOUNDARY CONDITIONS
I1=K+1
I2=K+2
I3=K-1
I4=K-2
D1=1.
D2=1.
D3=1.
D4=1.
IF(K.EQ.2) GO TO 1
IF(NSYM.EQ.2) GO TO 2
IF(K.EQ.KMAX) GO TO 3
IF(K.EQ.MM) GO TO 4
GO TO 5
1 I4=2
IF(NBC.EQ.1) D4=-1.
GO TO 5
3 I2=MM
GO TO 5
4 I1=MM
I2=MM-1
GO TO 5

```

C
C
C

[illegible]

1403
1404
1405
1406
1407
1408
1409
1410
1411
1412

```

SUBROUTINE MATMAT(MX1,MX2,MX3)
REAL MX1,MX2,MX3
DIMENSION MX1(2,2),MX2(2,2),MX3(2,2)
DO 1 I=1,2
DO 1 J=1,2
MX3(I,J)=0.
DO 1 K=1,2
1 MX3(I,J)=MX3(I,J)+MX1(I,K)*MX2(K,J)
RETURN
END

```

1413
1414
1415
1416
1417
1418
1419
1420

```

SUBROUTINE MATVEC(X,V1,V2)
DIMENSION X(2,2),V1(2),V2(2)
DO 1 I=1,2
V2(I)=0.
DO 1 K=1,2
1 V2(I)=V2(I)+X(I,K)*V1(K)
RETURN
END

```

1421
1422
1423
1424
1425
1426
1427
1428
1429
1430
1431
1432
1433
1434
1435
1436
1437
1438
1439
1440
1441
1442

```

SUBROUTINE WIDER2(K,L)
WIDER2 COMPUTES THE SECOND DERIVATIVES OF THE INITIAL IMPERFECTION
AS REQUIRED IN TNETA. THE SUBROUTINE IS BASED ON A PARTICULAR
AXIAL VARIATION AND MUST BE CHANGED TO ACCOMMODATE OTHER FUNCTIONAL
FORMS. (SEE THE COMMENTS AT THE BEGINNING OF SUBROUTINE WIDER1)

```

CCCCC

```

COMMON/A2/ D1,D2,D3,D4,D5,D6,D7,D8,D9,D10,D11
COMMON/A5/ NR,KR(3)
COMMON/A7/ MM,NN,D,FN,NBC,N(15),KMAX,NSYM,KSUM
COMMON/B2/ INMAX
COMMON/B7/ WIXY(20,15),WIXX(20,15),WIYY(20,15)
COMMON/ZO/ WI(15)
D7=NR+1
D8=KMAX
IF(NSYM.EQ.1) D8=2*MM-1
D7=6.2831843*D7
D8=D8*D
D6=K-1
D3=D6*D

```



```

WIXY(K,L)=-FN*WI(L)*D7*SIN(D7*D6/D8)/D8
WIXX(K,L)=WI(L)*D7**2*CCS(D7*D6/D8)/(D8**2)
WIYY(K,L)=-FN**2*WI(L)*(1.-COS(D7*D6/D8))
RETURN
END

```

1443
1444
1445
1446
1447

SUBROUTINE WIDER1(K,L)

WIDER1 COMPUTES THE FIRST DERIVATIVES OF THE INITIAL IMPERFECTION AS REQUIRED IN LAMIN2. THE SUBROUTINE IS BASED ON A PARTICULAR AXIAL VARIATION AND MUST BE CHANGED TO ACCOMMODATE OTHER FUNCTIONAL FORMS.

WIDER1 IS BASED ON THE ASSUMPTION THAT THE IMPERFECTION AND ITS FIRST AXIAL DERIVATIVE ARE ZERO AT THE ENDS OF THE SHELL AND AT STATIONS HAVING RINGS, I.E. THE IMPERFECTION IN MODE N(L) IS EQUAL TO $WI(L)*(1.-COS(2*PI*(NR+1)*X/L))$.

WHEN THE SHELL IS RING-STIFFENED, THE RINGS MUST BE LOCATED AT WHOLE STATIONS SUCH THAT THEY DIVIDE THE SHELL INTO EQUAL SEGMENTS. HENCE, THE NUMBER OF ACCEPTABLE RING LOCATIONS IS LIMITED.

IF THE RESPONSE IS ASSUMED TO BE SYMMETRIC WITH RESPECT THE MID-SPAN OF THE SHELL, THE FOLLOWING ARE ACCEPTABLE CONFIGURATIONS.

NO. OF RINGS	NO. OF AXIAL STATIONS	LOCATIONS OF RINGS
1	5	4
	8	6
	11	8
	14	10
	17	12
	20	14
2	8	4,7
	13	6,11
	18	8,15
3	11	4,7,10
	18	6,11,16

1448
1449
1450
1451
1452
1453
1454
1455
1456
1457
1458
1459
1460
1461
1462
1463
1464
1465
1466
1467
1468
1469
1470
1471
1472
1473
1474
1475
1476
1477
1478
1479
1480
1481
1482
1483
1484
1485
1486

IF THE RESPONSE IS NOT ASSUMED TO BE SYMMETRIC WITH RESPECT TO THE MIDSPAN, THE FOLLOWING ARE ACCEPTABLE CONFIGURATIONS.

NO. OF RINGS	NO. OF AXIAL STATIONS ANY ODD NUMBER<20	LOCATIONS OF RINGS CENTER
1	7	3,5
2		

CC

CCCCCCCC

10
13
16
19
9
13
17

4,7
5,9
6,11
7,13
3,5,7
4,7,10
5,9,13

3

```
COMMON/A2/ D1,D2,D3,D4,D5,D6,D7,D8,D9,D10,D11
COMMON/A5/ NR,KR( 3)
COMMON/A7/ MM,NN,D, FN,NBC,N(15),KMAX ,NSYM,KSUM
COMMON/B2/ INMAX
COMMON/B8/ WIXH(20,15),WIXW(20,15),WIYH(20,15),WIYW(20,15)
COMMON/Z0/ WI(15)
D7=NR+1
D8=KMAX
IF(NSYM.EQ.1) D8=2*MM-1
D7=6.2831843*D7
D8=D8*D
D6=K-1
D5=D6+.5
D6=D6*D
D5=D5*D
WIXH(K,L)=WI(L)*SIN(D7*D5/D8)*D7/D8
WIXW(K,L)=WI(L)*SIN(D7*D6/D8)*D7/D8
WIYH(K,L)=-FN*WI(L)*(1.-COS(D7*D5/D8))
WIYW(K,L)=-FN*WI(L)*(1.-COS(D7*D6/D8))
RETURN
END
```

1487
1488
1489
1490
1491
1492
1493
1494
1495
1496
1497
1498
1499
1500
1501
1502
1503
1504
1505
1506
1507
1508
1509
1510
1511
1512
1513
1514
1515

CCCCCCCC

SUBROUTINE AMPMAX

SUBROUTINE AMPMAX COMPUTES THE AMPLIFICATION OF THE MODES HAVING INITIAL IMPERFECTIONS. AMPMAX SHOULD BE USED IN CONJUNCTION WITH SUBROUTINES W11SIN AND W12SIN. THE AMPLIFICATION IS COMPUTED AT THE WHOLE STATION NEAREST TO THE SHELL MIDSPAN.

```
COMMON/A7/ MM,NN,D, FN,NBC,N(15),KMAX,NSYM,KSUM
COMMON/A9/ T,DTMAX
COMMON/B2/ INMAX
COMMON/Y1/ MMHALF,AMP(15), STPAM(15)
COMMON/Z0/ WI(15)
COMMON/Z3/ U(20,15),V(20,15),W(20,15),WI(20,15),WDOT(20,15),WDOT1
```

1516
1517
1518
1519
1520
1521
1522
1523
1524
1525
1526
1527
1528
1529
1530

```

1(20,15),WDDCT(20,15),WDDCT1(20,15)
C1=2*MM-1
KK=MM
D2=KMAX
IF(NSYM.EQ.1) GO TO 2
C1=MM-1
D2=MMHALF-1
KK=MMHALF
2 D3=SIN(3.141593*D2/D1)
DO 1 L=1,INMAX
IF(WI(L).EQ.0.) GO TO 1
D4=ABS(WI(KK,L))/(WI(L)*D3)
IF(D4.LE.AMP(L)) GO TO 1
AMP(L)=D4
STPAM(L)=T
1 CONTINUE
RETURN
END

```

1531
1532
1533
1534
1535
1536
1537
1538
1539
1540
1541
1542
1543
1544
1545
1546
1547
1548

SUBROUTINE PRLOAD

THIS VERSION OF PRLOAD COMPUTES THE LOAD FOR A TIME DECAYING
UNIFORM RADIAL PRESSURE

```

COMMON/A1/ P0,R,S,OMEGA
COMMON/A2/ D1,D2,D3,D4,D5,D6,D7,D8,D9,D10,D11
COMMON/A6/ PLCAD(20)
COMMON/A7/ MM,NN,D,FN,NBC,N(15),KMAX,NSYM,KSUM
COMMON/A9/ T,DTMAX
D1 = EXP(R*T)
D2 = P0/D1
DO 1 K=2,KSUM
PLCAD(K) = D2
1 RETURN
END

```

1549
1550
1551
1552
1553
1554
1555
1556
1557
1558
1559
1560
1561
1562
1563
1564
1565
1566

CCCCC

```

SUBROUTINE WI1SIN(K,L)
  WI1SIN COMPUTES THE FIRST DERIVATIVES OF THE INITIAL IMPERFECTION
  AS REQUIRED IN LAMIN2. THE SUBROUTINE IS USED WHEN THERE ARE NO
  FINGS AND THE IMPERFECTION VARIES AS SIN(PI*X/L).
  COMMON/A2/ D1,D2,D3,D4,D5,D6,D7,D8,D9,D10,D11
  COMMON/A7/ MM,NN,D, FN,NBC,N(15),KMAX,NSYM,KSUM
  COMMON/B2/ INMAX
  COMMON/B8/ WIXH(20,15),WIXW(20,15),WIYH(20,15),WIYW(20,15)
  COMMON/Z0/ WI(15)
  FN=N(L)
  D11=2*MM-1
  IF(NSYM.EQ.2) D11=KSUM
  D10=D11*D
  D9=K-1
  D8=D9+.5
  D5=3.1415927/D10
  D6=3.1415927*D9/D11
  D7=3.1415927*D8/D11
  WIXH(K,L)=WI(L)*D5*COS(D7)
  WIXW(K,L)=WI(L)*D5*COS(D6)
  WIYH(K,L)=-WI(L)*FN*SIN(D7)
  WIYW(K,L)=-WI(L)*FN*SIN(D6)
  RETURN
END

```

C
C
C
C
C
C

```

SUBROUTINE WI2SIN(K,L)
  WI2SIN COMPUTES THE SECOND DERIVATIVES OF THE INITIAL
  IMPERFECTION AS REQUIRED IN TNETA. THE SUBROUTINE IS USED WHEN
  THERE ARE NO RINGS AND THE IMPERFECTION VARIES AS SIN(PI*X/L)
  COMMON/A7/ MM,NN,D, FN,NBC,N(15),KMAX,NSYM,KSUM
  COMMON/A2/ D1,D2,D3,D4,D5,D6,D7,D8,D9,D10,D11
  COMMON/B2/ INMAX
  COMMON/B7/ WIXY(20,15),WIXX(20,15),WIYY(20,15)
  COMMON/Z0/ WI(15)
  FN=N(L)
  D8=2*MM-1
  IF(NSYM.EQ.2) D8=KSUM

```

C
C
C
C
C
C

```

D7=K-1
C7=3.1415927*C7
D6=D7/D8
D5=D8*D
D9=3.141593/D5
D3=D9**2
WIXY(K,L)=-WI(L)*FN*D9*COS(D6)
WIXX(K,L)=-WI(L)*D3*SIN(D6)
WIYY(K,L)=-WI(L)*FN**2*SIN(D6)
RETURN
END

```

```

1611
1612
1613
1614
1615
1616
1617
1618
1619
1620

```

INITIAL DISTRIBUTION LIST

	No. Copies
1. Defense Documentation Center Cameron Station Alexandria, Virginia 22314	20
2. Library Naval Postgraduate School Monterey, California 93940	2
3. Commander, Naval Air Systems Command Navy Department Washington, D.C. 20360	1
4. Professor R. E. Ball Department of Aeronautics Naval Postgraduate School Monterey, California 93940	4
5. Chairman, Department of Aeronautics Naval Postgraduate School Monterey, California 93940	1
6. Curricular Officer Aeronautical Engineering Programs Naval Postgraduate School Monterey, California 93940	1
7. D. W. Culbertson Warhead and Terminal Ballistics Laboratory Dahlgren, Virginia 22448	1
8. Professor D. J. Collins Department of Aeronautics Naval Postgraduate School Monterey, California 93940	1
9. Lieutenant Commander Charles C. Cromer 830 High Street Logansport, Indiana 46947	3

DOCUMENT CONTROL DATA - R&D

(Security classification of title, body of abstract and indexing annotation must be entered when the overall report is classified)

1. ORIGINATING ACTIVITY (Corporate author) Naval Postgraduate School Monterey, California 93940		2a. REPORT SECURITY CLASSIFICATION UNCLASSIFIED	
		2b. GROUP	
3. REPORT TITLE AN INVESTIGATION OF THE NONLINEAR DYNAMIC RESPONSE OF CYLINDRICAL SHELLS UNDER TRANSIENT PRESSURE			
4. DESCRIPTIVE NOTES (Type of report and inclusive dates) Thesis for Doctor of Philosophy, April 1969			
5. AUTHOR(S) (Last name, first name, initial) Charles Clinton Cromer, Lieutenant Commander, U. S. Navy			
6. REPORT DATE April 1969		7a. TOTAL NO. OF PAGES 280	7b. NO. OF REFS 48
8a. CONTRACT OR GRANT NO.		8a. ORIGINATOR'S REPORT NUMBER(S)	
b. PROJECT NO.			
c.		9b. OTHER REPORT NO(S) (Any other numbers that may be assigned this report)	
d.			
10. AVAILABILITY/LIMITATION NOTICES Distribution of this document is unlimited.			
11. SUPPLEMENTARY NOTES		12. SPONSORING MILITARY ACTIVITY Naval Postgraduate School Monterey, California 93940	
13. ABSTRACT A numerical algorithm was developed for computing the nonlinear dynamic response of a ring-stiffened, nearly circular cylindrical shell of finite length under transient, axisymmetric radial loads of arbitrary axial distribution. Nonlinear Donnell-type equations were solved using Fourier series expansions of the dependent variables in the circumferential coordinate, modified finite difference approximations of the axial derivatives, and Newmark's beta-method, combined with Gauss elimination, for the time integration. The response of a simply supported shell under an exponentially decaying, uniform pressure was computed for peak pressures and total impulses between the static buckling limit and the dynamic buckling limit. Near the dynamic buckling limit, the exponential growth of the static buckling modes dominated; but as the peak pressure was reduced, the parametrically excited Mathieu modes became increasingly important. The significance of damping, the initial imperfections, and nonlinear coupling was also investigated.			

CYLINDRICAL

SHELLS

NONLINEAR

DYNAMIC

RESPONSE

TRANSIENT

RINGS

BUCKLING

INSTABILITY

NUMERICAL

IMPULSE

COUPLING

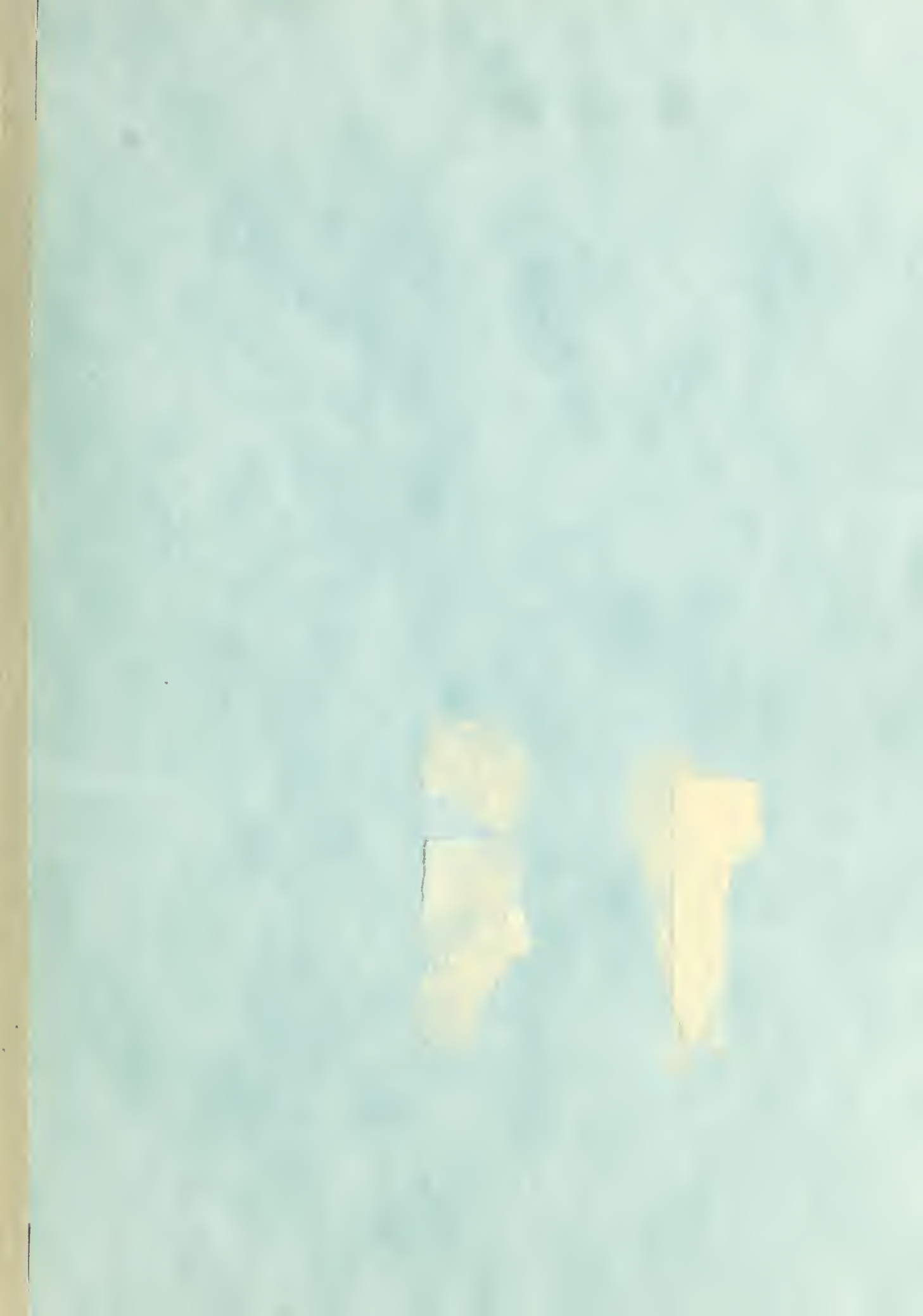
IMPERFECTIONS

STIFFENERS

FOURIER SERIES

FINITE DIFFERENCES

DAMPING



thesC8747

An investigation of the nonlinear dynami



3 2768 002 08934 4

DUDLEY KNOX LIBRARY